ISSN: 2153-1196 Volume 13, Number 11, November 2022

Scientific Research Publishing

# Journal of Modern Physics

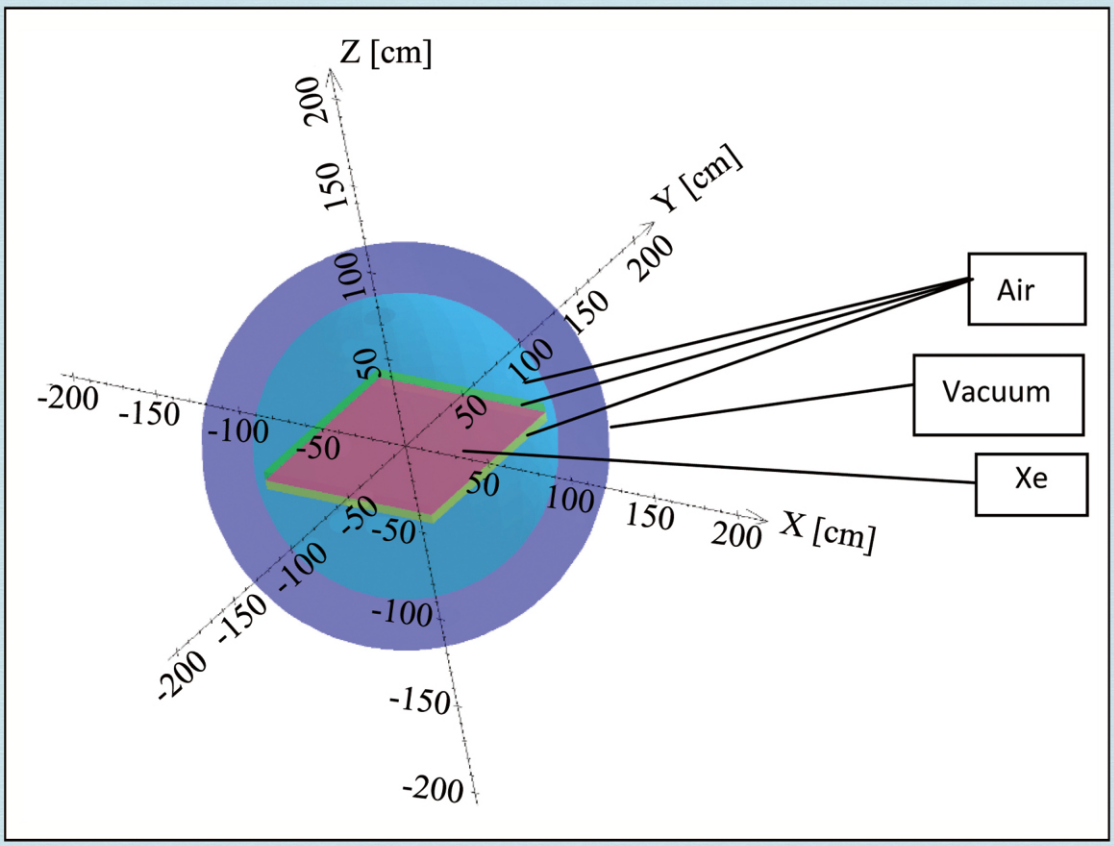


ISSN: 2153-1196

https://www.scirp.org/journal/jmp

# Journal Editorial Board

ISSN: 2153-1196 (Print) ISSN: 2153-120X (Online)
https://www.scirp.org/journal/jmp

## Editorial Board

Scientific Research Publishing

Journal of Modern Physics, 2022, 13, 1305-1517
https://www.scirp.org/journal/jmp
ISSN Online: 2153-120X
ISSN Print: 2153-1196

# Table of Contents

Volume 13 Number 11 November 2022

Journal of Modern Physics, 2022, 13, 1305-1517
https://www.scirp.org/journal/jmp
ISSN Online: 2153-120X
ISSN Print: 2153-1196



The figure on the front cover is from the article published in Journal of Modern Physics, 2022, Vol. 13, No. 11, pp. 1331-1340 by Michael Bettan, Jonathan Walg and Itzhak Orion.

# Journal of Modern Physics (JMP)
# Journal Information

## SUBSCRIPTIONS

The *Journal of Modern Physics* (Online at Scientific Research Publishing, https://www.scirp.org/) is published monthly by Scientific Research Publishing, Inc., USA.

**Subscription rates:**
Print: $89 per issue.
To subscribe, please contact Journals Subscriptions Department, E-mail: sub@scirp.org

## SERVICES

**Advertisements**
Advertisement Sales Department, E-mail: service@scirp.org

**Reprints (minimum quantity 100 copies)**
Reprints Co-ordinator, Scientific Research Publishing, Inc., USA.
E-mail: sub@scirp.org

## COPYRIGHT



## PRODUCTION INFORMATION

For manuscripts that have been accepted for publication, please contact:
E-mail: jmp@scirp.org

Scientific Research Publishing

Journal of Modern Physics, 2022, 13, 1305-1313
https://www.scirp.org/journal/jmp
ISSN Online: 2153-120X
ISSN Print: 2153-1196

# A Quantum Space Model of Cosmic Evolution: Dark Energy and the Cyclic Universe

**Carlos A. Melendres**

The SHD Institute 216 F Street, Davis, CA, USA
Email: camelendres@shdinstitute.org

**How to cite this paper:** Melendres, C.A. (2022) A Quantum Space Model of Cosmic Evolution: Dark Energy and the Cyclic Universe. *Journal of Modern Physics*, **13**, 1305-1313.
https://doi.org/10.4236/jmp.2022.1311079

**Received:** August 15, 2022
**Accepted:** October 29, 2022
**Published:** November 1, 2022



## Abstract

We present a Quantum Space Model (QSM) of cosmic evolution based on the theory that space consists of energy quanta from which our universe came about. We used the Friedmann equations to trace its history and predict its ultimate fate. Results provide further support to our recent proposal that the accelerating expansion of the universe is due to a scalar space field which has become known as Dark Energy. In our model, the universe started from high energy space quanta which were triggered by quantum fluctuations that caused the Big Bang. It then expanded and cooled undergoing phase transitions to radiation, fundamental particles, and matter. Matter agglomerated and grew into stars, galaxies, etc. and was eventually consolidated by gravity into Black Holes, which finally ended in a Big Crunch in a state of deep freeze inside the Black hole at 1.380 trillion years. Fluctuations, quantum tunneling, or some other mechanisms caused a new Bang to start another cycle in its life. Our results are in good agreement with the theoretical predictions of a cyclic universe by Steinhardt and his associates, and by Penrose. Space and energy are equivalent as embodied in the Planck energy equation. They give rise to the two principal long range forces in the universe: the gravitational force and the space force. The latter may be the fifth force in the universe. The two forces could provide the clockwork mechanism operating our cyclic universe. If the Law of Conservation of Energy is universal, then the cosmos is eternal.

## Keywords

Quantum Space Model, Spaceons, Dark Energy, Gravitational Waves, Cosmic Evolution, Expansion of the Universe, Black Holes, Big Bang, Big Crunch, Cyclic Universe

## 1. Introduction

The evolution of the universe is of great interest in astronomy, astrophysics, cosmology and science in general. It also has important implications in philoso-

phy and religion. Theories abound on how the universe started and evolved. Creationists begin with the biblical statement "Let there be light…", while non-believers and some others say that "The universe started from nothing… [1] [2]". Science has made great progress in answering the question of where the universe came from through the widely accepted Big Bang theory of Cosmology. However, many observations remain mysterious and unexplained; there is need for improvement in theories, better models, and more experimental work. This work attempts to do that.

In a recent paper [3], we presented a model that could help understand our universe better. We postulated that space consists of energy quanta. Using a themodyanamic approach, we showed how gravitational energy and the energy of space could give rise to dark energy which causes the accelerating expansion of the universe. We follow up on this approach to predict the future and the ultimate fate of the universe.

## 2. The Quantum Space Model (QSM)

Space consists of energy quanta which we call spaceons. It is a dynamical entity which actively participates in the creation and evolution of the universe rather than acting merely as a static background in which events are portrayed. The universe started as a quantum size volume of space of nearly infinite energy density. The wavelength of spaceons, $\lambda$, defines the size of space with its volume,

$$V = (4/3)\pi\left(\frac{\lambda}{2}\right)^3 \tag{1}$$

Its energy content is defined by the Planck equation, $E = hc/\lambda$, hence, $E$ is inversely proportional to $V^{1/3}$, *i.e.*, the smaller the volume (shorter wavelength, $\lambda$), the higher the energy.

From wave-particle duality, spaceons can be regarded as an ideal gas. From its initial state of a near-singular volume with near-infinite energy content, quantum fluctuations caused the release of energy in what we call the Big Bang, at high temperature and pressure. This tiny "ball of hot spaceons" expanded and cooled undergoing phase transitions forming ultra-high energy radiation and neutrinos, as well as, matter (dark and ordinary or baryonic). The expansion rate slowed down due to the action of gravity. It then re-accelerated at about $7.5 \times 10^9$ years due to dark energy [3]. We theorized earlier [3] that the re-aceceleration in expansion was due to the decrease in gravitational potential energy as matter was consolidated by agglomeration to form stars, galaxies and clusters. This energy was transformed into the energy of space which was dubbed "dark energy". Further consolidation by Black Holes resulted in a Big Crunch which brought back the universe to its beginning of a small point volume of space, *i.e.*, essentially a quantum dot.

## 3. Results and Discussions

1) The Universe from the Beginning to the present

Details of the calculational procedures appear in ref. 3. Briefly, we used the Friedmann equations to provide information on the evolution of the universe by constructing a plot of its composition as a function of time [3]. We used experimental data provided by the measurements of the Wilkinson Microwave Platform (WMAP) given previously. We plotted the fractional amount of radiation (high energy radiation plus neutrinos) and matter, "*f*", as a function of the scale factor "*a*". This was calculated using the Friedman equation,

$$H^2 = \left(\mathrm{d}a/\mathrm{d}t\right)^2 a^2 = \left(H_0\right)^2 \left[\Omega_m a^{-3} + \Omega_r a^{-4} + \Omega_s a^{-3(1+w_s)}\right] \quad (2)$$

where $H$ is the Hubble constant, a the scale factor, omega, Ω, the fractional energy density of each component, *i.e.*, matter (with $\Omega_m a^{-3}$), radiation (with $\Omega_r a^{-4}$), and space (with $\Omega a^{-3(1+w_s)}$) where $w_s$ is the equation of state parameter [4]. This has been explained in ref. [3] and appears in most books in Cosmology (see for example, ref. [4]).

Figure 1 gives the results of our calculations, which shows the evolution of the universe from the Big Bang (BB) up to the present time (13.8 billion years). In the figure, we have classified photons (radiation) and neutrinos as waves, which travel at the velocity of light, *c*. The other class is particulate matter which consists of dark matter and ordinary (baryonic) matter. In the beginning of the hot universe (the Big Bang), there were only spaceons, radiation and neutrinos (point I, BB, in Figure 1). This tiny ball of fire expanded and cooled. In the process of condensation, the elements of matter started to form (point II). We will refer to the forerunner of matter as gravitons, which has long been postulated by physicists to carry the force of gravity. They gave rise to the fundamental particles of matter, *i.e.*, quarks, leptons, etc. associated with gravity. There was no matter at the Big Bang. Fundamental particles were created 0.01 sec ($a = 10^{-10}$) later [5], point II. Figure 1 indicates that Dark and Ordinary matter did not exist before $1.4 \times 10^{-2}$ year ($a = 10^{-6}$). Our observation of matter for the first time came from the Wilkinson Microwave Auxiliary Platform measurements (WMAP) at $3.8 \times 10^5$ years ($a = 0.01$) at III, when electrons recombined

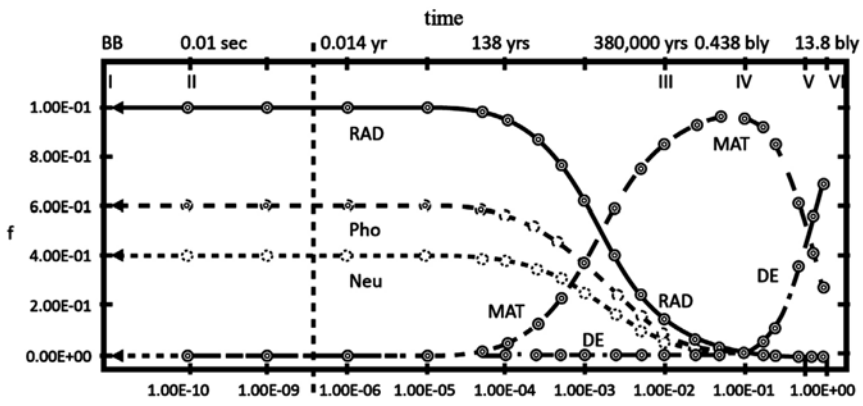


Figure 1. Fractional composition of the universe (f) vs scale factor (a) bly-billion light years; RAD-radiation; Pho-photons; Neu-neutrinos; MAT-matter; DE-dark energy, with equation of state parameter, $w_s = -0.7$.

with protons to form atomic hydrogen and released light. Thus the Big Bang was not an explosion of matter and radiation "all over the place" as commonly expressed; it was just a silent burst of spaceons and, high energy radiation. The amount of matter increased with time as the force of gravity consolidated it by agglomeration to form massive objects, stars, etc.. They continue to grow in mass, and eventually collapse to form Black Holes. The energy density of matter reached a maximum at about $4.36 \times 10^8$ yrs ($a = 0.1$) at point IV, Figure 1. The fractional energy density of spaceeons and radiation decreased correspondingly, reaching a minimum (nearly negligible) at point IV. This is the onset at which time the so-called Dark Energy appeared. The total energy density of matter started decreasing until the present time (point VI), at $13.8 \times 10^9$ years (a = 1). Dark Energy continued increasing, which correlated with the re-acceleration of the expansion of the universe that we observed [3], starting at about $7.5 \times 10^9$ years ($a = 0.65$), at point V, when the fractional density of total matter equaled that of dark energy. In effect, the gravitational energy decrease has been converted into the energy of the space field. This is the Dark Energy which is causing the reacceleration in expansion of the universe. It is the energy of space (the spaceons), just given the name "Dark Energy" because it was an unknown form of energy. A simple analogy to this mechanism is to imagine a quiet lake on a nice day. The ripples on the surface are small. When a motorboat passes by from a distance, the surface is disturbed and bigger waves are generated reinforcing the ripples which travel at higher velocity toward the shore. Gravitational waves are distortions in space [6]; they are generated, propagated and have been observed when two massive objects like neutron stars and Black Holes merge. The energy reinforces the energy of space which results in the acceleration of the expansion of the universe. Dark Energy is also Einstein's cosmological constant.

2) The Future and Ultimate Fate of the Universe

We use the Friedmann equation further to obtain information on the future of the universe beyond $13.8 \times 10^9$ years ($a = 1$). Figure 2, shows a plot of a vs the fractional energy density of particulate matter and Dark Energy (Spaceons) as a

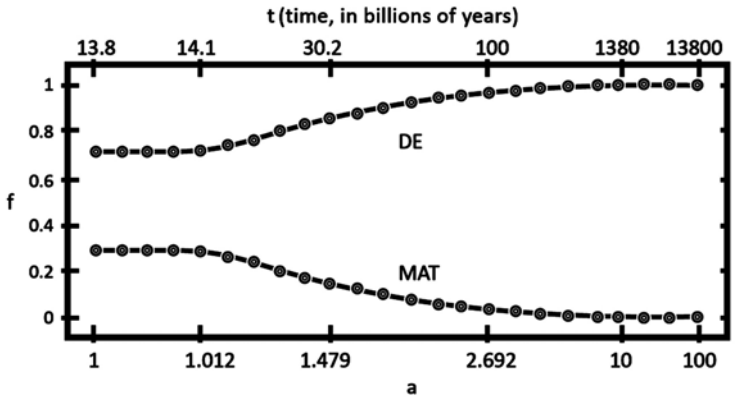


Figure 2. Fractional composition of the Universe in the future; a-scale factor; f-fractional energy density; MAT (Total Matter); DE (Dark Energy; with $w_s = -0.7$).

function of time (scale parameter, a) for the future; it is an extension of the curves of **Figure 1**, for $a > 1$. The DE curve rises very slowly but continuously then levels upon reaching a maximum. Likewise the energy density of matter decreases towards a minimum. The leveling occurs at about $a = 10$, equivalent to $1.380 \times 10^{12}$ years. At this point, all the matter in the universe has been consolidated and converted to Dark Energy by Black Holes. This is the energy of space (spaceons). Recall that this was actually the initial state of the universe before the Big Bang. But now all the energy of matter and space are inside a Black Hole! During the process of consolidation, Black Holes gobbled up everything in the universe, including space (in a waterfall effect), and converted them into Dark Energy (spaceons). It is interesting to think of or speculate on the state of spaceons inside inside a Black Hole. Some information can be gained from the theoretical works of Hawking (7) and Chapline (8, 9). The theory of Hawking Radiation [7] allows one to calculate the temperature inside a Black Hole to be nearly absolute 0 K (about $1 \times 10^{-14}$ K), for a supermassive black hole with a mass of about a million times that of the sun. Chapline's theory showed that the contents of Black Holes are Bose-Einstein condensates [8] [9]. This state of the universe inside the Black Hole can be called the "Big Crunch". But being at extremely low temperature it may also be called a "Big Freeze". We prefer to use the term "Big Crunch". The universe will remain in this state; but it is probable that this state of Big Crunch will not last forever. Fluctuations, quantum tunneling, or some other mechanism will likely occur, since they are random statistical processes. A new Big Bang is then quite likely which would lead to a new cycle in the life of the universe. As Krauss [1] said "… the state of nothing is unstable" and if there is nothing then there will be something though not visible to us, observers.

Our model thus shows that our universe can undergo at least one cycle in its evolution. Moreover, if the universe is closed where the law of conservation of energy is obeyed, then our universe can be eternal. It is important to point out that the theoretical work of Steinhardt and his co-workers first predicted the possibility of a cyclic and eternal universe without using a particular physical model and without invoking the need of a theory of Inflation [10] [11] [12]. Their calculated life of over 1 trillion years for one cycle is in agreement with our result of 1.4 trillion years. Penrose has also proposed a cyclic universe, which was met with much skeptism [13]. Our QSM is a good physical model for their theories. This agreement between theory and the results presented here is quite satisfying.

Another possibility for the fate of the university is that predicted by Rovelli's theory of Planck Stars [14] [15], *i.e.*, that a "bounce" is more likely rather than a crunch. Using a quantum gravity approach, he showed that there is no singularity in a Black Hole because the universe undergoes a bounce due to quantum pressure counteracting the force of gravity and the volume does not shrink beyond a certain size. The universe could therefore undergo a bounce, explode and eventually turn into a White Hole. However the time of conversion will take

about a thousand trillion times the current age of the universe [16]. White Holes have not been confirmed to exist. Rovelli and associates continue to improve their theory but at this time it does not appear viable [17].

3) The Consolidation of Matter and Space in Black Holes

We say a bit more on the conversion of matter back into space/dark energy. The universe evolved from fundamental particles to form atomic hydrogen which then formed stars by fusion. The stars formed galaxies, which then agglomerated to form clusters, then superclusters emerged. These massive bodies continue to grow in seize and mass. Eventually they (stars for example) collapse to form Black Holes. The force of gravity inside a Black Hole transform matter into space (spaceons) which is in effect Dark Energy, as they have become "baptized". In our model, Black Holes swallowed and devoured matter along with space (like a waterfall), until a near-singular volume of space is reached. Transformations occurred inside the Black Holes. The problem of singularity is avoided in our model. It cannot be present because space is almost infinitely compressible with increasing energy content. There will always be space if there is energy. Mathematics cannot theoretically describe the singularity in the structure of a Black Hole. But physically, one can imagine that matter in a Black Hole is compressed until they are broken down into fundamental particles and eventually transformed back into space/dark energy. Such transformation is already observed the formation of neutron stars which stop at neutrons as the final state (they also go through a superfluid state [15]). The forces in Back Holes are stronger such that the process of breakdown of particulate matter can go further all the way to spaceons/dark energy. This interconvertibility is embodied in Eistein's energy equation, $E = mc^2$ and Planck's equation, $E = (hc/\lambda) = hc/2)(4\pi/3\,V)^3$ from which follows,

$$m = \left(h/2c\right)\left(4\pi/3V\right)^3 \tag{3}$$

It shows the equivalence of matter and space. This equation provides the basis of our Quantum Space Model.

4) Epochs in the Evolution of the Universe

There are many versions of the history and chronology of the universe starting with the Big Bang. Ours started before the Big Bang. We will not go in as much detail as Silk [18], but briefly as befits our simple model. We divide its stage of evolution roughly into the following stages. Birth (Spaceons, Big Bang), Growth (matter formation, stars). Ageing and Consolidation (galaxies, clusters, Planck Stars, Black Holes), and the End (Big Crunch, Spaceons/Dark Energy, quantum dot). The chronology is shown in **Table 1** and illustrated in **Figure 3**. The universe started with quanta of space and ended in dark energy inside a Black Hole. From then on the universe undergoes cycles of "death" and "resurrection"/rebirth to exist possibly for eternity.

The evolution of the cosmos in accordance with our Quantum Space model is shown in **Figure 3** below.

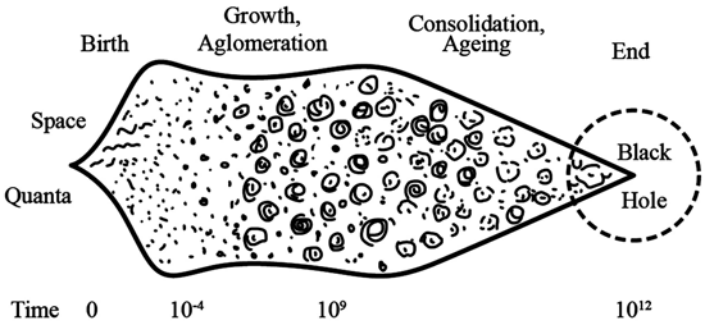


**Figure 3.** Epochs in the evolution of the quantum universe.

**Table 1.** Chronology of cosmic evolution.

| Epoch | Time (t) | Contents |
|---|---|---|
| Birth | $<10^{-12}$ sec $<10^{-4}$ yr | Space quanta, radiation, fundamental particles, matter |
| Growth and aggregation | $<10^{-4}$ to 138 yrs | matter formed nebulae, stars, planets, |
| Ageing and Consolidation | $>10^{7}$ to $10^{9}$ yrs | agglomeration to galaxies, clusters, Black Hole formation |
| The End | $10^{9}$ to $>10^{12}$ yrs | Stars died, Black Holes, Big Crunch |

## 4. Summary and Conclusion

We have presented a model which explains how dark energy emanates from the energy of space and provides the repulsive force to accelerate the expansion of the universe; it is in effect Einstein's cosmological constant. The model is based on a dynamical theory that space consists of energy quanta, and uses the Friedmann equations to describe the evolution of the universe from its beginning before the Big Bang until its ultimate end in a Big Crunch and Deep Freeze. The universe started from a near-singular volume of space with high energy density given by the Planck energy equation. It then expanded and cooled undergoing phase transitions to radiation, fundamental particles, and matter. The amount of matter grew, and was consolidated by gravity into stars, galaxies, clusters, and superclusters. Further consolidation by Black Holes continued ending in a Big Crunch at about 1.4 trillion years which brought the universe back to its initial state and started a new cycle in its life. If the Law of Conservation of Energy is universal, then the universe is eternal. In our model, energy and space are equivalent as, expressed by Planck's equation, similar to the equivalence of matter and energy as expressed in Einstein's energy equation. The two most fundamental quantities in the universe appear to be space and energy. The two principal long range forces are the gravitational force (compression) and the space force (expansion); the latter may be the fifth force in the universe. It is carried by bosonic spaceons while the gravitational force may be carried by an as yet undiscovered graviton. The two could constitute the clockwork mechanism that operates our cyclic and eternal Quantum Universe. The Quantum Space Model (QSM) pro-

vides a good physical model which is well supported by the theoretical work of Steinhardt and Penrose that predict an eternal phoenix universe. It provides an explanation of the creation, evolution, and ultimate fate of the universe, which is rational without arbitrary assumptions and consistent with prevailing theories. It may have further applications in the development of a theory of Quantum Gravity.

## Acknowledgements

The author enjoyed the lectures of Professor Robert Piccioni on cosmology conducted on-line and the stimulating discussions thereat. His dedication in the pursuit of his profession is remarkable and truly admirable. Funding of this work was provided by the SHD Institute.

## Conflicts of Interest

The author declares no conflicts of interest regarding the publication of this paper.

## References

[1] Krauss, L. (2012) A Universe from Nothing. Simon and Schuster, London.

[2] Krauss, L.M. and Starkman, G.D. (2000) *Astrophysical Journal*, **531**, 22-30. https://doi.org/10.1086/308434

[3] Melendres, C.A. (2021) *Journal of Modern Physics*, **12**, 1527-1544. https://doi.org/10.4236/jmp.2021.1211092

[4] Stenger, V.J. (2006) The Comprehensible Cosmos. Prometheus Books, New York.

[5] Weinberg, S. (1977) The First Three Minutes. Basic Books, New York.

[6] Piccioni, R.L. (2017) Einstein's Theories of Relativity. Real Science Publishing.

[7] Page, D.N. (1976) *Physical Review D*, **13**, 198-206. https://doi.org/10.1103/PhysRevD.13.198

[8] Chapline, G., Hohlfeld, E., Laughlin, R.B. and Santiago, D.I. (2003) *International Journal of Modern Physics A*, **18**, 3587-3590. https://doi.org/10.1142/S0217751X03016380

[9] Chapline, G., *et al.* (2005) Dark Energy Stars. *Proceedings of the Texas Symposium on Relativistic Astrophysics*, Stanford, December 2004, 101.

[10] Steinhardt, P.J. and Turok, N. (2002) *Science*, **296**, 1436-1439. https://doi.org/10.1126/science.1070462

[11] Lehners, J.L. and Steinhardt, P.J. (2009) *Physical Review D*, **79**, Article ID: 063503. https://doi.org/10.1103/PhysRevD.79.063503

[12] Ijjas, A. and Steindhart, P.J. (2022) *Physics Letters B*, **824**, Article ID: 136823. https://doi.org/10.1016/j.physletb.2021.136823

[13] Penrose, R. (2010) Cycles of Time: An Extraordinary New View of the Universe. The Bodley Head, London.

[14] Rovelli, C. (2007) *Nature Astronomy*, **1**, Article No. 0065. https://doi.org/10.1038/s41550-017-0065

[15] Barrau, A., Roveli and Vidotto, F. (2014) *Physical Review D*: *Particles and Fields*,

**90**, Article ID: 127503. https://doi.org/10.1103/PhysRevD.90.127503

[16] Cowen, R. (2014) Quantum Bounce Could Make Black Holes Explode. *Nature*. https://doi.org/10.1038/nature.2014.15573

[17] Rovelli, C. and Haggard, H.M. (2014) *Physical Review D*, **92**, Article ID: 104020. http://arxiv.org/abs/1407.0989

[18] Silk, J. (1989) The Big Bang. Freeman and Co., New York.

Journal of Modern Physics, 2022, 13, 1314-1323
https://www.scirp.org/journal/jmp
ISSN Online: 2153-120X
ISSN Print: 2153-1196

# Non-Linear Effects in Optical Systems by Lie Algebra and Symplectic Mapping

**Víctor M. Castaño**

Centro de Física Aplicada y Tecnología Avanzada/Secretaría de Desarrollo Institucional, Universidad Nacional Autónoma de México, Queretaro, México

Email: vmcastano@unam.mx

**How to cite this paper:** Castaño, V.M. (2022) Non-Linear Effects in Optical Systems by Lie Algebra and Symplectic Mapping. *Journal of Modern Physics*, **13**, 1314-1323.
https://doi.org/10.4236/jmp.2022.1311080

**Received:** August 22, 2022
**Accepted:** November 1, 2022
**Published:** November 4, 2022



## Abstract

The use of signals of different frequencies determines the geometrical deviation with respect to the optical axes of a given beam. This angle can be determined by Sympletic Map (SM), a powerful and simple mathematical tool for the characterization and construction of images in Geometrical Optics. The Sympletic Map constitutes a Lie Group, with an algebra associated: the Lie Algebra. In general, the SM can be expressed as an infinite series, where each term corresponds to different contributions produced by the optical devices that constitute the optical system (lenses, apertures, bandwidth cutoff, etc.). The level of correction to be performed on the image to recover the original object is clear and controllable by SM. This formalism can be extended easily to physical optics to describe diffraction and interference phenomena.

## Keywords

Symplectic Mapping, Geometrical Optics, Non-Linear Effects

## 1. Introduction

Geometrical optics is perhaps one of the oldest branches of physics. The observation of propagation and refraction of light date back to the ancient Greek world. However, it was during the XVII century when Snell and Descartes turned those empirical observations into physical laws. The principles of geometrical optics can be stated as a variational principle (Fermat) and the corresponding equations, that describe the geometrical properties of the light beams when passing through different media, can be then stated. The dependence on frequency in a specific medium determines the tilting angle of the propagating beam with respect to the optical axis.

To determine that deviation from the optical axis, the standard approach is by using the Hamiltonian. In this function, the refraction index can be made dependent on the medium and signal frequency. In most standard cases, the medium is assumed isotropic and linear.

For a more complex system, which consists of a Hamiltonian function dependent on the frequency by means of the refractive index, there exist several transformations, namely the Canonical Transformations (CT) dependent on frequency, which, when applied to the Hamiltonian, leave this unchanged, that is, the Hamiltonian is invariant to canonical transformations [1] [2].

The CT can be written as a Lie series of the Lie Transformation, where the first term corresponds to the Hamiltonian's Poisson Brackets of the dynamical variable of the system under study [1] [2]. The CT, Poisson Brackets and Lie Algebra constitute what is called the Symplectic Map (SM), a concept which allows to solve a wide number of problems in science and technology.

## 2. Geometrical Optics

Let us assume a medium characterized by a local refraction index $n(q)$, being

$$\boldsymbol{q}(s)=\left(q_x(s),q_y(s),q_z(s)\right)$$

the position vector relative to an arbitrary frame of reference, and $s$ the arc length, defined in the usual way:

$$\mathrm{d}s=\sqrt{\mathrm{d}q_x^2+\mathrm{d}q_x^2+\mathrm{d}q_x^2}$$

with the condition

$$\left|\mathrm{d}\boldsymbol{q}(s)/\mathrm{d}s\right|=1 \tag{1}$$

which corresponds to the inextensibility condition. From differential geometry, the tangent vector can be written as:

$$\boldsymbol{p}=n\left(\mathrm{d}\boldsymbol{q}(s)/\mathrm{d}s\right) \tag{2}$$

This vector is tangent to the light beam and it is used to indicate any deviation with respect to the optical axis.

$$\left|\boldsymbol{p}\right|=n(\boldsymbol{q})$$

Also, this tangent vector corresponds to the momentum vector $p$ in the Descartes' sphere [3] [4] [5] where, in each point the relation. The Hamilton equations state [3] [4] [5]:

$$\mathrm{d}p_i/\mathrm{d}z=\dot{p}_i=-\partial H^{opt}/\partial q_i\ ;\ \ \mathrm{d}q_i/\mathrm{d}z=\dot{q}_i=-\partial H^{opt}/\partial p_i\ ;\ \ i=1,2 \tag{3}$$

is satisfied. This sphere is built in such a way that the Snell-Descartes Law means a conservation of the tangent component of the momentum of the light along the surface between two media characterized with two different refractive index, where the optical Hamiltonian takes the form:

$$H^{opt}=-\sqrt{n(\boldsymbol{q}z)^2-p^2} \tag{4}$$

Here "$z$" indicates the optical axis, then the derivatives respect to $z$ indicates deviations from the optical axis.

These equations can also be obtained by using Fermat's principle, which is essentially a variational principle, where the distance traveled by a light beam to go, along the optical path, from one medium to another (with different refraction indexes) is minimized. By using Hamilton equations it is possible to obtain the deviation suffered by a light beam passing from one medium to another.

The Hamilton equations can be expanded in a power series in $\boldsymbol{p}$ to obtain:

$$H^{opt} = H^{paraxial} + O\left(\left(p^2\right)^2\right) = p^2/2n_0 - n(\boldsymbol{r}, z) + O\left(\left(p^2\right)^2\right) \tag{5}$$

where $n_0 = n(0,z)$ = constant.

This approximation is good when $|\boldsymbol{q}| \ll 1$ and $p^2 \ll n^2$; this means that the light beam is near to the optical axis ($z$ axis). As it can be noticed, these equations are very similar to the corresponding equation for mechanical systems, since by just exchanging $z$ by the time $t$, one obtains Newton's equations [3].

## 3. Hamiltonian Systems, Poisson Brackets and Canonical Transformation

For a mechanical system, the Hamiltonian $H(\boldsymbol{p}, \boldsymbol{q}, t)$ describes the time evolution of the system. The Hamiltonian $H(q, p, t)$ is a $2n$ variables function $q_i$; $p_i$; $i = 1, 2, \cdots, n$. $H : R^{2n} \to R$ with the dynamical equations [1] [2]:

$$\dot{p}_i = -\partial H^{opt}/\partial q_i \;;\; \dot{q}_i = -\partial H^{opt}/\partial p_i \;;\; i = 1, 2, \cdots, n \tag{6}$$

The solution of Hamilton equations allows to describe the trajectory of the system in phase space ($\boldsymbol{q}(t)$, $\boldsymbol{p}(t)$). These trajectories provide the position and momentum of the system as a function of time [1] [2].

The Poisson Brackets (PB) allow a simple representation of the dynamical equations of the system. These are defined as:

$$\{u, v\} \equiv \sum_{j=1}^{n} \left(\left(\partial u/\partial q_j\right)\left(\partial v/\partial p_j\right) - \left(\partial u/\partial p_j\right)\left(\partial v/\partial q_j\right)\right) \tag{7}$$

being $n$ the number of degrees of freedom. With this definition, two variables are called canonical conjugated, provided they satisfy:

$$\{q_i, q_j\} = 0 \;;\; \{p_i, p_j\} = 0 \;;\; \{q_i, p_j\} = \delta_{ij} \tag{8}$$

In this notation Hamilton's equations look like [1] [2]:

$$\{q_i, H\} = \dot{q}_i \;;\; \{p_i, H\} = \dot{p}_i \tag{9}$$

In order to solve specific physical problems, a coordinate system has to be specified. The choice of the coordinate system is important because an appropriated election produce what is called "cyclic coordinates" (coordinates that do not appear explicitly in the Hamiltonian) [1] [2]. The existence of these cyclic coordinates assures symmetries and conservation laws for the corresponding variables. Even when any coordinate system can be used to solve the problem, the election of a one who possess the largest number of cyclic coordinates, reduces

significantly the difficulty of finding the solution. The Hamilton-Jacobi method deals with this matter [1] [2].

It is possible to find a transformation between coordinate systems to obtain the adequate system to describe the problem. However, to find such transformation is not, generally, a simple task. From the large number of possible transformations, the canonical transformation deserves special attention because they leave invariant the Hamiltonian.

## 4. Lie Transformation and Lie Series

The Lie derivative of an analytical function f(q, p, t) associated with a Hamiltonian is defined as [6] [7]:

$$\mathrm{d}f/\mathrm{d}t = \{f, H\} \quad \text{and, in general} \quad \mathrm{d}^k f/\mathrm{d}t^k = \left\{\left\{\left\{\cdots k \text{ times} \cdots \{\{f, H\}\}\cdots\right\}\right\}\right\} \tag{10}$$

The function $f(\boldsymbol{q}, \boldsymbol{p}, t)$ can be expanded in a Taylor series around $t = 0$ to obtain:

$$f(\boldsymbol{q}, \boldsymbol{p}, t) = f(\boldsymbol{q}, \boldsymbol{p}, 0) + t\{f, H\}_{t=0} + \left(t^2/2!\right)\{\{f, H\}, H\} + \cdots \tag{11}$$

This expansion is usually called "Lie Series" of the function $f$. The $n^{\text{th}}$ order term contains the $n$ successive application, from the right, of the operator $\{\cdots, H\}$ which can be written as the operator to the $n^{\text{th}}$ power:

$$f(\boldsymbol{q}, \boldsymbol{p}, t) = \left[ f e^{t\{\cdot, H\}} \right]_{t=0} \tag{12}$$

Equation (13) is called Lie Transformation [7] [8]; this transformation is usually used in quantum and classic mechanics to describe the dynamics of physical systems.

## 5. Lie Algebra

The Lie Algebra (LA) is a non-commutative algebra where the product is defined as:

$$\{f, g\} \equiv \sum_{i=1}^{n} \left( (\partial f/\partial q_i)(\partial g/\partial p_i) - (\partial f/\partial p_i)(\partial g/\partial q_i) \right) \tag{13}$$

Let $f$, $g$, and $h$ three functions of $(q, p)$, then the following properties are fulfilled:

- Anti-symmetry: $\{g, h\} = -\{h, g\}$ and consequently $\{f, f\} = 0$
- Linearity: if $a$ and $b$ are constants, then $\{f, ag + bh\} = a\{f, g\} + b\{f, h\}$
- Product: $\{f, gh\} = \{f, h\}g + \{f, g\}h$
- Jacoby's Identity: $\{f, \{g, h\}\} = \{g, \{h, f\}\} = \{h, \{f, g\}\} = 0$

From this algebra, it is possible to show that there exists a sub-algebra called "Lie Differential Operator Algebra" defined as: $:f:g = \{f, g\}$. It is easy to show that this is a well-behaved algebra. The commutator between two operators is defined as the anti-symmetric operator: $[:f:, :g:] = :f::g: - :g::f:$

From this definition it is easy to prove that:

1) $[:f: + :g:, :h:] = [:f:, :h:] + [:g:, :h:]$

2) $[:f:,:g:+:h:]=[:f:,:g:]+[:f:,:h:]$

3) $a[:f:,:g:]=[a:f:,:h:]+[:f:,a:h:]$

4) $[:f:,:f:]=0$

5) $[:h:,[:f:,:g:]]+[:f:,[:g:,:h:]]+[:g:,[:h:,:f:]]=0$

The following theorem concerns to the well-behaved character of the LT [7]:

**Theorem**: Let two analytical functions $f$ and $g$ of ($q$, $p$), the function $G=G(\boldsymbol{q},\boldsymbol{p},t)$ can be written as $G=e^{(t:f:)}g=e^{(t\{f,\cdot\})}g$, where $G$ is a real analytical function of ($q$, $p$) when the parameter t is sufficiently small.

## 6. Lie Group

As it is known, a group is a set of elements that fulfill the following requirements [9]:

1) Let $a$ and $b$ two elements of the group, then $a\otimes b$ belongs to the group.

2) The multiplication $\otimes$ is associative: $(a\otimes b)\otimes c=a\otimes(b\otimes c)$.

3) The group contains the element identity e such that: $a\otimes e=e\otimes a$.

4) Each element a of the group has an inverse such that: $a\otimes a^{-1}=a^{-1}\otimes a=e$.

We shall restrict ourselves to continuous groups where the number of parameters is finite. Each of these parameters can vary continuously. Particularly, we are interested in the canonical transformation that forms a Lie Group.

$$Q_i=Q_i(\boldsymbol{q},\boldsymbol{p}),\quad P_i=P_i(\boldsymbol{q},\boldsymbol{p}) \tag{14}$$

In this particular case, this transformation connects two different coordinate systems of finite dimensionality. As known, the CT leaves invariant the Hamiltonian of the system, a fundamental requirement to leave unchanged the physical system. The CT can be written as a column vector of dimensionality $n$. The Lie group is isomorphic to a sub-group GL($n$, $R$).

## 7. Symplectic Group

The isomorphism between the Lie group and GL($n$, $R$) allows to characterize the CT by using the Symplectic Group (SG). The isomorphism between them allows to obtain a $2n$-dimensional matrix. In order to obtain this matrix it is necessary to define the following vectors:

$$\zeta=(P_1,\cdots,P_n,Q_1,\cdots,Q_n),\quad \eta=(p_1,\cdots,p_n,q_1,\cdots,q_n) \tag{15}$$

where $Q_i$ and $P_i$ are the end conditions, and $q_i$ and $p_i$ are the initial conditions.

With these definitions, the symplectic matrix can be written as [6] [7] [10] [11] [12] [13] [14]:

$$M_{ij}=\partial\zeta_i/\partial\eta_j \tag{16}$$

It is easy to prove that this matrix fulfills the symplectic conditions:

$$\boldsymbol{M}^t\boldsymbol{J}\boldsymbol{M}=\boldsymbol{J}\quad\text{where}\quad \boldsymbol{J}=\begin{bmatrix}0 & 1\\ -1 & 0\end{bmatrix} \tag{17}$$

where 1 and −1 are block matrices of $n\times n$ and the determinant of $M$ is:

$$\det(\boldsymbol{M}) = 1 \tag{18}$$

The infinitesimal transformation can be written as

$$\zeta = \eta + \delta\eta \tag{19}$$

and, after the substitution of the former equation, it is possible to obtain

$$M = 1 + \partial\delta\eta/\partial\eta \tag{20}$$

and applying the symplectic conditions it is possible to obtain the first order symplectic matrix.

## 8. Symplectic Maps Applied to Optical Systems

The transformation that takes from the initial condition to the end condition in phase space can be expressed formally as a Transference Map or Symplectic Map. In the same way that the Lie transformations are used in classical mechanics, these can be used in optical physics by using the following theorem [7]:

**Theorem** (Dragt-Finn): Let assume that $M$ is any simplectic map which maps the phase space into itself, *i.e.* if $h = 0$, then $z = 0$. In this case M can be factored as product of Lie transformations:

$$M = \cdots e^{:f4:} e^{:f3:} e^{:f2:} \tag{21}$$

where $f_n$ are polynomial homogeneous of $n$-degree in the variables ($q$, $p$). Furthermore, this map is symplectic for any set of polynomials. Additionally, if the product is cut at any stage of the expansion, the result is still a yimplectic map.

Each symplectic map whose existence is contemplated by the last theorem, can be used to represent optical systems. For example, lenses can be represented by Lie transformations whose exponent is polynomial of fourth-order [6] [11] [12] [13] [14].

The former definition of the symplectic matrix fulfills several properties [7] [12] [13]: suppose that $M$ is a transformation matrix, or a product of transformations, and be g a function in the phase space, then:

As a corollary of this result it can be demonstrated that for two functions in phase space f and g the following relationship is satisfied:

$$\boldsymbol{M}\left[f(\eta), g(\eta)\right] = \left[\boldsymbol{M}f(\eta)\right]\left[\boldsymbol{M}g(\eta)\right]$$

where $\boldsymbol{M}$ is isomorphic respect to the ordinary multiplication of functions. By using the former result, it is possible to show that $\boldsymbol{M}\{f, g\} = \{\boldsymbol{M}f, \boldsymbol{M}g\}$ which means that $\boldsymbol{M}$ is isomorphic respect to PB.

The following theorem relates the SM to LT [8]:

**Theorem:** If M is a LT associated with an analytical function $f$, then:

$$\zeta_i = \boldsymbol{M}\eta_i = e^{(:f:)}\eta_i \tag{22}$$

is a convergent series, *i.e.* a symplectic map.

The proof of the previous theorem is difficult because the convergence of the series in the general form has never been demonstrated, neither using symbolic programming nor numerical methods.

An optical system is generally symmetric around the optical axis (z axis). This means that the mapping must contain only polynomial of even order, *i.e.* no odds terms are allowed to be present in the polynomials, because these terms are related to an asymmetric behavior of the light beam around the optical axis. Then:

$$\boldsymbol{M} = \cdots e^{:f6:} e^{:f4:} e^{:f2:} \tag{23}$$

The first term from the right (where appears the 2nd-order polynomial) is the Lie transformation of the paraxial optics; the next term (corresponding to a 4th-order polynomial) is related to aberration and image deformation. High order terms are related to small corrections, produced by the optical system (lenses, apertures bandwidth cutoff, etc.), that have to be applied to the image to recover the object.

The order of the operators is arbitrary; this means that the same mapping can be stated in ascending order:

$$\boldsymbol{M} = e^{:f2:} e^{:f4:} e^{:f6:} \cdots \tag{24}$$

The election of the order of the operators in the symplectic matrix $\boldsymbol{M}$ (ascending or descending) changes the direction of the light beam [6] [7] [12]. From the mathematical point of view, to choose ascending or descending order in the polynomial is equivalent to transpose the symplectic matrix $\boldsymbol{M}$.

As an example of a symplectic map let us consider a light source who is emitting rays into a medium characterized by a constant refraction index. The symplectic matrix for a ray traveling in this medium from $z_i$ to $z_f$ is given by [6]:

$$M = e^{-\int_{z_i}^{z_f} :H^{opt}: \mathrm{d}z} = e^{l:\sqrt{n^2 - p^{i2}}} \tag{25}$$

where $H^{opt}$ is the Hamiltonian of the optical system, while $l$ is the difference $l = z_f - z_i$.

Expanding the Hamiltonian in a power series in $\boldsymbol{q}$ and $\boldsymbol{p}$ it is possible to obtain:

$$\begin{gathered} \left[:\sqrt{n^2 - p^{i2}}:\right]^m \boldsymbol{p}^i = 0 \ \ \therefore m = 1,2,3,\cdots \\ :\sqrt{n^2 - p^{i2}}: \boldsymbol{q}^i = \boldsymbol{p}^i \Big/ \sqrt{n^2 - p^{i2}} \\ \left[:\sqrt{n^2 - p^{i2}}:\right]^m \boldsymbol{q}^i = 0 \ \ \therefore m = 2,3,\cdots \end{gathered} \tag{26}$$

The last result is obtained by expanding the square root in a power series and retaining only the lower order terms corresponding to a small deviations respect to the optical axis.

Therefore:

$$\boldsymbol{p}^f = \boldsymbol{M}\boldsymbol{p}^i = \boldsymbol{p}^i, \ \ \boldsymbol{q}^f = \boldsymbol{M}\boldsymbol{q}^i = \boldsymbol{q}^i + l\boldsymbol{p}^i \Big/ \sqrt{n^2 - p^{i2}} \tag{27}$$

Expanding the Hamiltonian in a Taylor series, the symplectic map has the form (Equation (23)):

$$\boldsymbol{M} = \cdots e^{l1/16n^5\left[:\left(p^i\right)^2:\right]^3} e^{l1/8n^3\left[:\left(p^i\right)^2:\right]^2} e^{l1/2n\left[:\left(p^i\right)^2:\right]} \tag{28}$$

Retaining only the first exponential, the final coordinates and momentum have the form:

$$\boldsymbol{p}^f = e^{l1/2n\left[:\left(p^i\right)^2:\right]}\boldsymbol{p}^i, \quad \boldsymbol{q}^f = e^{l1/2n\left[:\left(p^i\right)^2:\right]}\boldsymbol{q}^i = \boldsymbol{q}^i + \left(1/n\right)\boldsymbol{p}^i \tag{29}$$

## 9. Frequency-Dependent Symplectic Map

We know that the Optical Hamiltonian is:

$$\boldsymbol{H} = -\sqrt{n\left(\boldsymbol{q}, z\right)^2 - \boldsymbol{p}^2} \tag{30}$$

If the medium only depends on the frequency, the refraction index is:

$$n = n\left(\omega\right) \tag{31}$$

Nevertheless, the refraction index depends on

$$n\left(\omega\right) = \sqrt{\epsilon\mu} \tag{32}$$

In the case that we have a isotropic and non-linear medium, we have modeled the electrical permittivity as:

$$\epsilon = a - \left(\omega_m/\omega\right)^2 + \left(\omega_m/\omega\right)^4 \tag{33}$$

We assumed that medium have a single resonance frequency. The "$a$" is a constant and "$\omega$" is the signal frequency. The refraction index behavior is:

$$n\left(\omega\right) = \sqrt{\mu\left(a - \left(\omega_m/\omega\right)^2 + \left(\omega_m/\omega\right)^4\right)} \tag{34}$$

since is constant we can obtain a new refraction index

$$n_\mu\left(\omega\right) = n\left(\omega\right)/\sqrt{\mu} = \sqrt{a - \left(\omega_m/\omega\right)^2 + \left(\omega_m/\omega\right)^4} \tag{35}$$

And the new Hamiltonian has the following form:

$$H = -\sqrt{a - \left(\omega_m/\omega\right)^2 + \left(\omega_m/\omega\right)^4 - \boldsymbol{p}^2} \tag{36}$$

With this Hamiltonian Equations (27) become:

$$\boldsymbol{p}^f = \boldsymbol{M}\boldsymbol{p}^i = \boldsymbol{p}^i, \quad \boldsymbol{q}^f = \boldsymbol{M}\boldsymbol{q}^i = \boldsymbol{q}^i + l\left(\boldsymbol{p}^i \Big/ \sqrt{a - \left(\omega_m/\omega\right)^2 + \left(\omega_m/\omega\right)^4 - \left(\boldsymbol{p}^i\right)^2}\right) \tag{37}$$

The coordinate presents a resonance when the medium frequency is equal to the signal frequency. In this frequency the ray has the maximum inclination with respect to the optical axis, that is, the $tg\left(\theta\right)$ is maximum is when $\omega = \omega_m$. When $\omega \ll 1$ we can expand the coordinate in a Taylor series:

$$\boldsymbol{q}^f - \boldsymbol{q}^i \cong \left(\omega^2/\omega_m^2\right) + \left(1/2\right)\left(\omega^4/\omega_m^4\right) \tag{38}$$

And if $\omega \gg 1$, the coordinate have the following form:

$$\boldsymbol{q}^f - \boldsymbol{q}^i \cong \left(1/\sqrt{n^2 - \left(p^i\right)^2}\right) + \left(1/2\right)\left(\omega_m^2 \Big/ \left(\left(n^2 - \left(p^i\right)^2\right)^{3/2}\omega^2\right)\right) \tag{39}$$

The most interesting case is when because, from of a certain frequency the

saturated medium behaves like vacuum (1st. term of the last series).

## 10. Conclusion

We have reviewed how a Lie transformation associated with an analytical function produces a Symplectic Map; this can be written as a product of Lie transformations. This formalism can be applied easily to complicated optical systems. The Lie group was used to construct the symplectic map which allows to obtain the equations that govern the behavior of a light beam passing through a system of thin lenses. When the medium is non-linear and isotropic and the signal depends on the frequency, this approach also allows to determine the ray propagation. In the case that the signal frequency is equal to the characteristic material frequency, the inclination angle is maxim: resonance point. By low signal frequency respect to material frequency, the inclination is quadratic; but by high signal frequency, the medium is saturated and its respond is the same, that it to say, it is like medium not depending to frequency with a refraction index equal one (vacuum).

## Acknowledgements

The technical help in formatting of Dr. Alejandro Castañeda-Miranda and Mr. Arturo Silva-Ordaz is gratefully acknowledged.

## Conflicts of Interest

The author declares no conflicts of interest regarding the publication of this paper.

## References

[1] Goldstein, H. (1996) Classical Mechanics. Second Edition, Editorial Reverte, Mexico City.

[2] Saletan, E.J. and Cromer, A.H. (1971) Theoretical Mechanics. Wiley, New York.

[3] Lopez Moreno, E. and Wolf, K.B. (1989) *Revista Mexicana de Física*, **35**, 291.

[4] Krotzsch, G. and Wolf, K.B. (1991) *Revista Mexicana de Física*, **37**, 540.

[5] Krotzsch, G. and Wolf, K.B. (1991) *Revista Mexicana de Física*, **37**, 136.

[6] Dragt, A.J., Forest, E. and Wolf, K.B. (1985) Foundations of a Lie Algebraic Theory of Geometrical Optics. In *Lectures Notes in Physics, Lie Methods in Optics*, Vol. 250, Spring-Verlag, Heidelberg, 105-157.

[7] Dragt, A.J. and Finn, J.M. (1976) *Journal Mathematical Physics*, **17**, 2215. https://doi.org/10.1063/1.522868

[8] Navarro Saad, M. (1985) Calculo de aberraciones en sistemas opticos con Teoria de Grupos. B.Sc. Thesis, UNAM, Mexico.

[9] Jacobson, N. (1979) Lie Algebras. Dover Publications, New York.

[10] Hamermesh, M. (1989) Group Theory and Its Applications to Physical Problems. Dover Publications, New York.

[11] Dragt, A. (1982) *Journal of the Optical Society of America*, **72**, 372. https://doi.org/10.1364/JOSA.72.000372

[12] Castaño, V.M. (2006) *International Journal of Mathematics, Game Theory, and Algebra*, **16**, 1-19.

[13] Reyes, J., Saenz, A., Silva, A. and Castaño, V.M. (1999) *Optik*, **110**, 527.

[14] Reyes, J. and Castaño, V.M. (2000) *Optik*, **111**, 219.

Scientific Research Publishing

Journal of Modern Physics, 2022, 13, 1324-1330
https://www.scirp.org/journal/jmp
ISSN Online: 2153-120X
ISSN Print: 2153-1196

# Single Charged Particle Motion in a Flat Surface with Static Electromagnetic Field and Quantum Hall Effect

**Gustavo V. López, Jorge A. Lizarraga**

Departamento de Física, Universidad de Guadalajara, Guadalajara, México
Email: gulopez@cencar.udg.mx, jorge.a.lizarraga.b@gmail.com

**How to cite this paper:** López, G.V. and Lizarraga, J.A. (2022) Single Charged Particle Motion in a Flat Surface with Static Electromagnetic Field and Quantum Hall Effect. *Journal of Modern Physics*, **13**, 1324-1330.
https://doi.org/10.4236/jmp.2022.1311081

**Received:** October 6, 2022
**Accepted:** November 1, 2022
**Published:** November 4, 2022



## Abstract

Taking into account the non separable solution for the quantum problem of the motion of a charged particle in a flat surface of lengths $L_x$ and $L_y$ with transversal static magnetic field $\boldsymbol{B}$ and longitudinal static electric field $\boldsymbol{E}$, the quantum current, the transverse (Hall) and longitudinal resistivities are calculated for the state $n=0$ and $j=0$. We found that the transverse resistivity is proportional to an integer number, due to the quantization of the magnetic flux, and longitudinal resistivity can be zero for times $t \gg L_x B/cE$. In addition, using a modified periodicity of the solution, a modified quantization of the magnetic flux is found which allows to have IQHE and FQHE of any filling factor of the form $\nu = k/l$, with $k, l \in \mathcal{Z}$.

## Keywords

Landau's Gauge, Quantum Hall Effect, Degeneration

## 1. Introduction

There are a lot of literature dealing with the phenomenon of Quantum Hall Effect [1]-[8], and most of them use the Landau's solution of the eigenvalue problem associated to the charged particle motion in a flat surface with static transversal magnetic field to the surface. This brings about the known Landau's levels for the energies and a separable variable solution for the eigenfunctions [9]. However, it has been shown that a non separable of variables solution exists for this problem with the same Landau's levels [10] [11], and these levels are numerable degenerated [12], determining the operators which causes this degeneration. In addition, the quantization of the magnetic flux appears naturally [10],

$$\frac{m\omega_c}{\hbar}A = 2\pi l, \quad l \in \mathcal{Z}, \quad \omega_c = \frac{qB}{mc}, \tag{1}$$

where $m$ is the mass of the charge $q$, $c$ is the speed of light, $\omega_c$ is the so called cyclotron frequency, $B$ is the magnitude of the static magnetic field, $A = L_x L_y$ is the area of the sample, and $2\pi\hbar = h$ is the Planck's constant. As we mentioned before, Landau's separable solution is normally used to try to explain the so called Integer Quantum and Fractional Quantum Hall Effects (IQHE and FQHE) [4] [5] [6] [7], which were first discovered experimentally [1] [2] [3]. The IQHE is normally explained as a single particle phenomenon; meanwhile, the FQHE is explained as a many particle event [4] [5] [6]. Experimentally, both of them occur in highly impure samples, where these impurities have the effect of extending the range of magnetic field intensity where the resistivity is quantized [2] [3] [7]. The main characteristic of the IQHE or FQHE is the resistivity (or voltage) which appears on the transverse motion of the charges, so called Hall's resistivity $\rho_H$. This Hall's resistivity acquires a constant value on certain regions of the magnetic field, and within these regions, the longitudinal resistivity is zero. The values of these constant $\rho_H$ turn out to be inverse to an integer number (IQHE) or proportional to an integer number (FQHE) multiplied by the constant $h/q^2$, called von Klitzing constant [2] [3] ($h/q^2 \approx 25812.80745\,\Omega$). In this paper, we calculate the quantum current and the expected value of the transverse and longitudinal resistivities for a single charged particle motion on a flat surface using the non separable solution in the lowest Landau level ($n = 0$) and using the first wave function ($j = 0$).

## 2. Quantum Current

The Hamiltonian associated to the motion of a charge particle $q$ with mass $m$ on a flat surface of lengths $L_x$ and $L_y$ with transverse magnetic field $\boldsymbol{B} = (0,0,B)$ and longitudinal electric field $\boldsymbol{E} = (0,E,0)$ is given by

$$\hat{H} = \frac{1}{2m}\left(\boldsymbol{p} - \frac{q}{c}\boldsymbol{A}\right)^2 + qV, \tag{2}$$

where $\boldsymbol{A}$ is the vector potential, $\boldsymbol{B} = \nabla \times \boldsymbol{A}$, and $V$ is the scalar potential, $\boldsymbol{E} = -\nabla V$. The Schrödinger's equation,

$$i\hbar\frac{\partial\Psi}{\partial t} = \hat{H}\Psi, \tag{3}$$

can be written, using the operator $\boldsymbol{p} = -i\hbar\nabla$, as

$$i\hbar\frac{\partial\Psi}{\partial t} = \frac{1}{2m}\left[-\hbar^2\nabla^2 + i\frac{\hbar q}{c}\left(\nabla\cdot\boldsymbol{A} + \boldsymbol{A}\cdot\nabla\right) + \frac{q^2A^2}{c^2}\right]\Psi + qV\Psi. \tag{4}$$

Taking the usual complex conjugated to this expression, a similar equation is gotten for the function $\Psi^*$. Multiplying this one by $\Psi$, (4) by $\Psi^*$ and subtracting both, the following continuity equation is obtained

$$\frac{\partial \rho}{\partial t} + \nabla \cdot \boldsymbol{J} = 0, \tag{5}$$

where $\rho$ and $\boldsymbol{J}$ are defined as

$$\rho = \Psi \cdot \Psi^* \tag{6}$$

and

$$\boldsymbol{J} = \frac{i\hbar}{2m}\left(\Psi \nabla \Psi^* - \Psi^* \nabla \Psi\right) - \frac{q}{mc}\rho \boldsymbol{A}. \tag{7}$$

Since $\Psi$ is a scalar complex function, it can be written as $\Psi = |\Psi| e^{i\theta}$, where $|\Psi|$ and $\theta$ are real functions, and $\theta$ is the argument of the function. Then, the current is given by

$$\boldsymbol{J} = \left(\frac{\hbar}{m}\nabla\theta - \frac{q}{mc}\boldsymbol{A}\right)|\Psi|^2. \tag{8}$$

For the general solution of (3), the function $\theta$ can be very complicated expression of all variables. However, for a particular state solution of the system, say

$$\psi_n(\boldsymbol{x}, t) = e^{i\phi_n(x,t)} f_n(\boldsymbol{x}), \tag{9}$$

the argument is just $\theta = \phi_n(\boldsymbol{x}, t)$, and the current associated to this state of the system is given by

$$\boldsymbol{J}_n = \left(\frac{\hbar}{m}\nabla\phi_n - \frac{q}{mc}\boldsymbol{A}\right)|f_n|^2. \tag{10}$$

## 3. Single Charged Particle Current

The non separable solution of (3) using the Landau's gauge $\boldsymbol{A} = B(-y, 0, 0)$ and the longitudinal constant electric field $\boldsymbol{E} = (0, E, 0)$ was given as

$$f_n^0 = \frac{1}{\sqrt{2^n n! L_y}}\left(\frac{m\omega_c}{\pi\hbar}\right)^{1/4} e^{i\phi_n} e^{-\frac{m\omega_c}{2\hbar}(x - c\mathcal{E}t/B)^2} H_n\left(\sqrt{\frac{m\omega_c}{\hbar}}(x - c\mathcal{E}t/B)\right), \tag{11a}$$

where $\mathcal{E} = qE$, $\omega_c$ is the cyclotron frequency (1), and $\phi_n$ is given by

$$\phi_n = -\left[\hbar\omega_c\left(n + \frac{1}{2}\right) - \frac{mc^2\mathcal{E}}{2B^2}\right]\frac{t}{\hbar} - \frac{m\omega_c}{\hbar}\left(x - \frac{c\mathcal{E}t}{B}\right)\left(y - \frac{mc^2\mathcal{E}}{qB^2}\right). \tag{11b}$$

These functions are degenerated in the sense that for each Landau's level ($\hbar\omega_c(n + 1/2)$), one has a numerable solutions $f_n^j = (\hat{p}_x)^j f_n^0$, $j \in Z$. Thus, the expressions (11a) define the state of the system. Using this function $\phi_n$ in (10) and for the index of degeneration $j = 0$, we have

$$\boldsymbol{J}_n = \left[\frac{cE}{B}\hat{\boldsymbol{i}} - \omega_c\left(x - \frac{c\mathcal{E}t}{B}\right)\hat{\boldsymbol{j}}\right]\left|f_n^0\right|^2. \tag{12}$$

In particular, for the ground state of Landau's energy, it follows that the components of the current are

$$J_0^x = \frac{c\mathcal{E}}{B}\left|f_0^0\right|^2, \tag{13}$$

and

$$J_0^y = -\omega_c\left(x - \frac{c\mathcal{E}t}{B}\right)\left|f_0^0\right|^2. \tag{14}$$

The electric conductivity along the x-axis is called Hall's conductivity and is given by

$$\sigma_H = \frac{q}{\mathcal{E}}J_0^x = \frac{qc}{B}\left|f_0^0\right|^2. \tag{15}$$

Thus, the Hall's resistivity is $\rho_H = 1/\sigma_H$, and the expected value of the resistivity in the state $f_0^0$ is

$$\left\langle f_0^0 \middle| \rho_H \middle| f_0^0 \right\rangle = \int_0^{L_x}\int_0^{L_y}\frac{\left|f_0^0\right|^2}{\sigma_H}\mathrm{d}x\mathrm{d}y = \frac{BA}{qc}. \tag{16}$$

Now, multiplying and dividing this quantity by $m\omega_c/\hbar$ and making some rearrangements, one gets

$$\left\langle f_0^0 \middle| \rho_H \middle| f_0^0 \right\rangle = \frac{\hbar}{q^2}\left(\frac{m\omega_c}{\hbar}A\right), \tag{17}$$

and taking into consideration the magnetic field flux quantization (1), it follows that

$$\left\langle f_0^0 \middle| \rho_H \middle| f_0^0 \right\rangle = \frac{h}{q^2}l, \quad l \in \mathcal{Z}. \tag{18}$$

The expected value in the state $f_0^0$ of the longitudinal resistivity $\rho_y$ is

$$\left\langle f_0^0 \middle| \rho_y \middle| f_0^0 \right\rangle = \int_0^{L_x}\int_0^{L_y}\frac{\left|f_0^0\right|^2\mathrm{d}x\mathrm{d}y}{\sigma_y} = \frac{\mathcal{E}}{q}\int_0^{L_x}\int_0^{L_y}\frac{\left|f_0^0\right|^2\mathrm{d}x\mathrm{d}y}{J_0^y} \tag{19}$$

$$= -\frac{\mathcal{E}}{q\omega_c}\int_0^{L_x}\int_0^{L_y}\frac{\mathrm{d}x\mathrm{d}y}{x - \frac{cEt}{B}} = -\frac{\mathcal{E}L_y}{q\omega_c}\ln\left(1 - \frac{L_xB}{c\mathcal{E}t}\right) \approx 0 \tag{20}$$

since one has normally in the experiments that $L_xB/c\mathcal{E}t \ll 1$, that is, the time in the experiments are such that

$$t \gg \frac{L_xB}{c\mathcal{E}}. \tag{21}$$

For example, on the reference [2] and with respect the voltage gate $V_g$, one has that $BL_x/c\mathcal{E} = BA/cV_g \sim 4.5\times10^{-8}$ sec. So, the condition (21) is well satisfied in this experiment.

Note that the expression (18) implies a filling factor $\nu = 1/l$, which correspond to the IQHE phenomenon for $l = 1$ and to the FQHE phenomenon for $l > 1$. However, this result is valid for an analysis of a single charged particle, and both QHE phenomena appear due to the quantization of the magnetic flux (1). In addition, one must note that this analysis is still valid for any $n > 0$ and $j = 0$.

## 4. Full IQHE and FQHE

The quantization of the magnetic flux (1) arises from the periodicity of the solutions of the Hamiltonian [10], which can be expressed using (11a) for $\mathcal{E}=0$ as

$$f_n^0\left(L_x, y+L_y, t\right)=f_n^0\left(L_x, y, t\right). \tag{22}$$

However (and also for $\mathcal{E}=0$), let us assume that $L_y=Nl_y$ where $l_y \ll L_y$ and $N\in\mathcal{Z}^+$, that is, the total area $L_xL_y$ is covered with slices of area $L_xl_y$, with horizontal length $L_x$ and width $l_y$. Let us impose the periodicity condition of the form

$$f_n^0\left(L_x, y+kl_y, t\right)=f_n^0\left(L_x, y, t\right), \quad k\in\mathcal{Z}, \tag{23}$$

such that with the phase (11b), one gets

$$\frac{m\omega_c}{\hbar}L_xkl_y=2\pi l, \quad l\in\mathcal{Z} \tag{24}$$

which brings about the relation

$$\frac{m\omega_c}{\hbar}a=2\pi\frac{l}{k}, \quad \text{with } a=L_xl_y. \tag{25}$$

Using (1) and making some rearrangements, the magnetic field can be given by

$$B=\alpha\frac{l}{k}, \quad \text{with } \alpha=\frac{hc}{qa} \tag{26}$$

and using (25) in (17), the expected value of the Hall resistivity would be

$$\left\langle f_0^0\middle|\rho_H\middle|f_0^0\right\rangle=\frac{h}{q^2}\frac{l}{k}, \quad k,l\in\mathcal{Z}, \tag{27}$$

implying now a filling factor of $\nu=k/l$, which represents the full IQHE (for $l=1$) and FQHE (for $l>1$). To determine the magnetic values $B$ where these phenomena occur, one looks for the value $B_0$ where the first IQHE ($l=k=1$) appears, which intersect the normal linear dependence behavior straight line, and this defines $\alpha=B_0$. Then, one uses the resulting expression

$$B=B_0\frac{l}{k} \tag{28}$$

to find the other quantized magnetic fields which correspond to IQHE or FQHE. For example, on the experimental data shown on the reference [3], one sees that $B_0\approx 5\text{ T}$ for $l=k=1$ (corresponding to an area $a\approx 8.27\times10^{-4}\ \mu\text{m}^2$), and the other FQHE are matched quite well for $l=3$ and $k=1$, that is $B\approx 15\text{ T}$. Another example is shown on the reference [8] page 886, one sees that $B_0\approx 9.8\text{ T}$ for $l=k=1$ (corresponding to an area $a\approx 4.22\times10^{-4}\ \mu\text{m}^2$), and the other IQHE and FQHE magnetic fields are matched quite well for $l>1$ and $k>1$. In addition, on reference [13] page 207, one sees that $B_0\approx 4.2\text{ T}$ for $l=k=1$ (corresponding to an area $a=9.85\times10^{-4}\ \mu\text{m}^2$), and the other IQHE and FQHE magnetic fields are matched quite well for $l>1$ and $k>1$. Finally, on reference [14] page 156801-2, one sees that $B_0\approx 5.3\text{ T}$ for $l=k=1$ (correspond-

ing to an area $a = 7.8\times10^{-4}\ \mu m^2$), and for the filling factor $\nu = 3/4$ one gets $B = 4B_0/3 = 7.06$ T, which is approximately the experimental value reported.

## 5. Conclusion

Using the known non-separable solution for the quantum motion of a charged particle in a flat surface with static fields, in the state $n = 0$ and $j = 0$, the Hall and the longitudinal resistivities were calculated. For the quantization of the magnetic flux, which can appear from the simple periodicity on the y-direction, the results bring about the IQHE and FQHE phenomena since from the expression (18) it appears a filling factor of $1/l$ for a single charged particle due to the quantization of the magnetic flux. If $l = 1$, one gets the IQHE phenomenon, and if $l > 1$, one gets the FQHE phenomenon. However, it is not possible to say anything about filling factors of the form $\nu = k/l$. For a more extended quantization of the magnetic flux (25), which appears of the extended periodicity (23), one gets also IQHE and FQHE but with a filling factor of $\nu = k/l$.

## Conflicts of Interest

The authors declare no conflicts of interest regarding the publication of this paper.

## References

[1] Wakabayashi, J.I. and Kawaji, S. (1978) *Journal of the Physical Society of Japan*, **44**, 1839-1849. https://doi.org/10.1143/JPSJ.44.1839

[2] Klitzing, K.V., Dorda, G. and Pepper, M. (1980) *Physical Review Letters*, **45**, 494-497. https://doi.org/10.1103/PhysRevLett.45.494

[3] Tsui, D.C., Stormer, H.L. and Gossard, A.C. (1982) *Physical Review Letters*, **48**, 1559-1562. https://doi.org/10.1103/PhysRevLett.48.1559

[4] Laughlin, R.B. (1981) *Physical Review B*, **23**, 5632-5633. https://doi.org/10.1103/PhysRevB.23.5632

[5] Laughlin, R.B. (1983) *Physical Review B*, **27**, 3383-3389. https://doi.org/10.1103/PhysRevB.27.3383

[6] Laughlin, R. B. (1983) *Physical Review Letters*, **50**, 1395-1398. https://doi.org/10.1103/PhysRevLett.50.1395

[7] Prange, R.E. (1981) *Physical Review B*, **23**, 4802-4805. https://doi.org/10.1103/PhysRevB.23.4802

[8] Stormer, H.L. (1999) *Reviews of Modern Physics*, **71**, 875-889. https://doi.org/10.1103/RevModPhys.71.875

[9] Landau, L.D. and Lifshitz, E.M. (2013) Quantum Mechanics: Non-Relativistic Theory. Volume 3, Elsevier, Amsterdam.

[10] López, G.V. and Lizarraga, J.A. (2020) *Journal of Modern Physics*, **11**, 1731-1742. https://doi.org/10.4236/jmp.2020.1110106

[11] López, G.V., Lizarraga, J.A. and Bravo, O.J.P. (2021) *Journal of Modern Physics*, **12**, 1464-1474. https://doi.org/10.4236/jmp.2021.1210088

[12] Lizarraga, J.A. and López, G.V. (2022) *Journal of Modern Physics*, **13**, 122-126.

https://doi.org/10.4236/jmp.2022.132010

[13] Stern, A. (2007) *Annals of Physics*, **232**, 204-249. https://doi.org/10.1016/j.aop.2007.10.008

[14] Wang, C., *et al.* (2022) *Physical Review Letters*, **129**, Article ID: 156801. https://doi.org/10.1103/PhysRevLett.129.156801

Journal of Modern Physics, 2022, 13, 1331-1340
https://www.scirp.org/journal/jmp
ISSN Online: 2153-120X
ISSN Print: 2153-1196

# Possible Neutrino-Antineutrino Production during Gamma Ray e−e+ Pair Production: Monte Carlo Simulation Study

**Michael Bettan[1,2], Jonathan Walg[1], Itzhak Orion[1*]**

[1]Department of Nuclear Engineering, Ben-Gurion University of the Negev, Beer-Sheva, Israel
[2]Soreq NRC, Yavne, Israel
Email: *iorion@bgu.ac.il

**How to cite this paper:** Bettan, M., Walg, J. and Orion, I. (2022) Possible Neutrino-Antineutrino Production during Gamma Ray e−e+ Pair Production: Monte Carlo Simulation Study. *Journal of Modern Physics*, **13**, 1331-1340.
https://doi.org/10.4236/jmp.2022.1311082

**Received:** October 6, 2022
**Accepted:** November 1, 2022
**Published:** November 4, 2022



## Abstract

An alternative Feynman diagram for electron-positron pair production, in which neutrino and antineutrino are also produced on the same pathway, is introduced here. In the proposed pair production process, a portion of the momentum is carried by neutrinos and antineutrinos, allowing the rest of the momentum for the electron-positron pair. Simulations to inspect the proposed pair production process were conducted in this research using the EGS5 code system while modifying its subroutine "PAIR". Liquid Xenon detector was then positioned in the path of various mono-energetic photon beams ranging from 2.6 to 12 MeV. These simulations were intended to inspect the detectability of the alternative pair production effects on radiation measurements in order to assess the detection conditions. Simulation results provided a comparison between the original pair production process and the proposed pair production process. Spectral results showed that changes in the region around 1 - 2 MeV and in the photopeak region were remarkable, therefore detectable. Further experimental research is recommended based on simulation findings. The alternative pair production process, firstly introduced in this paper, led to production of a larger flux of neutrinos from gamma radiation. This additional neutrino production and its contribution to non-baryonic dark matter are discussed.

## Keywords

Gamma, Pair-Production, Radiation, Neutrino, Dark-Matter

## 1. Introduction

### 1.1. The Neutrino Emission Prediction

When beta decay was first discovered, the process showed a continuous spec-

trum of the emitted electron from the nucleus. This continuous spectrum meant that some of the emitted electrons carry only part of the energy. Since energy must be conserved, the question arose: what happened to the missing energy? This continuous spectrum led to the assumption by Pauly of a new, small elementary particle emitted in the beta decay, the Neutrino [1]. The theoretically predicted Neutrino, a half-spin, zero-electric charge, and low mass elementary particle which carries energy and momentum interacts with the nuclear fields [2]. Later, the beta emission probabilities were formulated by the Fermi golden rules for beta decay.

### 1.2. Matter and Anti-Matter

In the wake of quantum theory development, P. Dirac established an equation to introduce relativistic Hamiltonian that includes the spin-1/2 property of particles. Solutions for this Dirac equation predicted that each elementary particle should have an anti-matter companion. Anti-matter particle has the same mass, an opposite electric charge, and opposite magnetic moment direction [3]. Hence, the counterpart of an electron is a positron. C. D. Anderson first detected in 1932 the anti-electron in cosmic rays, subsequently confirming the Dirac prediction of existence of anti-matter [4].

### 1.3. Rules for e−e+ Production

Photons transported through matter have the probability to produce pairs of matter-antimatter, such as e−e+, if two conditions are fulfilled: 1) photon energy is above a threshold dictated by the rest mass of the pair of particles, and 2) the presence of an electromagnetic field within the photon path. Thus, pair production cross section is linearly dependent on the atomic Z-number for atomic electron field interactions, as well as dependent on the square of Z for nuclear field interactions [5]. The theory of photon bound-free pair production has been gradually developed since the 1930s, while calculations of e−e+ cross sections for a vast range of photon energies and for various materials began accumulating during the 1960s. Full historical progress and references for the development of pair production theory and calculations are presented in detail in Reference [6]. Recently more detailed cross-section dependence on the target nucleus's magnetic field compared to the nucleus's electric field was investigated [7]. Several Monte Carlo code systems have been implemented for photon transport at energies of 1 keV up to 100 GeV after accomplishing numerical cross sections for photon interactions, including pair production. The most well-known Monte Carlo code system is the MCNP; first released in 1977, this initial version did not include the electron transport process [8]. Released in 1982 the MC tool kit GEANT-3 enabled full photon-electron transport; after 2000, this version was replaced by the upgraded GEANT4 code system [9]. EGS (Electron Gamma Shower) is one of the leading code systems for simulating high-energy gamma ray interactions in matter. Although the EGS3 version released in 1978 was designed to simulate

electromagnetic cascade for high physics experiments, simulation of pair production that can take place only by gammas with energies above 1.02 MeV and that becomes significant at energies above 2.5 MeV, was first introduced in the conversion of EGS3 to EGS4 in 1985 [10]. Each of these code systems was gradually upgraded, mostly by modifying cross section libraries. Approximately twenty years later, a tremendous change was made to every code that included modifications in transport handling.

### 1.4. Neutrino as a Dark Matter (Puzzle)

Dark matter is a cosmological term that expresses missing mass in the Universe due to the observed large-scale expansion rate, or the Hubble constant [11]. Current gravitational modeling indicates that whereas a great amount of the mass in the Universe influences Universe dynamics, it is not detectable by common observational methods [12]. Several theoretical proposals based on the Standard Model (SM) of particle physics (or beyond SM) explain this dark matter phenomenon; in these proposals hidden non-baryonic particle content is presumed. A review paper by G. Bertone, D. Hooper, and J. Silk introduces the particle dark matter candidates' properties and their detectability [13]. SM particle as the neutrino (or antineutrino) is likely to be a candidate for non-baryonic dark matter because of its low interaction probability due to its sub-electron Volt rest-mass [14], as well as its neutral electric charge, and minuscule absorption cross section. A detailed discussion by Kreisch *et al.* regarding neutrinos as dark matter was later published as "Neutrino puzzle: Anomalies, interactions, and cosmological tensions". In Reference [15], the known processes that produce neutrino flux in the galaxy are estimated to contribute a mass which is too small compared to the estimated total dark matter density [16]. This estimation of neutrino contribution to dark matter might be altered with the development of more highly efficient neutrino telescopes, or by discovering new neutrino emission processes.

## 2. Methods

In **Figure 1**, the Feynman diagram for pair production (PP) is shown. In this study we introduce an alternative Feynman diagram for pair production in which neutrinos and antineutrinos are also produced via the same pathway (**Figure 2(a)** and **Figure 2(b)**). In this case, neutrinos and antineutrinos should escape with a certain amount of the total momentum and energy, while conserving momentum and energy. Accordingly, we prepared a setup to simulate and track the response to this proposed change in the pair production process via the electron and positron contribution to an Xe detector. Liquid Xe detectors are state-of-the-art scintillation systems for radiation and particle tracking that could suit the PP interaction detection outcome [17] [18].

Significant improvements to the pair production subroutine that could better simulate the process using higher energy gamma rays were introduced only in

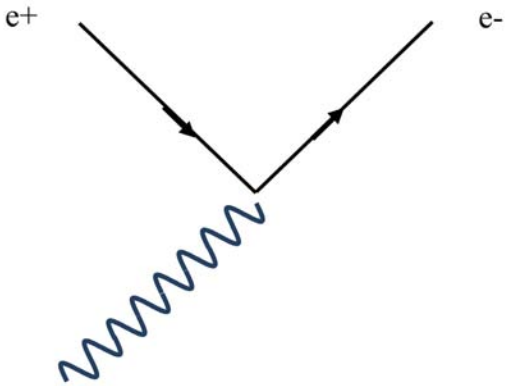


**Figure 1.** Feynman diagram of electron-positron pair production.

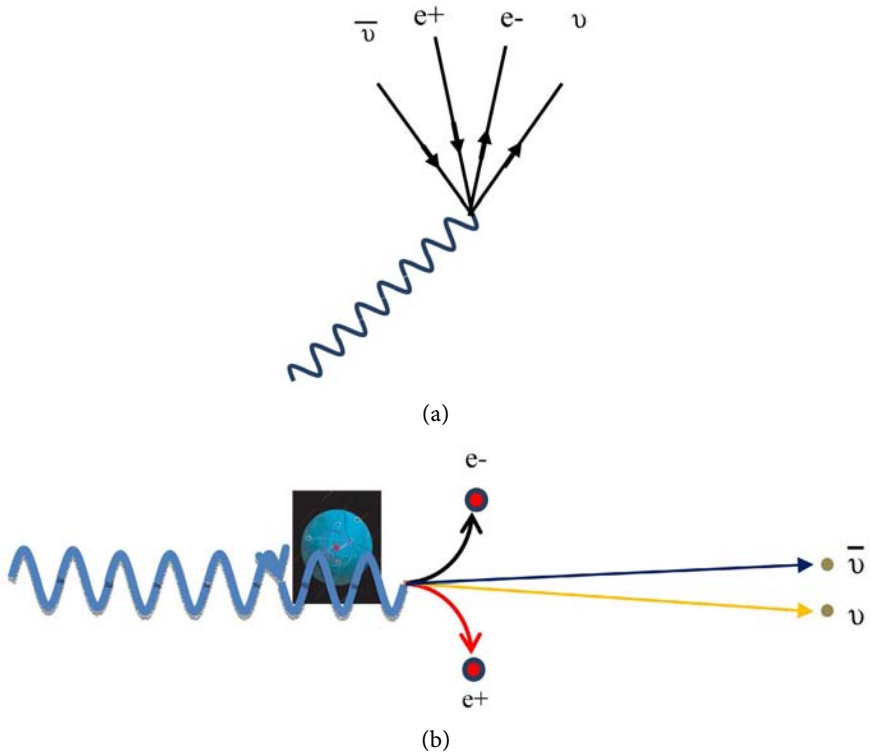


**Figure 2.** (a) Feynman diagram of electron-positron with neutrino-antineutrino pair production; (b) Illustration of proposed pair production process.

EGS5 [19]. Based on these improvements EGS5 calculations were used for the current study, with its geometry designed using CGVIEW, a program contained in the EGS5 code package, to describe a gamma ray beam passing through a Xenon detector (see **Figure 3**). The detector dimensions are 50 × 50 × 0.1 cm inside a 75 cm-diameter air sphere surrounded by vacuum. The detector is made of a liquid Xenon slab 1 mm thick sandwiched between two 5 cm-thick slabs of air. The beam location is on the X axis at coordinates (−60 cm, 0, 0) directed in the positive X direction. Since pair production in EGS5 is dependent on gamma energy, calculation was executed for various gamma ray beam energies suitable for future experiments.

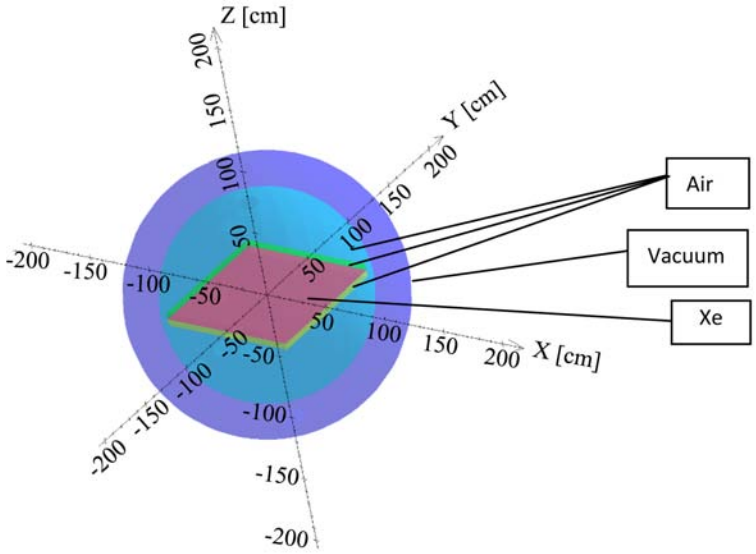


**Figure 3.** Simulation setup geometry and materials. The detector dimensions are 50 × 50 × 0.1 cm inside a 75 cm-diameter air sphere surrounded by vacuum.

In the "pair" subroutine of EGS5 ("egs5_pair.f") various energy ranges mark a difference in the way photon interaction is modeled. These energy edges are 2.1, 4.14, and 50 MeV; photons with energies within ranges between these energy levels are treated differently.

The energy carried out by the neutrino was simulated by making a change in two lines in the PAIR Subroutine, where the variables "theta" and "tteig" are calculated as follows:

$$\text{theta} = \text{RM}/(\text{eig}) \tag{1}$$

$$\text{tteig} = (\text{eig})/\text{RM} \quad \text{for} \quad \text{Eg} \geq 4.14 \ \text{MeV} \tag{2}$$

where,

RM = electron rest mass energy; and

eig = incident photon energy.

Theta is the polar angle of the outgoing electron, which correlates to the momentum conservation of the process. Therefore, the parameter "tteig" was calculated for the Motz-Olsen-Koch distribution that includes recoil energy and momentum [20]. The Motz-Olsen-Koch theoretical PP approach was implemented in EGS5 for gamma ray energy above 4.14 MeV.

In order to simulate the part of the photon energy that is carried out by the neutrino in the modified lines of the pair subroutine, for each gamma ray beam energy the variable "eig" was multiplied by 25% and 50%, meaning that the remainder of the energy was carried out by the neutrino-antineutrino.

## 3. Results and Discussion

We used a mono-energy gamma ray pencil beam source of 2.6 MeV, 4.5 MeV, 10 MeV, and 12 MeV to score the total deposited energy to the Xe detector for each case. Simulations were conducted using two different types of processes:

1) Original pair production process

2) Modified pair production process—a percentage of the momentum was transferred to the neutrino and the antineutrino, and was consequently reduced from the e−e+ pair.

We first simulated the system with its original condition, and then with modified pair production (PP), thereby showing that a percentage of momentum escaped with the neutrinos. Results of the absorption for 1E+07 histories are listed in Table 1 for each energy beam. A statistical error of about 0.15% was obtained for these results. The columns containing the scores for plain PP were compared to a case in which 50% of the momentum was carried by e+e−, and to a case in which 25% of the momentum was carried by e+e−. The neutrinos were not transported since the simulation does not have the capacity to track them, therefore were assumed to have escaped from the system without interactions.

Ratios presented in Table 1 reveal changes of less than 2% in detector response; hence, it would be very challenging to indicate whether or not neutrinos were created during the interaction.

In order to manifest resolution properties of the detector in the simulated liquid Xenon detector volume, two types of results were scored: a. spectral energy deposited in the Xenon detector; and b. the amount of energy transferred to produced positrons during a pair production occurrence. For each original run we changed the amount of momentum transferred to the e−e+ pair, a momentum deficit that was transferred to the hypothetical produced neutrino-antineutrino pair.

For photon energy below 4.14 MeV we simulated a gamma ray beam of 2.6 MeV, high enough above the PP energy threshold to produce a pair of e−e+. In Figure 4 spectrum ratios deposited in Xe by the 2.6 MeV beam are shown. Both calculated ratios introduce a relatively small difference of less than 3%, which would be barely detectable. Resulting events of energy transfer by produced positrons after pair production by 2.6 MeV beam are presented in Figure 5. In addition, n these counts, differences between each scenario events are hardly detectable along the detector depth.

In Figure 6, deposited spectra ratios of four incident photon energies in Xe are shown. The 50% ratios showed detectable anomalies below the photopeak energy. (For 5.0 MeV was not obtained.) The 25% ratios evinced a vast peak between 0.5 to 2.0 MeV, while for the 50% ratios that peak was barely detectable. These peaks' maxima varied from 4% to 10% depending on the beam's energy; therefore, we reckon that analysis of that region of the spectrum could reveal the proposed PP process. Even the anomalies around the photopeak are rather large, their detectability could be uncertain since multiple Compton scattering could interfere in that spectral region.

Events of energy transferred to produced positrons after pair production for 4.5 - 12 MeV beams are presented in Figure 7. The statistical error of these event values does not exceed 0.8%. The compared events for each model are presented in Figure 7; the changes are, for the most part, assumed as detectable in all cases.

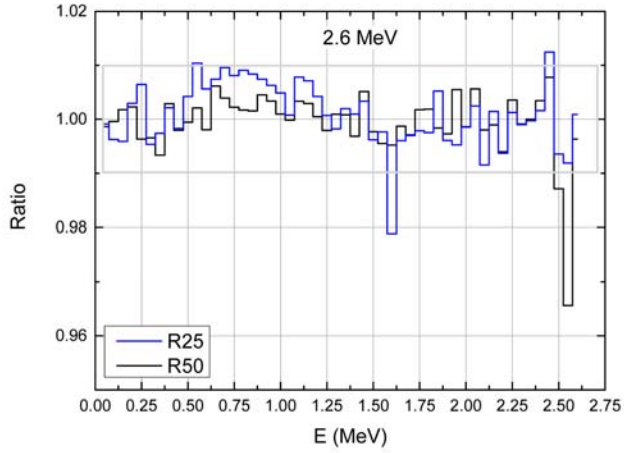


**Figure 4.** Spectral results of Xe response ratios of proposed to original pair production using 2.6 MeV photons. R25 - 25% of the total energy is transferred to e+e− while R50 - 50% of the total energy is transferred to e+e−.

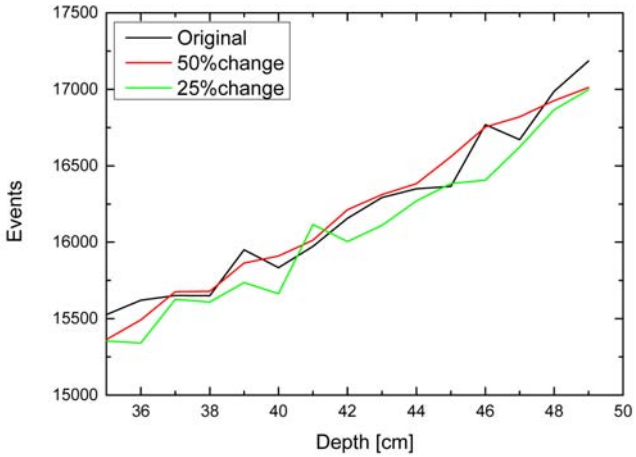


**Figure 5.** Photon beam of 2.6 MeV. Comparison of number of events resulting from produced positrons after pair production in the Xe. Original PP; 50% of the total energy transferred to e+e− while 25% of the total energy transferred to e+e−.

**Table 1.** Absorbed energy within the Xe detector as a result of 107 incident photons for these three cases: original PP process (without neutrino production); 50% of the PP energy transferred to electrons and positrons; and 25% of the PP energy transferred to electrons and positrons. Ratios obtained by normalizing the modified to the original process absorbed energy.

| Ebeam (MeV) | Plain PP | | 50% Energy to e+e− | | 25% Energy to e+e− | |
|---|---|---|---|---|---|---|
| | Absorbed (MeV) | Ratio | Absorbed (MeV) | Ratio | Absorbed (MeV) | Ratio |
| 2.6 | 11,679,138 | 1 | 11,678,047 | 0.9999 | 11,661,676 | 0.9985 |
| 4.5 | 16,874,336 | 1 | 16,827,416 | 0.9972 | 16,672,792 | 0.9881 |
| 10 | 26,739,942 | 1 | 26,638,851 | 0.9962 | 26,280,160 | 0.9828 |
| 12 | 29,802,801 | 1 | 29,703,683 | 0.9967 | 29,305,896 | 0.9833 |

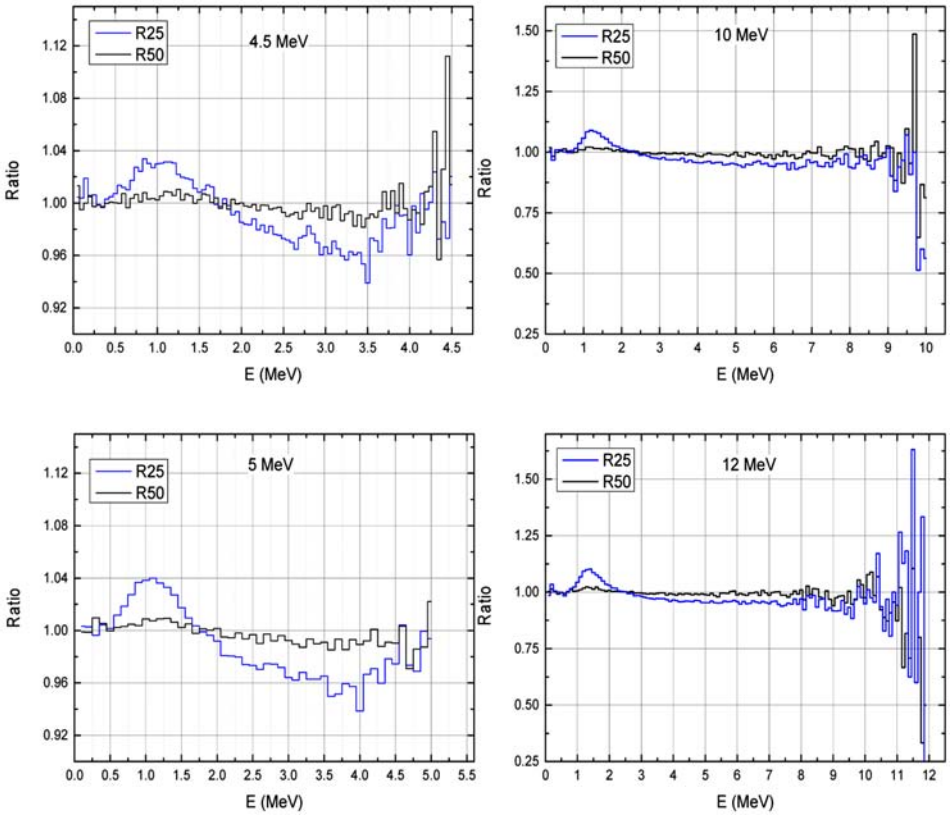


**Figure 6.** Spectral results of Xe response ratios of proposed to original pair production by photon beams of 4.5, 5, 10, and 12 MeV. R25 - 25% of the total energy is transferred to e+e−; while R50 - 50% of the total energy is transferred to e+e−.

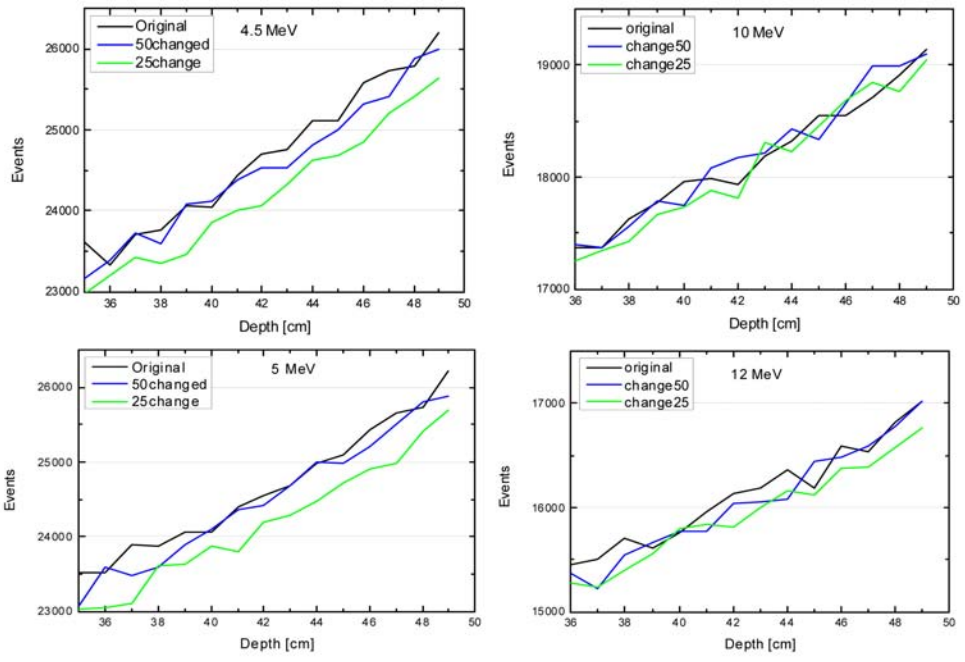


**Figure 7.** Photon beams of 4.5, 5, 10, and 12 MeV. Comparison of number of events from produced positrons after pair production. original PP; 50% of the total energy transferred to e+e−; while 25% of the total energy transferred to e+e−.

The new PP process presented in **Figure 2** that includes neutrinos, as might occur in reality, should also introduce a distribution of energy-momentum transfer to outgoing particles. Therefore, the percentage energy transfer to e+e− and to u, anti-u should be treated using a probability function. However, such process distribution rules are yet unknown, and require further exploration.

## 4. Conclusions

In the current study, the EGS5 Monte Carlo system was chosen to simulate a modified PP process that includes neutrino-antineutrino pair production. However, several other Monte Carlo codes also include PP interaction, electrons, and positrons transport. Comparing PP simulations using different Monte Carlo codes has been studied and reported [21], and their EGS5 results (marked as *EGS2*) plotted versus other much known codes. The same changes made for this study are applicable to these other codes (e.g., GEANT4), although factors extracted from published plot could spare one the effort.

The results in this paper indicate that a PP that includes neutrinos is detectable in cases in which the escaped neutrinos extract some fraction of the total momentum. The question is whether or not the PP process includes neutrino and antineutrino production, and it is recommended that this be experimentally studied.

Current estimates of neutrino flux in the galaxy contribute to small mass of the total estimated dark matter density to account for its entire amount. To date, the estimated total neutrino average number density is $n0\nu = 339.5\ cm^{-3}$ (The latest information on particle data is available on the web at: http://pdg.lbl.gov/pdg.html. This web page is maintained by the Particle Data Group at the Lawrence Berkeley laboratory). Gamma radiation from the sun at energies above 2.5 MeV is ~1 photons $cm^{-2}\cdot s^{-1}$ [22] that could produce an additional neutrino flux of ~20 $cm^{-2}\cdot s^{-1}$ neutrinos, at least. In the event that additional neutrino (antineutrino) flux is produced by gamma radiation from stars, as a result of the proposed PP process, the neutrino average number density would be higher by several orders of magnitude. Hence, a larger portion of the total estimated dark matter density may be contributed by neutrinos.

## Conflicts of Interest

The authors declare no conflicts of interest regarding the publication of this paper.

## References

[1] Brown, L.M. (1978) *Physics Today*, **31**, 23-28. https://doi.org/10.1063/1.2995181

[2] Bethe, H.A. and Peierls, R. (1934) *Nature*, **133**, 532. https://doi.org/10.1038/133532a0

[3] Dirac, P.A.M. (1928) *Proceedings of the Royal Society A*, **117**, 610-624. https://doi.org/10.1098/rspa.1928.0023

[4] Anderson, C.D. (1933) *Physical Review*, **43**, 491-494. https://doi.org/10.1103/PhysRev.43.491

[5] Hubbell, J.H. and Seltzer, S.M. (2004) *Nuclear Instruments and Methods in Physics Research B*, **213**, 1-9. https://doi.org/10.1016/S0168-583X(03)01524-6

[6] Hubbell, J.H. (2006) *Radiation Physics and Chemistry*, **75**, 614-623. https://doi.org/10.1016/j.radphyschem.2005.10.008

[7] Alkhateeb, S., Alshaery, A. and Aldosary, R. (2022) *Journal of Applied Mathematics and Physics*, **10**, 237-244. https://doi.org/10.4236/jamp.2022.102017

[8] Werner, C.J. (2017) LA-UR-17-29981: MCNP User's Manual, Code Version 6.2. https://mcnp.lanl.gov/pdf_files/la-ur-17-29981.pdf

[9] Allison, J., *et al.* (2016) *Nuclear Instruments and Methods in Physics Research A*, **835**, 186-225.

[10] Nelson, W.R., Hirayama, H. and Rogers, D.W.O. (1985) The EGS4 Code System. SLAC-Report-265.

[11] Peebles, P.J.E. and Ratra, B. (2003) *Reviews of Modern Physics*, **75**, 559-606. https://doi.org/10.1103/RevModPhys.75.559

[12] Frampton, P.H. (2018) Theory of Dark Matter. In: Fritzsch, H., Ed., *Cosmology, Gravitational Waves and Particles*, World Scientific, Singapore, 76-89. https://doi.org/10.1142/9789813231801_0008

[13] Bertone, G., Hooper, D. and Silk, J. (2005) *Physics Reports*, **405**, 279-390. https://doi.org/10.1016/j.physrep.2004.08.031

[14] Todorovic, Z. (2022) *Journal of High Energy Physics, Gravitation and Cosmology*, **8**, 593-622. https://doi.org/10.4236/jhepgc.2022.83042

[15] Kreisch, C.D., Cyr-Racine, F.-Y. and Dore, O. (2020) *Physical Review D*, **101**, Article ID: 123505. https://doi.org/10.1103/PhysRevD.101.123505

[16] Bertone, G. and Merritt, D. (2005) *Modern Physics Letters A*, **20**, 1021-1036. https://doi.org/10.1142/S0217732305017391

[17] Minamino, A. (XMASS Collaboration) (2010) *Nuclear Instruments and Methods in Physics Research—Section A*, **623**, 448. https://doi.org/10.1016/j.nima.2010.03.032

[18] Plante, G., Aprile, E., Budnik, R., Choi, B., Giboni, K.-L., Goetzke, L.W., Lang, R.F., Lim, K.E. and Melgarejo Fernandez, A.J. (2011) *Physical Review C*, **84**, Article ID: 045805. https://doi.org/10.1103/PhysRevC.84.045805

[19] Hirayama, H., *et al.* (2016) The EGS5 Code System. SLAC-R-730, KEK-2005-8, KEK-REPORT-2005-8, Version: January 13, 2016.

[20] Motz, J.W., Olsen, H.A. and Koch, H.W. (1969) *Reviews of Modern Physics*, **41**, 581-639. https://doi.org/10.1103/RevModPhys.41.581

[21] Gros, P. and Bernard, D. (2016) *Astroparticle Physics*, **88**, 60-67. https://doi.org/10.1016/j.astropartphys.2017.01.002

[22] Crannell, C.J., Crannell, H. and Ramaty, R. (1979) *The Astrophysical Journal*, **229**, 762-771. https://doi.org/10.1086/157012

Journal of Modern Physics, 2022, 13, 1341-1347
https://www.scirp.org/journal/jmp
ISSN Online: 2153-120X
ISSN Print: 2153-1196

# On Lorentz Transformations and the Theory of Relativity

**Fleur T. Tehrani**

School of Engineering and Computer Science, California State University, Fullerton, CA, USA
Email: ftehrani@fullerton.edu

**How to cite this paper:** Tehrani, F.T. (2022) On Lorentz Transformations and the Theory of Relativity. *Journal of Modern Physics*, **13**, 1341-1347.
https://doi.org/10.4236/jmp.2022.1311083

**Received:** October 11, 2022
**Accepted:** November 1, 2022
**Published:** November 4, 2022



## Abstract

In the course of a research study on Lorentz transformations and the theory of relativity, the fundamentals of the relativistic concepts of space and time, the relations of those concepts to Lorentz transformations, and equivalence of mass and energy were studied. Many important references on the said subjects were reviewed. This paper draws attention to some critical questions that have risen in the course of that research study on the concepts of expansion of time and unbounded increase of a particle's mass with velocity.

## Keywords

Lorentz Transformations, Relativity Theory, Mass, Energy

## 1. Introduction

Maxwell's equations have been used as the fundamental form of electromagnetic equations for more than a century. These equations in point form are:

$$\nabla \times E = -\frac{\partial B}{\partial t} \tag{1}$$

$$\nabla \times H = J + \frac{\partial D}{\partial t} \tag{2}$$

$$\nabla \cdot B = 0 \tag{3}$$

$$\nabla \cdot D = \rho \tag{4}$$

where $E$ is the electric field intensity, $B$ is the magnetic flux density, $H$ is the magnetic field intensity, $D$ is the electric flux density, $\rho$ is the volume charge density and $J$ is the current density.

The above equations are accompanied by:

$$B = \mu H \tag{5}$$

$$D = \epsilon E \tag{6}$$

$$J = \sigma E \tag{7}$$

$$J = \rho v \tag{8}$$

where $\epsilon$ is permittivity, $\mu$ is permeability, $\sigma$ is conductivity, $v$ is the velocity of charge, with Equation (8) defining the convection current density. The above set of Maxwell's equations is complemented by the Lorentz force equation as:

$$F = \rho\left(E + v \times B\right) \tag{9}$$

where $F$ is force per unit volume.

Lorentz transformations [1] [2] were introduced to enable physicists to apply the same equations in different coordinate systems with relative constant motion with respect to one another and also to explain the failure of the Michelson-Morley experiment [3]. Lorentz transformations were used as the basis of Einstein's special theory of relativity [4] which in turn was used later as the basis of general theory of relativity [5]. Lorentz transformations and the theory of relativity have been the subject of numerous studies to this date (e.g., [6] [7]). At the same time, the relativity theory and quantum mechanics have had significant contradictions which have been the subject of many debates and various new theories have been devised to bridge the gap between the two major theories. The purpose of this research was to get an in depth understanding of Lorentz transformations and the theory of relativity. This paper draws attention to some basic questions on these subjects that may need clarification.

## 2. Lorentz Transformations and the Relativistic Concepts of Space and Time

Considering two cartesian coordinate systems, one assumed as stationary ($x$, $y$, $z$, $t$), and the other in relative constant motion along the $x$ direction with respect to the other at a constant velocity, $v$, ($x'$, $y'$, $z'$, $t'$), Lorentz provided the following transformations so the physical equations would remain unchanged in the two coordinate systems:

$$x' = \frac{x - v \cdot t}{\sqrt{1 - \frac{v^2}{C^2}}} \tag{10}$$

$$y' = y \tag{11}$$

$$z' = z \tag{12}$$

$$t' = \frac{t - \frac{v \cdot x}{C^2}}{\sqrt{1 - \frac{v^2}{C^2}}} \tag{13}$$

where $C$ is the speed of light in free space considered as constant in all coordinate systems. In the well-known Michelson-Morley's experiment, in which a single source of light, a glass plate, and two mirrors were used, it was hypothesized that the earth velocity could be measured by measuring the difference in

the light travel time to and from the mirrors. That difference, however, turned out to be zero and the experiment did not produce any result. Lorentz transformations (Equations (10)-(13)) as stated above were used to describe the reason for the failure of the experiment. Focusing on Lorentz Equation (10) and applying that equation to two points $x_1'$, and $x_2'$ in the moving coordinate system yields:

$$x_1' = \frac{x_1 - v \cdot t_1}{\sqrt{1 - \frac{v^2}{C^2}}} \tag{14}$$

$$x_2' = \frac{x_2 - v \cdot t_2}{\sqrt{1 - \frac{v^2}{C^2}}} \tag{15}$$

where $x_1'$ and $x_2'$ are the positions measured along the $x'$ axis in the moving system, $x_1$ and $x_2$ are the positions along the $x$ axis in the stationary system, and $t_1$ and $t_2$ are the corresponding measured times in the stationary system. Subtracting Equation (14) from Equation (15) yields:

$$\Delta x' = \frac{\Delta x - v \cdot \Delta t}{\sqrt{1 - \frac{v^2}{C^2}}} \tag{16}$$

where $\Delta x = x_2 - x_1$, $\Delta x' = x_2' - x_1'$ and $\Delta t = t_2 - t_1$. Rearranging Equation (16) yields:

$$\Delta x = \Delta x' \sqrt{1 - \frac{v^2}{C^2}} + v \cdot \Delta t \tag{17}$$

The first term on the right side of Equation (17) shows that the distance between the two points in the moving system as viewed by an observer in the stationary system is multiplied by the factor $\gamma$:

$$\gamma = \sqrt{1 - \frac{v^2}{C^2}}$$

Therefore, this distance appears as contracted by the stationary observer as $v$ increases. This phenomenon as predicted by Lorentz transformations is referred to as contraction of space and could explain the null results of Michelson-Morley's experiment. Later, it was noted by a number of scientists that since the Michelson-Morley's measurement system was moving with the earth and was not stationary, the experiment could not produce the intended result. In relation to the same experiment, the concept of expansion of time was proposed as follows:

$$\tau = \frac{\tau'}{\sqrt{1 - \frac{v^2}{C^2}}} \tag{18}$$

where $\tau'$ is the travel time measured in the moving system and $\tau$ is the corresponding duration of time as observed in the stationary system. Focusing on Equation (13) of Lorentz transformations above and applying it to two points in

time in the moving system results as:

$$t_1' = \frac{t_1 - \frac{v \cdot x_1}{C^2}}{\sqrt{1 - \frac{v^2}{C^2}}} \tag{19}$$

$$t_2' = \frac{t_2 - \frac{v \cdot x_2}{C^2}}{\sqrt{1 - \frac{v^2}{C^2}}} \tag{20}$$

Subtracting Equation (19) from Equation (20) yields:

$$t_2' - t_1' = \Delta t' = \frac{\Delta t - \frac{v \cdot \Delta x}{C^2}}{\sqrt{1 - \frac{v^2}{C^2}}} \tag{21}$$

Rearranging Equation (21) yields:

$$\Delta t' = \frac{\Delta t}{\sqrt{1 - \frac{v^2}{C^2}}} - \frac{\frac{v \cdot \Delta x}{C^2}}{\sqrt{1 - \frac{v^2}{C^2}}} \tag{22}$$

This equation does not show the concept of expansion of time as shown in Equation (18). In Chapter 15 of a well-known reference book on this subject [8], an example of a light clock is used to demonstrate the concept of expansion of time in a moving system as observed from a stationary system. However, "time" can be measured in various ways. For example, the unit of time, second, may be defined as about 9 billion oscillations of the cesium atom or similarly in terms of biological procedures. Choosing a time clock in which the distance travelled by light is directly affected by the velocity of the coordinate system may result in different conclusions than by using a biological clock or a clock based on atomic oscillations. Another question that arises is that if the distance in a moving system as viewed by a stationary observer is contracted and the corresponding time is not contracted at the same rate and is expanded at that rate, how will that affect the speed of light which should remain constant in all coordinate systems.

## 3. Mass and Energy

While physicists were puzzled about the nature of light, Louis De Broglie proposed in 1923 that everything manifested both particle and wave properties, which became known as wave-particle duality. De Broglie came up with the following wave equation:

$$P = \frac{h}{\lambda} \tag{23}$$

where $P$ is the particle's momentum, $h$ is the Planck's constant, and $\lambda$ is the wavelength. The relation between the energy and frequency of a wave is given by

Planck's equation as:

$$\text{Energy} = h \cdot f \tag{24}$$

where $f$ is the wave frequency. Substituting $h$ from Equation (23) into Equation (24) yields:

$$\text{Energy} = P \cdot \lambda \cdot f \tag{25}$$

Since $f = \frac{C}{\lambda}$:

$$\text{Energy} = P \cdot C \tag{26}$$

For a mass $m_0$ at velocity, $v$:

$$\text{Energy} = m_0 \cdot v \cdot C \tag{27}$$

If the velocity of the particle, $v$, is raised to the maximum possible velocity which is the speed of light, $C$, at which point all the mass of the particle can be said to have been transformed to energy, Equation (27) can be written as:

$$\text{Energy} = m_0 \cdot C^2 \tag{28}$$

Equation (28) whose validity has been verified in many experiments was provided by Einstein. In Chapter 15 of Reference #8, a derivation of Equation (28) as well as the following equation is provided:

$$m = \frac{m_0}{\sqrt{1 - \frac{v^2}{C^2}}} \tag{29}$$

In the said reference, the derivation starts by assuming the validity of Equation (29) and ends up by concluding the validity of the said equation as well as Equation (28) above. There seem to be some issues with this approach. First, one may not begin by assuming the validity of a mathematical equation and use it as correct, in order to conclude the validity of the same equation. Second, Equation (29) which does not seem to have been supported by sufficient evidence to this date, expresses that the mass of a particle tends to become very large and approaches infinity as the velocity of that particle increases. Whether the resulting mass is called the "inertial mass", "the observed mass", or energy, the concept of a physical quantity to approach "infinity" does not seem to be plausible. The experiments performed to this date in which a lot of energy was given to a charged particle, resulted in the additional energy transformed to radiation energy given by the particle and not a measurable increase in mass.

## 4. Summaries

Relativity and quantum physics are two major theories that have significant contradictions. Some aspects of relativity have been verified experimentally while some others have not. At the same time, quantum physics has been used quite successfully to predict many experimental results, particularly at the atomic and sub-atomic levels. Albert Einstein once stated "… the great initial success of the

quantum theory does not make me believe in the fundamental dice game," and his famous quote was "I cannot believe that god plays dice". Einstein might have been quite right that the world does not function based on probabilities. However, quantum physics is based on probabilistic mathematics which is devised for and is quite successful when the amount of data is enormous, maybe partially unknown, and deterministic analysis is practically impossible; these conditions exist in the atomic and subatomic world.

However, as described in this paper, there are some important questions on Lorentz transformations and the theory of relativity that need to be addressed. Notwithstanding that Lorentz transformations are empirical, the concept of contraction of space in a moving coordinate system as viewed by a stationary observer can be derived from Lorentz transformations. The main questions raised in this paper are the following:

1) With regard to the concept of expansion of time in a moving system as seen by a stationary observer, there does not seem to be a clear derivation of that concept based on Lorentz transformations that are themselves empirical in nature, or otherwise, as discussed above. Also, taking the concepts of expansion of time and contraction of space together may present a contradiction with the principle of constancy of the speed of light in all coordinate systems.

2) Another issue is with Equation (29) that describes a particle's mass (or inertial mass) as a function of velocity and predicts that it will increase unbounded to infinity as velocity increases. There does not seem to be sufficient proof of this concept to this date. Furthermore, the use of Equation (29) by some authors to derive Equation (28) that has been verified in many experiments and can be derived from Equations (23)-(27) as shown above, does not seem to be warranted. These issues deserve more attention and may need to be addressed.

## Conflicts of Interest

The author declares no conflicts of interest regarding the publication of this paper.

## References

[1] Lorentz, H.A. (1904) *Proceedings of the Royal Netherlands Academy of Arts and Sciences*, **6**, 809-831. https://en.wikisource.org/wiki/Electromagnetic_phenomena

[2] Poincaré, H. (1905) *Comptes Rendus Hebdomadaires des Séances de l'Académie des Sciences*, **140**, 1504-1508. https://en.wikisource.org/wiki/Translation:On_the_Dynamics_of_the_Electron_(June)

[3] Michelson, A.A. and Morley, E.W. (1887) *American Journal of Science*, **34**, 333-345. https://en.wikisource.org/wiki/On_the_Relative_Motion_of_the_Earth_and_the_Luminiferous_Ether https://doi.org/10.2475/ajs.s3-34.203.333

[4] Einstein, A. (1905) *Annalen der Physik*, **322**, 891-921. https://doi.org/10.1002/andp.19053221004

http://www.physik.uni-augsburg.de/annalen/history/einstein-papers/1905_17_891-921.pdf

[5] Einstein, A. and Grossmann, M. (1913) *Zeitschrift fur angewandte Mathematik und Physik*, **62**, 225-261. http://www.pitt.edu/~jdnorton/teaching/GR&Grav_2007/pdf/Einstein_Entwurf_1913.pdf

[6] Ogura, A. (2019) *World Journal of Mechanics*, **9**, 267-284. https://doi.org/10.4236/wjm.2019.912018

[7] Zhao, J. (2022) *Journal of Modern Physics*, **13**, 851-857. https://doi.org/10.4236/jmp.2022.136048

[8] Feynman, R.P., Leighton, R.B. and Sands, M. (2010) The Feynman Lectures on Physics. Basic Books, New York, Chapter 15. https://www.feynmanlectures.caltech.edu/

Journal of Modern Physics, 2022, 13, 1348-1368
https://www.scirp.org/journal/jmp
ISSN Online: 2153-120X
ISSN Print: 2153-1196

# How the Redshift of Gravitons Explains Dark Matter and Dark Energy

**Firmin J. Oliveira**

East Asian Observatory/James Clerk Maxwell Submillimetre Telescope, Hilo, Hawai'i, USA
Email: firmjay@hotmail.com

**How to cite this paper:** Oliveira, F.J. (2022) How the Redshift of Gravitons Explains Dark Matter and Dark Energy. *Journal of Modern Physics*, **13**, 1348-1368.
https://doi.org/10.4236/jmp.2022.1311084

**Received:** September 26, 2022
**Accepted:** November 1, 2022
**Published:** November 4, 2022



## Abstract

The theory that gravitons lose energy by way of gravitational redshift while traveling in a gravitational field is applied to the expansion of the universe and to spiral and dwarf galaxy rotation curves using General Relativity. This is a graviton self interaction model which derives an expansion equation which is identical in form to the standard Lambda Cold Dark Matter model. In the domain of galaxies, spiral and dwarf galaxy rotation curves are matched using only baryonic mass. Thus, the requirement for dark matter and dark energy in the universe is replaced by this paradigm.

## Keywords

Gravitons, Gravitational Redshift, Baryon Mass Density, Supernovae, Spiral Galaxies

## 1. Introduction

This paper describes a theory of gravitons acting in the universe and it supersedes the theory expressed in [1] in regards to the expansion of the universe. We will also describe the action of gravitons in galaxies [2]. Assuming that gravitons are the agents of interaction in a gravitational field, then our goal is to describe how the gravitational redshift of gravitons shows up as what has traditionally been labeled as dark matter and dark energy. We will show how the redshift of gravitons can explain both of these phenomena using high precision data. Throughout this paper, all reference to sources of mass and test particles are assumed to be of baryonic nature, unless otherwise specified. When we speak of the graviton mass $m_g$, it is a relativistic mass.

We assume gravitons are bosonic particles which travel at constant speed $c$ in vacuum, where $c$ equals the speed of light. Gravitons traveling in a gravitational

field between a source mass $M$ and a test mass $m$, modeled by the equivalence principle as an accelerating system, should experience an average energy loss of $\delta\xi$ due to motion in that field, over a short time period $\delta t = \delta r/c$, where the acceleration $a$ at a point $r$ in the field is given by $a = -GM/r^2$. The energy loss is expressed differentially as

$$\delta\xi = -\left(m_g c^2\right)\frac{\delta v}{c} = -\left(m_g c\right)a\delta t = -\left(\frac{GMm_g}{r^2}\right)\delta r, \tag{1}$$

where $m_g = m/n$ is the average relativistic graviton mass, $n$ is the number of gravitons, $m$ is the test mass, $\delta v$ is the change in the free fall velocity of the system observed from an inertial reference frame, $G$ is Newton's gravitational constant, $M$ is the baryonic mass of the field source, $r$ is the distance between the center of the source and the location of the moving gravitons, $\delta t$ is the short travel time of the gravitons at speed $c$ over distance $\delta r$. The energy change is a loss (negative), because the velocity change $\delta v$ is in the same direction as the motion of the gravitons, so that for an inertial observer moving in the same direction as the graviton, the energy of the graviton is redshifted. We call this effect of energy loss a gravitational redshift which, as we have described it resembles a Doppler effect. Since gravitons are agents of the gravitational field, our model is essentially an attempt to describe the graviton-graviton interaction as in the self interaction of a quantum gravity theory [3].

Gravitons exist and travel in a gravitational field, which in principle is equivalent to an accelerating system. Assume that the total graviton energy for a system of two masses is expressed by,

$$\Xi = \frac{GMm}{r}, \tag{2}$$

where $m = nm_g$ is the total graviton mass associated with the test mass $m$, where $m_g$ is the average graviton mass and $n$ is the number of gravitons. The total graviton energy decrease $\delta\Xi$ due to its freefall in the gravitational field of mass $M$, when viewed from an inertial system, is expressed by

$$\delta\Xi = -\Xi\frac{\delta v}{c} = -\left(\frac{GMm}{r}\right)\frac{\delta v}{c} = -\left(\frac{GMm}{r}\right)\left(\frac{GM}{c^2r^2}\right)\delta r, \tag{3}$$

where, as in (1), $\delta v = \left(GM/cr^2\right)\delta r$ is the velocity increase in the accelerated reference frame equivalent, according to the principle of equivalence, to the gravitational field of mass $M$ at the position $r$.

## 2. Gravitons in an Expanding Universe

Consider the universe as a sphere of interior baryonic mass $M$ with a thin spherical shell of mass $m$. The masses $M$ and $m$ are constants. The thin shell has a radius $r(t)$ at time $t$. Only the mass interior to the shell has an effect on the shell. The total graviton energy $\Xi(t)$ within the shell at time $t$ is given by (2), where $r = r(t)$. Assuming isotropic uniformity, the mass density $\rho(t)$ within the shell at time $t$ is

$$\rho\left(r\left(t\right)\right)=\frac{3M}{4\pi r^3\left(t\right)}. \tag{4}$$

At the present epoch of time $t_0$ the baryon mass density is $\rho_b$, which is given by,

$$\rho_b=\frac{3M}{4\pi\bar{a}^3}, \tag{5}$$

where $\bar{a}=r\left(t_0\right)$ is the radius of the universe at the present epoch.

### 2.1. Energy Loss Due to Gravitational Redshift

Since the potential function $\Phi\left(r\right)=GMm/r$ is defined as having zero energy at infinity and having a negative energy at position *r*, likewise we define the graviton energy loss to be zero at infinity and negative at position *r*. Applying (1) to the *n* gravitons in free fall in the expanding universe we have the energy loss,

$$\Delta\Xi_{dm}=K_{dm}\int_0^{\Delta\Xi}n\delta\xi=-K_{dm}\int_\infty^r-\frac{GMm}{r^2}\mathrm{d}r=-K_{dm}\left(\frac{GMm}{r}\right), \tag{6}$$

where $K_{dm}$ is a coupling constant to be determined by observation and the extra minus sign accounts for an energy loss because the gravitons travel in the same direction as the free fall velocity change and appear redshifted to an inertial observer also moving in the same direction. Substituting for *M* from (5) and simplifying yields,

$$\Delta\Xi_{dm}=-K_{dm}\left(\frac{4\pi G\bar{a}^3}{3}\right)\frac{m\rho_b}{r}. \tag{7}$$

This component is the energy loss of the so called dark matter.

### 2.2. Energy Loss Due to Expansion

Gravitons traveling at speed *c* in the vacuum of the expanding universe undergo cosmological redshift in three dimensions on the way to interaction with the masses. We express this redshift by applying the 3-D velocity differential ($\delta v_x\delta v_y\delta v_z/c^3$) to the total graviton energy $\Xi$ from (2), and applying (3) in the three spatial dimensions, given in the form,

$$\delta\xi=-\frac{GMm}{r}\left(\frac{\delta v_x\delta v_y\delta v_z}{c^3}\right), \tag{8}$$

where the negative sign is applied because the motion of the gravitons is in the same direction as the freefall in the field. We can convert the 3-D velocity differential to a ratio of 3-D volume differential by the construction,

$$\frac{\delta v_x\delta v_y\delta v_z}{c^3}=\left(\frac{\delta x}{c\delta t_x}\right)\left(\frac{\delta y}{c\delta t_y}\right)\left(\frac{\delta z}{c\delta t_z}\right)=\frac{\delta x\delta y\delta z}{c^3\delta t_x\delta t_y\delta t_z}, \tag{9}$$

where *x*, *y* and *z* are Cartesian co-ordinates, $t_x$, $t_y$ and $t_z$ are independent times and where $\delta v_x=\delta x/\delta t_x$, $\delta v_y=\delta y/\delta t_y$ and $\delta v_z=\delta z/\delta t_z$. Furthermore, we convert the volume differential in Cartesian co-ordianes to radial co-ordiates,

in the form

$$\delta x\delta y\delta z = 4\pi r^2\delta r. \tag{10}$$

Now, applying the transformations (9) and (10) to (8), while also moving the volume differential $c^3\delta t_x\delta t_y\delta t_z$ to the left hand side of the equation we get,

$$\delta\xi\left(c^3\delta t_x\delta t_y\delta t_z\right) = -\frac{GMm}{r}\left(4\pi r^2\delta r\right). \tag{11}$$

The left hand side of (11) is a quadruple differential whilst the right hand side is a single differential. Integrating both sides of (11) yields,

$$\begin{aligned}\left(\frac{\bar{a}^3}{\sigma_{de}}\right)\Delta\Xi_{de} &= \int_0^T\int_0^T\int_0^T\int_0^{\Delta\Xi}\delta\xi\left(c^3\delta t_x\delta t_y\delta t_z\right) = \int_{r_0}^{r}\left(\frac{-mGM}{r}\right)4\pi r^2\delta r \\ &= \int_{r_0}^{r} -4\pi mGMr\delta r = -\frac{8\pi^2G}{3}\bar{a}^3 m\rho_b r^2,\end{aligned} \tag{12}$$

where the expansion time is taken to be

$$T = \bar{a}/c, \tag{13}$$

where $\bar{a}$ is the present radius of the universe and $\sigma_{de}$ is a dimensionless coupling constant and where, in the final line we substituted for M from (5). Rearranging (12) we get the graviton energy loss due to the expansion of the universe, the so called dark energy component,

$$\Delta\Xi_{de} = -\sigma_{de}\left(\frac{8\pi^2G}{3}\right)m\rho_b r^2. \tag{14}$$

We will subsequently show that the graviton energy losses $\Delta\Xi_{dm}$ and $\Delta\Xi_{de}$ can account for the expansion rate of the universe without dark matter or dark energy which is required by the Lamda Cold Dark Matter cosmological model [4].

### 2.3. Equation of the Expanding Universe

The total energy of the shell of mass $m$, where $m \ll M$, having kinetic energy, gravitational potential energy and energy loss due to the cosmological redshift of gravitons (14), is expressed by

$$\begin{aligned}&\frac{1}{2}mv^2 - \frac{GMm}{r} + \Delta\Xi_{dm} + \Delta\Xi_{de} \\ &= \frac{1}{2}mv^2 - \left(\frac{4\pi G\bar{a}^3}{3}\right)\frac{m\rho_b}{r} - K_{dm}\left(\frac{4\pi G\bar{a}^3}{3}\right)\frac{m\rho_b}{r} - \sigma_{de}\left(\frac{8\pi^2G}{3}\right)m\rho_b r^2 \\ &= -\frac{1}{2}mc^2k\bar{a}^2,\end{aligned} \tag{15}$$

where the term on the far right is the total energy, where $k$ is a constant (curvature) with dimensionality [length]$^{-2}$, $\bar{a}$ is the present radius of the universe and $M$ is the mass of the universe. Multiplying (15) by $2/mr^2$ and simplifying, we get the expression for the expansion of the shell,

$$\frac{v^2}{r^2} = \frac{8\pi G\bar{a}^3\rho_b}{3}\frac{1}{r^3} + K_{dm}\left(\frac{8\pi G\bar{a}^3\rho_b}{3}\right)\frac{1}{r^3} + \sigma_{de}\left(\frac{16\pi^2G\rho_b}{3\bar{a}^3}\right) - \frac{kc^2\bar{a}^2}{r^2}. \tag{16}$$

Note that the shell mass $m$ can be made arbitrarily small compared to the universe mass $M$.

Define the distance $r$ by

$$r = \bar{a}a, \tag{17}$$

where the time varying scale factor $a$ is dimensionless with $0 < a \le 1$. Using (17), the velocity $v$ takes the form

$$v = \frac{\mathrm{d}r}{\mathrm{d}t} = \bar{a}\frac{\mathrm{d}a}{\mathrm{d}t}. \tag{18}$$

Substituting (18) into (16) gives us,

$$\left(\frac{1}{a}\frac{\mathrm{d}a}{\mathrm{d}t}\right)^2 = \frac{8\pi G\left(1+K_{dm}\right)\rho_b}{3a^3} + \frac{16\pi^2 G\sigma_{de}\rho_b}{3} - \frac{kc^2}{a^2}. \tag{19}$$

Putting (19) in terms of the mass densities we have,

$$\left(\frac{1}{a}\frac{\mathrm{d}a}{\mathrm{d}t}\right)^2 = \frac{8\pi G}{3}\left(\rho_m(a) + \rho_{dm}(a) + \rho_{de}(a) + \rho_k(a)\right), \tag{20}$$

where

$$\rho_m(a) = \frac{\left(1+K_{dm}\right)\rho_b}{a^3} \tag{21}$$

is the mass density composed of baryons and graviton energy loss mass due to gravitational redshift (an apparent dark matter mass density),

$$\rho_{de}(a) = 2\pi\sigma_{de}\rho_b \tag{22}$$

is the graviton energy loss due to the expanding universe (an apparent dark energy mass density) and

$$\rho_k(a) = \frac{-3kc^2}{8\pi G a^2} \tag{23}$$

is the curvature mass density.

Define the Hubble parameter $H(t)$ by

$$H(t) = \frac{1}{r}\frac{\mathrm{d}r}{\mathrm{d}t}, \tag{24}$$

where, by (17), $r = \bar{a}a$. Equation (24) can also be written as

$$v = \frac{\mathrm{d}r}{\mathrm{d}t} = H(t)r(t), \tag{25}$$

which is the Hubble law for $H_0 = H(t_0)$ where $t_0$ is the present epoch of cosmic time. Thus, $H(t)$ defined by (24) is the general form of Hubble's law [5]. Substituting $H(t)$ for $\mathrm{d}a/a\mathrm{d}t$ in (20), with some manipulation, we get

$$\rho_c(t) = \frac{3H^2(t)}{8\pi G} = \rho_m(t) + \rho_{de}(t) + \rho_k(t), \tag{26}$$

where $\rho_c(t)$ is called the critical mass density at time $t$. Dividing (26) by $\rho_c(t)$ yields the parametric equation

$$\frac{\rho_c(t)}{\rho_c(t)} = \Omega_c = 1 = \Omega_m(t) + \Omega_{de}(t) + \Omega_k(t), \tag{27}$$

where $\Omega_m(t) = \rho_m(t)/\rho_c(t)$, $\Omega_{de}(t) = \rho_{de}(t)/\rho_c(t)$ and $\Omega_k(t) = \rho_k(t)/\rho_c(t)$. At the present epoch $t_0$, the mass density parameter is

$$\Omega_m(t_0) = (1 + K_{dm})\Omega_b, \tag{28}$$

where $\Omega_b$ is the baryon mass density parameter, the graviton expansion energy loss mass density parameter is

$$\Omega_{de}(t_0) = 2\pi\sigma_{de}\Omega_b \tag{29}$$

and the curvature density parameter is

$$\Omega_k(t_0) = -\frac{kc^2}{H_0^2}. \tag{30}$$

## 3. General Relativity for an Expanding Universe with Graviton Interaction

The Friedmann-Lemaître-Robertson-Walker (FLRW) metric line element [6] [7] [8] [9] in terms of the scale factor $a(t)$ is

$$\mathrm{d}s^2 = -c^2\mathrm{d}t^2 + a^2(t)\left(\frac{\mathrm{d}r^2}{1-kr^2} + r^2\mathrm{d}^2\theta + r^2\sin^2(\theta)\mathrm{d}^2\phi\right), \tag{31}$$

where the scale factor $0 < a(t) \le 1$ and the curvature $k$ has units of $[length]^{-2}$ where $k < 0$, $k > 0$ or $k = 0$. The Einstein equations [10] [11] in trace reverse form is

$$R_{\mu\nu} = \kappa\left(T_{\mu\nu} - \frac{1}{2}Tg_{\mu\nu}\right), \tag{32}$$

where $R_{\mu\nu}$ is the Ricci tensor, $T_{\mu\nu}$ is the energy-momentum tensor, $T$ is the contracted energy-momentum tensor, $g_{\mu\nu}$ is the metric tensor defined by (31) and $\kappa = 8\pi G/c^4$. Define the energy-momentum tensor $T_{\mu\nu}$ of a perfect fluid,

$$T_{\mu\nu} = \begin{pmatrix} \rho c^2 & 0 & 0 & 0 \\ 0 & p & 0 & 0 \\ 0 & 0 & p & 0 \\ 0 & 0 & 0 & p \end{pmatrix}, \tag{33}$$

where, referring to (21) to (23) for the mass densities, the total mass density $\rho$ is given by

$$\rho = \rho_m + \rho_{de} + \rho_k, \tag{34}$$

where

$$\rho_m = \frac{(1 + K_{dm})\rho_b\bar{a}^3}{r^3}, \tag{35}$$

$$\rho_{de} = 2\pi\sigma_{de}\rho_b, \tag{36}$$

$$\rho_k = \frac{-3k\bar{a}^2c^2}{8\pi Gr^2}, \tag{37}$$

and where the current baryon mass density is

$$\rho_b = \rho_c \Omega_b, \tag{38}$$

where $\Omega_b$ is the baryon mass density parameter. We have assumed the equation of state for the relativistic particles $p_{de} = \omega_{de} \rho c^2$, with $\omega_{de} = -1$. We are neglecting the radiation density (photon and neutrinos) and we will justify this when we fit the model to SNe Ia data.

Solving the Einstein Equations (32) given the mass-energy tensor (33), and simplifying the results, yields the equation for the rate of change of the scale factor,

$$\left(\frac{\dot{a}}{a}\right)^2 = \frac{8\pi G}{3}\rho - \frac{k}{a^2}. \tag{39}$$

Assuming $k = 0$ for no curvature, and the total mass density given by (34) - (38), the Hubble parameter $H(a)$ is

$$H(a) = H_0 \sqrt{\frac{(1+K_{dm})\Omega_b}{a^3} + 2\pi\sigma_{de}\Omega_b}, \tag{40}$$

where $\Omega_b = 8\pi G\rho_b / 3H_0^2$.

## 4. Fits to Type Ia Supernova Data and Comparison with the Standard Model

The scale factor *a* has the relation to the cosmological redshift *z* expressed by

$$a = \frac{1}{1+z}. \tag{41}$$

An increment of comoving distance $\delta d_c$ defined in terms of the scale factor is

$$\delta d_c = c\frac{\mathrm{d}t}{a} = c\frac{\mathrm{d}a}{a^2 H(a)}, \tag{42}$$

where we used the definition (24) of the Hubble parameter. In terms of the cosmological redshift $z$, the comoving distance is

$$\delta d_c = c\frac{\mathrm{d}z}{H(z)}, \tag{43}$$

where we used the fact that $\mathrm{d}a = -\mathrm{d}z/(1+z)^2 = -a^2\mathrm{d}z$ to transform (42), dropping the minus sign.

The flux $\Phi_0$ from a distant light source at redshift *z* is defined in terms of the observed luminosity $L_o = L/(1+z)^2$, where *L* is the luminosity of the emitting source,

$$\Phi_0 = \frac{L}{4\pi(1+z)^2 d_p^2}, \tag{44}$$

where $d_p$ is the proper distance. The luminosity distance, from (44) is

$$(1+z)d_p = \sqrt{\frac{L}{4\pi\Phi_0}}. \tag{45}$$

The luminosity distance, from (43), is

$$D_L(z) = (1+z)d_c = (1+z)\int_0^z \frac{cdz}{H(z)}, \tag{46}$$

where $d_c$ is the co-moving distance and where

$$H(z) = H_0\sqrt{(1+K_{dm})\Omega_b(1+z)^3 + 2\pi\sigma_{de}\Omega_b}, \tag{47}$$

and we changed the negative sign to positive by inverting the limits of integration. The form (47) of the Hubble parameter $H(z)$ is identical to that of the standard model. Therefore, fitting to the SNe Ia data will be identical. The magnitude is defined, in the standard way,

$$Mu(z) = 5\log(D_L(z)) - \mu_B + a_{off}, \tag{48}$$

where $\mu_B$ is the source magnitude and $a_{off}$ is an offset. Generally, the source magnitude is combined into $a_{off}$.

We applied (48) in a fit to 580 Type Ia supernovae (SNe Ia) magnitude data from the Super Nova Cosmology Project Union 2.1 data set [12]. With Hubble constant $H_0 = 70\ \mathrm{km}\cdot\mathrm{s}^{-1}\cdot\mathrm{Mpc}^{-1}$, densities $\Omega_m = 0.271$, $\Omega_{de} = 0.729$ [12] and offset $a_{off} = -87.441$, the fit to the SNe Ia data set obtained a two parameter $\chi^2 = 0.9769$. Figure 1 shows the fit to the data. Regarding neglecting the radiation density in our model, the radiation density parameter of photons, with $h = 0.7$ is given by [13], $\Omega_r = \left(2.47\times10^{-5}\right)/h^2 = 5.04\times10^{-5}$. At the maximum redshift

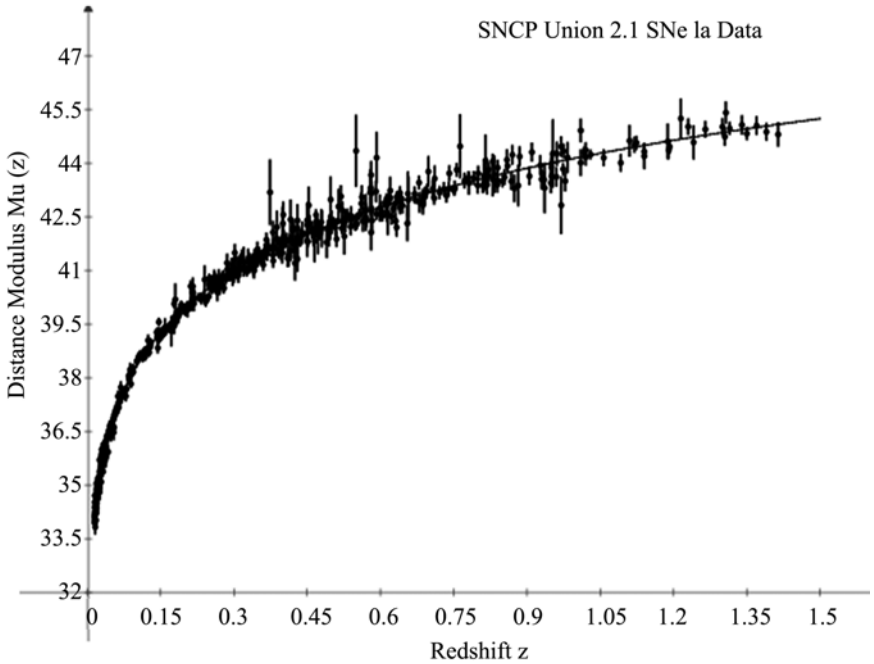


Figure 1. Supernova cosmology project union 2.1 SNe Ia magnitude vs redshift data points with error bars. The solid line is the fit for the graviton model with $\Omega_m = 0.271$ and $\Omega_{de} = 0.729$ with a two parameter $\chi^2 = 0.9769$. The dotted line is the fit for the LCDM model with the same parameters and the same $\chi^2$. The graviton model and the LCDM model fits are (obviously) identical.

of $z_{\max}=1.5$ for the SNe Ia data, the relative magnitude of the error $\varepsilon_{rad}$ in comparing the radiation and matter densities is

$$\varepsilon_{rad}=\frac{\Omega_r\left(1+z_{\max}\right)^4}{\Omega_m\left(1+z_{\max}\right)^3}=4.6\times10^{-4}, \tag{49}$$

which justifies ignoring the radiation density in the fitting.

Assuming that the curvature $k=0$, so that $\Omega_k=0$, then from (27) we have for the present epoch

$$1=\left(1+K_{dm}\right)\Omega_b+2\pi\sigma_{de}\Omega_b, \tag{50}$$

and from (29),

$$\sigma_{de}=\frac{\Omega_{de}}{2\pi\Omega_b}. \tag{51}$$

For example, for $\Omega_{de}=0.721$ and $\Omega_b=0.049$ which is in the big bang nucleosynthesis (BBN) allowable range [14] we get a value of the coupling constant $\sigma_{de}=2.342$. Also, from (28) we get $K_{dm}=\left(\Omega_m/\Omega_b\right)-1=4.694$. The expansion time, from (13) has the value $T=1/H_0=13.97\times10^9$ yr.

## 5. Gravitons in Galaxies

Integrating (1) up to radial distance $r$ we obtain the average energy change per graviton $\Delta\Xi_g$ expressed by

$$\Delta\Xi_g=-\int_0^r\left(m_gc^2\right)\frac{\mathrm{d}u}{c}=-\int_0^r m_g\left(\frac{GM_b}{r^2}\right)\mathrm{d}r. \tag{52}$$

Equation (52) describes the gravitational redshift of the energy of the average graviton as it travels from a lower, more negative potential to a position r of higher, less negative potential and is consistent with energy conservation.

Now, consider the energy for a galaxy of mass $M$ interior of a small mass $m$ in a circular orbit of radius $r$. The gravitons traversing the distance at lightspeed from the interior mass to the orbiting mass will experience a decrease in energy as described by (52), $\Delta\Xi=n\Delta\Xi_g$, where $n$ is the number of gravitons. Taking the energy loss of the gravitons into account, the total orbital energy of the orbiting mass $m$ is

$$\frac{1}{2}mv^2-\frac{GMm}{r}+K_gn\Delta\Xi_g=E, \tag{53}$$

where $v$ is the rotational velocity of the orbiting mass, $K_g$ is a coupling coefficient, a constant for each galaxy, and the total energy $E=-GM/2r$. Using (53) by expanding $\Delta\Xi_g$ using (52), with $m=nm_g$, multiplying by $2/m$ and moving all terms except $v^2$ to the right hand side, we obtain the expression for the orbital velocity,

$$v^2=\frac{GM\left(r\right)}{r}+2K_g\int_0^r\left(\frac{GM\left(r\right)}{r^2}\right)\mathrm{d}r. \tag{54}$$

As an approximation, we model the mass distribution of a spiral galaxy by a

spherically symmetric distribution $\rho(r)$, even though a mass density distribution consisting of a spherically symmetric central bulge surrounded by an axially symmetric thin disk would be more realistic. Then the mass $M(r)$ of the galaxy within the radial distance $r$ from the galaxy center is given by,

$$M(r)=\int_0^r 4\pi\rho(r)r^2\mathrm{d}r. \tag{55}$$

### Coupling Coefficient $K_g$

Under our assumption that the coupling coefficient is constant for each galaxy, (54) can be solved for $K_g$ at the galaxy edge, where $r=r_f$ and $v=v_f$, giving

$$K_g=\frac{v_f^2-\dfrac{GM(r_f)}{r_f}}{2\displaystyle\int_0^{r_f}\left(\frac{GM(r)}{r^2}\right)\mathrm{d}r}, \tag{56}$$

where $M(r_f)=M_b$ is the total baryonic mass in the galaxy. By Newton's gravitational law, at the galaxy edge, the final velocity $v_f$ is related to the total mass $M_g$ contained within the radial distance $r_f$ by,

$$v_f^2=\frac{GM_g}{r_f}=\frac{G(M_b+M_d)}{r_f}, \tag{57}$$

where $M_g=M_b+M_d$, where $M_d$ is the total apparent mass due to the graviton energy loss, the mass of the so called "dark matter". The total apparent dark matter in a galaxy is given at the galaxy edge by,

$$M_{d\,obs}=\frac{v_f^2r_f}{G}-M_b. \tag{58}$$

Using the results from analyzing galaxy rotational data we can estimate the dark matter by (58) as $M_d$, and substituting that and (57) into (56) we arrive at a formula for estimating $K_g$ as,

$$K_g=\frac{M_{d\,obs}}{2r_f\displaystyle\int_0^{r_f}\left(\frac{M(r)}{r^2}\right)\mathrm{d}r}. \tag{59}$$

## 6. The Einstein Equations for Galaxies with Gravitons

Assuming a spherically symmetric mass distribution for a galaxy we will use the Schwarzschild metric to describe the motions within the galaxy. The Einstein equations for the region outside of a spherical mass distribution is

$$R_{\mu\nu}=0 \tag{60}$$

where $R_{\mu\nu}$ is the Ricci tensor. The metric element we use is defined in spherical coordinates,

$$\mathrm{d}s^2=-\mathrm{e}^{\nu}c^2\mathrm{d}t^2+\mathrm{e}^{\lambda}\mathrm{d}r^2+r^2\left(\mathrm{d}\theta^2+\sin(\theta)\mathrm{d}\phi^2\right), \tag{61}$$

where

$$e^{\nu} = 1 - \frac{2GM(r)}{c^2 r}, \tag{62}$$

$$e^{\lambda} = \left(1 - \frac{2GM(r)}{c^2 r}\right)^{-1}, \tag{63}$$

and where $M(r)$ is the mass within radius $r$. From the metric element (61) the metric tensor is

$$g_{\mu\nu} = \begin{pmatrix} -e^{\nu} & 0 & 0 & 0 \\ 0 & e^{\lambda} & 0 & 0 \\ 0 & 0 & r^2 & 0 \\ 0 & 0 & 0 & r^2 \sin^2(\theta) \end{pmatrix}. \tag{64}$$

Since the metric (64) does not depend on time $t$ and angles $\theta$ and $\phi$, it follows from Hamilton's principle and the Lagrange equations[1] that

$$\frac{d}{d\tau}\left(e^{\nu}\frac{dt}{d\tau}\right) = 0, \tag{65}$$

implying that the total energy $E$ is

$$e^{\nu}\frac{dt}{d\tau} = \frac{E}{mc^2}, \tag{66}$$

from which we get

$$e^{\nu}\left(\frac{c^2 dt^2}{d\tau^2}\right) = e^{-\nu}\left(\frac{E^2}{m^2 c^2}\right). \tag{67}$$

And similarly for the $\phi$ component, we have that

$$\frac{d}{d\tau}\left(r^2 \sin^2(\theta)\frac{d\phi}{d\tau}\right) = 0, \tag{68}$$

implying that the specific angular momentum is

$$r^2 \sin^2(\theta)\frac{d\phi}{d\tau} = h, \tag{69}$$

from which we get,

$$r^2 \sin^2(\theta)\frac{d\phi^2}{d\tau^2} = \frac{h^2}{r^2}. \tag{70}$$

For motion in the plane defined by $r$ and $\phi$, $d\theta/d\tau = 0$, where $\theta$ is defined as

$$\theta = \frac{\pi}{2}. \tag{71}$$

## Equation of Motion

We derive the equation of motion using the metric element (61), where $ds^2 = -c^2 d\tau^2$ where $d\tau$ is the differential of proper time $\tau$. Dividing the metric element by $d\tau^2$ and substituting from (66)-(71) with the metric element

[1]Wikipedia: Schwarzschild geodesics, https://en.wikipedia.org/Schwarzschild_geodesics.

we get, dropping the $\theta$ term since $\mathrm{d}\theta = 0$,

$$\frac{\mathrm{d}s^2}{\mathrm{d}\tau^2} = -c^2 = -\mathrm{e}^{-\nu}\frac{E^2}{m^2c^2} + \mathrm{e}^{\lambda}\frac{\mathrm{d}r^2}{\mathrm{d}\tau^2} + \frac{h^2}{r^2}, \tag{72}$$

Multiplying (72) by $\mathrm{e}^{-\lambda}$ and simplifying yields

$$\frac{\mathrm{d}r^2}{\mathrm{d}\tau^2} = \mathrm{e}^{-(\nu+\lambda)}\left(\frac{E^2}{m^2c^2}\right) - \mathrm{e}^{-\lambda}\left(c^2 + \frac{h^2}{r^2}\right). \tag{73}$$

Substituting for $\mathrm{e}^{-\lambda}$ from (63) into (73) and, since $\mathrm{e}^{\lambda} = \mathrm{e}^{-\nu}$ from (62) and (63) so that $\mathrm{e}^{-(\nu+\lambda)} = \mathrm{e}^{0} = 1$, we get after simplification,

$$\frac{\mathrm{d}r^2}{\mathrm{d}\tau^2} = \frac{E^2}{m^2c^2} - c^2 + \frac{2GM(r)}{r} - \frac{h^2}{r^2} + \frac{2GM(r)h^2}{c^2r^3}. \tag{74}$$

We assume that the mass $M(r)$ within distance $r$ from the galaxy center is given by the sum of the baryonic mass $M_b(r)$ within $r$ and the mass $M_g(r)$ equivalent to the graviton gravitational redshift energy loss mass within $r$. The mass density of the baryons is given $\rho_b(r)$. The total mass within $r$, which is the sum of baryonic mass and gravitonic energy loss mass, is expressed by

$$M(r) = M_b(r) + M_g(r), \tag{75}$$

where the baryonic mass is

$$M_b(r) = \int_0^r 4\pi s^2 \rho_b(s)\mathrm{d}s, \tag{76}$$

where $\rho_b$ is the baryonic mass density and from (54) we express the gravitonic energy loss mass in terms of the baryonic mass density by,

$$M_g(r) = 2K_g r\int_0^r \frac{M_b(s)}{s^2}\mathrm{d}s, \tag{77}$$

where $K_g$ is a constant coupling coefficient which is peculiar to each galaxy. For circular motion the specific angular momentum term in (74) is

$$\frac{h^2}{r^2} = \frac{GM(r)}{r}. \tag{78}$$

Dropping the constant terms in (74) and substituting with (78), the velocity of a particle in orbit in the galaxy is expressed by

$$v^2 = \frac{\mathrm{d}r^2}{\mathrm{d}\tau^2} = \frac{GM(r)}{r} + 2c^2\left(\frac{GM(r)}{c^2r}\right)^2. \tag{79}$$

## 7. Results for SPARC Galaxies

We use the velocities from the Spitzer Photometry and Accurate Rotation Curves (SPARC) data base [15] [16], derived from near-infrared (NIR) surface photometry at 3.6 μm. We select the spiral galaxies NGC 2403, NGC 2841 and dwarf galaxies DDO 154 and NGC 2915. From the photometric data which has been reduced to the equivalent velocities for the galaxy bulge, disk and gas mass content, we approximate the baryonic mass as due to a spherically symmetric distribution, which is given by the Newtonian relation for the velocity to mass con-

tained within the radius $r$ from the galaxy center, expressed by

$$M_b(r)=\left(\frac{r}{G}\right)\left(\left|v_{gas}(r)\right|v_{gas}(r)+\Upsilon_{dsk}(r)\left|v_{dsk}(r)\right|v_{dsk}(r)+\Upsilon_{bul}(r)\left|v_{bul}(r)\right|v_{bul}(r)\right), \tag{80}$$

where $r=r_i$, $i=1,2,\cdots,N$, $N>1$, $N$ the number of radial distances observed, and the absolute values of the velocities are needed because they can sometimes be negative (Ref. [16], p. 5) . The velocities for the disk and gas from **Table 2** of [15] are taken with $\Upsilon_*=1$. In our **Table 2**, $\Upsilon_{dsk}$ and $\Upsilon_{bul}$ are the $\mathrm{M}_\odot/\mathrm{L}_\odot$ used in (80) to make the fits. Using the SPARC results for the mass at $r$ in terms of the gas, disk and bulge velocities, where the mass internal to $r$ is given by $M_b(r)$ of (80), the equivalent graviton energy loss mass is

$$M_g(r)=\left(2K_g r\right)\sum_{j=1}^{n}\left(\int_{r_{j-(j>1)}}^{r_{j+(j<2)}}\left(\frac{M_b(s)}{s^2}\right)\mathrm{d}s\right). \tag{81}$$

The predicted velocity (79) is expressed in the form

$$v^2(r_n)=\frac{G\left(M_b(r_n)+M_g(r_n)\right)}{r_n}+2c^2\left(\frac{G\left(M_b(r_n)+M_g(r_n)\right)}{c^2 r_n}\right)^2, \tag{82}$$

where $n=1,2,\cdots,N$, $N>1$.

We strived to obtain good fits to the velocity $v_{obs}(r_k)$ at each radial distance $r_k$ by minimizing the mean absolute error MAE between $v(r_k)$ and $v_{obs}(r_k)$ while iterating $\Upsilon_{dsk}(r_k)$ for the disk and, when available, $\Upsilon_{bul}(r_k)$ for the bulge. We constrained the mass to agree with the baryonic Tully-Fisher relation (BTFR) [17] [18] mass for each galaxy. **Table 1** lists for each galaxy the baryonic mass $M_b$ determined by the velocity profiles used in (80), the BTFR estimated galaxy mass, the mean data rotation velocity error $V_{err}$, the mean absolute fitted error MAE and the coefficient $K_g$.

**Table 2** lists the average values for disk $\Upsilon_{dsk}$ and bulge $\Upsilon_{bul}$ mass to light ratios which were used in making each galaxy fit. Also listed in the table are minimum and maximum $\Upsilon_{dsk}$ taken from Table 4 and Table 5 of [19] for

**Table 1.** Results of fits to SPARC galaxy data using the graviton model (82) with masses from (80) and (81). The $V_{err}$ are the mean error of the reported stellar velocities. The MAE errors are the average absolute error for the fits.

| Galaxy | $M_b$ ($\mathrm{M}_\odot\times10^{10}$) | † $M_b$ BTFR ($\mathrm{M}_\odot\times10^{10}$) | $V_{err}$ ($\mathrm{km\cdot s^{-1}}$) | MAE ($\mathrm{km\cdot s^{-1}}$) | $K_g$ |
|---|---|---|---|---|---|
| NGC 2403 | 1.612 | 1.612 | 2.421 | 0.528 | 0.424 |
| NGC 2841 | 37.277 | 37.356 | 7.67 | 1.476 | 0.189 |
| DDO 154 | 0.06474 | ‡ 0.02143 | 0.625 | 0.225 | 0.578 |
| NGC 2915 | 0.2810 | 0.2799 | 8.064 | 0.814 | 0.653 |

† Using final velocity as flat velocity. ‡ Rotation curve does not flatten.

**Table 2.** Results of fits to SPARC galaxy data using the graviton model (82). The columns for $\Upsilon_{dsk}$ and $\Upsilon_{bul}$ are the averages for the disk and bulge mass to light ratios determined by modeling the rotation velocity curve.

| Galaxy | Avg $\Upsilon_{dsk}$ | Avg $\Upsilon_{bul}$ | † min $\Upsilon_{dsk}$ | † max $\Upsilon_{dsk}$ |
|---|---|---|---|---|
| NGC 2403 | 0.579 | 0 | 1.3 | 1.8 |
| NGC 2841 | 1.039 | 0.833 | 2.0 | 5.1 |
| DDO 154 | 6.183 | 0 | 1.1 | 1.2 |
| NGC 2915 | 1.874 | 0 | na | na |

0 in the $\Upsilon_{bul}$ column means the bulge velocity is zero in the data. † Min and max $\Upsilon_{dsk}$ values for high surface mass galaxies from [19]. NA means the result is not available.

comparison. The fitted spiral galaxy disk mass to light ratios are $\Upsilon_{dsk} < 1.0$ except for NGC 2841 which fitted with $\Upsilon_{dsk} < 2.0$. A good reference for fits to SPARC data can also be found in [20], especially for spiral galaxy NGC 2841, where from our **Table 2** we have an average of $\Upsilon_{dsk} = 0.856\ \mathrm{M}_{\odot}/\mathrm{L}_{\odot}$ and $\Upsilon_{bul} = 1.254\ \mathrm{M}_{\odot}/\mathrm{L}_{\odot}$, each of which is of the same order of magnitude as the fitted values $\Upsilon_{disk} = 0.81 \pm 0.05\ \mathrm{M}_{\odot}/\mathrm{L}_{\odot}$ and $\Upsilon_{bul} = 0.93 \pm 0.05\ \mathrm{M}_{\odot}/\mathrm{L}_{\odot}$, respectively, from **Figure 1** of [20]. For each plot of the galaxy rotation velocity, the Newtonian velocity curve is also displayed. Plots for the results of the SPARC galaxies can be found in **Figure 2** and **Figure 3**.

### SPARC Galaxies DDO 154 and NGC 2915

Two dwarf galaxies that have been difficult to understand in terms of missing mass are DDO 154 and NGC 2915. **Figure 3** shows the results for the fits using the graviton model. The upper curve shows the mass density, the middle curve displays the M/L ratios and the lower plot shows the observed and predicted rotation velocities. With the graviton model for DDO 154 we obtained a total baryonic mass of $M_{bary} = 6.47 \times 10^{8}\ \mathrm{M}_{\odot}$, which is less than 2× the detected luminous mass [21] of $M_{*} + M_{HI+He} = 3.65 \times 10^{8}\ \mathrm{M}_{\odot}$. Significantly, it is only one-fifth of the estimated dark plus luminous matter of $M_{dark+lum} = 3.1 \times 10^{9}\ \mathrm{M}_{\odot}$. Our fitted disk mass to light ratios have an average of $\Upsilon_{dsk} = 6.183\ \mathrm{M}_{\odot}/\mathrm{L}_{\odot}$ which is 3× the published value of $\Upsilon_{dsk} \approx 2\ \mathrm{M}_{\odot}/\mathrm{L}_{\odot}$.

For NGC 2915 we obtained a total baryonic mass of $M_{bary} = 2.81 \times 10^{9}\ \mathrm{M}_{\odot}$, where the stellar mass and luminous HI mass [22] [23] $M_{HI} + M_{*} = 1.06 \times 10^{9}\ \mathrm{M}_{\odot}$. This compares with the total dynamical mass $M_{T} = 21 \times 10^{9}\ \mathrm{M}_{\odot}$ which is 7× the total baryonic mass derived by the graviton model.

## 8. Discussion

Regarding the baryon acoustic oscillations (BAO) in the primordial plasma and the resulting cosmic microwave background radiation (CMB), if the energy loss in the gravitational field due to the gravitational redshift of graviton energy is the cause of the apparent dark matter in the universe, implying that dark matter

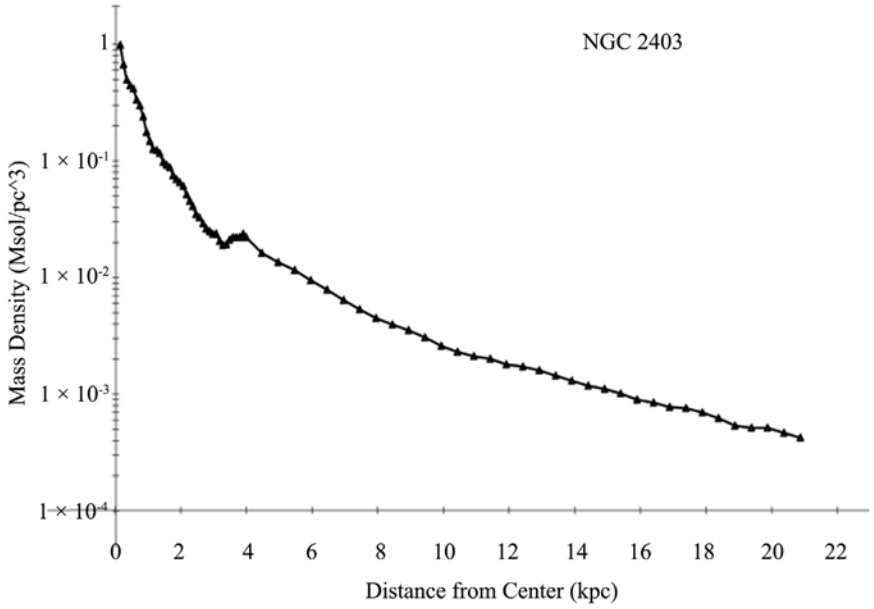
NGC 2403
Mass Density (Msol/pc^3)
1
1 × 10-1
1 × 10-2
1 × 10-3
1 × 10-4
0 2 4 6 8 10 12 14 16 18 20 22
Distance from Center (kpc)

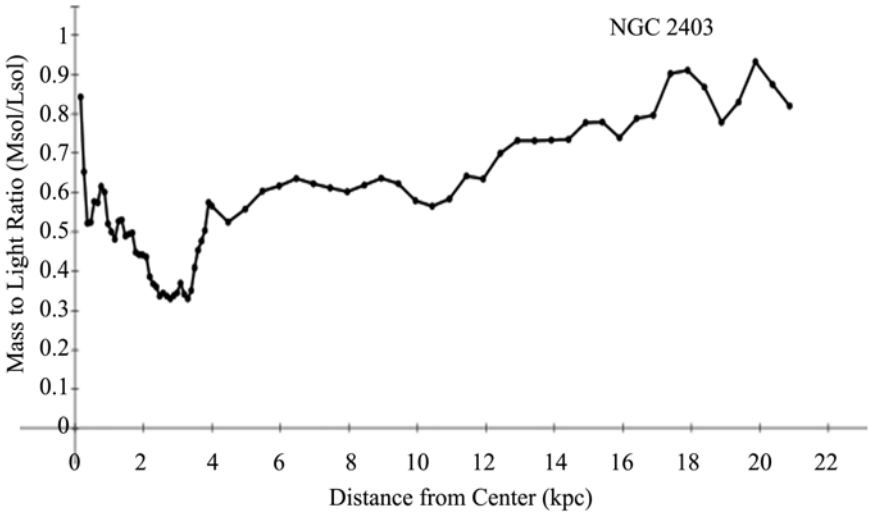
NGC 2403
Mass to Light Ratio (Msol/Lsol)
1 0.9 0.8 0.7 0.6 0.5 0.4 0.3 0.2 0.1 0
0 2 4 6 8 10 12 14 16 18 20 22
Distance from Center (kpc)

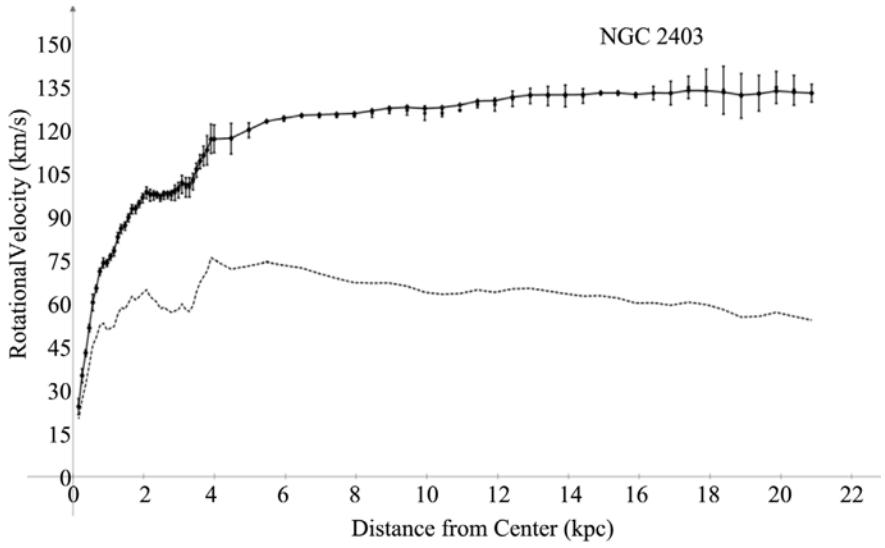
NGC 2403
RotationalVelocity (km/s)
150 135 120 105 90 75 60 45 30 15 0
0 2 4 6 8 10 12 14 16 18 20 22
Distance from Center (kpc)

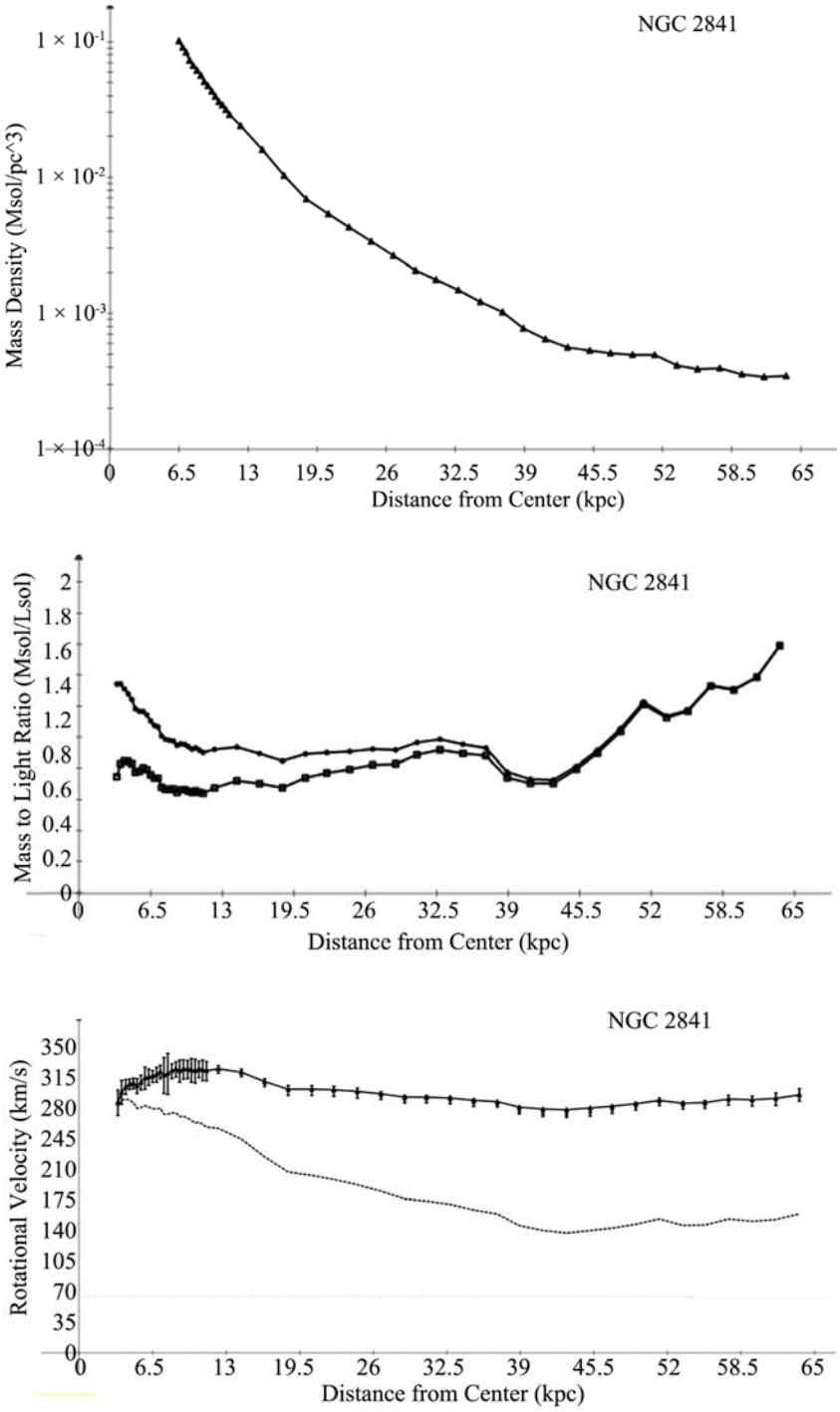


**Figure 2.** NGC 2403 and NGC 2841. Fits with SPARC data, the masses derived from (80) and (81) with velocity profiles for gas, disk and bulge. For mass to light curves, $\Upsilon_{dsk}$ is the solid line and filled circles, $\Upsilon_{bul}$ is the solid line and open squares. For rotation velocity curves, the solid line is the minimised fit to the data with the graviton model (82) and the dashed line is the Newtonian velocity. Top Half: Upper: Mass density. Middle: Mass to light ratio. Lower: The model velocity vs. radial distance from the galactic center and the Newtonian velocity. Bottom Half: Upper: Mass density. Middle: Mass to light ratio. Lower: The model velocity vs. radial distance from the galactic center and the Newtonian velocity.

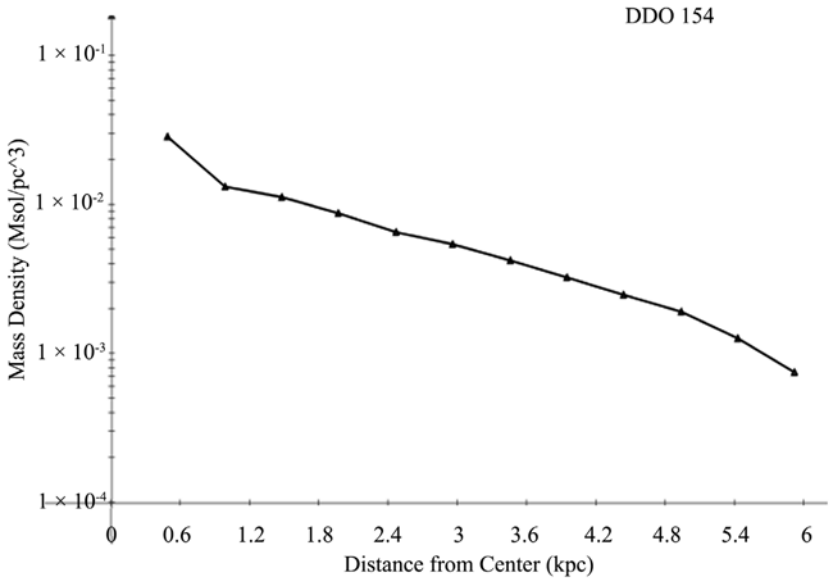
DDO 154
Mass Density (Msol/pc^3)
1 × 10-1
1 × 10-2
1 × 10-3
1 × 10-4
0
0.6
1.2
1.8
2.4
3
3.6
4.2
4.8
5.4
6
Distance from Center (kpc)

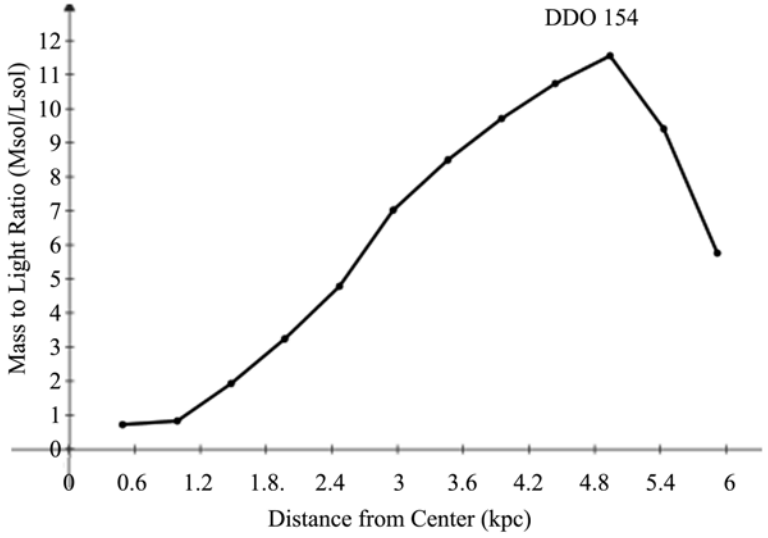
DDO 154
Mass to Light Ratio (Msol/Lsol)
0
1
2
3
4
5
6
7
8
9
10
11
12
0
0.6
1.2
1.8.
2.4
3
3.6
4.2
4.8
5.4
6
Distance from Center (kpc)

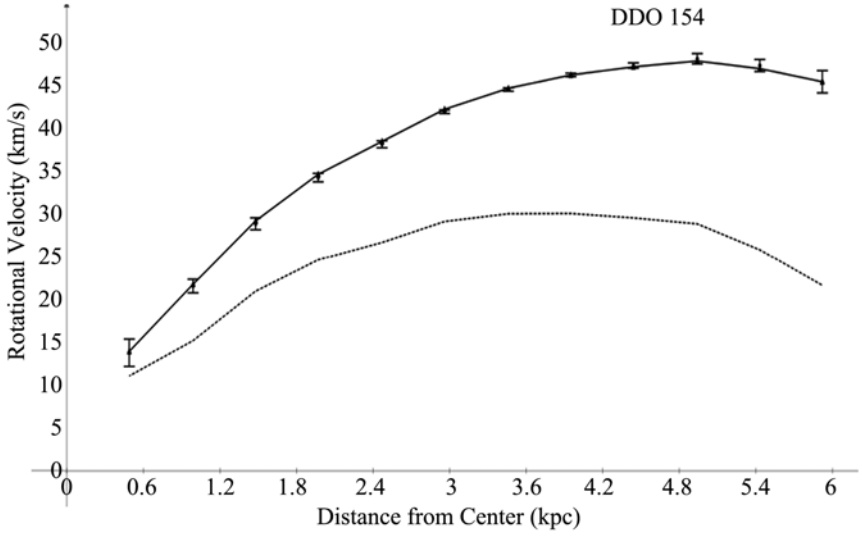
DDO 154
Rotational Velocity (km/s)
0
5
10
15
20
25
30
35
40
45
50
0
0.6
1.2
1.8
2.4
3
3.6
4.2
4.8
5.4
6
Distance from Center (kpc)

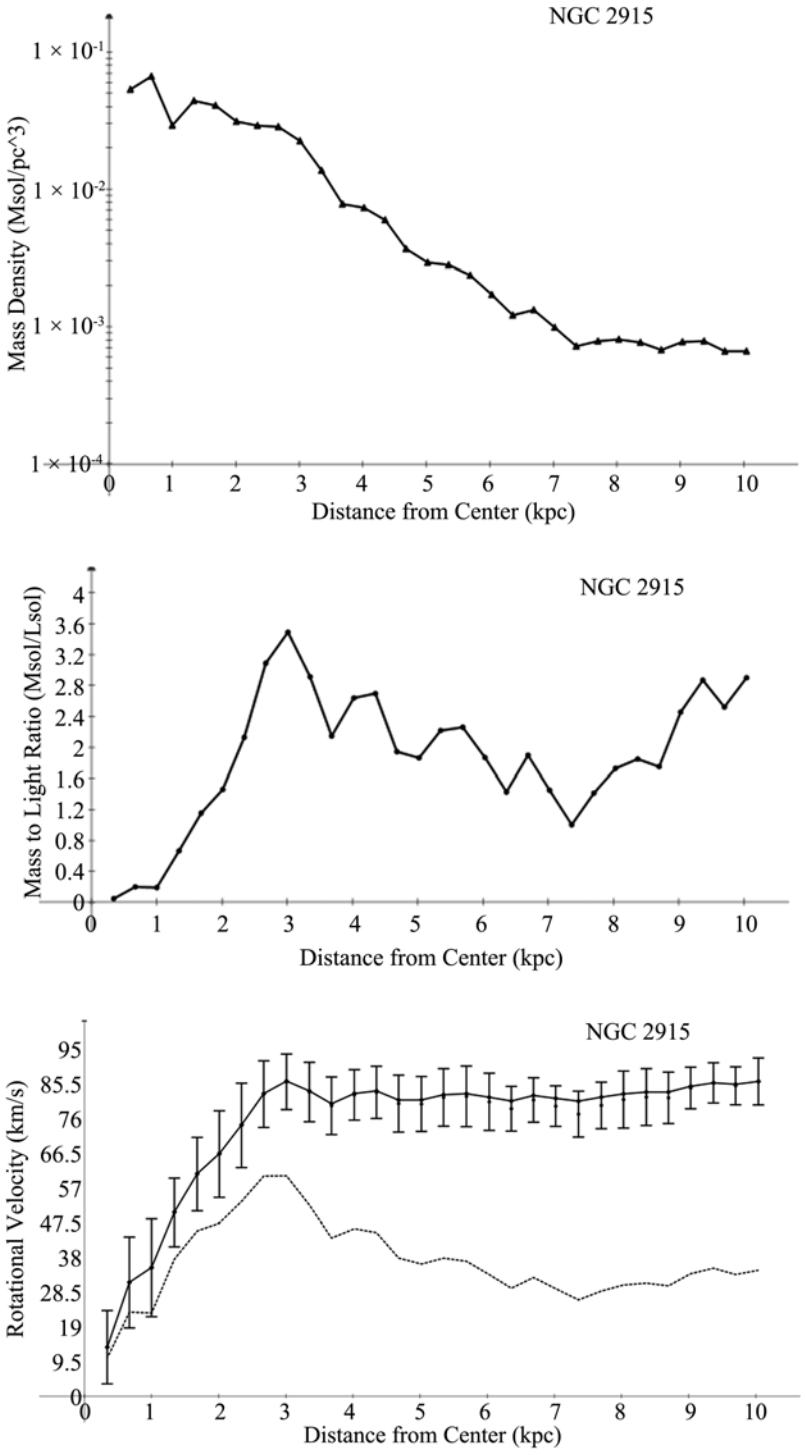


**Figure 3.** DDO 154 and NGC 2915. Fits with SPARC data, the masses derived from (80) and (81) with velocity profiles for gas, disk and bulge. For mass to light curves, $\Upsilon_{dsk}$ is the solid line and filled circles. For rotation velocity curves, the solid line is the minimised fit to the data with the graviton model (82) and the dashed line is the Newtonian velocity. Top Half: Upper: Mass density. Middle: Mass to light ratio. Lower: The model velocity vs. radial distance from the galactic center and the Newtonian velocity. Bottom Half: Upper: Mass density. Middle: Mass to light ratio. Lower: The model velocity vs. radial distance from the galactic center and the Newtonian velocity.

particles do not exist, then in density perturbations of the primordial plasma just before recombination, the baryons, photons and gravitons are synchronized and there is not a central region of dark matter particles as theorized in the standard model [24], so that when recombination begins the photons dissociate from the electrons and the resultant hydrogen atoms begin to attract and form dense regions in the perturbation. Just how the graviton redshift energy loss affects the density formations in the primordial plasma and how this affects the determination of the Hubble constant from the BAO and CMB modeling [25] is an area which needs to be studied.

Regarding galaxy dynamics, with the modified Newtonian dynamics (MOND) [26] [27] there may be a way to compare it with the graviton gravitational redshift theory. MOND takes effect in galaxies at a distance where the central acceleration is around $1.2 \times 10^{-10}$ m·s$^{-2}$ by effecting a transition in the gravitational attractive force from a $r^{-2}$ to a $r^{-1}$ form. On the other hand, the graviton gravitational redshift theory augments the Newtonian rotational velocity beginning from the galactic center, which allows to distinguish it from MOND. Referring to **Figure 2**, at a radius of $r = 24.59$ kpc the spiral galaxy NGC 2841 has an observed velocity of $V = 298.0\ \mathrm{km \cdot s^{-1}}$ and we calculate the Newtonian velocity of $V_N = 191.5\ \mathrm{km \cdot s^{-1}}$ using the SPARC data. The radial acceleration at this distance is $Acc = V^2/r = 1.171 \times 10^{-10}\ \mathrm{m \cdot s^{-2}}$ which is at the beginning of the MOND regime and, assuming we have the correct baryon mass within that radius, MOND would predict an orbital velocity smoothly connected to the Newtonian value $V_N$ but we see that it would be smaller than $V$ by 106.5 km·s$^{-1}$.

Another interesting alternative approach to modified Newtonian dynamics is given in [28] which, by way of an additive inverse Yukawa-like term to Newtonian gravitation, purports to account for gravitational dynamics from solar systems to galaxies and galaxy clusters and to the large scale universe expansion. There is an analogy between (Ref. [29] Equation (19)) and our (54) which can to be further explored.

## 9. Conclusions

The graviton self interaction model describes the effect of gravitons in free fall in the gravitational field, losing energy by way of gravitational redshift and cosmological redshift without emitting any radiation. General Relativity was applied for both the universe expansion and for spiral galaxy rotation curves. By assuming a coupling coefficient $K_{dm}$ for the graviton redshift in free fall, the graviton model can account for the apparent dark matter in the universe being related to the baryon density. Likewise, the dark energy depends on the coupling constant $\sigma_{de}$ and the baryon density. Thus, the apparent dark matter and dark energy are replaced by two constants and the hypothesized redshift of graviton energy.

In the case of the rotational characteristics of spiral galaxies, the graviton theory well explains the greater than expected galaxy rotational velocities in the SPARC data with only the baryonic mass derived from the gas, disk and bulge

velocity data with fitted $\Upsilon_*$ ratios, with a galaxy dependent coupling coefficient $K_g$ and with the total baryon mass conforming to the BTFR.

It is apparent that the fundamental aspect of graviton redshift points to the need to include this in the General Relativity field equations.

## Conflicts of Interest

The author declares no conflict of interest.

## References


[1] Oliveira, F.J. (2022) *Journal of High Energy Physics, Gravitation and Cosmology*, **8**, 579-592.

[2] Oliveira, F.J. (2022) *Journal of High Energy Physics, Gravitation and Cosmology*, **8**, 810-834. https://doi.org/10.4236/jhepgc.2022.83055

[3] Deur, A. (2009) *Physics Letters B*, **676**, 21-24. https://doi.org/10.1016/j.physletb.2009.04.060

[4] Wikipedia. Lambda-CDM Model. https://en.wikipedia.org/wiki/Lambda-CDM_model

[5] Hubble, E. (1929) *Proceedings of the National Academy of Sciences*, **15**, 168-173. https://doi.org/10.1073/pnas.15.3.168

[6] Friedmann, A. (1922) *Zeitschrift für Physik*, **10**, 377-386. https://doi.org/10.1007/BF01332580

[7] Lemaître, G. (1931) *Monthly Notices of the Royal Astronomical Society*, **91**, 483-490. https://doi.org/10.1093/mnras/91.5.483

[8] Robertson, H.P. (1935) *The Astrophysical Journal*, **82**, 284-301. https://doi.org/10.1086/143681

[9] Walker, A.G. (1937) *Proceedings of the London Mathematical Society, Series* 2, **42**, 90-127. https://doi.org/10.1112/plms/s2-42.1.90

[10] Einstein, A. (1918) Über Gravitationswellen. Sitzungsberichte der Königlich Preußischen Akademie der Wissenschaften (Berlin), Seite 154-167. https://ui.adsabs.harvard.edu/abs/1918SPAW.....154E/abstract

[11] Einstein, A. (1952) The Foundation of the General Theory of Relativity. Dover Publications, Inc., New York.

[12] Suzuki, N., Rubin, D., Lidman, C., Aldering, G., Amanullah, R., Barbary, K., *et al.* (2011) *The Astrophysical Journal*, **746**, Article ID: 22011768. https://doi.org/10.1088/0004-637X/746/1/85

[13] Lahav, O. and Liddle, A.R. (2010) The Cosmological Parameters. Chapter 21. https://pdg.lbl.gov/2011/reviews/rpp2011-rev-cosmological-parameters.pdf

[14] Tanabashi, M., *et al.* (2018) *Physical Review D*, **98**, Article ID: 030001. https://pdg.lbl.gov/2018/reviews/rpp2018-rev-bbang-nucleosynthesis.pdf

[15] http://astroweb.cwru.edu/SPARC

[16] Lelli, F., McGaugh, S.S. and Schombert, J.M. (2016) *The Astronomical Journal*, **152**, 157-170. https://doi.org/10.3847/0004-6256/152/6/157

[17] McGaugh, S.S. (2005) *The Astrophysical Journal*, **632**, 859-871. https://doi.org/10.1086/432968

[18] Lelli, F., McGaugh, S.S. and Schombert, J.M. (2016) *The Astrophysical Journal Letters*, **816**, L14-L19. https://doi.org/10.3847/2041-8205/816/1/L14

[19] De Blok, W.J.G. and McGaugh, S.S. (1997) *Monthly Notices of the Royal Astronomical Society*, **290**, 533-552. https://doi.org/10.1093/mnras/290.3.533

[20] Li, P., Lelli, F., McGaugh, S.S. and Schombert, J.M. (2018) *Astronomy & Astrophysics*, **615**, A3. https://doi.org/10.1051/0004-6361/201732547

[21] Carignan, C. and Purton, C. (1998) *The Astrophysical Journal*, **506**, 125-134. https://doi.org/10.1086/306227

[22] Meurer, G.R., Carignan, C., Beaulieu, S.F. and Freeman, K.C. (1996) *The Astronomical Journal*, **111**, 1551-1575. https://doi.org/10.1086/117895

[23] Meurer, G.R., Blakeslee, J.P., Sinanni, M., Ford, H.C., Illingworth, G.D., Benitez, N., *et al.* (2003) *The Astrophysical Journal Letters*, **599**, L83-L86. https://doi.org/10.1086/381317

[24] Beutler, F., Blake, C., Colless, M., Jones, D.H., Staveley-Smith, L., Campbell, L., *et al.* (2011) *Monthly Notices of the Royal Astronomical Society*, **416**, 3017-3032. https://doi.org/10.1111/j.1365-2966.2011.19250.x

[25] Planck Collaboration, Aghanim, N., Akrami, Y., Ashdown, M., Aumont, J., Baccigalupi, C., Ballardini, M., *et al.* (2020) *Astronomy & Astrophysics*, **641**, 67-139.

[26] Milgrom, M. (1983) *The Astrophysical Journal*, **270**, 365-370. https://doi.org/10.1086/161130

[27] Milgrom, M. (1983) *The Astrophysical Journal*, **270**, 371-383. https://doi.org/10.1086/161131

[28] Falcón, N. (2013) *Journal of Modern Physics*, **4**, 10-18. https://doi.org/10.4236/jmp.2013.48A003

[29] Falcón, N. (2021) *Journal of Astrophysics and Astronomy*, **42**, Article No. 102. https://doi.org/10.1007/s12036-021-09752-0

Scientific Research Publishing

Journal of Modern Physics, 2022, 13, 1369-1381
https://www.scirp.org/journal/jmp
ISSN Online: 2153-120X
ISSN Print: 2153-1196

# Real Quanta and Continuous Reduction

**Antony J. Bourdillon**

UHRL, San Jose, CA, USA
Email: bourdillona@sbcglobal.net

**How to cite this paper:** Bourdillon, A.J. (2022) Real Quanta and Continuous Reduction. *Journal of Modern Physics*, **13**, 1369-1381.
https://doi.org/10.4236/jmp.2022.1311085

**Received:** September 14, 2022
**Accepted:** November 4, 2022
**Published:** November 7, 2022



## Abstract

Previous theories of quasicrystal diffraction have called it "Bragg diffraction in Fibonacci sequence and 6 dimensions". This is a misnomer, because quasicrystal diffraction is not in integral linear order $n$ where $n\lambda = 2d\sin(\theta)$ as in all crystal diffraction; but in irrational, geometric series $\tau^m$, that are now properly indexed, simulated and verified in 3 dimensions. The diffraction is due not to mathematical axiom, but to the physical property of dual harmony of the probe, scattering on the hierarchic structure in the scattering solid. By applying this property to the postulates of quantum theory, it emerges that the 3rd postulate (continuous and definite) contradicts the 4th (instantaneous and indefinite). The latter also contradicts Heisenberg's "limit". In fact, the implied postulates of probability amplitude describe hidden variables that are universally recognized, in all sensitive measurement, by records of error bars. The hidden variables include momentum quanta, in quasicrystal diffraction, that are continuous and definite. A revision of the 4th postulate is proposed.

## Keywords

Quasicrystal, Icosahedra, Hierarchic, Periodic, Harmonic, Irrational, Geometric Series, Metric, Resonant Response, Dispersion Dynamics

## 1. Introduction

Einstein claimed Bohr's theory is incomplete: "the wave function does not provide a complete description of the physical reality" [1]. Their views represented two physics in schism [2]. Quanta are fundamental. Our theory of diffraction in quasicrystals is falsifiable and verified [3].

The quanta are not only harmonic; but harmonic in dual series: geometric and linear. Many have believed the quantum is real, rather than conceptual and axiomatic. The quasicrystal proves its reality. The formula for the free electron or photon probe, that consistently and realistically describes interactions by the dual wave-particles, can be further used to describe the reduction of the wave

packet in space and time. The real probe bridges a short-cut that is taken by the method of mathematical probability amplitudes. The quantum finds new expression in the peculiar diffraction that we observe in quasicrystals [3].

Consider the quantum wave-packet in momentum space: in a scattering crystal, both the probe wave-packet and Bragg diffraction are periodic, while their interaction is *harmonic* in space and time, by *linea*r, *integral* orders. By contrast, diffraction from quasicrystals occurs *in geometric series* of *irrational* orders [4]. This scattering corresponds to hierarchic structure in the quasicrystal. It turns out that the quasi-Bloch waves—that are generated by the hierarchic scatterer and that mediate the quasi-Bragg diffraction—are dual harmonic in both geometric and linear series: the periodic probe scatters into geometric space.

How, we ask, does this realistic, dual harmony in the quasicrystal compare with the following 4 postulates of orthodox quantum mechanics [5]:

1) *Representational completeness of $\phi$.* The rays of Hilbert space correspond one-to-one with the physical states of the system.

2) *Measurement.* If the Hermitian operator $A$ with spectral projectors $\{P_k\}$ is measured, the probability of outcome $k$ is $\langle\phi|P_k|\phi\rangle$. These probabilities are objective, *i.e.* indeterminate.

3) *Unitary Evolution of isolated systems:*

$$|\phi\rangle \to U|\phi\rangle = \exp\left(-\hbar^{-1}Ht|\phi\rangle\right)$$

and therefore deterministic and continuous.

4) *Evolution of systems undergoing measurement.*

If Hermitian operator $A$ with spectral projectors $\{P_k\}$ is measured and outcome $k$ is obtained, the physical state of the system changes discontinuously:

$$|\phi\rangle \to |\phi_k\rangle = P_k(\phi)\Big/\sqrt{\langle\phi|P_k|\phi\rangle}$$

Notice the opposites in the 3rd and 4th postulates: the unitary evolution is continuous and deterministic; the measurement is discontinuous and indeterminate. Heisenberg's uncertainty "limit" seems to have been arbitrarily discarded. The examination of dual harmonies in the wave-packet, preserves his limits.

In this paper, we consider first the probe, with group velocity and phase velocity variables; then illustrate dual quanta in quasicrystals; and finally describe the evolutionary reduction of the wave-packet using the known variables. The treatment is not so much probabilistic as classically crystallographical. Wherever measurement predictions are calculated to be the same in realistic theory as in probabilism, the theories are, in logic, equally "true"; however, the dual harmonics in quasicrystals demand redefinition of the quantum, and they are consistent with continuous change during measurement.

## 2. Wave-Packet

Consider the interaction, in time and space, between an X-ray or electron wave-packet and a quasicrystal. This stable wave-packet [6] is deduced from the combination of wave-particle duality, Maxwell's electromagnetism, special relativity,

Planck's law, and the de Broglie hypothesis, all expressed in simplified units with unified reduced Planck constant $\hbar = 1 = c$, the speed of light. The rest mass (zero for the photon) of the probe is given by:

$$m_o^2 = \omega^2 - k^2 = (\omega + k)(\omega - k) \tag{1}$$

where $\omega$ is its angular frequency; $k$ its wavevector; and $m_o$ its rest mass (zero for the photon). The equation is separable into conservative and responsive parts. For a normal free particle, the wave function may be expressed[1]:

$$\varphi(t,x) = A\exp\left(\frac{X^2}{2\sigma^2} + X\right) \text{ with imaginary: } X = i(\bar{\omega}t - \bar{k}x) \tag{2}$$

where uncertainty $\sigma$ depends on initial conditions that determine coherence of a packet in space and time (in manifold rank $\Re^4$) and where $A^2$ is a normalizing constant[2]. The variables $\bar{\omega}$ and $\bar{k}$ are mean values. The Gaussian envelope function is conservative and contains energy, momentum, mass density, intrinsic spin etc. The imaginary factor in exp($X$) is responsive as an infinite wave with uniform density for all $x$ and $t$: ($e^X$) * ($e^X$) = 1. It describes interference, superposition, entanglement, creation, annihilation, harmony, resonance, etc. Equation (2) is not only *stable* mathematically with energy and momentum conservation; but it represents stable photons from the microwave background that have travelled 13 billion light years (cf. [7]).

The packet has many special properties. Differentiation of Equation (1) provides the equations for dispersion dynamics [6] in simplified units, including:

$$\frac{\omega}{k} \cdot \frac{\mathrm{d}\omega}{\mathrm{d}k} = 1 \tag{3}$$

where the normalized phase velocity of the wave $v_p/c = \omega/k$. Notice this phase velocity, *in vacuo*, is—for particles with mass $m_o > 0$—faster than the speed of light $c$. It does not conflict with relativity because the phase does not carry energy and is not measurable directly, but it is a real part of physics and we apply it below. The beat velocity is the normalized group velocity, $v_g/c = \mathrm{d}\omega/\mathrm{d}k$ [3] [6]. Notice that the group, velocity $v_g/c = (\mathrm{d}\omega/\mathrm{d}k)^{-1}$ = energy/momentum, and is the velocity of the reference frame in relativity, *i.e.* less than the speed of light. For a free particle, $v_g/c = k/m'$, *i.e.* momentum/relativistic mass.

The phase velocity $v_p$ is the ratio of the two most measured variables in atomic physics and is very easily derived from the free particle wave equation $e^X$, while it is totally ignored in texts about quantum theory and even denied [7]. Its inverse $v_g$ by comparison, that is theoretically derived with comparative difficulty as beat velocity, is the dominant variable in special relativity and even in quantum mechanics. As we illustrate below, the neglect of $v_p$ causes major confusion, *e.g.* in collapse.

The probe is uncertain in space and time [8]:

[1]We let $\phi$ stand for a density function of either photon or electron.

[2]In the simplest case with $k$ linear, $A^*A = 2\Big/\left(\int \exp\left(X^2/\sigma^2\right)\mathrm{d}\tau\right)$.

$$\Delta\omega \cdot \Delta t = 8;\ \Delta k_i \cdot \Delta i = 8,\ i = x, y, z \tag{4}$$

since $\sigma$ (in Equation (2)) cancels after Fourier transformation. We shall consider uncertainty in collapse after reporting on the reality of dual harmonics in quasicrystals.

Notice that this physical result is sharply distinguished from signal processing of electromagnetic waves: in *the latter case*, $c$ depends on physical laws that are invariant in all inertial reference frames, so that, wherever $m_o = 0$, $v_p = c = v_g$. The speeds may be measured by reflections of signals into space, or from interferometry. However, in *the former case*, as applied to electron microscopy, $v_g \ll c$ so that $v_p \gg c$. We will apply this internal motion of the wave packet in double slit interference.

Moreover, the wave-packet has remarkable properties that have been overlooked in standard quantum mechanics. The packet enables spatial entanglement in the propagation direction as in the transverse directions, and also enables action at distances, with speeds faster than $c$, in waves representing massive particles. We shall return to this property in the context of Young's double slit experiment, but are uncommitted regarding and Bell's inequalities and observations from crossed polarizers.

## 3. Hierarchic Structure

The probe just described diffracts off a hierarchical quasicrystal (QC) with icosahedral symmetry in its diffraction pattern. Not only is the pattern forbidden in Bragg diffraction from crystals, but so also are the diffraction orders which are in geometric series that is emphatically inconsistent with the integral orders $n$ in Bragg's law: $n\lambda = 2d\sin(\theta)$, where $\lambda = 2\pi/k$ is the probe wavelength; $d$ is the interplanar spacing for a particular diffraction beam; and $\theta$ is half the scattering angle. The law is very well understood in terms of harmonic reflections of the periodic probe from atomic sites that are periodic and crystalline. By contrast, quasicrystal diffraction is often misnamed "Bragg diffraction in Fibonacci series", which is a contradiction in terms for reasons already given. *A priori*, relationships between $n$, $\lambda$, $d$ and $\theta$ are undefined. We had to work out both the law of quasicrystal diffraction and to understand the harmonies that are required between the periodic probe and the geometric series diffraction. It is obvious that the quasicrystal is structured from *hierarchically* arranged icosahedra because—especially after the unit cell is identified and measured—this introduces the geometric series with the point group symmetry of the pattern. Moreover, the unit cell is icosahedral and is extremely dense owing to the precise diameters not only of *Mn* and *Al* atoms in the first quasicrystal observed [4] but of all of the diatomic 1:6 quasicrystals subsequently reported. The structure is therefore *uniquely* icosahedral.

Furthermore, complete indexation in three dimensions was developed from a stereogram of the icosahedral structure, both for the principal axes as for the diffraction planes that are normal to them. The indexation was three dimension-

al and geometric, which excludes the prior usage of six dimensions. Dimensions should not be multiplied without necessity. The indexation of the diffraction pattern is complete [4].

From the hierarchic structure, quasi-structure factors could be calculated by formulae [4] that are modified from classical structure factors for crystals. The modifications included, firstly a scaling factor $c_s$ to compensate for the (linear) aperiodicity of the structure that causes surprisingly sharp diffraction; and secondly an iterative procedure that summed quasi-structure factors over a large quasicrystal of selected order so as to account for the aperiodicity of the unit cell. By numerically scanning values for $c_s$, it was found to maximize at a unique value for all quasi-Bragg reflections. Applying this value, the calculations provided a range of intensities that matched very well the wide range of experimental values observed in the diffraction patterns. Not surprisingly, the structure factor intensities were all close to zero at Bragg scattering angles, but consistent with experimental line intensities at scattering angles that were larger than defined by Bragg's law[3]. The divergence from the Bragg condition depends on the coherence factor, $c_s = \theta/\theta'$: the Quasi-Bragg law was therefore deduced:

$$\tau^m \lambda = 2d' \sin\left(\theta'\right) \tag{5}$$

for the simplest index ($h$, 0, 0) with $\tau = \left(1+\sqrt{5}\right)\Big/2$, *i.e.* the golden section, and with interplanar spacing:

$$d' = a'\left(h^2 + k^2 + l^2\right)^{-1/2} \tag{6}$$

having generally irrational values $h$, $k$, $l$, for each a member of the series 0, $\tau^{-1}$, 1, $\tau$, …, $\tau^m$, …, and having quasi-lattice parameter $a'$, which was consistently measured in the conventional way [9]. The primes indicate modified versions of Bragg variables as they apply to QC diffraction (Equation (5)).

## 4. Summary of the Analytic Derivation

Whether the QC diffraction series is Fibonacci or geometric is nominal, since the following identities can easily be demonstrated by mathematical induction: [9]:

$$\tau^m = F_m\left(1,\tau\right) = \delta_{m,1} + F_m\left(0,1\right) + F_m\left(0,1\right)\tau \tag{7}$$

where the brackets define the bases for the $m^{\text{th}}$ term of the Fibonacci series $F_m$ and $\delta_{m,1}$ is the Kronecker delta. The geometric series is irrational, but Equation (7) shows how it can be separated into a natural part, $\delta_{m,1} + F_m(0, 1)$, and irrational part, $F_m(0, 1)\tau$. By substituting the last $\tau$ by 3/2, an approximate natural value for $\tau^m$ is obtained, and subtraction of this approximate natural value from the original irrational geometric number, yields an extraordinary and exact value

[3]In crystals, structure factors are calculated from atoms in a unit cell, and the number of values is therefore restricted. In pure *Al*, for example, there are only two values: 0 (when half the atoms scatter in antiphase) or 4. In quasicrystals, the quasi-structure factors are calculated over all the scattering atoms in selected structural orders of clusters, superclusters *etc.* This calculation is performed iteratively.

$1/c_s$. which we will call also the metric function (Equation (8)). The match is emphatically extraordinary because the comparison is between numeric and analytic answers**,** that are the same for all $m$, *i.e.* $\tau - 0.5$.

The exact match clarifies the nature of $c_s$. The irrational part of the index provides a scaling factor for the scattering of probe by specimen, that results in dual harmonics in the diffraction (Section 4). The scaling factor describes a ratio between a Bragg angle from a cubic crystal having lattice parameter $a$ and integral indexation, from a corresponding quasi-Bragg angle in quasicrystals with quasi-lattice parameter $a'$ and geometric indexation. The ratio results from path differences between neighboring rays in the quasi-Bragg scattering [10]. The irrational part, phase shifts the ray paths that are longer than in Bragg diffraction. The result is that corresponding quasi-Bragg diffraction angles are not only sharply defined; but are fractionally larger by ~11.18… % after allowing for different indexations in electron microscopy where $\sin(\theta) \sim \theta$. The fraction is the peculiar consequence of the ideal icosahedral, hierarchic structure. The diffraction pattern is a map of quantized momentum transfers. The dual harmonics determine the momentum quanta that define quasicrystal diffraction patterns. The following illustration is by quasi-Bloch waves that are stimulated by the interaction of the probe that scatters inside the quasi-lattice.

## 5. Dual Harmonies That Occur in Irrational, Geometric Order

The diffraction mechanism by quasi-Bloch waves in QCs at the quasi-Bragg condition, illustrates consequences of the irrational QC diffraction. In a crystal oriented to a first order Bragg condition, an advancing high-energy electron-beam interacts with the reflecting lattice to form two momentum dispersed Bloch wave bands [11]. Relative intensities of the zeroth order and first order beams depend on specimen thickness and on specimen orientation, and they form regular fringes in wedge foils; and lattice images in high resolution imaging [12]. The images are commensurate with the unit cell and with all cells periodically repeating. This is represented in the blue wave of **Figure 1**. However, these periodic Bloch waves are incommensurate with the hierarchic quasi-lattice that is geometric and irrational. However if their scale is multiplied by the metric function (Equation (8)) [3] [9];

$$\frac{1}{c_s} = 1 + \frac{\tau^m - F_{m+4}/2}{F_{m+1}} = \frac{1}{0.894} \tag{8}$$

the (red) wave becomes commensurate with the geometric quasi-lattice both long-range, and simultaneously at linear short-range on each geometric intercept, *i.e.* for all $m$. In Equation (8), $F_m$ represents the Fibonacci sequence, base (0, 1). The quasi-Bloch wave is translationally invariant about all geometric intercepts $a'\tau^m$. Notice that the spacings between intercepts are in Fibonacci series that are represented by the denominator in Equation (8), $F_{m+1}$.

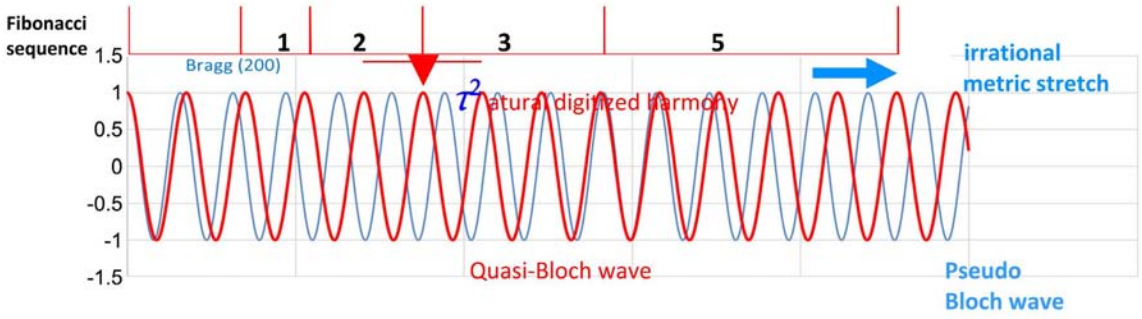


**Figure 1.** Crystalline Bloch waves (blue) are commensurate with their unit cell and corresponding periodic crystal lattice at the Bragg condition. When this wave is stretched horizontally by the inverse coherence factor $1/c_s$, the quasi-Bloch-wave (QBW in red) commensurates with the irrational, geometric and hierarchic, quasi-lattice. Its geometric order is represented by the intercepts on the horizontal line above it. The digitized number of periodic cycles between successive intercepts is in Fibonacci sequence (denominator in equation 8), and the diffraction is logarithmically periodic. The natural and irrational parts of the indices are separable: the irrational part is expressed by the metric stretch; the natural part scatters with sharp, coherent diffraction [3].

*Most Important is the fact that the quasi-Bloch wave is dual harmonic.* The irrational part of any index is represented by the metric function (Equation (8)) and this digitizes the periodic probe, which commensurates with the hierarchic lattice. The fractional increase in ray paths causes an 11.18… per cent increase in scattering angle. The dual harmony enables the periodic probe to scatter coherently from the hierarchic lattice onto a geometric reciprocal lattice with a peculiar and precise quasi-lattice constant $a'$ [3].

It is obvious that the dual harmony forces the quantization of the momentum that is evident in the diffraction pattern. *It is reasonable to make the hypothesis that all quantization is the result of—not the cause of—harmonic dynamic variables.* Further confirmation may, in future, be found from multi-slice calculations of quasi-Bloch wave intensities as probe interacts with specimen. This becomes more feasible now that $c_s$ is known, understood and applied with geometric band-gaps in momentum space [11].

Notice that this discovery of dual harmony in QC diffraction is realistic rather than mathematical: the solution is three dimensional, geometric, and classical with harmonies in space and time. By contrast mathematicians have digressed with six dimensions for "Fibonacci sequences" in abstruse tiling and unexplained diffraction [13].[4]

## 6. Hidden Variables

> "It was [Einstein's] almost solitary conviction that quantum mechanics is logically consistent but that it is an incomplete manifestation of an underlying theory in which an objectively real description is possible—a position he maintained until his death" ([14] p. 433).

Einstein's EPR thought experiment has not resolved his differences with

[4]Incidentally, another example of dual harmony is the 12 point chromatic scale in Western music, which is, conversely, irrational short range ( $\times\sqrt[12]{2}$ ) and linear long range (×2).

Bohr[5]: the former realistic, the latter probabilistic. The difference is partly nominal because a realist variable that is truly hidden can be represented, in epiphenomenal mathematics, by a probability amplitude. That is why mathematicians have been content to "choose" their lattice parameter [3] [4], instead of measuring it, and thereafter to "apply" Bragg's law in six invented dimensions. By contrast, the metric function is derived, observed and verified in three dimensions. The derivation occurs by applying observed, irrational indices to a modification of the classical theory, and the derivation is therefore realistic.

This is not to deny that the probability amplitude, that is used for example in elementary particle interactions, has been extraordinarily successful. However, the standard theory is indistinguishable from a realist theory when the probability amplitude expresses hidden variables. This is consistent with "mad-dog Everettianism" [5]: we have the Schrödinger equation and a wave function and that is all, with no metaphysics and no phenomenalism.

Sometimes a "hidden variable", such as phase velocity, becomes useful to explain a long-known property such as intrinsic spin, and to discover new dependent properties such as its magnetic radius [15]. As another example, the hidden variable that determines the direction of spontaneous emission is, by momentum conservation, atomic recoil, the same recoil as is acknowledged in the Schrodinger eigenvalues by reduced mass on the electron. In this paper, we use phase velocity that derives directly from special relativity and can be used to describe the otherwise instantaneous and problematic collapse of the wave packet when a measurement is made (Section 6). The phase velocity is hidden because it is faster than the speed of light, and because it does not carry energy; this is carried by conservation in the group velocity. However, when the angular frequency and wavelength of an interacting particle is known, the phase velocity is sometimes informative. It is simpler in concept ($\omega/k$) than the more easily measured group velocity $\mathrm{d}\omega/\mathrm{d}k$. For many such reasons, the wavefunction cannot be complete. The realistic quantum that we have described implies continuity in the final realistic collapse upon measurement (*cf.* postulate 4).

## 7. Operators and Reduction of the Wave-Packet

Equations (1) and (2) describe a *stable* wave-packet because $\bar{\omega}$ and $\bar{\boldsymbol{k}}$ are conserved. They represent photons that are more than 13 billion light years old, when measured in the microwave cosmic background, to an accuracy of $1{:}10^5$. They are mathematically conserved by mean energy and momentum; so can hardly be unstable (cf. [7]). The equations also apply to free electrons in high energy electron diffraction.

To show that the photon is consistent with mainstream quantum mechanics, we need to show that it responds consistently with known operators. Consider firstly, the energy operator in Schrödinger's equation:

[5]Though it is obvious that if reference frames are not held stable, Einstein could not measure, by conservation laws, the momentum on Bohr's electron.

$$\hat{\varepsilon} = -i\hbar \cdot \partial\phi/\partial t \tag{9}$$

Then by applying to Equations (2) with the chain rule:

$$\left\langle \phi^* \right| -i\hbar \frac{\partial}{\partial t} \left| \phi \right\rangle = \left\langle \phi^* \right| \omega(2X+1) \left| \phi \right\rangle \tag{10}$$

the integral over $X$, in the antisymmetric first term of the bracket operating on symmetric $\phi$ is zero. The second term provides the expectation $\langle \varepsilon \rangle = \bar{\omega}$, in absence of Schrödinger's central potential etc.

Similarly,

$$\langle \boldsymbol{k} \rangle = -\bar{\boldsymbol{k}}_x \tag{11}$$

With this consistency, we proceed to consider the reduction of the wave-packet in space and time. Particularize with observations on a Young's slit experiment in strong beam and weak beam (Figure 2) ([16] p. 262). After taking account of different $\lambda$ and $m_o$, electrons produce corresponding interference patterns to Young's. Suppose an *electron is a point particle* that may be incident on slit B as a single time-resolved event. In weak beam, individual scintillations are observed in the image plane (green pattern), but the pattern is different if slit A is open (upper red pattern) or closed (lower red pattern). Bohr claimed that the calculated wave function is a probability amplitude. He held no way of predicting precisely where an individual event would be recorded on the image plane. Einstein objected that his interpretation of probability amplitudes implies "spooky action at a distance", which is unsatisfactory as an explanation because information about the state of A would be needed at B by a speed faster than light.

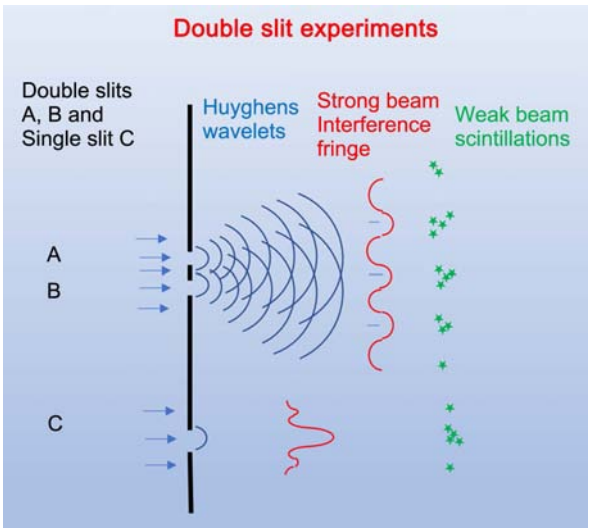


Figure 2. A bright incident beam, transmitted by Young's double slit, forms a regular interference pattern in the image plane (upper red). When the beam intensity is weak, scintillations may be counted on the plane (green) while, after a long time, the pattern approximates to the strong beam pattern. A single electron passing through slit B would require "spooky action at a distance" to respond to either slit A open (upper red) or A closed (lower red).

However, when we consider the wave function to be a probability amplitude that is due to hidden variables, including $v_p$, then the information at A (whether open or closed) may be carried to B through those variables in the following way.

The wave-packet described by Equation (2) is extended by $\sigma_x$ in both time and $x$-space so that transverse waves have time $\Delta t$ to interact after passing through the slit(s), and the interference is as Young observed it (Figure 2) with the transverse uncertainty $\sigma_y$ that can be estimated. There is no spooky action at a distance, and no instantaneous collapse: Notice that across the wavefronts in Figure 2, time is constant and locally Newtonian. The waves, as they advance, interact long range with scintillator atoms in their general path: some will resonate in phase causing the transverse density function to accelerate across the front in response, further exciting a scintillating molecule. Any resonant molecule will compete with other molecules to absorb energy from the electron, so that energy will eventually be captured when the wave front becomes localized. Subsequently decay occurs by photo-emission.

Electron-scintillator resonance corresponds to photon resonance, which is simple since in vacuo, the components $v_p^i = v_g = c$. Absorption depends on the oscillator strength $|<|er/4\pi\epsilon_0|>|^2$ around the excited molecule. Typically, since the scintillation energy of de-excitation is similar to the probe photon energy, its absorption is an all-or-nothing event.

Consider the "collapse" of Bohr's wave-packet that is supposed to occur when an event is recorded by scintillation or chemical reaction on photographic emulsion. In the standard theory, by definition of the wavefunction, the event is only probable and never predictable for particular quanta. However, as with the interference pattern, a realistic wavefunction undergoes a different sequence. The real interference occurs throughout the space between slits and image plane, as a superposition of excitations from the double slit. Moreover, this pattern extends in both time and space (Equations (2)). As the superposition approaches the image plane it interacts, in time and space, with the chemicals on the image plane, some of which will—depending on hidden variables—resonate, typically through electric permittivity. Resonances will appear and there may be a mutual forward-backward response through the extended wave-packet, leading to concentration of the wave-packet near a molecule and localization as the excitation grows. Final absorption will occur in time $\Delta t \sim 8/\Delta\omega$, within typical scattering angle of $<45^\circ$ from the axial line through the slits. The absorption event is, within this time scale, all-or-nothing, and contrasts with the gradual decay of energy when the probe is a high energy electron beam. The resonance occurs continuously.

High-energy electron diffraction may scintillate more than one atom sequentially with small energy losses, so that the absorptive beam spread is small across a thin detector. Furthermore, over a short decay path, multiple excitations, if they occur, will result typically in a single recorded pulse owing to the uncertainty in time $\sigma$ (in Equation (2)) controlling the resonant interaction.

Because the quantum has finite uncertainty, and because the electron has in-

trinsic magnetic moment with dimensions $L^3T^{-1}Q$ in length, time and charge respectively [15], we can drop the supposition that the quantum is a point particle. Instead, Huyghens' wavelet is real and is described mathematically in the $\Re^4$ complex space. Consider further, the phase velocities that are described in the wave-packet (Section 2) in all three spatial dimensions. On the photon they are all equal to $c$: $v_p = v_g$. However in the electron with finite $m_o$, $v_p > c$, and the transverse velocities are greater than the velocity in the propagation direction, $v_p^y, v_p^z \gg v_p^x$, since transverse momenta are small: $1/v_p^i = v_g^i = p^i/m'^i$ ; $i = x, y$ or, $z$ (momentum/relativistic mass $m'$, in simplified units). Applications of these principles to Bell's inequalities and to crossed polarizers will be described in future work [17][6].

## 8. Conclusions

Easy it is for a mathematician to invent axioms that describe an infinite wave that is attached to a quantum as if the wave were a probability amplitude for the positions and momenta of atoms in an ideal gas. The invention was discontinuous and indefinite during measurement, and therefore not subject to the laws of physics. It is lucky that such an invention should have been useful in developing the standard model for elementary particles.

However, it is difficult for a physicist to discover the continuous and definite laws in physics that can be used to predict future measurements on such complicated systems. This is done here by employing the reality of the wave function, including its physical properties of phase velocity that is measured by real components $\omega$, $k_b$, $\nu$, $\lambda$ etc.

We propose a change in postulate 4 of quantum theory (in the Introductory section above) to account for physical variables that can always be described, even if not actually measured on individual atoms:

*4. Evolution of systems undergoing measurement.*

If Hermitian operator $A$ with spectral projectors $\{P_k\}$ is measured and outcome k is obtained, the physical state of the system changes continuously: $|\phi\rangle \to |\phi_k\rangle = P_k(\phi)/\sqrt{\langle\phi|P_k|\phi\rangle}$ within time $\Delta t \sim 8/\Delta\omega$.

The notions, that the probability amplitude is extended in time and space, while that the quantum is a point particle, are multiplication of entities. By contrast, we have shown how the real wave-packet describes the effects of Young's slits completely, as it does indeed for other diffraction effects: Quasicrystal diffraction has proved the quantum to be dual harmonic and real in this instance. We understand that phase velocity $v_p = \omega/k$ is hidden in the sense that it is measured through its inverse, $v_g = \mathrm{d}\omega/\mathrm{d}k$. Independently, the constituent va-

[6]The following identities, that are used in this paper, are consistent. Relativity: $E^2 = p^2c^2 + m_o^2c^4$; $E = \hbar\omega = m'^2c^4 = m_o^2c^4/\sqrt{1-\beta^2}$; $\beta = v_g/c$ ; $p = \hbar k = m'v_g = m_o v_g/\sqrt{1-\beta^2}$ . Corrollary: Frequency $\nu$, angular frequency $\omega$, wavelength $\lambda$, and wavector $k$ are all relativistic; $m_oc^2$ is normally constant. On the analysis used, after massive annihilation, energy conservation would require the rate of increase in $c$ is half the rate of decrease in rest mass $m_o$: $\mathrm{d}c/\mathrm{d}m_o = -c/2m_o$.

riables are also measurable.

In physical quantum mechanics, reduction of the packet is continuous in time, having typical uncertainty, $\Delta t = 8/\mathrm{d}\omega$. This contradicts postulate 4 in mathematical quantum theory, where the evolution is instantaneous. On their hypotheses, arbitrary change in reference frame is a mathematical option for Bohr in the EPR experiment [1]; but is confusing in the wider scope of physics.

In other words, the fact of real quanta in quasicrystals implies that extreme probabilism is an analytic theory of math. If Probabilism expresses the effects of hidden variables in measurement, then it is indistinguishable from real physical theory since they describe the same experimental results.

## 9. Postscript on Intuition

Many, from freshman undergraduates to seasoned mechanists, have been mystified by physical quanta. Einstein famously objected, "God does not play dice with nature".

> "[Einstein] was said to reject the idea of a personal God, but I am fairly sure he meant by that the anthropomorphic figure of the Blake pictures—God with a great beard. He accepted the idea of a spirit of righteousness and for one who had not fed on the Gospels that is surely a just paraphrase of what the true idea of God might mean." [18]
>
> Dirac on Einstein: "He wasn't merely trying to construct a theory to agree with observation. So many people do that. Einstein wrote quite differently. He tried to imagine, 'If I were God, would I have made the world like this.' And according to the answer to that question, he would decide whether he liked a particular theory or not." [19]
>
> Pauli quipped, "Dirac has a religion, 'There is no God and Dirac is his prophet'" [20].

All science begins with intuition. One intuition need not depend on another. Einstein's calculation of the perihelion of Mercury and concern for light bending during the 1917 total eclipse show Dirac mistaken on the necessity for evidence, at least for general relativity. Intuition belongs not to the core logic of science that has been described by Popper [21]; but to the psychology of scientists before they formulate a law and begin to systematize and verify it. Einstein's profound belief in objective reality for the wave function [1] ([22] ch.25c) has been debated over a long time e.g. ([14] p. 433).

## Conflicts of Interest

The author declares no conflicts of interest regarding the publication of this paper.

## References

[1] Einstein, A., Podolski, B. and Rosen, N. (1935) *Physical Review*, **47**, 777-780. https://doi.org/10.1103/PhysRev.47.777

[2] Popper, K. (1982) Quantum Theory and the Schism in Physics. Routledge, London.

[3] Bourdillon, A.J. (2022) *Journal of Modern Physics*, **13**, 918-931. https://doi.org/10.4236/jmp.2022.136052

[4] Bourdillon, A.J. (2012) Metric, Myth and Quasicrystals. UHRL, San Jose.

[5] Carroll, S., (2022) Mad-Dog Everettianism. YouTube. https://www.youtube.com/watch?v=2R7elwozou4

[6] Bourdillon, A.J. (2017) Dispersion Dynamics in the Hall Effect and Pair Bonding in HiT. Nova Science N.Y., Hauppauge.

[7] Dirac, P.A.M. (1958) The Principles of Quantum Mechanics. 4th Edition, Clarendon Press, Oxford.

[8] Bourdillon, A.J. (2015) *Journal of Modern Physics*, **6**, 2011-2020. https://doi.org/10.4236/jmp.2015.614407

[9] Bourdillon, A.J. (2020) *Journal of Modern Physics*, **11**, 581-592. https://doi.org/10.4236/jmp.2020.114038

[10] Bourdillon, A.J. (2022) Youtube Physical Quanta v Weird Math. https://www.youtube.com/watch?v=F3kPmm3Vtxw

[11] Bourdillon, A.J. (2010) Quasicrystals' 2D Tiles in 3D Superclusters. UHRL, San Jose.

[12] Hirsch, P., Howie, A., Nicholson, R.B., Pashley, D.W. and Whelan, M.J. (1977) Electron Microscopy of Thin Crystals. Krieger, New York.

[13] Steurer, W. (2004) *Zeitschrift für Kristallographie*, **219**, 391-446. https://doi.org/10.1524/zkri.219.7.391.35643

[14] Pais, A. (1991) Niels Bohr's Times in Physics, Philosophy and Polity. Clarendon Press, Oxford.

[15] Bourdillon, A.J. (2018) *Journal of Modern Physics*, *Special Issue on Magnetic Field and Magnetic Theory*, **9**, 2295-2307. https://doi.org/10.4236/jmp.2018.913145

[16] Jenkins, F.A. and White, H.E. (1957) Fundamentals of Optics. 4th Edition, McGraw-Hill, London.

[17] (2022) Bell's Theorem—The Quantum Venn Diagram Paradox. https://www.youtube.com/watch?v=zcqZHYo7ONs

[18] Harp, R. (2009) From the Archive of Father D'Arcy Times Literary Supplement.

[19] Dirac, P.A.M. (2018) Dirac on Einstein Youtube. https://www.youtube.com/watch?v=JZAISWKj3Pk

[20] Pais, A., Jacob, M., Olive, D.I. and Atiyah, M.F. (1998) The Man and His Work. Cambridge University Press, Cambridge.

[21] Popper, K. (1980) The Logic of Scientific Discovery and the Schism in Physics. Hutchison, London.

[22] Pais, A. (1982) Subtle Is the Lord…, the Science and Life of Albert Einstein. Oxford University Press, Oxford.

Journal of Modern Physics, 2022, 13, 1382-1402
https://www.scirp.org/journal/jmp
ISSN Online: 2153-120X
ISSN Print: 2153-1196

# Electrodynamics in Curvilinear Coordinates and the Equation of a Geodesic Line

**Anatoly V. Parfyonov**

Ulyanovsk State Technical University, Ulyanovsk, Russia
Email: avparfo@gmail.com, parfyonov.anatoly.v@yandex.ru

**How to cite this paper:** Parfyonov, A.V. (2022) Electrodynamics in Curvilinear Coordinates and the Equation of a Geodesic Line. *Journal of Modern Physics*, **13**, 1382-1402.
https://doi.org/10.4236/jmp.2022.1311086

**Received:** September 30, 2022
**Accepted:** November 5, 2022
**Published:** November 8, 2022



## Abstract

The creation of the theory of relativity, which discovered the equivalence of mass and energy, showed that the concept of a point charge, used in the formulation of Coulomb's law, one of the basic laws of classical electrodynamics, contradicts the famous formula establishing the equivalence of mass and energy. But the discovery of quarks makes it possible to present classical electrodynamics in a form free from the indicated contradiction. In the article, having considered the electromagnetic field in a curvilinear coordinate system, a theory has been created that expands our understanding of the electromagnetic field, the nature of quarks, the nature of strong interaction, and the connection between strong interaction and electromagnetic interaction. This theory is based on the principle of equivalence of an electromagnetic field to a free material particle formulated in the article and the law of formation of elementary particles from an electromagnetic field that follows from it.

## Keywords

Electrodynamics, Electromagnetic Field, Curvilinear Coordinates, Quarks, Strong Interaction, Equation of a Geodesic Line

## 1. Introduction

In the theory of relativity, every elementary particle must be considered as a point particle. Therefore, according to classical electrodynamics, any elementary particle would have to have an infinite "intrinsic" energy, and, consequently, mass. To solve this problem, people tried in many ways. For example, the finiteness of the mass of an elementary particle can be interpreted by introducing an infinite negative mass of non-electromagnetic origin. This mass compensates for the infinity of the electromagnetic mass. This method is known as "renormalization" of the mass. But this method does not eliminate all the internal contradic-

tions of classical electrodynamics. The main problem of such solutions is that, when passing to sufficiently small distances, classical electrodynamics becomes an internally contradictory theory. It became possible to overcome these contradictions only after the discovery of quarks. This allows us to speak not only about the electromagnetic interaction but also about the strong interaction in the transition to sufficiently small distances. Therefore, in this article, the solution of the problem is achieved by combining the electromagnetic and strong interactions.

Classical theories, such as Newtonian Mechanics, Maxwell's Electrodynamics are theories that do not have complete generality. So, Classical Mechanics cannot describe mechanical systems in the entire range of speeds with which these systems can move. It describes mechanical systems that move at speeds, the magnitude of which is so much less than the speed of light that the speed of light can be considered an infinitely large value. As you know, mechanics, which have complete generality, since it describes mechanical systems over the entire range of speeds with which these systems can move, are called relativistic mechanics, and were created by Einstein. Classical Electrodynamics does not have complete generality, since it cannot describe the electromagnetic field in the entire four-dimensional space. It becomes an internally inconsistent theory in the field surrounding a point elementary charged particle. Indeed, when tending to the point at which a point charged particle is located, the electric field according to Coulomb's Law will tend to infinity. Consequently, the field energy, and hence the mass corresponding to this energy, will also tend to infinity. The physical meaninglessness of this result is the essence of this contradiction. This immediately implies the need to create electrodynamics with complete commonality. However, before creating such electrodynamics, one should get rid of the contradiction, which can be done only by refusing to consider elementary particles as point particles. Moreover, we now know that elementary particles are not so elementary; they have a very complex internal structure. So, protons, neutrons, and a number of other particles consist of quarks; then, if they are considered point particles, not only do we neglect their size, but also their complex internal structure.

Refusing to consider elementary particles to be point particles, we must consider them particles having finite sizes. But if we consider them particles having finite sizes, then we must know the law by which the shape of the surface of the particles will change, because we cannot consider particles to be absolutely solid bodies, which is prohibited by the basic principles of the theory of relativity, working for electrodynamics. And we will know this law if we know the nature of the mass of elementary particles. To reveal the nature of the mass of elementary particles, we will use a hint. During the interaction of a particle and its antiparticle that is during the annihilation reaction, the particle and antiparticle disappear and gamma quanta appear, which are electromagnetic waves. Electromagnetic waves, in their turn, are vibrations of electric and magnetic fields. Therefore, it is natural to assume that the nature of the mass of an elementary particle and its antiparticle also has an electromagnetic character. In other words, this means that the electromagnetic field is equivalent to an elementary particle.

For the entire subsequent presentation, this conclusion is of fundamental importance. It lays down the mathematical foundations. Therefore, let's call it the Principle of equivalence of an electromagnetic field to a free material particle. Here, we need to make the following clarifications. The article will show that the use of curvilinear coordinates makes it possible to represent the electromagnetic interaction and the strong interaction as two manifestations of one single interaction. And in order not to come up with a name for it, we will call it electromagnetic interaction. Well, the field of this interaction will be called the electromagnetic field. It is this electromagnetic field (which includes the "ordinary" electromagnetic field and the field of strong interaction) that is equivalent to the mass of an elementary particle. An elementary particle can be a free material particle. This equivalence principle makes it possible to create electrodynamics capable of describing the electromagnetic field in the entire four-dimensional space.

## 2. Method

Obviously, such electrodynamics should be created using curvilinear coordinates. But here we have a problem of how to connect the electromagnetic field with some curvilinear coordinate system. Unlike the gravitational field, which is directly related to the space-time metric, the electromagnetic field does not have such a direct connection. To overcome this problem, we will use one more hint. We know that electric and magnetic fields can be represented in the form of force lines, and if we direct the coordinate axes of a curvilinear coordinate system along the force lines of an electromagnetic field, then this problem can be solved. But this is only an idea; to make it work, it is necessary to find a mathematical expression of this idea. And here we have a clue—we know that if a vector field is specified in three-dimensional space, then the equations describing the lines of a given vector field can be found as follows: taking the vector of a given vector field at an arbitrary point of this field, and multiplying it vectorially by the radius vector element and equating the result to zero, we obtain a system of equations describing the lines of this vector field. Moving on to four-dimensional space, if we consider electromagnetic fields in four-dimensional space, and if the magnitude of the electromagnetic field is determined by the second-rank antisymmetric tensor and, using the analogy with three-dimensional space, we must therefore find another antisymmetric second-rank tensor in four-dimensional space that would describe some geometric object defined in this space. And we do have such an antisymmetric tensor of the second rank which describes a two-dimensional surface defined in four-dimensional space. Based on these two antisymmetric second-order tensors, a number of quantities can be compiled, starting from a scalar, that is a zero-rank tensor, and ending with two second-rank tensors. Considering these two second-rank tensors in rectangular coordinates (in four-dimensional non-curved space they are called Galilean Coordinates), we see that each of these two tensors can be represented as the sum of a symmetric and antisymmetric tensor. The importance of this result is that the

symmetric tensor for each of these two tensors of the second rank is the metric tensor of the four-dimensional non-curved space. Thus, we have found the connection of the electromagnetic field with the space-time metric using two tensors of the second rank compiled on the basis of two antisymmetric tensors of the second rank, one of which describes the electromagnetic field, while the second describes a two-dimensional surface.

The main method, which is the basis of many mathematical calculations performed in the article, is as follows. The article deals with four-dimensional vectors and four-dimensional tensors and their "changes" caused by transformations from one coordinate system to another. In this case, transformation laws are used, which are a natural generalization to curvilinear coordinates of the definitions of four-dimensional vectors and four-dimensional tensors made in Galilean coordinates.

## 3. Harmonized Electromagnetic Field

The trace of the stress-energy tensor of the electromagnetic field is zero: $T_i^i = 0$, therefore, the scalar curvature of space-time $R$ in the presence of a single electromagnetic field is also zero [1]. Thus, it may be concluded that the electromagnetic field has no connection with the space-time metric, in contrast to the gravitational field, where the metric tensor $g_{ik}$ plays the role of "potentials". Therefore, to describe the electromagnetic field in curvilinear coordinates, we must first match the electromagnetic field with a system of curvilinear coordinates. Coordination is an operation that resembles the introduction operation for a vector field $\mathbf{F}$, defined in three-dimensional space, of vector lines using differential equations describing these same vector lines: $\mathbf{F} \times \mathrm{d}\mathbf{r} = 0$, where $\mathbf{r}$ is a radius vector. Moving to a four-dimensional space and having an antisymmetric tensor of the second rank $F_{ik}$, describing an electromagnetic field, we take an antisymmetric tensor of the second rank

$$\mathrm{d}f^{ik} = \mathrm{d}x^i \mathrm{d}x'^k - \mathrm{d}x^k \mathrm{d}x'^i, \tag{1}$$

describing an infinitesimal element of a two-dimensional surface $x^i = x^i(u,v)$, where $u$ and $v$ will be considered as curvilinear coordinates on the specified surface. We choose these coordinates so that the four-dimensional vectors $\mathrm{d}x^i$ and $\mathrm{d}x'^i$ are tangent vectors to the coordinate lines $u$ and $v$, respectively. This allows writing expression (1) as follows:

$$\mathrm{d}f^{ik} = f^{ik}\mathrm{d}u\mathrm{d}v,$$

where

$$f^{ik} = \frac{\partial x^i}{\partial u}\frac{\partial x^k}{\partial v} - \frac{\partial x^k}{\partial u}\frac{\partial x^i}{\partial v}. \tag{2}$$

Using the tensors $F_{ik}$ and $f^{ik}$, we construct two tensors of the second rank $A^{ik}$ and $B^{ik}$:

$$A^{ik} = F^i_{\ l} f^{kl} - F^{*i}_{\ \ l} f^{*kl}, \tag{3}$$

$$B^{ik} = F^{i}_{l} f^{*kl} + F^{*i}_{l} f^{kl}, \tag{4}$$

where the pseudo-tensors $F^{*ik}$, $f^{*ik}$ and accordingly the tensors $F^{ik}$ and $f^{ik}$ are dual to each other. We show that tensors (3) and (4) can be written as the sum of a symmetric tensor and an antisymmetric tensor. To do this, we write them in the Galilean coordinate system [1]. The quantities considered in the Galilean coordinate system will be denoted by the index Γ. Thus, in the Galilean coordinate system we have:

$$A^{ik}_{\Gamma} = \frac{1}{4} A_{\Gamma} g^{ik}_{\Gamma} + a^{ik}_{\Gamma}, \tag{5}$$

$$B^{ik}_{\Gamma} = \frac{1}{4} B_{\Gamma} g^{ik}_{\Gamma} + a^{*ik}_{\Gamma} \tag{6}$$

where $A_{\Gamma} = A^{i}_{\Gamma i}$, $B_{\Gamma} = B^{i}_{\Gamma i}$. The tensor $a^{ik}_{\Gamma}$ and pseudo-tensor $a^{*ik}_{\Gamma}$ are dual to each other. The correctness of the equalities (5) and (6) can be verified by direct calculation, which gives the values to which are included in these equalities:

$$A_{\Gamma} = 4\left(\mathbf{E}_{\Gamma}\mathbf{f}_{\Gamma} - \mathbf{H}_{\Gamma}\mathbf{s}_{\Gamma}\right), \tag{7}$$

$$B_{\Gamma} = 4\left(\mathbf{E}_{\Gamma}\mathbf{s}_{\Gamma} + \mathbf{H}_{\Gamma}\mathbf{f}_{\Gamma}\right), \tag{8}$$

where $\mathbf{E}_{\Gamma}$ and $\mathbf{H}_{\Gamma}$ are electric and magnetic field tension vectors,

$$\mathbf{f}_{\Gamma} = \left(\mathrm{f}^{01}, \mathrm{f}^{02}, \mathrm{f}^{03}\right), \tag{9}$$

$$\mathbf{s}_{\Gamma} = \left(\mathrm{f}^{23}, \mathrm{f}^{31}, \mathrm{f}^{12}\right), \tag{10}$$

where, for instance,

$$\mathrm{f}^{01} = \frac{\partial ct}{\partial u}\frac{\partial x}{\partial v} - \frac{\partial x}{\partial u}\frac{\partial ct}{\partial v}, \tag{11}$$

and so on; $ct = x^{0}_{\Gamma}$, $x = x^{1}_{\Gamma}$, $x^{i}_{\Gamma}$: Galilean coordinates.

The components of the antisymmetric tensor of the second rank $a^{ik}_{\Gamma}$ are components of the two vectors:

$$\mathbf{a} = \mathbf{E}_{\Gamma} \times \mathbf{s}_{\Gamma} + \mathbf{H}_{\Gamma} \times \mathbf{f}_{\Gamma}, \tag{12}$$

$$\mathbf{b} = \mathbf{E}_{\Gamma} \times \mathbf{f}_{\Gamma} - \mathbf{H}_{\Gamma} \times \mathbf{s}_{\Gamma}, \tag{13}$$

where

$$a^{ik}_{\Gamma} = \begin{pmatrix} 0 & a_x & a_y & a_z \\ -a_x & 0 & -b_z & b_y \\ -a_y & b_z & 0 & -b_x \\ -a_z & -b_y & b_x & 0 \end{pmatrix}. \tag{14}$$

The connection of the tensor component $A^{ik}$ written in curvilinear coordinates $x^{i}$ with the tensor component $A^{ik}_{\Gamma}$ written in Galilean coordinates is given by the law of transformation:

$$A^{ik} = \frac{\partial x^{i}}{\partial x^{l}_{\Gamma}}\frac{\partial x^{k}}{\partial x^{m}_{\Gamma}} A^{lm}_{\Gamma}. \tag{15}$$

Substituting the right side of the Equation (5) instead of the tensor $A^{lm}_{\Gamma}$, we

take into account that the components of the tensors $g^{ik}$ and $g_{\Gamma}^{ik}$, $a^{ik}$ and $a_{\Gamma}^{ik}$ are also connected by the same transformation law (15) as the components of the tensors $A^{ik}$ and $A_{\Gamma}^{ik}$. Thus, after the substitution, we obtain that the tensor $A^{ik}$ can be represented as a sum of symmetric and antisymmetric tensors:

$$A^{ik} = \frac{1}{4} A_{\Gamma} g^{ik} + a^{ik}. \tag{16}$$

Simplifying this equation and taking into account the antisymmetric nature of the tensor $a^{ik}$, we find: $A_i^i = A_{\Gamma}$. Denoting $A = A_i^i$, we have a relation stating that the value of $A$ remains unchanged in any coordinate system: $A = A_{\Gamma}$. From here we finally obtain the following for the equation considered:

$$A^{ik} = \frac{1}{4} A g^{ik} + a^{ik}. \tag{17}$$

Similarly, we find:

$$B^{ik} = \frac{1}{4} B g^{ik} + a^{*ik}. \tag{18}$$

where $B = B_i^i = B_{\Gamma}$.

### 3.1. Equations of Motion

Starting to find the equations to which the values under consideration are subjected, we pay attention to the antisymmetric character of the tensors $a^{ik}$ and $a^{*ik}$. It implies the equation to zero of the double covariant derivatives of the indicated tensors:

$$a_{;i;k}^{ik} = 0, \tag{19}$$

$$a_{;i;k}^{*ik} = 0. \tag{20}$$

In this article, we consider only the electromagnetic field, which, as mentioned above, is not related to the space-time metric, therefore, any coordinate transformations considered in the article should not change the space-time metric. Such infinitesimal coordinate transformations are determined by the so-called Killing equations [1] $\xi^{i;k} + \xi^{k;i} = 0$, where $\xi^i$ are small values that describe the transformation from the coordinates $x^i$ to coordinates $x'^i = x^i + \xi^i$. Killing equations mean that with the specified coordinate transformations the variation of the metric tensor is zero: $\delta g^{ik} = 0$. From here it is easy to get that the Jacobians of such coordinate transformations are equal to one. To do so, we consider the indicated transformation from the Galilean coordinates $x_{\Gamma}^i$ to the curvilinear coordinates $x^i = x_{\Gamma}^i + \xi^i$. With this coordinate transformation, the components of the metric tensor are transformed according to the law:

$$g^{ik} = \frac{\partial x^i}{\partial x_{\Gamma}^l} \frac{\partial x^k}{\partial x_{\Gamma}^m} g_{\Gamma}^{lm}. \tag{21}$$

We first find the determinant from the left and right side of this transformation law, which leads to the following relation:

$$\frac{1}{\sqrt{-g}} = \left|\frac{\partial x^i}{\partial x_\Gamma^l}\right| \approx 1 + \xi^i_{,i}, \tag{22}$$

where $g = |g_{ik}|$ is a determinant of the metric tensor $g_{ik}$. Killing's equations in Galilean coordinates are as follows: $\xi^{i,k} + \xi^{k,i} = 0$. Simplifying them, we get the following: $\xi^i_{,i} = 0$. Thus, in Galilean coordinates we have $\sqrt{-g} = 1$, as it should be. It will be proved below that this equality holds not only in Galilean coordinates, but also in curvilinear coordinates describing spherically symmetric systems (80).

Taking into account this condition, twice covariantly differentiating between the left and right parts of Equations (17) and (18) and considering Equations (19) and (20), we obtain equations resulting from the matching of the electromagnetic field and the curvilinear coordinate system $\left(x^0, x^1, x^2, x^3\right)$:

$$\frac{\partial}{\partial x^i}\left(g^{ik}\frac{\partial A}{\partial x^k}\right) = 4A^{ik}_{;i;k}, \tag{23}$$

$$\frac{\partial}{\partial x^i}\left(g^{ik}\frac{\partial B}{\partial x^k}\right) = 4B^{ik}_{;i;k}. \tag{24}$$

In electrodynamics, considered in curvilinear coordinates, the Equations (23) and (24) play the role of equations of motion.

### 3.2. Variational Problem

Let us consider an electromagnetic field that is not limited in space or time and does not experience any influences.

We write the law of transformation connecting the components of the tensor $F^i_l f^{kl}$, given in the curvilinear coordinates $x^i$, and the components of the tensor $F^i_{\Gamma l} f^{kl}_\Gamma$, given in the Galilean coordinates $x^i_\Gamma$. We write the law of transformation connecting the components of the tensor $F^i_{(1)l} f^{kl}_{(1)}$, given in the curvilinear coordinates $x^i_{(1)}$, and the components of the same tensor $F^i_{\Gamma l} f^{kl}_\Gamma$, given in the Galilean coordinates $x^i_\Gamma$. Since the left sides of the relations obtained are equal, we equate the right sides of these relations and then, simplifying them, we get [2]:

$$F_{(1)ik} f^{ik}_{(1)} = F_{ik} f^{ik}. \tag{25}$$

We multiply the left and right sides of Equation (25) by *dudv*. Then, integrating over an arbitrary domain $S$ lying on a two-dimensional surface $x^i(u,v)$, we get the following equation:

$$\iint_S F_{(1)ik} f^{ik}_{(1)} \mathrm{d}u\mathrm{d}v = \iint_S F_{ik} f^{ik} \mathrm{d}u\mathrm{d}v. \tag{26}$$

We transform from the curvilinear coordinates $x^i$ to the curvilinear coordinates $x^i_{(1)} = x^i + \xi^i$, where $\xi^i$ means small values. Substituting $x^i_{(1)} = x^i + \xi^i$ in left part of the Equation (26) and decomposing the integrand in a series of powers $\xi^i$, we get after reduction:

$$\delta \iint_S F_{ik} f^{ik} \mathrm{d}u\mathrm{d}v = 0. \tag{27}$$

When matching the electromagnetic field with a curvilinear coordinate system, the components of the tensor $F_{ik}$ should be considered as functions of the coordinates $x^i$: $F_{ik} = F_{ik}\left(x^i\right)$. Thus, from the Equation (27) we get the following variational problem:

$$\delta \iint_S \Lambda\left(x^i, x^i_{,u}, x^i_{,v}\right) \mathrm{d}u\mathrm{d}v = 0, \tag{28}$$

where $\Lambda = \frac{1}{2} F_{ik} f^{ik} = F_{ik} x^i_{,u} x^k_{,v}, x^i_{,u} \equiv \frac{\partial x^i}{\partial u}, x^i_{,v} \equiv \frac{\partial x^i}{\partial v}$.

Performing the variation in the left-hand side of the Equation (28), we arrive at the Euler equation and the natural boundary conditions

$$\frac{\partial \Lambda}{\partial x^i} - \frac{\partial^2 \Lambda}{\partial u \partial x^i_{,u}} - \frac{\partial^2 \Lambda}{\partial v \partial x^i_{,v}} = 0, \tag{29}$$

$$\iint_S \left[ \frac{\partial}{\partial u}\left( \frac{\partial \Lambda}{\partial x^i_{,u}} \delta x^i \right) + \frac{\partial}{\partial v}\left( \frac{\partial \Lambda}{\partial x^i_{,v}} \delta x^i \right) \right] \mathrm{d}u\mathrm{d}v = 0 \tag{30}$$

Substituting the value $\Lambda$ in the Euler equation and performing differentiation, we find: $F_{ik;l} + F_{kl;i} + F_{li;k} = 0$. This is the first pair of Maxwell's equations. It follows that the Euler equation is carried out automatically.

Since the region $S$ is arbitrary, therefore, it can be chosen so small that it is close to the plane. Let's designate this region as $\Delta S$. Consider the natural boundary conditions for the region $\Delta S$ of a two-dimensional surface. Let us apply to the integral (30) written for the region $\Delta S$ the Green formula. Thus we get:

$$\oint_{\Delta C} \left( \frac{\partial \Lambda}{\partial x^i_{,u}} \delta x^i \mathrm{d}v - \frac{\partial \Lambda}{\partial x^i_{,v}} \delta x^i \mathrm{d}u \right) = 0 \tag{31}$$

where $\Delta C$ is a closed loop enclosing $\Delta S$.

We introduce another system of curvilinear coordinates $x'^0, x'^1, x'^2, x'^3$, the first two coordinates of which are coordinates on the two-dimensional surface under consideration $x'^0 = u, x'^1 = v$. The two remaining coordinates will be denoted as $x'^2 = w, x'^3 = n$. The ( ) sign was used only once in the Formula (1), so its new use should not cause any confusion. The tangent vectors to the coordinate lines $w$ and $n$ are denoted by: $x^i_{,w} \equiv \partial x^i / \partial w$, $x^i_{,n} \equiv \partial x^i / \partial n$.

Let $\Delta S$ tend to zero and reach zero at some point M. Let us place the origin of coordinates $x^i$ at the point M. Thus, at point M we have: $x^i = 0$. Let us pass at the point M to the locally geodesic coordinate system. To do this, we use the expression [1]:

$$x'^i = x^i + \frac{1}{2}\left(\Gamma^i_{kl}\right)_M x^k x^l \tag{32}$$

From here at point M we have:

$$\left(\frac{\partial x'^i}{\partial x^k}\right)_M = \delta^i_k; \quad \left(\delta x'^i\right)_M = \left(\delta x^i\right)_M. \tag{33}$$

Therefore, at point M, we can write:

$$\frac{\partial\Lambda}{\partial x^i_{,u}}\delta x^i = F_{ik}x^k_{,v}\delta x^i = F'_{l1}\frac{\partial x'^l}{\partial x^i}\delta x^i = F'_{01}\delta x'^0 + F'_{21}\delta x'^2 + F'_{31}\delta x'^3; \quad (34)$$

$$\frac{\partial\Lambda}{\partial x^i_{,v}}\delta x^i = F_{ki}x^k_{,u}\delta x^i = F'_{0l}\frac{\partial x'^l}{\partial x^i}\delta x^i = F'_{01}\delta x'^1 + F'_{02}\delta x'^2 + F'_{03}\delta x'^3. \quad (35)$$

We substitute the value of Λ into the integral (31) and after differentiation we substitute the right side of expressions (34) and (35), we obtain:

$$\begin{aligned}&\oint_{\Delta C}\left[F'_{01}\left(\delta x'^0\mathrm{d}v - \delta x'^1\mathrm{d}u\right) + F'_{21}\delta x'^2\mathrm{d}v + F'_{31}\delta x'^3\mathrm{d}v\right.\\&\left. - F'_{02}\delta x'^2\mathrm{d}u - F'_{03}\delta x'^3\mathrm{d}u\right] = 0\end{aligned} \quad (36)$$

We choose natural boundary conditions (36) so that the variational problem has a solution. This variational problem has three solutions. First decision: all components of the antisymmetric tensor $F'_{ik}$ are equal to zero, except for the component $F'_{23}$. Let's call this solution a neutron. Second solution: all components of the tensor $F'_{ik}$ are equal to zero, except for $F'_{01}$ and $F'_{23}$. Let's call this solution a proton. Third solution: all components of the tensor $F'_{ik}$ are equal to zero, except for $F'_{01}$. Let's call this solution electron. The meaning of these decisions will become clear below. Here it is necessary to say the following. When $F'_{01} \neq 0$, in order for the variational problem to have a solution, the following natural boundary conditions must be satisfied:

$$\delta x'^0 = \delta x'^1 = 0 \quad (37)$$

and

$$F'_{02} = F'_{03} = F'_{12} = F'_{13} = 0. \quad (38)$$

Taking into account the arbitrary choice of the $\Delta S$ region on the surface $x^i(u,v)$, we can say that condition (37) must be satisfied at any point of the surface $x^i(u,v)$. Variations $\delta x'^0$ and $\delta x'^1$ occur in the tangent plane to surface $x^i(u,v)$. Therefore, condition (37) means that the distances between infinitely close points on the surface $x^i(u,v)$ remain unchanged. Thus condition (37) means that the two-dimensional surface $x^i(u,v)$ behaves like an incompressible and inextensible film. Variations $\delta x'^2$ and $\delta x'^3$ lead to such consequences which in mathematics are called bendings. They do not change anything on surface $x^i(u,v)$. Therefore, they can be different from zero.

Let's make an important remark. In [1] it is said: it can be shown that a locally geodesic system can be obtained not only at a point, but also along the world line [3]. Therefore, the solutions obtained are valid not only at the point M, but also along the world line. Therefore, we do not write the letter M in the obtained solutions of the variational problem. The obtained solutions are achieved by applying the following transformation law:

$$F_{ik}\frac{\partial x^i}{\partial x'^l}\frac{\partial x^k}{\partial x'^m} = F'_{lm}. \quad (39)$$

It follows from (38) that the tensor $F'_{ik}$ has only two non-zero components $F'_{01}$ and $F'_{23}$. For them, the transformation law (39) can be written as follows,

for example:

$$\frac{1}{2}F_{ik}f^{ik} = F'_{01} \quad \text{or} \quad \frac{1}{2}F_{\Gamma ik}f_{\Gamma}^{ik} = F'_{01}, \tag{40}$$

if we write the transformation law (39) connecting the components of the tensors $F_{\Gamma ik}$ and $F'_{ik}$, considered in the Galilean coordinates $x_{\Gamma}^{i}$ and the curvilinear coordinates $x'^{i}$, respectively. From the obtained equations we find:

$$F'_{01} = \frac{1}{4}A. \tag{41}$$

Now we consider the value $\frac{1}{4}B_{\Gamma}$. Since $B = B_i^i = B_{\Gamma}$, we will do all calculations in Galilean coordinates. It is easy to verify that

$$F_{\Gamma ik}f_{\Gamma}^{*ik} = F_{\Gamma ik}^{*}f_{\Gamma}^{ik}, \tag{42}$$

but

$$\frac{1}{2}F_{\Gamma ik}^{*}f_{\Gamma}^{ik} = F_{\Gamma ik}^{*}\frac{\partial x_{\Gamma}^{i}}{\partial x'^{0}}\frac{\partial x_{\Gamma}^{k}}{\partial x'^{1}} = F'^{*}_{01}. \tag{43}$$

Thus, we get:

$$F'^{*}_{01} = \frac{1}{4}B. \tag{44}$$

### 3.3. Two-Dimensional Spaces

Let us return to condition (37) and its corollary: the surface $x^{i}(u,v)$ is an incompressible and inextensible film. All this suggests that the surface $x^{i}(u,v)$ can be considered a two-dimensional space, which has certain properties and preserves them with variation. Indeed, with variation, the distances between any two points of the surface, and hence the two-dimensional space, remain constant. When bending, the Gaussian curvature at each point of the surface $x^{i}(u,v)$, and therefore at every point of two-dimensional space, remains unchanged. Additional confirmation of the above can be obtained by considering the following calculations. We write the first pair of Maxwell's equations in curvilinear coordinates $x'^{i}$ taking into account the condition (38): $F'_{01,2} = F'_{01,3} = F'_{23,0} = F'_{23,1} = 0$. It follows there from that $F'_{01} = F'_{01}\left(x'^{0}, x'^{1}\right)$, *i.e.* this component is a function of the coordinates $x'^{0} = u$ and $x'^{1} = v$, and $F'_{23} = F'_{23}\left(x'^{2}, x'^{3}\right)$, *i.e.* this component is a function of the coordinates $x'^{2} = w$ and $x'^{3} = n$. Thus, we find that in the curvilinear coordinates $x'^{i}$ each of the two nonzero components of the electromagnetic field tensor depends on a strictly individual set of coordinates consisting of only two curvilinear coordinates. This fact is another confirmation of the fact that we are dealing with two two-dimensional spaces. One of them is formed by a two-dimensional surface $x^{i}(u,v)$; the second two-dimensional space is formed by a two-dimensional surface $x^{i}(w,n)$. Since these surfaces are coordinate surfaces of four-dimensional curvilinear coordinate system ($u$, $v$, $w$, $n$), therefore, their geometry, and hence, the geometry of two-dimensional spaces, is determined by metric tensors [3]:

$$g'_{ab} = \frac{\partial x^i_\Gamma}{\partial x'^a}\frac{\partial x^k_\Gamma}{\partial x'^b} g_{\Gamma ik}, \tag{45}$$

$$g'_{\hat{a}\hat{b}} = \frac{\partial x^i_\Gamma}{\partial x'^{\hat{a}}}\frac{\partial x^k_\Gamma}{\partial x'^{\hat{b}}} g_{\Gamma ik}, \tag{46}$$

where $a,b,\cdots = 0,1$; $\hat{a},\hat{b},\cdots = 2,3$.

Each of these tensors is obviously connected with the metric tensor of a curvilinear coordinate system ($u$, $v$, $w$, $n$):

$$g'_{ik} = \frac{\partial x^l_\Gamma}{\partial x'^i}\frac{\partial x^m_\Gamma}{\partial x'^k} g_{\Gamma lm}. \tag{47}$$

Using the calculation of Riemannian spaces [3], it is arguable that the surface $x^i(u,v)$ is a two-dimensional space with a metric tensor (45). It is clear that all this can be repeated for a two-dimensional space with the metric tensor $g'_{\hat{a}\hat{b}}$. In each of these two-dimensional spaces, respectively, one can enter the tensor of the electromagnetic field:

$$F'_{ab} = \begin{pmatrix} 0 & F'_{01} \\ -F'_{01} & 0 \end{pmatrix}, \quad F'_{\hat{a}\hat{b}} = \begin{pmatrix} 0 & F'_{23} \\ -F'_{23} & 0 \end{pmatrix} \tag{48}$$

and write accordingly the following tensor equation:

$$F'_{ab} = g'_{ac}g'_{bd}F'^{cd} = \frac{1}{2}\left(g'_{ac}g'_{bd} - g'_{ad}g'_{bc}\right)F'^{cd}, \tag{49}$$

$$F'_{\hat{a}\hat{b}} = g'_{\hat{a}\hat{c}}g'_{\hat{b}\hat{d}}F'^{\hat{c}\hat{d}} = \frac{1}{2}\left(g'_{\hat{a}\hat{c}}g'_{\hat{b}\hat{d}} - g'_{\hat{a}\hat{d}}g'_{\hat{b}\hat{c}}\right)F'^{\hat{c}\hat{d}}. \tag{50}$$

From here we get:

$$F'_{01} = qF'^{01}, \tag{51}$$

$$F'_{23} = \hat{q}F'^{23}, \tag{52}$$

where

$$q = g'_{00}g'_{11} - g'^2_{01} = \det\left[g'_{ab}\right], \tag{53}$$

$$\hat{q} = g'_{22}g'_{33} - g'^2_{23} = \det\left[g'_{\hat{a}\hat{b}}\right]. \tag{54}$$

The Formulas (51) and (52) establish a connection between the covariant and contravariant components of the electromagnetic field in the corresponding two-dimensional space. We note that if two-dimensional surfaces are represented as planes and viewed in Galilean coordinates, then for the values (53) and (54) we will have the following values: $q = -1$ and $\hat{q} = 1$. Substituting these values in (51) and (52) we arrive at a well-known connection between the various types of components of the tensor of the electromagnetic field, given in Galilean coordinates.

### 3.4. The Law of Stress-Energy Tensors Equality

For further calculations, we consider the stress-energy tensor of the electromagnetic field, and then we write it in Galilean coordinates as follows:

$$4\pi T_{\Gamma ik} = -F_{\Gamma il}F_{\Gamma k}{}^{l} + \frac{1}{4}g_{\Gamma ik}F_{\Gamma lm}F_{\Gamma}^{lm}. \tag{55}$$

We prove that for a given tensor the equation is true:

$$T_{\Gamma ik} = T_{\Gamma ik}^{(*)}, \tag{56}$$

where

$$4\pi T_{\Gamma ik}^{(*)} = -F_{\Gamma il}^{*}F_{\Gamma k}^{*\,l} + \frac{1}{4}g_{\Gamma ik}F_{\Gamma lm}^{*}F_{\Gamma}^{*lm}. \tag{57}$$

To do this, we substitute the right-hand sides of the calculations (55) and (57) in the Equation (56), after multiplying the left and right sides of Equation (56) by 4π. Considering that

$$-\frac{1}{2}F_{\Gamma lm}^{*}F_{\Gamma}^{*lm} = \frac{1}{2}F_{\Gamma lm}F_{\Gamma}^{lm} = \mathbf{H}_{\Gamma}^{2} - \mathbf{E}_{\Gamma}^{2}, \tag{58}$$

we get:

$$F_{\Gamma il}F_{\Gamma k}{}^{l} - F_{\Gamma il}^{*}F_{\Gamma \mathrm{k}}^{*\,l} = \left(\mathbf{H}_{\Gamma}^{2} - \mathbf{E}_{\Gamma}^{2}\right)g_{\Gamma ik}. \tag{59}$$

The validity of tensor Equation (59) can be checked directly for each of its components. That proves the validity of the Equation (56). Next, applying the transformation law connecting the components of the tensor $T_{\Gamma lm}$, given in the Galilean coordinates $x_{\Gamma}^{i}$, with the components of the tensor $T_{ik}$, given in curvilinear coordinates $x^{i}$, and applying the same law respectively for the tensors $T_{\Gamma lm}^{(*)}$ and $T_{ik}^{(*)}$, to the left and right sides of Equation (56), we obtain:

$$T_{ik} = T_{ik}^{(*)}. \tag{60}$$

The validity of this equation follows from the validity of Equation (56). The form of the stress-energy tensors of the electromagnetic field, which are in the Equation (60), can be established by using the laws of transformation given above. Substituting in their right-hand side, respectively, the values of $T_{\Gamma ik}$ or $T_{\Gamma ik}^{(*)}$, found from the calculations (55) and (57), and taking into account that their values are related by the same transformation laws, we get:

$$4\pi T_{ik} = -F_{il}F_{k}{}^{l} + \frac{1}{4}g_{ik}F_{\Gamma lm}F_{\Gamma}^{lm}, \quad 4\pi T_{ik}^{(*)} = -F_{il}^{*}F_{k}^{*l} + \frac{1}{4}g_{ik}F_{\Gamma lm}^{*}F_{\Gamma}^{*lm}. \tag{61}$$

Simplifying these calculations and taking into account that the trace of the stress-energy tensor of the electromagnetic field is zero, and from (60) it follows that $T_{i}^{(*)i} = 0$, we find: $F_{ik}F^{ik} = F_{\Gamma lm}F_{\Gamma}^{lm}$, $F_{ik}^{*}F^{*ik} = F_{\Gamma lm}^{*}F_{\Gamma}^{*lm}$. Considering these equalities, we can write down the calculations of the stress-energy tensors of the electromagnetic field in the system of curvilinear coordinates $x^{i}$ in the following form:

$$4\pi T_{ik} = -F_{il}F_{k}{}^{l} + \frac{1}{4}g_{ik}F_{lm}F^{lm}, \quad 4\pi T_{ik}^{(*)} = -F_{il}^{*}F_{k}^{*l} + \frac{1}{4}g_{ik}F_{lm}^{*}F^{*lm}, \tag{62}$$

where all members of these calculations are expressed in the same coordinate system $x^{i}$. Once again applying the transformation law now to the left and right side of the tensor Equation (59), we get:

$$F_{il}F_k^{\ l} - F_{il}^{*}F_k^{*l} = \left(\mathbf{H}_\Gamma - \mathbf{E}_\Gamma\right) g_{ik}. \tag{63}$$

The validity of this formula follows from the validity of Formulas (59) and (60). Note that Formula (63) can also be obtained by substituting the calculations of the stress-energy tensors of the electromagnetic field in the Equation (60), considered in the curvilinear coordinates $x^i$. The Equation (60) extends our understanding of the properties of electromagnetic fields, therefore, to emphasize this, it can be called the law of stress-energy tensor equality, composed of the electromagnetic field tensors dual to each other.

### 3.5. Field in Two-Dimensional Spaces

Since the Formula (63) is another form of writing the law the law of stress-energy tensor equality of an electromagnetic field, therefore, writing down the Formula (63) in curvilinear coordinates $x'^i$ and taking into account

$$g'^{il} g'_{kl} = \delta_k^i, \tag{64}$$

we write the Formulas (63) and (64) in the components. In order not to give all thirty-two equations, which are obtained by writing the Formulas (63) and (64) in the components, we restrict ourselves to the minimum number of equations necessary to demonstrate the method of calculations. From (63) we have in curvilinear coordinates $x'^i$:

$$g'^{00}\left(F'^2_{01} - F'^{*2}_{01}\right) = \left(\mathbf{H}_\Gamma^2 - \mathbf{E}_\Gamma^2\right) g'_{11}, \quad g'^{01}\left(F'^2_{01} - F'^{*2}_{01}\right) = -\left(\mathbf{H}_\Gamma^2 - \mathbf{E}_\Gamma^2\right) g'_{01}, \tag{65}$$

$$g'^{02}\left(F'_{01}F'_{23} - F'^{*}_{01}F'^{*}_{23}\right) = \left(\mathbf{H}_\Gamma^2 - \mathbf{E}_\Gamma^2\right) g'_{13}, \tag{66}$$

$$g'^{03}\left(F'_{01}F'_{23} - F'^{*}_{01}F'^{*}_{23}\right) = -\left(\mathbf{H}_\Gamma^2 - \mathbf{E}_\Gamma^2\right) g'_{12}. \tag{67}$$

Multiply the first equation by $g'_{00}$, the second equation by $g'_{01}$, the third equation by $g'_{02}$ and the fourth equation by the value $g'_{03}$. From (64) we have:

$$g'_{00}g'^{00} + g'_{01}g'^{01} + g'_{02}g'^{02} + g'_{03}g'^{03} = 1. \tag{68}$$

We substitute here the values of the components from the left-hand side of this equation, which can be found from the four equations obtained after multiplying by the components of the metric tensor. Performing similar calculations for the other components of the Formulas (63) and (64) and taking into account the calculations (53) and (54), we arrive at the following equation:

$$\hat{q}\left(F'^2_{01} - F'^{*2}_{01}\right) = q\left(F'^2_{23} - F'^{*2}_{23}\right), \tag{69}$$

Considering the condition $\sqrt{-g'} = 1$, we can write for a pseudo-tensor given in curvilinear coordinates, $F'^{*}_{ik} = \frac{1}{2} e_{iklm} F'^{lm}$. Hence, using the Equations (51) and (52), we find:

$$F'^{*}_{01} = -\frac{F'_{23}}{\hat{q}}, \tag{70}$$

$$F'^{*}_{23} = -\frac{F'_{01}}{q}. \tag{71}$$

Substituting (70) and (71) in (69), we finally get:

$$\frac{F'^2_{01}}{q} = \frac{F'^2_{23}}{\hat{q}}. \tag{72}$$

From (38) it follows that

$$F'_{ik} = \begin{pmatrix} 0 & F'_{01} & 0 & 0 \\ -F'_{01} & 0 & 0 & 0 \\ 0 & 0 & 0 & F'_{23} \\ 0 & 0 & -F'_{23} & 0 \end{pmatrix}. \tag{73}$$

The components of the tensor (73) $F'_{a\hat{b}} = 0$ that are equal to zero are connected with the components $F'^{a\hat{b}}$ of the tensor $F'^{ik}$ by the relation: $F'_{a\hat{b}} = g'_{ac} g'_{\hat{b}\hat{d}} F'^{c\hat{d}} = 0$, from which it follows that $F'^{a\hat{b}} = 0$, therefore

$$F'^{ik} = \begin{pmatrix} 0 & q^{-1}F'_{01} & 0 & 0 \\ -q^{-1}F'_{01} & 0 & 0 & 0 \\ 0 & 0 & 0 & \hat{q}^{-1}F'_{23} \\ 0 & 0 & -\hat{q}^{-1}F'_{23} & 0 \end{pmatrix}. \tag{74}$$

From (72), (73) and (74) we find:

$$F'_{01} - \frac{1}{2}\sqrt{F'_{ik}F'^{ik}}\sqrt{q} = 0, \tag{75}$$

$$F'_{23} - \frac{1}{2}\sqrt{F'_{ik}F'^{ik}}\sqrt{\hat{q}} = 0. \tag{76}$$

These equations determine the electromagnetic field in two-dimensional spaces. The Equations (75) defines an electromagnetic field in a two-dimensional space ($u$, $v$), and the Equation (76) defines a field in a two-dimensional space ($w$, $n$), and establishes a relationship between the electromagnetic field and determinants of the metric tensors (45) and (46) that define the two-dimensional spaces.

### 3.6. Spherically Symmetric Systems

We show that the Formula (75) is the Coulomb law written in curvilinear coordinates. To do this, we write the Formula (75) in three-dimensional space in orthogonal coordinates. Using the formulas [1]:

$$\gamma_{\alpha\beta} = -g'_{\alpha\beta} + \frac{g'_{0\alpha}g'_{0\beta}}{g'_{00}}, \alpha, \beta = 1,2,3, \tag{77}$$

$$-g' = g'_{00}\gamma, \tag{78}$$

where $\gamma = \det\left[\gamma_{\alpha\beta}\right]$ is the determinant, and $\gamma_{\alpha\beta}$, is three-dimensional metric tensor. Considering that $\sqrt{-g'} = 1$ from (78) we find: $g'_{00} = 1/\gamma$. From (77) we find: $g'_{11} = -\gamma_{11} + g'^2_{01}/g'_{00}$. Substituting instead of $g'_{00}$ and $g'_{11}$ the right parts of these equalities in (53) and taking into account that in orthogonal coordinates $\gamma = \gamma_{11}\gamma_{22}\gamma_{33}$ we get:

$$q = -\frac{1}{\gamma_{22}\gamma_{33}}. \tag{79}$$

The electric field, which is considered in the Coulomb law, is spherically

symmetric. Such a field is most conveniently viewed in spherical coordinates. Therefore, to determine $\gamma_{22}$ and $\gamma_{33}$, we write the square of the element of length in spherical coordinates $\mathrm{d}S^2 = \mathrm{d}r^2 + r^2\mathrm{d}\vartheta^2 + r^2\sin^2\vartheta\mathrm{d}\varphi^2$. But in this form it is impossible to use this equation to determine the components of the three-dimensional metric tensor. The fact is that the spherical coordinates $\vartheta$ and $\varphi$ enter it non-symmetrically and, moreover, they are dimensionless.

To eliminate these shortcomings, one should consider an infinitely small neighborhood of a point with the spherical coordinates $(\rho_0, \vartheta_0, \varphi_0)$. Then we draw through this point a tangent plane to a sphere of the radius $\rho_0$. Let us introduce on this plane a rectangular coordinate system ($\tilde{x}$, $\tilde{y}$) with the origin at a point $(\rho_0, \vartheta_0, \varphi_0)$ so that the coordinate axis $\tilde{x}$ is tangent to the coordinate line $\vartheta$, and the coordinate axis $\tilde{y}$ is tangent to the coordinate line $\varphi$. In an infinitely small neighborhood of the point, we have: $\mathrm{d}\tilde{x} \approx \rho_0\mathrm{d}\vartheta$; $\mathrm{d}\tilde{y} \approx \rho_0\sin\vartheta_0\mathrm{d}\varphi \approx \rho_0\sin\vartheta\mathrm{d}\varphi$. From here, we get:

$$\mathrm{d}S^2 = \mathrm{d}r^2 + \frac{r^2}{\rho_0^2}\mathrm{d}\tilde{x}^2 + \frac{r^2}{\rho_0^2}\mathrm{d}\tilde{y}^2. \tag{80}$$

From (80), we have the following values for the components of the three-dimensional metric tensor in an infinitely small neighborhood of the point ($\rho_0$, $\vartheta_0$, $\varphi_0$):

$$\gamma_{22} = \gamma_{33} = \frac{r^2}{\rho_0^2}. \tag{81}$$

For the transformations considered in the article from (37) we have $\delta x'^0 = \delta x'^1 = 0$. Consequently, for the variation of the metric tensor, we obtain, further omitting the prime sign ('):

$$\delta g_{ik} = \frac{\partial g_{ik}}{\partial x^l}\delta x^l = \frac{\partial g_{ik}}{\partial x^2}\delta x^2 + \frac{\partial g_{ik}}{\partial x^3}\delta x^3. \tag{82}$$

Hence, if the components $g_{ik}$ depend only on the coordinates $x^0$, $x^1$, for example, as in the spherically symmetric system (80), then in this system $\delta g_{ik} = 0$. Let us construct a tensor $g_{ik}$, satisfying the above conditions. We find the component $g_{00}$ from (78). The components $g_{\alpha\beta}$ are determined from (77). They will depend on $\frac{r^2}{\rho_0^2}$ (81) and on the components $g_{0\alpha} = g_{0\alpha}\left(x^0, x^1\right)$. It is easy to check that the determinant of this tensor is −1. Let us find the values of the diagonal components of the metric tensor $g_{ik}$ given in curvilinear coordinates $x^i$. We neglect the terms $\frac{r^4}{\rho_0^4}g_{0\alpha}^2$, which have a higher order of smallness. Using $x_\Gamma^i = x^i - \xi^i$, we get: $g_{00} = 1 - 2\xi^0_{,0}$; $g_{11} = -1 + 2\xi^1_{,1}$; $g_{22} = -1 + 2\xi^2_{,2}$; $g_{33} = -1 + 2\xi^3_{,3}$. In Galilean coordinates, the values of the diagonal components of the metric tensor on the left side of these equalities will be as follows: 1, −1, −1, −1. Hence, we obtain that the derivatives on the right-hand side of these equalities will be equal to zero. This is one more proof that the equality $\xi^i_{,i} = 0$ holds in Galilean coordinates. Now let us consider the curvilinear coordinates

$x^i$ describing a spherically symmetric system. As mentioned above, such a system should be considered in the tangent plane to a sphere of radius $\rho_0$ in an infinitesimal neighborhood of the point of tangency $(\rho_0, \vartheta_0, \varphi_0)$ of the plane with the sphere. In an infinitely small neighborhood of this point, we can write $\frac{r}{\rho_0} \approx 1+\delta$, where $\delta$ is a small quantity, therefore, for the diagonal components of the metric tensor of a spherically symmetric system, we have: $g_{00} = 1-4\delta$; $g_{11} = -1$; $g_{22} = g_{33} = -1-2\delta$. Comparing these values with the previously obtained ones, we find: $\xi^0_{,0} = 2\delta$; $\xi^1_{,1} = 0$; $\xi^2_{,2} = \xi^3_{,3} = -\delta$. From this, we see that for a spherically symmetric system $\xi^i_{,i} = 0$.

Substituting (81) into (79) and the result of this substitution into (75), we arrive at the formula:

$$F'_{01} = \frac{1}{2}\sqrt{-F'_{ik}F'^{ik}}\,\frac{\rho_0^2}{r^2}. \tag{83}$$

Considering that $A = A_\Gamma$, the Equation (41) and the calculation (7), we find $F'_{01} = \mathbf{E}_\Gamma \mathbf{f}_\Gamma - \mathbf{H}_\Gamma \mathbf{s}_\Gamma$. But we consider only the electric field, therefore $\mathbf{H}_\Gamma = 0$. In the absence of any movement and change, time remains unchanged, therefore $u \equiv x'^0 = x^0_\Gamma \equiv ct$. Thus, everything comes down to the transformation of spatial coordinates: the rectangular Cartesian coordinates $x, y, z$ and the curvilinear coordinates $v, w, n$, which naturally should be taken as spherical coordinates. So, for instance, $v = r$, and for the electric field we have $E_r = E$; $E_\vartheta = E_\varphi = 0$. It follows that $\mathbf{E}_\Gamma = E\left[\sin\vartheta\cos\varphi, \sin\vartheta\sin\varphi, \cos\vartheta\right]$. From (9), (11), etc., we obtain: $\mathbf{f}_\Gamma = \left[\sin\vartheta\cos\varphi, \sin\vartheta\sin\varphi, \cos\vartheta\right]$. Considering the above, we arrive at this value $F'_{01} = \mathbf{E}_\Gamma \mathbf{f}_\Gamma = E$. Now the Formula (83) can be written as follows:

$$E = \frac{1}{2}\sqrt{-F'_{ik}F'^{ik}}\,\frac{\rho_0^2}{r^2}. \tag{84}$$

From this formula it follows that a physical value equal to

$$2\pi\varepsilon_0\rho_0^2\sqrt{-F'_{ik}F'^{ik}}, \tag{85}$$

is an electric charge $e$, where $\varepsilon_0$ —electric constant. Thus, we get the formula $E = \frac{e}{4\pi\varepsilon_0 r^2}$, which completely coincides with Coulomb's law.

Now we will consider the Formula (76) in a three-dimensional space in spherical coordinates. To do this, we again use the Formulas (77), (78) and again we take into account that $\sqrt{-g'} = 1$. Thus, after the transformation, we obtain the determinant (54):

$$\hat{q} = \gamma_{22}\gamma_{33} - \frac{g_2^2}{\gamma_{11}\gamma_{22}} - \frac{g_3^2}{\gamma_{11}\gamma_{33}}, \tag{86}$$

where $g_\alpha = -\frac{g'_{0\alpha}}{g'_{00}}$ [1]. Substituting in this expression the values of the components of the three-dimensional metric tensor (81), as well as $\gamma_{11} = 1$, see (80), we arrive at the following formula:

$$\hat{q} = \frac{r^4}{\rho_0^4} - \frac{\rho_0^2}{r^2}\left(g_2^2 + g_3^2\right). \tag{87}$$

We multiply the left side and the right side of the Formula (87) by the value $\frac{r^2}{\rho_0^2}$. Then, denoting $\chi = \frac{r^2}{\rho_0^2}$, we represent (87) as a cubic equation

$$\chi^3 - \hat{q}\chi - g_2^2 - g_3^2 = 0. \tag{88}$$

Its solution is three roots:

$$\chi_1 = \frac{r_1^2}{\rho_0^2}; \chi_2 = \frac{r_2^2}{\rho_0^2}; \chi_3 = \frac{r_3^2}{\rho_0^2}. \tag{89}$$

These roots satisfy the following relations:

$$\chi_1 + \chi_2 + \chi_3 = 0. \tag{90}$$

$$\chi_1\chi_2 + \chi_2\chi_3 + \chi_3\chi_1 = -\hat{q}. \tag{91}$$

$$\chi_1\chi_2\chi_3 = g_2^2 + g_3^2. \tag{92}$$

Raising the left side of the Equation (90) to the square and taking into account (91), we get:

$$\hat{q} = \frac{r_1^4 + r_2^4 + r_3^4}{2\rho_0^4}. \tag{93}$$

We divide the left side of the Equation (91) by the left side of the Equation (92) and, accordingly, the right side of the Equation (91) by the right side of the Equation (92), and thus, we find:

$$\hat{q} = -\rho_0^2\left(\frac{1}{r_1^2} + \frac{1}{r_2^2} + \frac{1}{r_3^2}\right)\left(g_2^2 + g_3^2\right). \tag{94}$$

From (94) it follows that the value $\hat{q}$ is formed by three separate "particles" with relative charges as follows:

$$\frac{1}{\chi_1} = \frac{\rho_0^2}{r_1^2}; \frac{1}{\chi_2} = \frac{\rho_0^2}{r_2^2}; \frac{1}{\chi_3} = \frac{\rho_0^2}{r_3^2}. \tag{95}$$

Their total relative charge is equal to the relative charge of the proton. Taking the relative charge of the proton equal to unity, from (94) we obtain the relationship between the coefficient and the free term of Equation (88): $\hat{q} = -g_2^2 - g_3^2$. Obviously, only quarks can be such "particles". It is easy to verify as for quarks forming a proton and having charges of $\frac{2}{3}; \frac{2}{3}; -\frac{1}{3}$ the relation (90) is really fulfilled: $\frac{3}{2} + \frac{3}{2} - \frac{3}{1} = 0$. From these simple considerations, it follows that the two-dimensional space $(w, n)$ has finite dimensions and it, in fact, is what we call an elementary particle, for example, a proton.

Here is one more proof of the correctness of the theoretical calculations and the conclusions made on their basis. From (75) and (76), we find:

$$\frac{F'_{23}}{F'_{01}} = \sqrt{\frac{\hat{q}}{q}}. \tag{96}$$

For the proton $\hat{q} = -g_2^2 - g_3^2$, and from (78) and (79) we have $q = -g'_{00}$. If we use these values, by means of (87), we obtain:

$$\frac{F'_{23}}{F'_{01}} = \frac{\frac{r^5}{\rho_0^5}}{\sqrt{1-\frac{r^2}{\rho_0^2}}}. \tag{97}$$

At $\frac{r^2}{\rho_0^2} \to 0$, $\frac{F'_{23}}{F'_{01}} \to 0$; at $\frac{r^2}{\rho_0^2} \to 1$, $\frac{F'_{23}}{F'_{01}} \to \infty$. This result proves that Formula (76) describes a strong interaction acting in a finite region of space, the magnitude of which is determined by the radius $\rho_0$. And in this region of space, the magnitude of the strong interaction grows with the increasing radius *r*.

### 3.7. Evidence

The solution to Equation (88) was obtained for $\hat{q} > 0$. This inequality is fulfilled in the region of four-dimensional space, which in spherical coordinates is defined as follows: $\rho_0 < r \le \infty$. It is in this region that the quark nature of an elementary particle is manifested. This can be explained by the fact that two invariants $\hat{q}$ and $F'_{ik}F'^{ik}$ (their invariance follows from the equality to unity of the Jacobian transformation, since $\sqrt{-g} = 1$) in Galilean coordinates decompose into three invariants of Lorentz transformations [2]. For example, $H_{\Gamma x}^2 - E_{\Gamma x}^2$; $H_{\Gamma z}^2 - E_{\Gamma y}^2$; $H_{\Gamma y}^2 - E_{\Gamma z}^2$ which behave like independent entities. But in curvilinear coordinates, these three invariants will no longer be invariants. Therefore, their complete independence is impossible. Because of this, quarks are not particles in the usual sense. In the absence of a magnetic field $F'_{ik}F'^{ik} = -2\mathbf{E}_\Gamma^2 < 0$, and in the indicated region of space, a complex quantity appears in equality (76), which is unacceptable. Therefore, Equality (76) is inapplicable in this region of four-dimensional space. Equality (76) will consist of real values for $\hat{q} < 0$. This inequality holds in the region defined as $0 \le r < \rho_0$. This is easy to prove if we notice that it is in this region of the four-dimensional space that Equation (88) has one more solution. Substituting the equal value $\hat{q} = -g_2^2 - g_3^2$ into Equation (88) instead of the free term, we find

$$\hat{q} = \frac{\chi^3}{\chi - 1}. \tag{98}$$

Hence it follows that for $\chi \le 1$ we have $\hat{q} \le -\infty$. It can be seen that the indicated solution is obtained for $\chi \sim 1$, when $|\hat{q}| \gg \chi^3$, therefore $\chi^3$ in the equation can be neglected. Note, that in the region $0 \le r < \rho_0$ the electromagnetic field radically changes its dependence on the spatial coordinates (76) and completely coincides with the dependence that is observed for the strong interaction.

## 4. Geodesic Line Equation

The principle of equivalence of an electromagnetic field and a free material particle allows us to apply the principle of least action to an electromagnetic field. As is known, the principle of least action establishes the law of motion of a free material particle. Application of the principle of least action to an electromagnetic field allows us to find a law explaining how an elementary particle is formed from an electromagnetic field.

Thus, the geometry of the electromagnetic field, determined by the field lines of force, must obey the principle of least action, which determines the motion of a free material particle [1]:

$$-mc\delta\int \mathrm{d}s = 0. \tag{99}$$

The following physical quantities were used here: $m$-mass of a free material particle; $c$-speed of light; d$s$-interval, equal: $\mathrm{d}s^2 = g_{ik}\mathrm{d}x^i\mathrm{d}x^k$, $(i,k,\cdots = 0,1,2,3)$; $\mathrm{d}x^i$-differential of curvilinear coordinates $x^i$.

Let us vary the integral on the left side of expression (99). At the same time, we take into account that the variations $\delta x'^0$ and $\delta x'^1$ are equal to zero (37). Taking into account the above, the result of the variation is the equation:

$$\frac{\mathrm{d}u_{\hat{a}}}{\mathrm{d}s} - \frac{1}{2}\frac{\partial g_{ik}}{\partial x^{\hat{a}}}u^i u^k = 0, \tag{100}$$

$u^i = \dfrac{\mathrm{d}x^i}{\mathrm{d}s}$ is the four-dimensional speed; $\hat{a} = 2,3$. In Equation (100), the prime sign is omitted.

Equation (100) is the equation of a geodesic line for an electromagnetic field. The field is not limited by anything, does not experience any influences and is completely equivalent to a free material particle.

Let us consider Equation (100) in more detail. We write the second term in Equation (100) using the three-dimensional metric tensor $\gamma_{\alpha\beta}$ (77) and the three-dimensional vector: $g_\alpha = -g_{0\alpha}/g_{00}$. Considering transformations:

$$u^0 - g_\alpha u^\alpha = \frac{g_{00}\mathrm{d}x^0 + g_{0\alpha}\mathrm{d}x^\alpha}{g_{00}\mathrm{d}s} = \frac{g_{0i}\mathrm{d}x^i}{g_{00}\mathrm{d}s} = \frac{\mathrm{d}x_0}{g_{00}\mathrm{d}s}, \tag{101}$$

the second term in Equation (100) can be rewritten as follows:

$$-\frac{1}{2g_{00}^2}\frac{\partial g_{00}}{\partial x^{\hat{a}}}\left(\frac{\mathrm{d}x_0}{\mathrm{d}s}\right)^2 + \frac{\partial g_\alpha}{\partial x^{\hat{a}}}u^\alpha\frac{\mathrm{d}x_0}{\mathrm{d}s} + \frac{\partial \gamma_{\alpha\beta}}{\partial x^{\hat{a}}}u^\alpha u^\beta. \tag{102}$$

Let us represent the third term of the sum (102) in the following form:

$$\lambda_{\alpha,\beta\hat{a}}u^\alpha u^\beta. \tag{103}$$

To do this, we use three-dimensional Christoffel symbols:

$$\lambda_{\alpha,\beta\gamma} = \frac{1}{2}\left(\frac{\partial \gamma_{\alpha\beta}}{\partial x^\gamma} + \frac{\partial \gamma_{\alpha\gamma}}{\partial x^\beta} - \frac{\partial \gamma_{\beta\gamma}}{\partial x^\alpha}\right). \tag{104}$$

Consider the electric field of an immobile and non-interacting elementary charged particle. Such a field will be spherically symmetrical. Therefore, in three-dimensional space we will use spherical coordinates $(r,\vartheta,\varphi)$. In three-

dimensional space in spherical coordinates, non-zero Christoffel symbols are equal to the following values: $\lambda_{1,22} = -r$; $\lambda_{2,12} = r$; $\lambda_{1,33} = -r\sin^2\vartheta$; $\lambda_{3,13} = r\sin^2\vartheta$; $\lambda_{2,33} = -r^2\sin\vartheta\cos\vartheta$; $\lambda_{3,23} = r^2\sin\vartheta\cos\vartheta$. These values turn expressions (103), and hence the third term of the sum (102), to zero:

$$\frac{1}{2}\frac{\partial\gamma_{\alpha\beta}}{\partial x^{\hat{a}}}u^{\alpha}u^{\beta} = \lambda_{\alpha,\beta\hat{a}}u^{\alpha}u^{\beta} = 0. \tag{105}$$

Let an elementary charged particle move at a constant speed. As a result of the Lorentz contraction of the length along the direction of motion, the electric field of the elementary particle will be cylindrically symmetrical. Let's consider this field in three-dimensional space in cylindrical coordinates ($\rho, \varphi, z$). In three-dimensional space in cylindrical coordinates, non-zero Christoffel symbols are equal to the following values: $\lambda_{1,22} = -\rho$; $\lambda_{2,12} = \rho$. These values also satisfy equality (105). Thus, equality (105) is also fulfilled in a cylindrically symmetric electromagnetic field.

Now let's find the conditions under which the first two terms in expression (102) are equal to zero. This becomes possible if the clocks in the system under consideration are synchronized. The clock synchronization condition means that expression (101) is equal to zero. This is possible if

$$\mathrm{d}x_0 = 0. \tag{106}$$

Clock synchronization is not possible along a line whose ends converge at one point. An example of such a line is a circle. In spherical coordinates, such a line is the coordinate line of the $\varphi$ ($i = 3$) coordinate. Therefore, condition (106) is not applicable along this coordinate. But the components of the metric tensor, which describes a spherically symmetric system, do not depend on the coordinate $\varphi$. It means that

$$\frac{\partial g_{00}}{\partial x^3} = \frac{\partial g_{\alpha}}{\partial x^3} = 0. \tag{107}$$

Therefore, in a spherically symmetric system, expression (102) is equal to zero.

In cylindrical coordinates, the coordinate line coordinates ($i = 2$) $\varphi$ is also a circle. Therefore, condition (106) is not applicable along this coordinate. But the components of the metric tensor describing a cylindrically symmetric system do not depend on the coordinate $\varphi$. It means that

$$\frac{\partial g_{00}}{\partial x^2} = \frac{\partial g_{\alpha}}{\partial x^2} = 0. \tag{108}$$

Therefore, in a cylindrically symmetric system, expression (102) is also equal to zero.

The equality to zero of expression (102) means that the second term in Equation (100) is equal to zero. Therefore, the equation of the geodesic line (100) for an electromagnetic field with spherical or cylindrical symmetry will be as follows:

$$\frac{\mathrm{d}u_{\hat{a}}}{\mathrm{d}s} = 0. \tag{109}$$

But the same equation of a geodesic line will have an electromagnetic field in the Galilean four-dimensional coordinate system. This means that we have found two types of curvilinear coordinates (spherical and cylindrical) for which Equation (109) coincides with the equation obtained in Galilean coordinates. This means that the transition from spherical (and cylindrical) coordinates to Galilean coordinates does not change the electromagnetic field. Since Equation (109) does not change during this transition. Summarizing the above, we can formulate a law explaining how an electromagnetic field turns into an elementary particle. It follows from the principle of least action that it is the spherically (cylindrically) symmetric configuration of the electromagnetic field that provides the minimum for the action integral. This law explains that the mass and charge of an elementary particle is a consequence of the spherical configuration of the field.

An experimental confirmation of this law can be considered the creation of particle-antiparticle pairs from a gamma-ray quantum. This process was first observed in 1933 by the Joliot-Curies.

## 5. Conclusions

Summing up, it must be said that in electrodynamics, considered in curvilinear coordinates, the second pair of Maxwell's equations can be obtained using the antisymmetric character of the electromagnetic field tensor. From this antisymmetry, it follows: $F^{ik}_{;i;k} = 0$. If we mark

$$-\frac{c}{4\pi}F^{ik}_{,k} \tag{110}$$

as a four-dimensional vector of current density, we obtain the second pair of Maxwell's equations in a known form, and from the equation $F^{ik}_{;i;k} = 0$, taking into account the introduced notation, we get the continuity equation. So, classical electrodynamics which neglects the internal structure of elementary particles can be called a macroscopic theory that considers electromagnetic fields on the scale of the macro-world.

## Conflicts of Interest

The author declares no conflicts of interest regarding the publication of this paper.

## References

[1] Landau, L.D. and Lifshitz, E.M. (1980) The Classical Theory of Fields. Course of Theoretical Physics. Volume 2, Butterworth-Heinemann, an Imprint of Elsevier Science.

[2] Parfyonov, A.V. (2018) Electrodynamics in Curvilinear Coordinates. IPK "Venets" Ulstu, Ulyanovsk.

[3] Rashevsky, P.K. (2006) Rimanova Geometry and Tensor Analysis. URSS, Moscow, 383, 387, 445.

Journal of Modern Physics, 2022, 13, 1403-1410
https://www.scirp.org/journal/jmp
ISSN Online: 2153-120X
ISSN Print: 2153-1196

# An SU(3) Electroweak Unified Model Using Generalized Yang-Mills Theory

**Lu Wang[1], Xinyu Zhou[1], Dianfu Wang[1], Sizhao Huang[2*], Yanqing Guo[1*]**

[1]School of Science, Dalian Maritime University, Dalian, China
[2]School of Physics, University of Electronic Science and Technology of China, Chengdu, China
Email: wangdfu@dlmu.edu.cn, *huangsz301@163.com, *yqguo@dlmu.edu.cn

**How to cite this paper:** Wang, L., Zhou, X.Y., Wang, D.F., Huang, S.Z. and Guo, Y.Q. (2022) An SU(3) Electroweak Unified Model Using Generalized Yang-Mills Theory. *Journal of Modern Physics*, **13**, 1403-1410.
https://doi.org/10.4236/jmp.2022.1311087

**Received:** October 11, 2022
**Accepted:** November 13, 2022
**Published:** November 16, 2022



## Abstract

Generalized Yang-Mills theory has a covariant derivative which contains both vector and scalar gauge bosons. Based on this theory, we construct an $SU(3)$ unified model of electromagnetic and weak interactions to simplify the Weinberg-Salam model. By using the Nambu-Jona-Lasinio mechanism, the symmetry breaking can be realized dynamically. The masses of $W^{\pm}$, $Z^0$ are obtained and interactions between various particles are the same as that of the Weinberg-Salam model. At the same time, $\sin^2\theta_w = 1/4$ can be given.

## Keywords

Yang-Mills Theory, Dynamical Symmetry Breaking, Nambu-Jona-Lasinio Mechanism

## 1. Introduction

Up to now, many experimental results have proved that the Weinberg-Salam (WS) model [1] [2] is correct in the current energy range, but as Weinberg himself pointed out, the WS model still has some unsatisfactory points [3]. The WS model describes the weak and electromagnetic interactions in the energy range ≤ $10^2$ GeV with two different coupling constants $g$ and $g'$ for the gauge groups $SU(2)$ and $U(1)$, respectively. Thus, there is no real explanation of the different strengths displayed by the two interactions. For example, the experimentally determined Weinberg angle is approximately equal to 30˚, which cannot be directly obtained by WS model itself. On the other hand, although the 125 GeV Higgs boson has been discovered in 2012 [4] [5], there is still no evidence that Higgs particles are basic or compound particles and the number of Higgs particles is without theoretical guidance. Therefore, the improvement of the WS model is still necessary.

There have been different types of ideas to improve these situations. The most widely accepted one by far has been to use a large group of which $SU(2)\otimes U(1)$ is just a small subgroup. The original work is an old idea proposed by Fairlie [6] and Ne'eman [7], of using supergroup $SU(1/2)$ as the unification group and putting the Higgs fields in the adjoint along with the vector fields. But it increases the dimensions of space-time; meanwhile, the number of the Higgs bosons increases, which is not expected to be seen in theory. In Ref. [8], the authors have constructed an $SU(3)$ unified model of electroweak interaction; by using different realizations of $SU(3)$ algebra, the correct quantum numbers of the leptons and the Weinberg angle can be given. However, since $SU(3)$ group has eight generators, there are four more vector gauge fields $V^{\pm}$ and $U^{\pm}$ than the WS model, as well as some heavy fermions and scalar particles in the model.

Then, is there a more natural way for us to introduce the Higgs fields to physical theories? Many scholars have taken efforts to solve this problem. In Ref. [9], the authors have constructed a unified $U(3)$ model of electroweak interaction using a generalized Dirac covariant derivative, that contained both vector and pseudo-scalar fields. However, since $U(3)$ group has nine generators, it will have a extra field that does not interact with other particles than the WS model. And what's more, there is no the Higgs potential $V(\varphi)$ in the model; thus the spontaneous symmetry breaking cannot be applied, and the particles in the model cannot obtain masses. Recently, some authors have attempted to construct the so-called generalized Yang-Mills theory (GYMT) [10] [11] [12] [13] [14], which the generalized Dirac covariant derivative $D$ is besides the vector part $A_{\mu}$; it can also contain a scalar part $\varphi$, a pseudo-scalar part $P$, an axial-vector part $V_{\mu}$ and a tensor part $T_{\mu\nu}$. In Ref. [12], by using a covariant derivative with both vector and scalar gauge fields, the authors have constructed a generalized Yang-Mills model, which is invariant under local gauge transformations of a Lie group. Since the GYMT does not involve the potential energy term about the scalar fields, it is difficult to realize the Higgs mechanism [15] directly. It is shown, in terms of the Nambu-Jona-Lasinio (NJL) mechanism [16], that the gauge symmetry breaking can be realized dynamically.

Based on the GYMT given in Ref. [12], the work of the present paper is to construct an $SU(3)$ gauge-invariant unified model of electroweak interaction and that it naturally assigns the correct quantum numbers to the leptons and Higgs bosons. By using the GYMT, we introduce vector fields and scalar fields as the gauge fields into the model by the requirement of localization gauge invariance. We will show that, in terms of the NJL mechanism, the symmetry breaking can be realized dynamically and the masses of $W^{\pm}$ and $Z^{0}$ particles are obtained. Meanwhile, interactions between various particles are the same as that of the WS model.

## 2. Generalized Yang-Mills Theory

The main idea of the GYMT in Ref. [12] is as follows: Corresponding to each

generator of the Lie group there is a gauge field, it does not matter whether vector fields or scalar fields. The generalized Dirac covariant derivative $D$ can be constructed by taking each of the $N$ generators and multiplying it by one of its associated gauge fields and summing them together

$$D = \gamma_\mu \partial_\mu - i\gamma_\mu A_\mu + \varphi, \tag{1}$$

where

$$A_\mu = gA_\mu^a T_a, \varphi = g\varphi^b T_b, \tag{2}$$

with the subscript $a$ varies from 1 to $N_A$, $b$ varies from $N_A + 1$ to $N$. Define the transformation for the gauge fields as

$$-i\gamma_\mu A_\mu + \varphi \to U\left(-i\gamma_\mu A_\mu + \varphi\right)U^{-1} - \left(\gamma_\mu \partial_\mu U\right)U^{-1}, \tag{3}$$

from which we can obtain that the covariant derivative must transform as $D \to UDU^{-1}$. When the covariant derivative acts on the matter field $\psi$, its gauge fields $A_\mu$ and $\varphi$ will acquire certain coefficients called the charges $Q_A$ and $Q_\varphi$ of each gauge field with respect to $\psi$ with the result

$$D_\psi = \gamma_\mu \partial_\mu - iQ_A \gamma_\mu A_\mu + Q_\varphi \varphi. \tag{4}$$

From our knowledge of the standard model we can only conclude that $Q_A = 1$. As for $Q_\varphi$, it is only known that parameter $gQ_\varphi$ is related to the mass of the matter field. If $Q_A = Q_\varphi = 1$, the expressions of covariant derivatives $D$ and $D_\psi$ will be the same form, which is a considerable question that will be discussed in the next part.

The Lagrangian density of the GYMT contains only covariant derivatives and matter fields, and that it possesses both gauge and Lorentz invariance:

$$L = -\bar{\psi} D_\psi \psi + \frac{1}{2g^2}\widetilde{Tr}\left(\frac{1}{8}\left(TrD^2\right)^2 - \frac{1}{2}TrD^4\right), \tag{5}$$

in which the trace with the tilde is over the matrices of the Lie group and the one without tilde is over the matrices of the spinorial representation of Lorentz group.

## 3. The *SU*(3) Unified Model of Electroweak Interaction

In this section, in terms of the above GYMT, we will construct an $SU(3)$ unified model of electromagnetic and weak interactions of electron-type leptons. By considering an $SU(3)$ gauge invariant GYMT, it will be naturally assign the correct isospin $T_3$ and hypercharge $Y$ quantum numbers to the neutrino and the electron, so long as we place them in $SU(3)$ fundamental representation

$$\psi = \begin{pmatrix} \nu_L \\ e_L \\ e_R \end{pmatrix}. \tag{6}$$

In the Lagrangian density (5), the covariant derivative $D$ will be of the form Equation (1) where $A_\mu = gA_\mu^a T_a \left(a = 1,2,3,8\right)$ is the vector gauge field, $\varphi = g\varphi^b T_b \left(b = 4,5,6,7\right)$ is the scalar gauge field, and $g$ is the coupling constant,

we have

$$D=\gamma_\mu\partial_\mu-i\gamma_\mu gA_\mu^a T_a+g\varphi^b T_b, \tag{7}$$

in which $T_i=(1/2)\lambda_i$ are the generators of $SU(3)$ group in three-dimensional representation, the $\lambda_i$ are $3\times3$ traceless Hermitian matrices, which can be chosen to have the form

$$\begin{aligned}
&\lambda_1=\begin{pmatrix}0&1&0\\1&0&0\\0&0&0\end{pmatrix},\lambda_2=\begin{pmatrix}0&-i&0\\i&0&0\\0&0&0\end{pmatrix},\\
&\lambda_3=\begin{pmatrix}1&0&0\\0&-1&0\\0&0&0\end{pmatrix},\lambda_4=\begin{pmatrix}0&0&1\\0&0&0\\1&0&0\end{pmatrix},\\
&\lambda_5=\begin{pmatrix}0&0&-i\\0&0&0\\i&0&0\end{pmatrix},\lambda_6=\begin{pmatrix}0&0&0\\0&0&1\\0&1&0\end{pmatrix},\\
&\lambda_7=\begin{pmatrix}0&0&0\\0&0&-i\\0&i&0\end{pmatrix},\lambda_8=\frac{1}{\sqrt{3}}\begin{pmatrix}-1&0&0\\0&-1&0\\0&0&2\end{pmatrix}.
\end{aligned} \tag{8}$$

One can see that the matrices from $\lambda_1$ to $\lambda_7$ are still the usual Gell-Mann matrices. Meanwhile the last one $\lambda_8$ takes the minus sign. Correspondingly, the components containing indices 8 in the structure constants $f_{ijk}$ and $d_{ijk}$ of $SU(3)$ group will take the minus sign too.

Next, we will give the specific form of the covariant derivative $D_\psi$ in Equation (5). Following from Ref. [8], in order to obtain the correct hypercharge of $e_R$, we choose one of the four realizations of $SU(3)$ algebra. Then the above eight generators $T_i$ can be divided into two groups $T_n\,(n=2,4,6)$ and $T_s\,(s=1,3,5,7,8)$ respectively. Define $T_i^{(5)}\,(i=1,\cdots,8)$ as

$$T_n^{(5)}=T_n,T_s^{(5)}=T_s\gamma_5. \tag{9}$$

It can be easily proved that $T_i^{(5)}$ satisfy the same commutation rules as $T_i$

$$\left[T_i^{(5)},T_j^{(5)}\right]=if_{ijk}T_k^{(5)}. \tag{10}$$

Here, $T_i^{(5)}$ is the one of the four realizations of $SU(3)$ algebra.

Following the above discussion we can give the covariant derivative $D_\psi$ as

$$D_\psi=\gamma_\mu\partial_\mu-i\gamma_\mu A_\mu^{(5)}+Q_\varphi\varphi^{(5)}, \tag{11}$$

where $A_\mu^{(5)}=gA_\mu^a T_a^{(5)}\,(a=1,2,3,8),\varphi^{(5)}=g\varphi^b T_b^{(5)}\,(b=4,5,6,7)$. By using $\gamma_5L=L$, and $\gamma_5R=-R$, we can obtain

$$\begin{aligned}
i\bar\psi\gamma_\mu A_\mu^{(5)}\psi&=ig\bar\psi\gamma_\mu\left[\gamma_5\left(A_\mu^1T_1+A_\mu^3T_3+A_\mu^8T_8\right)+A_\mu^2T_2\right]\psi\\
&=ig\bar\psi\gamma_\mu\left[A_\mu^1T_1+A_\mu^2T_2+A_\mu^3T_3+A_\mu^8T_8'\right]\psi,
\end{aligned} \tag{12}$$

in which $T_8'=1/\left(2\sqrt{3}\right)diag\left(-1,-1,-2\right)$. This means that the hypercharges of

$\nu_L, e_L$ and $e_R$ are $-1, -1, -2$, respectively.

Substituting Equation (12), Equation (11) and Equation (7) into Equation (5), the Lagrangian density changes to be

$$\begin{aligned} L = & -\bar{\psi}\gamma_\mu\partial_\mu\psi + i\bar{\psi}\gamma_\mu A_\mu^{(5)}\psi - Q_\varphi\bar{\psi}\varphi^{(5)}\psi \\ & -\frac{1}{2g^2}\widetilde{Tr}\left(\partial_\mu A_\nu - \partial_\nu A_\mu - i\left[A_\mu, A_\nu\right]\right)^2 - \frac{1}{g^2}\widetilde{Tr}\left(\partial_\mu\varphi - i\left\{A_\mu, \varphi\right\}\right)^2. \end{aligned} \tag{13}$$

By using the Pauli matrices $\sigma_{a'}\left(a'=1,2,3\right)$, Equation (6) and Equation (12), one can give the expansion of the Lagrangian density (13) as

$$\begin{aligned} L = & -\bar{\theta}_L\gamma_\mu\left(\partial_\mu - \frac{1}{2}igA_\mu^{a'}\sigma_{a'} + \frac{1}{2}ig'A_\mu^8\right)\theta_L - \bar{e}_R\gamma_\mu\left(\partial_\mu + ig'A_\mu^8\right)e_R \\ & -\frac{G_F}{\sqrt{2}}\bar{e}_R\phi^{(5)+}\theta_L - \frac{G_F}{\sqrt{2}}\bar{\theta}_L\phi^{(5)}e_R - \frac{1}{4}F_{\mu\nu}^{a'}F_{\mu\nu}^{a'} - \frac{1}{4}F_{\mu\nu}^8F_{\mu\nu}^8 \\ & -\left|\left(\partial_\mu - \frac{1}{2}igA_\mu^{a'}\sigma_{a'} - \frac{1}{2}ig'A_\mu^8\right)\phi\right|^2, \end{aligned} \tag{14}$$

where, $F_{\mu\nu}^{a'} = \partial_\mu A_\nu^{a'} - \partial_\nu A_\mu^{a'} + gf_{a'b'c'}A_\mu^{b'}A_\nu^{c'}\left(a',b',c'=1,2,3\right)$, $F_{\mu\nu}^8 = \partial_\mu A_\nu^8 - \partial_\nu A_\mu^8$, $G_F = gQ_\varphi$, $\phi = \left(\varphi^4 - i\varphi^5, \varphi^6 - i\varphi^7\right)^{\mathrm{T}}/\sqrt{2}$, $\phi^{(5)} = \left(\varphi^4 - i\gamma_5\varphi^5, \varphi^6 - i\gamma_5\varphi^7\right)^{\mathrm{T}}/\sqrt{2}$, $\theta_L = \left(\nu_L, e_L\right)^{\mathrm{T}}$ and $g' = g/\sqrt{3}$. By considering $g' = g/\sqrt{3}$, one can conclude that $\sin^2\theta_w = 1/4$ easily. Seeing from Equation (14), one can obtain the correct hypercharge $Y=1$ of the scalar field (the Higgs field) as in the WS model.

In Equation (14), the factor $G_F/\sqrt{2} = gQ_\varphi/\sqrt{2}$ is the Yukawa coupling constant for the coupling between the scalar gauge field and the fermion field. The fermion masses are proportional to $gQ_\varphi/\sqrt{2}$ after electroweak symmetry breaking. And the different masses of all elementary fermions are determined by the different values of $Q_\varphi$. If $Q_\varphi = 1$, as we have mentioned above, is there any possibilities that the elementary fermion mass spectrum can be obtained as usual? In Ref. [17], the authors have discussed this problem and proposed a possible way to solve it.

## 4. Dynamical Breaking of *SU*(3) Gauge Symmetry

As is known to us, Equation (14) is almost the Lagrangian density of the WS model, except that no the Higgs potential $V\left(\varphi\right)$, which means that the spontaneous symmetry breaking mechanism cannot be utilized directly. In this section, we will show that by using the NJL mechanism, the *SU*(3) gauge symmetry breaking can be realized dynamically.

Substituting Equation (13) into Euler equation, one can obtain the equations of motion for the fermion field $\psi$, the scalar gauge fields $\varphi^b$, and the vector gauge fields $A_\mu^{a'}$

$$\gamma_\mu\left(\partial_\mu - igA_\mu^aT_a^{(5)}\right)\psi + G_F\varphi^bT_b^{(5)}\psi = 0, \tag{15}$$

$$\left(\partial_\mu^2 - g^2dA_\mu^aA_\mu^a\right)\varphi^b - G_F\bar{\psi}T_b^{(5)}\psi = 0, \tag{16}$$

$$\left(\partial_\mu F_{\mu\nu}^{a'} + gf_{a'b'c'}A_\mu^{b'}F_{\mu\nu}^{c'}\right) + g^2d\left(\varphi^b\right)^2A_\nu^{a'} - ig\bar{\psi}\gamma_\nu T_{a'}^{(5)}\psi = 0. \tag{17}$$

With $d = d_{abc}d_{abc}\left(a = 1,2,3,8, b = 4,5,6,7\right)$. Multiplying $A_\nu^{a'}$ on both sides of Equation (17), we obtain

$$\left[\left(\partial_\mu F_{\mu\nu}^{a'} + gf_{a'b'c'}A_\mu^{b'}F_{\mu\nu}^{c'}\right) + g^2 d\left(\varphi^b\right)^2 A_\nu^{a'} - ig\bar{\psi}\gamma_\nu T_{a'}^{(5)}\psi\right]A_\nu^{a'} = 0, \tag{18}$$

after taking the vacuum expectation value of Equation (18), to the lowest-order approximation in $\hbar$, we obtain a simple formula

$$f\left\langle A_\mu^{a'}A_\mu^{a'}\right\rangle = d\left\langle\left(\varphi^b\right)^2\right\rangle, \tag{19}$$

where $f = f_{a'b'c'}f_{a'b'c'}\left(a', b', c' = 1,2,3\right)$. We can see that in the ground state, Equation (19) gives an important relationship between the vector gauge fields and the scalar gauge fields. One can denote the vacuum expectation of the scalar fields as

$$\left\langle\varphi^b\right\rangle = \left\langle\varphi^6\right\rangle = \upsilon \neq 0, \tag{20}$$

which means

$$\left\langle\phi\right\rangle = \left\langle\phi^{(5)}\right\rangle = \frac{1}{\sqrt{2}}\begin{pmatrix}0\\ \upsilon\end{pmatrix}. \tag{21}$$

Substitute Equation (21) into Equation (14), we can give the masses of the neutrino and the electron

$$m_e = \frac{G_F\upsilon}{2}, m_\nu = 0. \tag{22}$$

Let us now take the vacuum expectation value of Equation (16). To the lowest-order approximation in $\hbar$, by using Equation (19), the self-consistency equation can be given as

$$g^2d^2f^{-1}\left\langle\varphi^6\right\rangle^3 = -\frac{1}{2}G_F\left\langle\bar{e}e\right\rangle. \tag{23}$$

In Equation (23), with an invariant momentum cut-off at $p^2 = \Lambda$ in the momentum integral, $\left\langle\bar{e}e\right\rangle$ will be finite value as

$$\begin{aligned}\left\langle\bar{e}e\right\rangle &= -TrS_F\left(0\right) = 2G_F\left\langle\varphi^6\right\rangle\int\frac{\mathrm{d}^4p}{\left(2\pi\right)^4}\frac{i}{p^2 + G_F^2\left\langle\varphi^6\right\rangle^2/4}\\ &= -\frac{G_F\left\langle\varphi^6\right\rangle}{4\pi^2}\left[\Lambda^2 - \frac{G_F^2\left\langle\varphi^6\right\rangle^2}{4}\ln\left(\frac{4\Lambda^2}{G_F^2\left\langle\varphi^6\right\rangle^2} + 1\right)\right].\end{aligned} \tag{24}$$

Substituting Equation (24) into Equation (23), we have

$$\left\langle\varphi^6\right\rangle^2 = \frac{G_F^2f}{8\pi^2d^2g^2}\left[\Lambda^2 - \frac{G_F^2\left\langle\varphi^6\right\rangle^2}{4}\ln\left(\frac{4\Lambda^2}{G_F^2\left\langle\varphi^6\right\rangle^2} + 1\right)\right]. \tag{25}$$

From Equation (25), one can finally obtain the non-vanishing vacuum expectation value $\left\langle\varphi^6\right\rangle$ of the scalar field, which is determined by the self-energy of the fermion field. And then the *SU*(3) gauge symmetry is broken down dynamically.

Substituting the definition

$$W_\mu^\pm = \frac{1}{\sqrt{2}}\left(A_\mu^1 \mp iA_\mu^2\right), Z_\mu = \frac{1}{2}\left(-\sqrt{3}A_\mu^3 + A_\mu^8\right), B_\mu = \frac{1}{2}\left(A_\mu^3 + \sqrt{3}A_\mu^8\right), \quad (26)$$

and Equation (21) into Equation (14), we can obtain the masses of the vector gauge particles

$$m_W^2 = \frac{1}{4}g^2\upsilon^2, m_Z^2 = \frac{4}{3}m_W^2, m_B^2 = 0. \quad (27)$$

This result is exactly the same as that of the WS model.

## 5. Summary and Remarks

In this paper, based on the generalized Yang-Mills theory, we have constructed an $SU(3)$ unified model of electromagnetic and weak interactions. By using the NJL mechanism, the $SU(3)$ gauge symmetry breaking can be realized dynamically, although there is no the Higgs potential $V(\varphi)$ in the GYMT. The masses of $W^\pm$ and $Z^0$ particles are obtained. Interactions and quantum numbers of various particles are the same as that of the WS model. Compared to the WS model, the present model has several advantages. Firstly, since the present model is based on $SU(3)$ gauge group, there is only one coupling constant, and $\sin^2\theta_w = 1/4$ can be obtained directly. Secondly, the scalar fields are considered to be as gauge fields in the present model, then the introduction of the scalar fields becomes natural, and the number of the scalar fields can become certain too.

## Acknowledgements

Sincere thanks to the members of JMP for their professional performance.

## Conflicts of Interest

The authors declare no conflicts of interest regarding the publication of this paper.

## References

[1] Goldstone, J., Salam, A. and Weinberg, S. (1962) *Physical Review*, **127**, 965-970. https://doi.org/10.1103/PhysRev.127.965

[2] Weinberg, S. (1967) *Physical Review Letters*, **19**, 1264-1266. https://doi.org/10.1103/PhysRevLett.19.1264

[3] Weinberg, S. (1972) *Physical Review D*, **5**, 1962. https://doi.org/10.1103/PhysRevD.5.1962

[4] Chatrchyan, S., Khachatryan, V., Sirunyan, A.M., *et al.* (2012) *Physics Letters B*, **716**, 30-61.

[5] Aad, G., Abajyan, T., Abbott, B., *et al.* (2012) *Physics Letters B*, **716**, 1-29.

[6] Fairlie, D.B. (1979) *Physics Letters B*, **82**, 97-100. https://doi.org/10.1016/0370-2693(79)90434-9

[7] Neeman, Y. (1979) *Physics Letters B*, **81**, 190-194. https://doi.org/10.1016/0370-2693(79)90521-5

[8] Zhou, G.Z. and Gao, C.S. (1980) *Chinese Physics C*, **4**, 609-622.

[9] Chaves, M. and Morales, H. (1998) *Modern Physics Letters A*, **13**, 2021-2023. https://doi.org/10.1142/S0217732398002126

[10] Langmann, E. (2001) *Journal of Mathematical Physics*, **42**, 5238-5259. https://doi.org/10.1063/1.1399297

[11] Chaves, M. and Morales, H. (2000) *Modern Physics Letters A*, **15**, 197-206. https://doi.org/10.1142/S0217732300000190

[12] Wang, D.F. and Song, H.S. (2005) *Communications in Theoretical Physics*, **43**, 1083-1086. https://doi.org/10.1088/0253-6102/43/6/025

[13] Wang, D.F. and Song, H.S. (2006) *Communications in Theoretical Physics*, **45**, 297-300. https://doi.org/10.1088/0253-6102/45/2/022

[14] Wang, D.F. and Zhong, H.Y. (2008) *Communications in Theoretical Physics*, **50**, 703-706. https://doi.org/10.1088/0253-6102/50/3/36

[15] Higgs, P.W. (1964) *Physics Letters*, **12**, 132-133. https://doi.org/10.1016/0031-9163(64)91136-9

[16] Nambu, Y. and Jona-Lasinio, G. (1961) *Physical Review*, **122**, 345-358. https://doi.org/10.1103/PhysRev.122.345

[17] Wang, D.F., Liang, X. and Guo, Y.Q. (2020) *Journal of Modern Physics*, **11**, 448-454. https://doi.org/10.4236/jmp.2020.113028

Journal of Modern Physics, 2022, 13, 1411-1439
https://www.scirp.org/journal/jmp
ISSN Online: 2153-120X
ISSN Print: 2153-1196

# A Non-Newtonian View of the Universe Derived from Hydrodynamic Gravitation and Expanding Earth

**Giancarlo Scalera**

INGV, Rome, Italy
Email: giancarlo.scalera@ingv.it

**How to cite this paper:** Scalera, G. (2022) A Non-Newtonian View of the Universe Derived from Hydrodynamic Gravitation and Expanding Earth. *Journal of Modern Physics*, **13**, 1411-1439.
https://doi.org/10.4236/jmp.2022.1311088

**Received:** September 26, 2022
**Accepted:** November 19, 2022
**Published:** November 22, 2022



## Abstract

Earth Science observations and the Borexino and KamLAND geoneutrino experiments provide clues on the role of aether in the evolution of the Earth, planets, and all other universal structures. Analysis of the problem of storage of aether entering celestial bodies led to a hydrodynamic explanation of gravitation which in turn was found to be closely related to the expanding Earth and to several other phenomena. Variable radius paleogeography provides an approximate assessment of the quantity of ordinary matter added to the planet per time unit, and some inferences about the Earth's inner energy balance. The aether density, flow rate, and velocity are computed with the help of astrophysics. The origins of cosmological and gravitational redshift are unified under the single cause of gravitation. This is linked to the similar but not interchangeable concept of tired light, which was considered very plausible by cosmologists like Edwin Hubble and Fritz Zwicky. A superluminal speed was calculated for aether at the Earth's surface. INFN experiments confirm hydrodynamic gravitation and superluminal velocities, and it is possible to identify interrelations of aether parameters with the currently known cosmological parameters $H_0$, $G$, and $c$. Unification of hydrodynamic gravitation and the expansion of the celestial bodies through the existence of a minor dissipative force, a non-Newtonian concept, involves a revision of the theories of physics and cosmology, in which the currently accepted laws of physics will be only considered good approximations of a more complex reality.

## Keywords

Expanding Earth, Aether Central Flow, Hydrodynamic Gravity, Red Shifts, New Evolutionary Cosmology

## 1. Historical Perspective of the *Central Torrent*

Newton's research into gravity was never without the conviction that gravitation should be explainable by physical mechanisms. Newton (1642-1727) admitted the existence of aether pervading everything [1], and he was surrounded by scientific peers who proposed mechanical explanations of gravitation. One of his good friends and confidants, Fatio De Duillier (1664-1753; on 1690) believed gravity was caused by mechanical collisions of infinitesimal particles wandering in random directions and velocities in space. This mechanism was further developed some time later by George Le Sage (1724-1803; on 1750) [2] [3]. However, Newton preferred other hypotheses about the nature and dynamics of the aether. He defined an initial hypothesis in 1675 in a communication [4] to the Royal Society:

*The vast body of the earth, which may be everywhere to the very centre in perpetual working, may continually condense so much of this spirit as to cause it from above to descend with greater celerity for a supply*; […] *nature making a circulation by the slow ascent of as much matter out of the bowels of the earth in aerial form, which, for a time, constitutes the atmosphere*; […] *And, as the earth, so perhaps may the sun imbibe this spirit copiously, to conserve his shining, and keep the planets from receding further from him. And they, that will, may also suppose that … the vast aetherial spaces between us and the stars are for a sufficient repository for this food of the sun and planets.* (Newton, 1675; text reproduced in [5], p. 181).

This was possibly the first proposal of a central torrent and an explanation for the rapid flow of aether towards the interior of celestial bodies. Aether as food for the Sun and planets is also a first vague prelude to the Expanding Earth concept. A few years later, he conceived a second possible mechanism for gravity. This was: an aether of increasing consistency and particle size as you moved away from the Earth [6], which started another line of research at the time by Euler (1707-1783) on a similar basis (increasing pressure instead of density). Despite conjecture on possible flows of aether towards the Earth's interior as the cause of weight, Newton and many of his successors could not accept a progressive accumulation of matter in the planet due to their philosophical and religious beliefs, instead conceiving improbable mechanisms for the elimination of aether. Newton thought that it must return to outer space, and the problematic contrast between the arrival and return mechanisms was one of the reasons that led him to give up trying to establish further hypotheses.

The Swiss scientist Johann Bernoulli (1667-1748), although well aware of the De Duillier-Le Sage-like mechanism (since he had translated De Duillier's text), proposed a true hydrodynamic flow of aether penetrating perpendicularly to the Earth's surface towards the center of the planet—which he called the *central torrent* [7]. He wrote:

*The gravitation of the planets toward the center of the sun, and the weight of bodies toward the center of the earth, are not caused either by the attraction of*

*Newton, or by the rotary force of the vortex medium of Descartes, but by the immediate impulsion of a substance which under the form of what I call a "central torrent", is continually thrown from the whole circumference of the vortex to its center, and consequently impresses on all bodies encountered by it in its path the same tendency toward the center of the vortex. … And all that Newton has derived from his "attractions" are by my theory, derived from the impulsions of the central torrent* (Bernoulli, 1735 [7]; translated and quoted in [8]).

Although not without contradictions and incompleteness, Bernoulli believed he was blending the best of the (incompatible) concepts of Newton (spherical symmetry of gravity) and Descartes (axial symmetry), convinced that this reproduced all aspects of Newtonian gravity, but without a rigorous formal demonstration [7] [8]. The problem of whether or not the incoming aether was stored in celestial bodies remained vague.

Pierre Simon Laplace (1749-1827), who considered hydrodynamic gravity plausible, calculated that the propagation speed of gravitation fluid had to exceed the speed of light by many orders of magnitude to make the effect of gravitational aberration negligible:

*If gravitation were produced by the impulse of a fluid towards the center of the attracting body; the previous analysis, relating to the impulse of sunlight, would give the secular equation due to the successive transmission of the attractive force*. […]; *we must suppose that the gravitational fluid has a speed at least a hundred million times greater than that of light* […]. *Geometers can therefore, as they have done hitherto, suppose this speed to be infinite* (Laplace, 1802 [9]; pp. 325-326; translated from French).

Otherwise, with aether flowing at speeds comparable to $c$, the planetary orbits would have destabilized within a few thousand years. Laplace does not express an opinion on the issue of final storage of aether. However, the superluminal properties of gravific fluid within the solar system seem to have been confirmed in very recent experiments (see Section 7 of the present paper).

In the nineteenth century at least two scientists again addressed the issue, James Clerk Maxwell (1831-1879) and Bernhard Riemann (1826-1866). Starting from the field of electrostatics, Maxwell offered a hydrodynamic interpretation of Faraday's lines of force, describing them as tubes within which a fluid (but imaginary!) flowed at speeds decreasing as $1/r^2$ relative to charge [10]. The analogy between electromagnetism and gravitation was later elaborated by Oliver Heaviside (1850-1925) [11]. Riemann's 1853 work (published posthumously) called *New Mathematical Principles of Natural Philosophy*, postulated a hydrodynamic model for an incompressible fluid aether [12], but again without suggesting where the incoming stream of aether might be stored. He wrote:

*I make the hypothesis that space is filled with a substance which continually flows into ponderable atoms, and vanishes there from the world of phenomena, the corporeal world. Both hypotheses may be replaced by a single one, that in all ponderable atoms, a substance perpetually appears from the corporeal world in-*

*to the mental world* (Riemann, 1853 [12]; pp. 505-517).

Maxwell and Riemann thus solved the storage problem in an idealistic way.

A place for aether to settle in our real world was found a few decades later in a rather obvious solution proposed by the Russian-Polish engineer and astronomer Jean O. Yarkovsky (1844-1902), best known in astronomy for a thermodynamic effect on the rotation of small celestial bodies [13] [14]. He suggested that incoming aether formed new atoms in the depths of the Earth, giving rise to various phenomena like planetary expansion, internal heat and earthquakes [15]. In the early 1900s he published a short pamphlet in Russian regarding the density of aether, giving a value eleven orders of magnitude greater than the one calculated here [16]. Without providing a bibliographic reference, he cited the value published by Lord Kelvin as erroneous (which instead is near to the order of magnitude deduced here in section 4). Yarkovsky's ideas had an affinity with those of De Duillier-Le Sage, from which it was possible to deduce the existence of a gravitational shielding effects sought without positive results during 1900s [17] [18] [19].

Ott Hilgenberg (1896-1976) was a well-known scientist and Expanding Earth sustainer in Berlin from the early 1900s [20] [21]. At a late stage in his career he resumed his youthful interest in flowing aether [22] [23]. Setbacks prevented his oral presentation on hydrodynamic gravity as the cause of expansion at a conference organized by the British geophysicist Keith Runcorn in Newcastle upon Tyne. Shortly afterwards he published the text of his talk in a 16-page booklet [22] criticizing Riemann for his idealistic idea of aether simply disappearing following penetration into material bodies, and he tried to derive the density of aether with the help of the red shift of solar light. The data available at the time did not allow him to succeed, but it is notable that he followed a path that was in principle correct.

The concept of aether has never been abandoned [24] [25] [26] [27] and numerous groups or individual researchers have considered hydrodynamic gravitation [28] [29] [30] and various other concepts (a short review in [31]) but many of these studies fell within the theoretical ambit of general relativity, without considering the Expanding Earth concept. Only Wang, without considering expansion of celestial bodies as really plausible, is acknowledged that if gravity is formulated hydrodynamically, there is an implied increase in mass and a variation in $G$ [32]. In his master thesis Ngucho observed that the existence of a thin material field leads to a slow kinetics energy loss by planets along their orbits [33]. In his long scientific activity Blinov offers a concept of gravity as a form of energy transfer from space to objects [34], a concept similar to that proposed [35] by Petry. Cahill identifies aether with flowing space [36], while Consoli and coauthors prefer a flowing aether in the form of a Bose-Einstein condensate [37]. Even Euler's idea of aether causing gravity from a pressure gradient is sustained today [38].

However, for the vast majority of the scientific community, the situation to-

day does not differ substantially from that described clearly by Riemann:

*Rather, we should look to the circumstance that Newton's law of attraction has operated so long on the notions of researchers that they seek no further for explanations* (Riemann, 1853 [12]; pp. 505-517).

Finally, in modern manuals and treatises on hydrodynamics, the sink and source entities are considered with dismay because of the singularities present at their centers, defined as pure theoretical abstractions. In none of these manuals is formal proof provided that singularities are eliminated by Newton's laws (see section 8 in the present paper).

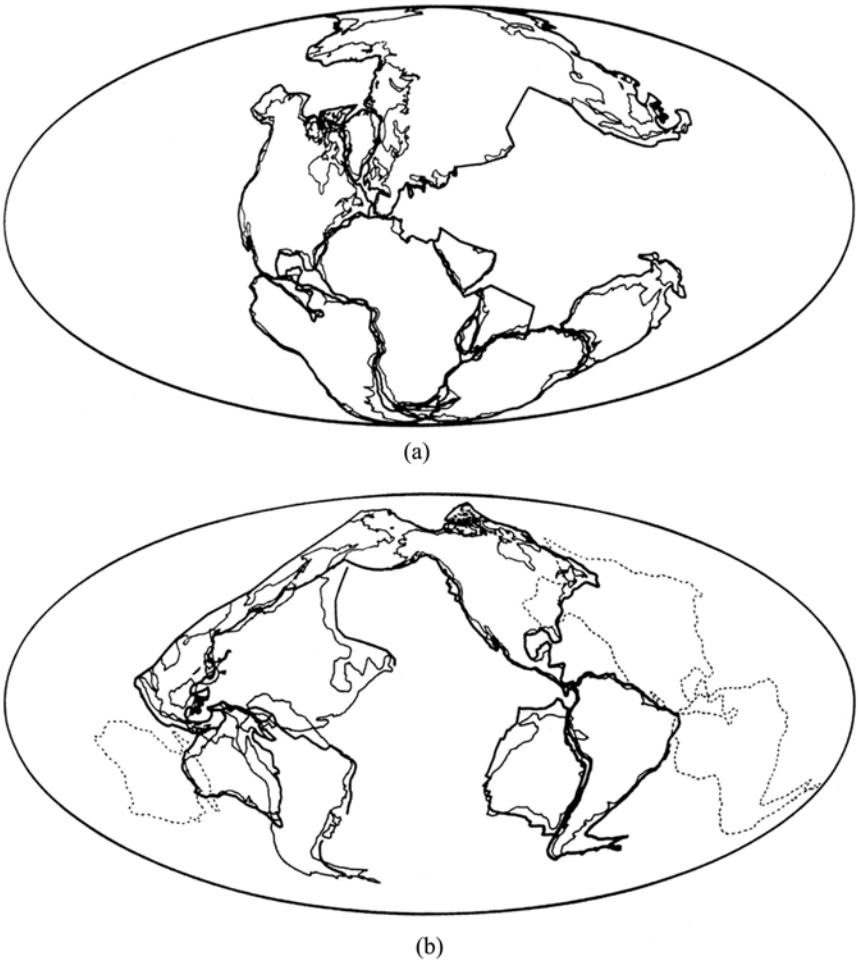


**Figure 1.** Cartographic experiment performed in [64] (pag. 50, **Figure 3**). (a) Reference Pangaea. The supercontinent reconstructed following the classic works [39] [40] [41]. (b) Circumpacific continental scarps (bold line) and coastlines in their modern position showing all the conformities between continents and basins [64] together with the outlines of Australia, Laurentia and South America (dotted lines) in the positions which they assume in (a) in the reference Pangaea. It is impossible to imagine how the conformities could be formed by convergence of Laurentia, South America and Australia coming from Pangea and drifting towards their modern position and towards the Pacific. The circumpacific conformities overlap adequately with the relative basins and there is reciprocal juxtaposition if the mutual position of continents is reconstructed on a half radius globe as in the next **Figure 2**.

## 2. The Earth's Heat Flux Budget Is Not Balanced

The Earth Sciences provide plentiful evidence for planetary expansion [21] [22] [23] [42]-[80]. All the preceding quoted papers derive from the diverse spheres of geology, paleontology, geomorphology, paleogeography, paleomagnetism, geochronology, geodetics etc. However none of them necessarily implies a link between Expanding Earth and hydrodynamic gravitation with a central torrent. Recently, from some more refined experiments including the Borexino at Gran Sasso in Italy, and KamLAND on the island of Honshu in Japan, designed to measure the radiogenic heat of the Earth from neutrino flux [81] [82] and from a series of cartographic experiments (see **Figure 1** and **Figure 2**) awareness has grown that the cause of expansion could be a flow of aether converging into the planet and transforming into ordinary structured matter (first particles and then atoms) along the journey from surface to geocenter [21].

The problem of the Earth's energy balance has been extensively debated [83] [84] without reaching a definitive solution. Today we can re-examine the issue from the new perspective of a centripetal flow of constitutive matter. To resolve the Earth's heat balance the total of 45 - 47 TW, as measured in wells and mines, should equal the sum of primeval heat—generated during the formation of the planet, which has slowly dissipated down to the modern residual heat, estimated to be between 5 TW and 15 TW—plus radiogenic heat. However, this is not the case. The exiguous tidal dissipation (≈0.1 TW) and gravitational potential energy released in the differentiation of crust from mantle (≈0.2 TW) can be neglected [85]. The geodynamic approach with its hypothesis of convective currents in the mantle would imply a faster dissipation of primordial heat, estimating values below the average of ≈10 TW. For the three radiogenic heat flux values predicted by the models (**Table 1**) the Borexino and KamLAND experiments [81] [82] provide result of 8 - 16 TW (best value) and 18-28 TW (best value) respectively (**Table 1**). With these values, the sum of radiogenic (average KamLAND-Borexino ≈ 18 TW, average Borexino ≈ 24 TW, maximum Borexino ≈ 28 TW) and primordial heat (mean ≈ 10 TW) differs more markedly from the surface heat flux value. Some geophysicists ([84], among others) suggest the possibility of applying the highest values allowed by standard deviations, but the problem persists and should not be underestimated.

It has been hypothesized that the missing heat could be provided by an exothermic process of fission in a nuclear reactor generated by the gravitational migration of the radioactive elements towards the region near the Earth's center [86]. This would produce no more than 5 - 7 TW, but some researchers reject it for various reasons, including geochemical considerations [87]. The same doubts arise for the possibility of nuclear reactors in the *D*" layer, a thin shell enclosing the liquid core. Both these nuclear fission reactors hypotheses suffer from the major problem of the lack of an efficient mechanism for elimination of the nuclear fission waste that would inexorably contaminate and halt the reaction.

**Table 1.** Decay of radioactive elements: comparison between models and experimental results.

| | | |
|---|---|---|
| Cosmochemical approach | The composition of the Earth is based on the enstatite chondrites, which show a closer isotopic similarity with the mantle and an iron content high enough to explain the terrestrial metallic core | 11 ± 2 TW |
| Geochemical approach | For the relative abundances of the lithophile refractory elements it adopts a chondritic composition, then placing limits on the absolute abundances from terrestrial samples | 20 ± 4 TW |
| Geodynamical approach | It is based on the hypothetical energetics of mantle convection and on the observed heat flux on the surface | 33 ± 4 TW |
| Borexino experiment | Observed best value | 18 - 28 TW |
| KamLAND experiment | Observed best value | 8 - 16 TW |

The neutrino experiments suggest that the terrestrial radiogenic heat flux predicted by the convective cell geodynamic model (33 ± 4 TW) is not confirmed [21] [81] [82] (**Table 1**) and cannot be correct. Even taking the Borexino mean value of ≈23 TW, it is necessary to add a primeval heat value taken from the lower end of its estimated range, due to the higher dissipation caused by convective motions, but even conservatively adding a mean of ≈10 TW would be far off the 45 - 47 TW total.

Furthermore, it is important to consider that the feedback from an Expanding Earth on primeval heat evaluation would lead to a primitive heat re-evaluation much lower than 5 - 15 TW, making the lack of a plausible heat source more dramatic. This serious question of the Earth's actual evolution skews all estimates of the Earth's primordial heat, without the authors being aware since they are mainly interested in balancing the Earth's heat budget within the framework of current knowledge, in which the expansion of celestial bodies is not considered [83] [84] [85]. The budget can only be balanced by arguing the existence of an unidentified source of heat possibly linked to the unknown physical phenomenon that drives terrestrial expansion. It is therefore necessary to ask whether a part of the neutrinos detected by Borexino and KamLAND were produced by matter-genesis, and whether the unexplained missed fraction of the heat flux is due to an increase in the kinetic (thermal) energy of the Earth's core materials not due to radioactive decay but rather to the convergence of aether and its transformation into ordinary matter.

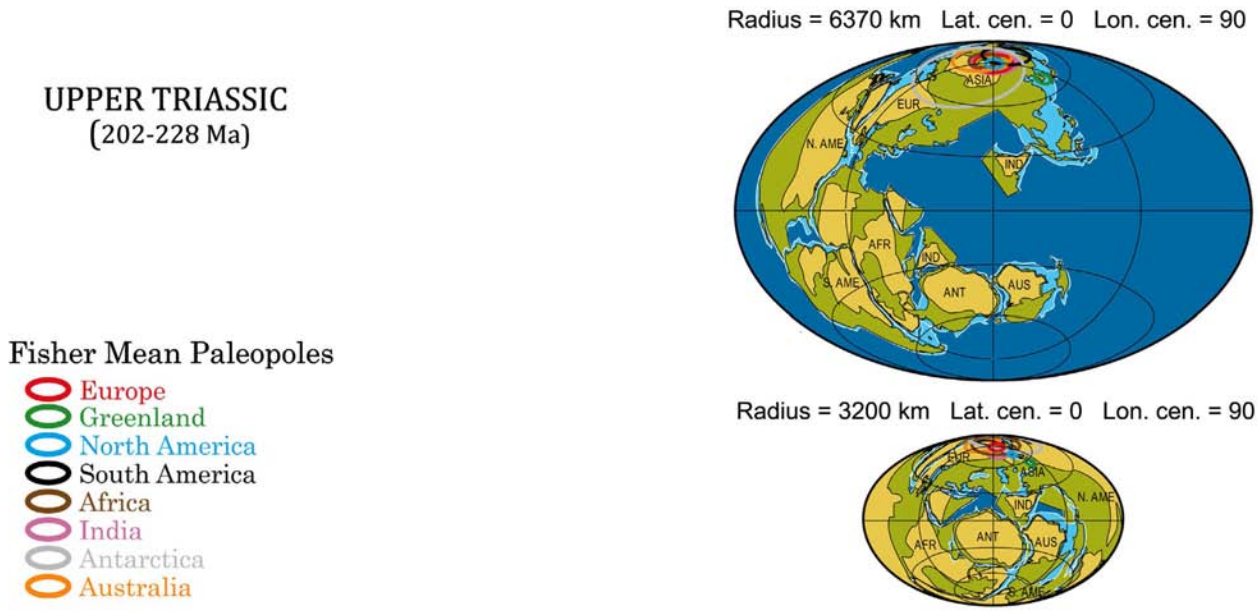


**Figure 2.** Paleogeographic reconstructions performed for the Triassic [21] [88], assisted by the GPMDB (Global Paleomagnetic Database) [89]. Paleopoles were traced as Fisher averages. The beige color defines the Paleozoic shields; olive green the mainland of the current continents; and light blue the modern continental shelves. More details and the lists of GPMDB data used, can be found in the Supplementary Materials file accompanying [21]. This is a typical cartographic experiment enabling estimation of the Earth's annual mass growth. It constituted also evidence for an Expanding Earth because the same selection of poles (see data lists in [21], supplementary materials) enables reconstruction of both the classical Pangea with all its exaggerations (Tethys Sea too vast, pre-Triassic Pacific crust more than hemispherical and today completely disappeared, India too isolated from Asia, etc.) and the globe of 3200 km, the Triassic terrella without oceans. If the pole selections were incorrect or biased for the 3200 km globe, then the reconstruction of Pangea with the modern radius would also be wrong, and/or the GPMDB catalog would be useless.

## 3. Geological Quantification of Incoming Aether

What we call the gravity field, the intensity of which decreases as $1/r^2$, is nothing more than the force exerted on a unitary mass $m$ positioned at a given point. The force does not exist at any other point without the presence of a unitary mass $m$. The field is therefore a point-by-point mapping of what a unit mass $m$ would experience if located at an infinite numbers of points in the space surrounding the central massive body with $M \gg m$. There is no perception of what really exists at all the infinite points in which $m$ could be located, which is what exerts physical action on $m$ (something present even without the presence of the test mass $m$). The Newtonian gravitational field is therefore an incomplete phenomenological description of physical reality (also true for the electromagnetic field).

We can thus start interpreting gravitation as resulting from the material field of an incompressible perfect fluid aether of density $\rho$, converging towards the Earth at a speed depending on $1/r^2$ (above the surface of the planet; $r$ = distance from the geocenter). Starting from the known relationship for the force $f = \rho Q \upsilon$ (known as the dissipative term) exerted by a fluid current of uniform flow of velocity $\upsilon$ on a sink singularity with flow rate $Q$, we arrive at an expression of the attractive force between two static sinks (or even between two sources) analog-

ous to the expression of Newtonian gravity [90]:

$$f = \frac{\rho}{4\pi} \cdot \frac{Q_1 Q_2}{R^2},$$

which can be compared with the force of gravity between two masses:

$$F = G \cdot \frac{mM}{R^2}.$$

Obvious dimensional problems do not allow identification of $G$ with $\rho/4\pi$. What makes this (only apparently old) conception very attractive is that it is not a Newtonian conception, since the expression of force in the non-static case depends on the speed of the sinks or sources.

The same attractive force would be obtained either with high flow rates $Q_i$ and low density $\rho$, or low flow rates and increasing $\rho$, and the velocity field $\upsilon$ also plays a part in the dissipative term. There are only clues that the density of aether must be very low [21] [32] [90], otherwise the dissipative term would be too important and the founding fathers of modern science could not have posited the principle of inertia, the concept of conservative field, of escape velocity, etc. as good approximations.

From the sciences of the Earth, using paleogeography (**Figure 1** and **Figure 2**) with awareness of its precision limits [21], the mass in the spherical shell added up to now to our globe can be evaluated and thus it is possible to approximately calculate the rate of transformation of aether into ordinary matter as energy transferred to the planet per unit of time (per second; averaging from the Triassic to Recent, 250 My; assuming a conservative terrestrial radius at the Triassic time $R_{Trias} \approx 3400$ km) [21]. The volume of the Earth (today $V_T$) in the Triassic was $V_{Trias} \approx 0.152 \cdot V_T$. So the volume acquired over 250 My would be $V_{acq} = V_T - V_{Trias} \approx (1 - 0.152) \cdot V_T = 0.848 \cdot V_T$.

This does not guarantee that the acquired mass was $M_{acq} \approx 0.848 \cdot M_T$ (with $M_T$ = Earth's current mass), because a poorly known process of differentiation of materials may have been taking place in the deep planet with phase changes and large volume increases. Therefore, assuming very crudely that the acquired mass is only $M_{acq} = 0.5 \cdot (0.848 \cdot M_T) = 0.424 \cdot M_T$ and linear growth (in reality it is exponential) we can evaluate the approximate amount of energy per second absorbed at the expense of the constituent matter:

$$E_s = \left(M_{acq} c^2\right) \Big/ \left(2.5 \times 10^8 \text{ y} \times 3.1557 \times 10^7 \text{ s}\right) = 2.889 \times 10^{25} \text{ J/s}.$$

The Earth Sciences alone cannot uniquely solve the problems of establishing the density $\rho$ of aether, aether flow rates, or its velocities $\upsilon(x, y, z)$ around sinks (celestial bodies). Perhaps this lack of definitiveness prevented Bernoulli and his successors' conception of gravity from spreading and gaining acceptance in the scientific community.

## 4. Help from Astrophysics

In order to establish at least an approximate value for $\rho$, assistance was sought

from astrophysics, an option not available in the times of Yarkovsky and Hilgenberg [16] [22]. We hypothesize that the velocity-dependent dissipative hydrodynamic term, the force $f = \rho qc$, is responsible for the phenomenon of redshift $z = (\nu_0 - \nu_1)/\nu_1$ of electromagnetic radiation coming from celestial bodies, which gives rise to Hubble's law $z = (H_0 D)/c$. This idea is similar, but not identical, with that of tired light, considered as much more plausible than the Doppler effect by cosmologists such as Edwin Hubble, Fritz Zwicky, and other colleagues who first worked on the redshift-distance relationship [91] [92].

Today it can be argued that the energy variation $E$ of each photon emitted with frequency $\nu_0$ and received with frequency $\nu_1$, $E = h(\nu_0 - \nu_1)$, is caused by the work $L = E = fD = \rho qcD$ of the dissipative term on the motion of a sink with flow rate $q$ (the photon), over the distance $D$ between the emitter and the observer. It can be written as follows: $\rho q = E/Dc$. The same quantity $\rho q$ can be obtained from the hydrodynamic force (equal to the Newtonian $F$) between a black hole of flow rate $Q_{BH}$ and a photon of flow rate $q$ forced to orbit around it circularly at our set distance $R$: $F = f_I = (\rho/4\pi)\cdot(qQ_{BH})/R^2$; from which we have: $\rho q = F(4\pi R^2)/Q_{BH}$.

By combining the previous relations, the aether flow rate of the black hole can be determined: $Q_{BH} = F(4\pi R^2)/EDc$. Knowing that the circular orbital velocity for negligible masses relative to the central one is $\upsilon_0 = \sqrt{GM/r}$, we can obtain the mass of the black hole that causes the photon to orbit around it at velocity $\upsilon_0 = c$ at our set distance $R$: $M_{BH} = (c^2 R)/G$, and then:

$$F = G\frac{mM_{BH}}{R^2} = G\frac{M_{BH}h\nu}{R^2c^2} = \frac{h\nu}{R}. \tag{1}$$

Equation (1) and Hubble's law can be used to derive the constant ratio between any flow rate $Q$ and its associated mass $M$, in this case between $Q_{BH}$ and $M_{BH}$:

$$\frac{Q_{BH}}{M_{BH}} = \frac{Q}{M} = GF\frac{4\pi R}{Ec}D = 4\pi G\frac{h\nu}{R}\frac{R}{h\Delta\nu c}\frac{zc}{H_0} = 4\pi\frac{G}{H_0} = \ell, \tag{2}$$

with $\ell = 3.6\times10^8\ \mathrm{m^3/(kg\cdot s)}$, a universal constant, at present time, of "transfer" from the phenomenological world of masses to the real hydrodynamic world of flow rates. Finally, applying some algebra to (2) gives $\rho$ starting from the constant ratio between flow rates and masses of black holes and photons:

$$\frac{Q_{BH}}{M_{BH}} = \frac{q}{m} = \ell,$$

from which:

$$q = \frac{Q_{BH}}{M_{BH}}m = 4\pi\frac{G}{H_0}\frac{h\nu}{c^2} = \frac{k}{c^2}\nu = \frac{\ell}{c^2}h\nu,$$

or, following a different more direct way:

$$\frac{q}{m} = \ell, \quad \Rightarrow \quad q = \ell m = \frac{\ell}{c^2}h\nu,$$

which has a degree of analogy, in the flow rates world, with Plank quantization. Reordering the Newtonian force: $m = FR^2/(GM_{BH})$, we obtain the flow rate of photons:

$$q = F\frac{Q_{BH}}{GM_{BH}^2}R^2,$$

and finally, from the latter, recalling the dissipative term, the force of the black hole on the photon and Hubble's law, we obtain the long-sought after fundamental parameter:

$$\rho = \frac{1}{4\pi}\frac{H_0^2}{G} \tag{3}$$

with the value $\rho = 0.647\times10^{-26}\ \mathrm{kg/m^3}$.

## 5. Two Roads That Should Converge

With (3) it is possible to define the velocity field $\upsilon(x,y,z)$ of the fluid (with $Q_T$ = Earth's flow rate; $R_T$ = Earth's radius):

$$\upsilon = \frac{Q_T}{4\pi R_T^2} = \frac{M_T\ell}{4\pi R_T^2} = \frac{M_T G}{H_0 R_T^2}, \tag{4}$$

with the value $\upsilon = 0.42\times10^{19}\ \mathrm{m/s}$ at the Earth's surface, 10 orders of magnitude greater than $c$, decreasing as $1/r^2$ similarly to the classical field of gravity $g$.

The value (4) obtained from astrophysics must be compatible with the value of energy per unit of time injected into the Earth by the aether and transformed into mass of ordinary matter $E_s = 2.889\times10^{25}\ \mathrm{J/s}$, already obtained as the averaged value over 250 My from paleogeographic reconstructions. This gives:

$$\rho\frac{\mathrm{d}V}{\mathrm{d}t} = \rho 4\pi R_T^2\frac{\mathrm{d}x}{\mathrm{d}t} = \frac{E_s}{c^2}; \tag{5}$$

and:

$$\upsilon = \frac{\mathrm{d}x}{\mathrm{d}t} = \frac{E_s}{\rho 4\pi R_T^2 c^2} \tag{6}$$

with the value $\upsilon = 9.72\times10^{19}\ \mathrm{m/s}$ at the Earth's surface. Although different, the values (4) and (6) are in adjacent order of magnitude (there would be no reason for this if terrestrial expansion, or hydrodynamic gravitation, or both were false) confirming their link with physical reality. The value (4) should be considered closer to true, with $H_0$ the most uncertain parameter.

The value of $\upsilon$ derived from geology is however higher than that derived from astrophysics and various approaches could be hypothesized to make them converge.

1) The importance of volume increases due to phase changes in the crystal lattice may be greater. For example, it could be assumed that additional dilation phenomena occur related to a hydridic Earth [53].

2) The radius of the Triassic globe could be further increased—albeit only slightly.

3) Finally, additional special properties of aether could also be hypothesized: e.g. the "gravific" aether, of density $\rho$ expressed in (3), may be just a component of the central flow of aether transforming into new mass within the planet. If this is really the case, then the total density of the aether flux $\rho_m > \rho$ should appear in (6), with a consequent lower value for velocity $\upsilon$. Alternatively a "non-gravific" aether could constitute a stationary background on which the central torrent acts germinating new ordinary matter.

All of these three possibilities could apply simultaneously, but currently there is no way to confirm or reject them.

## 6. Additional Improvements

As previously mentioned, while the Earth's mass and flow rate increase with exponential regularity (ignoring depletion of aether from the space reservoir), the same cannot be said for volume, which could grow according to an irregular and even non-monotonic function. Assuming therefore an exponential increase in mass or terrestrial flow rate $M_T(t) = (Q_0/\ell)\cdot e^{t/\tau}$, it is possible to derive the value of $\tau$ (time of increase of $M_T$ by a factor *e*). Initially, we proceed starting from a Triassic Earth mass equal to about $M_{Trias} \approx 0.5 M_T$ of the current value (and not 0.1 as would be the case following volume increase), taking into consideration the additional processes of volume variation caused by reorganization of the crystal lattice.

This gives:

Using

$$Q(t) = Q_0 \cdot e^{t/\tau} \quad \text{and} \quad \int_{-\infty}^{0} \rho \cdot Q(t)\,dt = M_T$$

With the values

$$Q(t) = 0 \quad \text{when} \quad t = -\infty;$$

$$Q(t) = 0.5 \cdot Q_T \quad \text{when} \quad t = -250 \text{ My};$$

$$Q(t) = Q_T \quad \text{when} \quad t = 0;$$

then:

$$Q(-250) = 1/2 \cdot Q_T = Q_T \cdot e^{-250/\tau}$$

and then:

$$e^{-250/\tau} = 1/2 \quad \Rightarrow \quad e^{250/\tau} = 2 \quad \Rightarrow \quad 250/\tau \approx 0.7,$$

and finally:

$$\tau = 250/0.7 \approx 357 \text{ My}.$$

All this will help to calibrate paleogeographic reconstructions and estimate the terrestrial paleoradius.

The effect of decreasing density of aether $\rho$ over time due to its transfer from space to celestial bodies must be carefully evaluated in the future.

## 7. Old and Recent Experiments

An old experiment: as we have seen in this view of the universe, light cannot propagate engaged to aether. The speed $\upsilon \gg c$ of aether entering celestial bodies would make it impossible for light to move away from them. Light rays propagate by self-induction phenomena, and are only weakly influenced by aether, giving rise to cosmological and gravitational redshift, and the deflection of light by hydrodynamic gravity. Michelson and Morley's attempt to reveal the aether wind was a poorly conceived concept. Only one type of aether wind acting on light in one of the possible ways was studied, ignoring the others and in particular the central torrent that causes gravity.

Recent experiments: if gravitation propagated at finite speed $\upsilon_g = c$, it could be shown that planets feel the force of the sun as it was some minutes before (depending on the distance of the planet). The planets would accelerate in the direction of motion, and the orbits would expand rapidly, as forecast by Laplace.

Recently Van Flandern [93] confined the values $\upsilon_g$ to a range greater than $2.0\times10^{10}c$ which are in the order of those estimated here—Equations (4) and (6), for near the Earth. An INFN experiment (in Frascati, Italy) proved that the Coulomb field of charges in motion behaves rigidly [94], a result that can be interpreted as a very high speed of propagation of the fields within their hydrodynamic formulation (more complete than the classical theory). The unrealistic exclusion of the dissipative hydrodynamic term (small but not negligible if $\rho \neq 0$) leads to theoretical results that are again unrealistic, with instantaneous propagation of the Coulomb field (the delayed potentials of Liénard-Weichert are cited in [94]), generating misleading interpretations that would justify both action at a distance and non-locality.

However, the existence of gravitational aberration is not excluded for very large distances. For example, a field velocity of 1.0 m/s is reached for the Earth at about $1.3 \times 10^{16}$ m (1.4 light years), for the Sun at $7.55 \times 10^{18}$ m (163 light years), for the galaxy—assuming a galactic mass of $10^{12}$ solar masses, at $7.55 \times 10^{24}$ m ($8 \times 10^{8}$ light years). Gravitational aberration is therefore probably important for galactic dynamics, and its contribution to the unsolved problem of the anomalous flattening of the galactic rotation velocity curve with increasing distance should be considered.

## 8. Aether Velocity Field into the Earth's Interior

Given the analogy between the $1/r^2$ trend of the Newtonian gravity field and the hydrodynamic velocity field moving away from the surface of the Earth, and given that it is precisely the speeds of the omnipresent fluid that produce forces identifiable with those of gravity, the same analogy must be considered for the terrestrial interior. In fact, given that $g$ and $\upsilon$ under the Earth's surface are both obtained as an integration of the contributions of all the elements of mass $\mathrm{d}m$ or flow rate $\mathrm{d}Q$, the result of the integrals will have the same trend but on different scales (**Figure 3**).

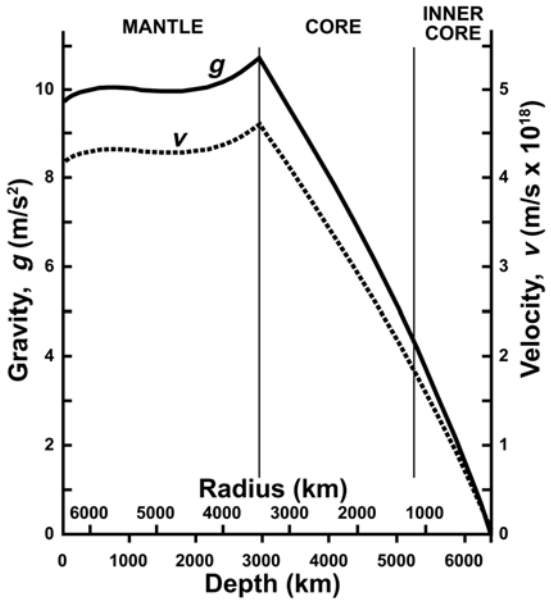


**Figure 3.** Variation of the acceleration of gravity ($g$, solid line) in the Earth's interior.

The value of both the $g$ and $\upsilon$ fields from the surface to the geocenter do not increase without limits towards infinite singular values (as in hydrodynamic sinks) but, starting from the core-mantle boundary, an almost linear decrease begins towards zero in the terrestrial center (**Figure 3**). The accumulation of a small amount of matter in the center is sufficient for Newton's laws to prohibit the existence of the singularities so feared by Riemann and the authors of modern fluid dynamics treatises.

In this region of the core, with the deceleration of the incoming flux, a more efficient transformation from aether to ordinary matter must be expected, with probable exothermic reactions which would constitute the unknown source of heat in the Earth's energy balance. A second zone of self-overlapping flow, which maintains an almost constant speed from depths of 700 km to about 2000 km (**Figure 3**), could be related to the maximum observed depth of earthquakes, which in the Wadati-Benioff regions is 700 km. These regions are interpreted in plate tectonics theory as lithospheric subduction zones, but in an Expanding Earth interpretation they are areas of material extrusion [21] the origin of which is now identifiable.

## 9. Discussion of Alleged Problems

### 9.1. Criticisms of Matter-Genesis within the Earth

Some criticisms of the matter-genesis process have already been made explicit. The most frequent is that *aether would generate subatomic particles that would combine to form protons, neutrons and electrons, finally producing hydrogen. However, our planet is not made of hydrogen, while heavy elements require specific conditions for synthesis from hydrogen, conditions that do not exist inside planets like the Earth and are only found in stars and supernovas.*

The reply is that the chemical constitution of the Earth's core is still under debate and the possibility that a small or even large part of it comprises hydrogen (whether in a metallic state or not) has never been ruled out (see [95] [96]). In addition, an erroneous logical assumption is committed when claiming that the conditions for formation of heavy elements only occur inside stars and supernovae. This is based on an incomplete theory of stars that erroneously exclude a main actor: the convergent flow of aether towards the center of bodies. This flow is subject to extreme deceleration and accumulation, creating conditions and processes the details of which are unknown (see also point 3) in section 5). The specific environment (chemical, static, dynamic) in the interior of real planets is still without a complete theoretical description (see a review of the Earth's core problems in [97]). The two matter-genesis theories (stellar and aether central flow) are not incompatible but simply regard different environments and conditions.

It should be clear from the above that Expanding Earth is compatible with Laplace nebula cosmogonies, in which heavy elements have already been produced in processes described by the theory of stars and supernovae. This theory of precursory matter-genesis could be seen as producing additional and cumulative effects together with central aether flow matter-genesis, a concept that should be developed in the future.

### 9.2. Criticisms about Neutrino Generation within the Earth

Again it is supposed that *generation of heavy elements from elementary particles implies fusion reactions that would generate emissions of geoneutrinos. The geoneutrino flows detected in the Borexino and KamLAND experiments were not even close to what could be expected from large amounts of new matter being generated inside the Earth*.

It must be recalled once more that this kind of objection is raised within a stellar and supernovae creation context, while a theory for matter-genesis from a "central torrent" of aether does not yet exist. There is thus no clear basis for the objections of critics who compare the experimental results with non-existent theoretically predicted values.

A final criticism is that *neutrinos are generated in both nuclear fusion and nuclear fission reactions. Geoneutrinos are generated by nuclear decay of radioactive elements in the crust, mantle and core of the Earth. Therefore, the ability of detectors to measure the flux of geoneutrinos means they can discriminate neutrinos generated from different sources. If new matter was being generated inside the planet, we would expect a strong emission of neutrinos from nuclear fusion of terrestrial origin greatly in excess of the flux of geoneutrinos from nuclear decay*.

Nuclear fission generates many neutrons, which then decay by emitting antineutrinos $\overline{\nu}_e$ according to the reaction:

$$\mathrm{n} \rightarrow \mathrm{p}^{+} + \mathrm{e}^{-} + \overline{\nu}_e. \tag{7}$$

During matter-genesis inside stellar matter, neutrinos are produced by the fusion of 4 hydrogen atoms according to the reaction (99.77% prevalent compared to other reactions):

$$4\mathrm{H} \rightarrow {}^{4}\mathrm{He} + 2\mathrm{e}^{+} + 2\nu_{e}. \tag{8}$$

However, if new matter was generated inside the planet from convergence of aether, the process of creation could be assumed to act on a more microscopic level than the known particle level (quarks, fermions, bosons) in a chaotic environment that might partially resemble the primordial soup hypothesized during the initial phases of the expanding universe theory. The presence of this active germinating soup could constitute an as yet unknown and highly complex physical environment able to activate different processes and reactions from (7) and (8) while inhibiting or screening others, without excluding possible catalyzing effects.

### 9.3. Some Controversial Topics

What is certain today is just that the experimental outcomes of Borexino and KamLAND were different from those expected, and that the speculations regarding the specific provenance of neutrinos remain far short of a final stable theoretical description traceable back to physical reality. The observed discrepancy provides a further piece of evidence in the known anomalous energy emission of the giant planets (like Jupiter and Saturn, which emit 150 and 50 times the Earth's emission respectively). On 1990 this phenomenon was generalized and explained by Wang as the effect of specific thermonuclear fusion reactions [98].

While the subject is still controversial, many researchers have followed Wang [98] proposing a geo-fusion process catalyzed by heavy metals in the depths of the Earth's core [99] or thermonuclear fusion in the deep Earth as the cause for formation of nitrogen, oxygen, and water over geological time [100] [101]. Also the surface degassing from volcanic vents and lakes of $^{3}$He and $^{3}$H (tritium only has a 12 year half-life, and, if not replenished fed from the atmosphere, must be produced in situ in the depths of the mantle or beyond) have been ascribed to nuclear reactions in the Earth's interior [102] [103]. Finally, Makarenko [104] agreed with [98] when noting anomalous heat emission from the planets, proposing an as yet unidentified cause of cosmic origin for this surplus energy.

The presence of a stream of aether decelerating towards the Earth's core could therefore be an important missing element to help explain experimental observations or to improve modeling for catalysis of "juvenile" elements, and generation of excess heat. Critics should reflect that if aether does not reach the center of the Earth (where its velocity $\upsilon = 0$) it must necessarily be transformed along the way.

### 9.4. Criticisms Regarding Terrestrial Energetics

Some papers [105] [106] [107] [108] [109] indicate that expansion with a marked increase in radius would be impossible due to the lack of sufficient

energy sources to produce the necessary variation in potential energy of the materials gradually moving away from the geocenter. This argument is referenced and adopted by followers of the "slow" version of Expanding Earth [110]. The necessary energy that cannot be accounted for is equal to $E \approx 10^{31}$ J over about 400 Ma. Such an enormous quantity of energy was considered impossible to justify within the framework of commonly accepted physical theories, and constituted a crucial argument against the expansion of celestial bodies without a central aether torrent.

However, assuming the physical reality of a central flow of aether as the cause of gravitation and expansion completely overturns any such objections [105]-[110]. Indeed, the energy injected by aether into our planet from the Triassic to the Recent era is:

$$E \approx 10^{41} \text{ J}.$$

This is many orders of magnitude higher than that estimated (for a longer period of time! From 400 Ma to the Recent) by critics of Expanding Earth. The smallness of the variation in potential energy in the expansion models without convergent flow of aether can be compared to the tiny amount of energy that our arms require to lift a load of one kilogram, relative to the total energy contained in the matter of the pack according to the formula $E = mc^2$. In his paper of 1961 Beck was aware that if Earth had doubled its radius then different sources of energy must exist [106]. He wrote:

*But even here the maximum expansion that can plausibly be expected is less than 1500 km. For the approximate doubling of the Earth's radius implicit in the ideas of Carey and Heezen a completely unknown source of energy must be postulated.* (Beck, 1961 [106]; p. 1489)

### 9.5. Criticism Regarding the Stability of the Orbits of Celestial Bodies Due to Mass Increase

The Universe described in the present paper is evolutionary and stability of planetary orbits is not foreseen. Stars and planets (also galaxies etc.) are increasing in mass, and the Earth's mass is increasing exponentially with $\tau \approx 350$ Ma. The orbits of the Earth and other planets could be strongly affected in the absence of compensating influences.

However, the laws that regulate the transformation of aether into matter (or rather into additional sinks) are not know, and it is not known if the new mass is created having already a speed equal to that of the mass of the planetary body.

The process could be analogous to placing a heavy brick on a small light carriage already loaded with an identical brick, and already traveling by inertia at a constant speed with respect to the laboratory. If you put the brick down—when it is stationary with respect to the laboratory—by dropping it on the carriage the speed of the carriage is approximately halved. Conversely, if the brick's speed is first raised to that of the carriage, the carriage speed does not change when the brick is added. At the moment we have no way distinguishing between the two modes of action, although invariance of speed (the second mode) seems more

likely, otherwise the galactic (or even more general) reference system would come into play, with disastrous effects.

However, the increase in solar mass certainly causes a shrinkage of planetary orbits which becomes significant over periods in the order of hundreds of millions of years.

### 9.6. Criticism Regarding the Stability of the Orbits Due to the Dissipative Term

The current kinetic energy of the Earth (disregarding spin) is:

$$E_c \approx 26.87\times10^{32}\ \mathrm{J}.$$

While, not considering an increase in mass, the work $E_w$ of the dissipative term on the length $D_o$ of a current Earth's orbit (for a current year) is:

$$f\cdot D_o = E_w \approx 39.48\times10^{22}\ \mathrm{J}.$$

The ratio between the annual friction work of the aether and the Earth's kinetic energy (excluding that of rotation) is:

$$E_w/E_c = 1.47\times10^{-10}$$

Thus the kinetic energy of the Earth could be significantly decreased (halved for example) in a time of the order of 10 billion years. The dissipative term alone has a negligible influence on the shortening of orbits compared to the effect of the increasing mass of the Sun.

## 10. No Relationship between the Dissipative Term and Pioneer Anomaly

A possible relationship between the dissipative term and the Pioneer Anomaly might be conjectured. Assuming the values provided by NASA for the mass and velocity of the Pioneer 10 probe ($M_{P10} = 222\ \mathrm{kg}$; $V_{P10} = 36737\ \mathrm{m\cdot s^{-1}}$) a value can be calculated for the additional acceleration due to aether:

$$f = \rho V_{P10} Q = \rho V_{P10} M_{P10} \ell = 18.996\times10^{-12}\ \mathrm{kg\cdot m/s^2}$$

$$a = f/M_{P10} = 8.557\times10^{-14}\ \mathrm{m/s^2}$$

Which is 4 orders of magnitude less than the anomalous acceleration measured for the probe, equal to $a = 8.47\times10^{-10}\ \mathrm{m/s^2}$.

Credit must therefore be given to the explanation based on recoil of the probe by thermal radiation from the circuits. The progressive attenuation over time of the anomalous acceleration value is in fact compatible with the progressive exhaustion of the on-board batteries. We can conclude that the aether's viscous force has nothing to do with the Pioneer Anomaly.

## 11. Compatibility of Aether Flux with Observed Polar Motion (PM)

The mass absorbed every second by Earth from gravific aether flux at the present time is:

$$M_s = \rho \mathrm{d}V \cdot 1\,\mathrm{s} = \rho \mathrm{d}x 4\pi r^2 \cdot 1\,\mathrm{s} = \rho \upsilon \mathrm{d}t 4\pi r^2 = 1.387 \times 10^7\ \mathrm{kg/s}\,.$$

And the mass per year:

$$M_y = M_s \times 3.1557 \times 10^7\ \mathrm{s} = 4.377 \times 10^{14}\ \mathrm{kg/y}\,,$$

which is $7.33 \times 10^{-11}$ of the Earth's mass ( $M_T = 5.972 \times 10^{24}$ kg ).

While more refined treatments exist taking into account the viscoelastic behavior of the Earth [111], a simplified rigid behavior is assumed in the following PM computation with the aim of assessing only orders of magnitude. This is based on the consideration that the probable absence of mantle convection in the expanding Earth framework would result in a more rigid behavior of the planet as a whole.

The Earth rotation pole displacement $PP'$ in the rigid case is (following [111] [112]):

$$PP' \approx W \cdot \frac{rm}{M_T} \sin(2\varphi)\,, \text{ with } W = \frac{M_T br}{2(B-A)} \approx 460\,,$$

($m$ = added mass; $\varphi$ = colatitude; $(B - A)$ = difference between the Earth's polar and equatorial inertial moments; $b$ = Earth's polar semi-axis; $r$ = Earth's radius).

If hypothetically all the mass $m = M_y$ was added annually at the geographic point 30˚S, 79˚W (colatitude $\varphi = 60^\circ\,\mathrm{S}$ ), near Nazca, the following Polar Motion drift would be obtained:

$$PP' \approx W \cdot \frac{rM_y}{M_T} \sin(2 \times 30^\circ) = 18\ \mathrm{cm/y}$$

towards Nazca. A factor of ≈0.5 applied to $M_y$ is then sufficient to reach the value of the observed annual Polar Motion of ≈10.0 cm/y.

At the present time only about an half of the mass injected by the gravific aether, extruded asymmetrically each year, would be enough to cause the observed PM. However, because of the consideration in point (3) of section 5, the yearly accumulated total mass could be due to an additional flow or *in situ* transformation of "non-gravific" aether, and the unbalanced asymmetrically emplaced mass would be less than 1/20 of the yearly total. A different behavior (more intense asymmetrical extrusion) in different epochs cannot be ruled out, especially during periods of the Earth's highest expansion rate.

It can be concluded that the PM values obtained starting from aether flux are compatible with those currently observed, once again suggesting that the adopted concepts are in line with physical reality.

## 12. An Aether Advantage: The Reappearance of Antimatter in the Universe

The rationalist attitude physics postulates that every structure would be made up of ever smaller structures in a sort of infinite regression (see **Figure 4**). From this perspective, particles are similar to indivisible points only because of our

temporary ignorance of what constitutes them. A general conception of aether and its infinite and increasingly microscopic levels can be framed within this scheme, open to future progress.

The nucleosynthesis and origin of chemical elements have been explained for a few decades in the scenario of an expanding universe. This starts with the fusion of baryons and leptons, within a primordial quark soup, always set in the high temperatures and pressures of the initial phases of the big-bang and then into the interior of stars. This view assumes that in the early stages of the universe matter was already constituted only by particles and not by antiparticles. However, for reasons of symmetry, the initial explosion or primitive singularity would have produced matter and antimatter in equal quantities. It is therefore necessary to hypothesize generation of surplus of matter in the first moments of expansion. After a rapid annihilation of matter with antimatter, the surplus persisted on to our time by aggregating according to the mechanisms of nucleosynthesis.

Andrei Sakharov [113] postulates three conditions that need to be satisfied for an excess of baryogenesis to occur:

1) Violation of the baryonic number according to laws of physics yet to be discovered.

2) Violation of C and CP symmetry. The hypothetical process that changes the baryon number must act to favor the production of baryons over the production of antibaryons.

3) Conditions far outside of thermodynamic equilibrium.

If all levels are populated according to a Boltzmann distribution, because CPT guarantees that each level with a positive number of baryons has a corresponding level with a negative baryon number, the total baryon number is zero. At equilibrium, transformations in one sense would be equiprobable to inverse transformations, but if an arrow of time acts together with thermodynamic non-equilibrium, direct and inverse processes would not be zero-sum. There is a vast literature that attempts to find sufficiently efficient processes of baryon number violation without contradicting aspects of big-bang cosmology, but yet all unsuccessful.

Instead, thinking once again in terms of aether and infinite regression opens up completely different scenarios. The universe would appear to possess infinitely more microscopic levels (**Figure 4**) and in one or more of these levels matter and antimatter could coexist—in structures unknown to us—separated by fields of emergent forces at that level. The matter we observe today at our level would therefore already contain both tiny matter and antimatter, and the "antiparticles" that we are able to produce in laboratories would also be manifestations of matter. The problem of the disappearance of antimatter in our universe would appear to be ill-posed. So, the mere persistence in "main stream" cosmology of this unresolved problem could be seen as evidence that aether and Expanding Earth are part of physical reality.

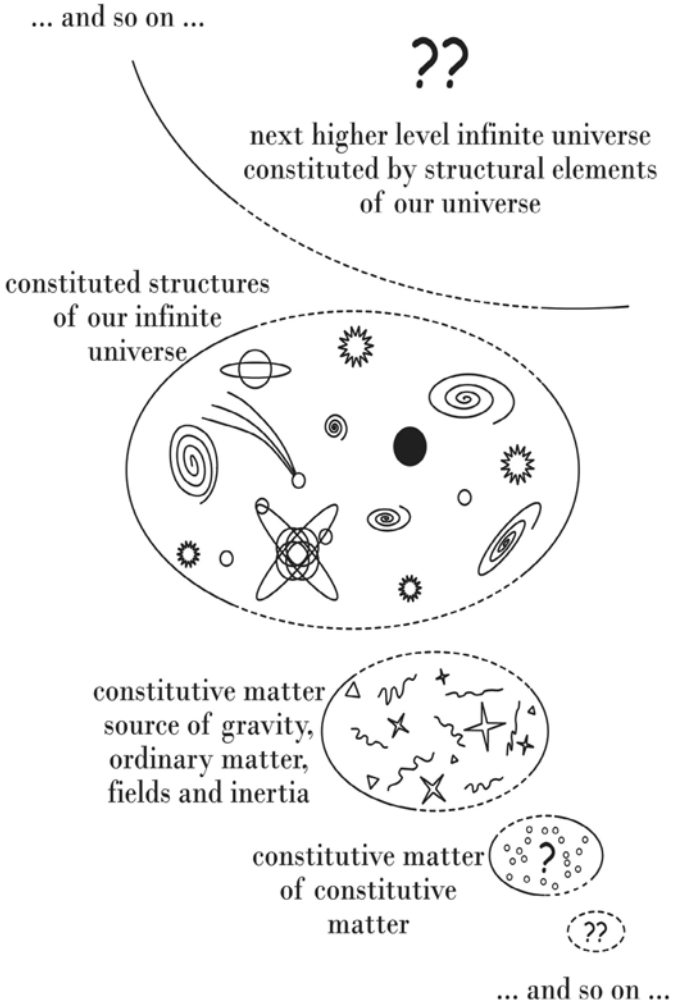


**Figure 4.** The evolutionary universe derived from hydrodynamic gravitation and the Earth Sciences. The universe that we can now observe directly or indirectly, from large-scale cosmic structures to microphysics, is being comprised at the expense of a constitutive material, the aether, which can be identified through the expansion of celestial bodies. This impalpable matter is being formed through absorption of a constituent material of a lower order, and so on. Our ordinary matter and its structures (micro and macro) are constituent matter (effectively an "aether") for a universe of higher order of spatial and temporal scales immeasurably greater than ours. All these *Chinese-boxes* universes are supplied from the lower order structures and they form a continuum in mutual evolution. The boundaries between one universe and the next of major or minor order are not well defined. For example, the micro and macro boundaries of our universe are only due to our current ability to build devices and observational experiments, and they are progressively extending.

## 13. Concluding Remarks

The last century was a historical period in which a "virtuosic" approach to physics prevailed, moving ever further away from the will to faithfully describe reality. We are not referring here to the splendid experiments in large colliders in search of new particles, which are still an expression of microscopic vibrational properties of the aether.

With the advent of relativistic theories, *horror vaqui* has been replaced by *horror pleni*, with a consequent demonization of the concept of aether along with anyone who considered it or tried to study it. Today, however, the simple acknowledgment that the expansion of celestial bodies is a natural phenomenon once more assigns to aether a leading role in order to integrate multiple physical phenomena while simultaneously providing an interpretation for several of them:

1) Origin and action of the gravitational field, rediscovering a concept that has been around for a few centuries in Western science, without becoming established due to the limited geological and astrophysical knowledge (marginality of Expanding Earth, low awareness of redshift). More generally, it clarifies the cause of the phenomenological fields of acceleration, calling into question the material field in motion as the cause of those accelerations. It also gives rise to a formula that has the elegance of physical reality:

$$\rho = \frac{1}{4\pi}\frac{H_0^2}{G},$$

which determines the mechanism of the Universe, with mass increase and expansion of celestial bodies. A centuries-old conundrum is resolved for scientists (for example Newton, Riemann, Maxwell etc.) and authors of manuals and treatises on hydrodynamics regarding infinite speeds in the centers of sinks and sources. In real sinks (the celestial bodies), the inevitable accumulation of material around the center and Newton's laws of gravitation, mean that singularities are not created.

2) Origin of cosmological and gravitational redshift, unifying the cause of gravitation with that of redshifts. The presence of a very rarefied aether and its dissipative term gives rise to both these phenomena. The dissipative term is fundamental as a moderator, homogenizer, and large-scale stabilizer of the Universe. It is also critical in making this version of gravitation non-Newtonian. Additionally, its frequency damping effect gives rise to a plausible solution for Olbers' paradox.

3) The analogy between gravitation and forces between sinks in hydrodynamics—both with a trend of $1/r^2$ outside the bodies, extends the correspondence to the inside of planets. The area of maximum deceleration of the aether flow coincides with the liquid and solid core, where consequently the aether must transform efficiently into ordinary matter. This role of the core should generalize across planets and other celestial bodies. Unlike theoretical sink or source entities, no singularity occurs at the planetary center.

4) The superluminal speeds of aether near celestial bodies explain the apparent "rigidity" of moving Coulomb fields, as revealed by the experiments at INFN [94]. This is linked to the *querelle* on gravitational aberration resolved by Laplace through the assumption of a superluminal velocity for gravitation, a solution confirmed by [93] with its value $\upsilon_g \geq 2\cdot 10^{10} c$, comparable with that obtained in the present text on the Earth's surface.

5) Sound waves travel by vibration of the medium they pass through and they

are transported by the medium if it is in motion. The central torrent does not carry light radiation and consequently it needs to be clarified whether a non-gravific Lorentzian aether is part of physical reality, as some evidence (see point 3 in Section 5) would appear to indicate. The universe in turn provides us with the evidence of the dipole anisotropy of the CMBR (Cosmic Microwave Background Radiation) which identifies a reference system at rest. Furthermore, observed in the deep infrared field with the Webb telescope, the Universe exhibits an infinite time axis towards the past.

6) The presence of the gravific fluid and the consequent dissipative term $f = \rho q \upsilon$ (a static fluid tends to slow down the motion of the singularities of sinks or sources) means that the principle of inertia, conservative field, escape velocity, etc., apply only as good local approximations of a more complex non-Newtonian reality. It would be possible to try and develop a hydrodynamic interpretation of the quantum world (one example—among others—in [114]). The expansion of celestial bodies is therefore inextricably linked to a general revision of the concepts of physics and cosmology, prefiguring a more unitary and realistic image, in which an upper limit to achievable speed values is no longer required.

In particular, classical field theory needs to be revised because it is formulated without the dissipative term, which, although tiny (the density of the aether is $\rho \approx 10^{-26}\ \mathrm{kg/m^3}$) and with generally negligible astronomical effects on orbits (apart from small effects on the perihelia of the planets) is of enormous importance for the structure, dynamics and evolution of the universe on a large spatial and temporal scale.

While the Expanding Earth concept is finally starting to demonstrate that it can realistically integrate multiple phenomena of physics with each other, no detailed demonstration has yet been provided of the full compatibility of the concept of hydrodynamic gravitation with relativistic effects. The present author is nevertheless confident that this will be possible, both because fields dependent on $1/r^2$ can be described by equations analogous to those of Maxwell, which are known to contain Lorentzian special relativity, and also because a vast literature exists claiming the capacity to deal with the effects predicted by general relativity, applying only classical physics. Moreover, recent papers that recalculate the drift of Mercury's perihelion with more precise methods and data do not seem to confirm the value of 42" of arc per century predicted by general relativity. All these issues, along with the study and assessment of the related literature remain for future investigation.

The present paper explains some new solutions and possible advantages of adopting the non-Newtonian concept of flowing aether derived from hydrodynamic gravitation and Earth Sciences, but many other issues must necessarily remain open.

## Acknowledgements

My thanks go to the anonymous referees who made me aware of a numerical

error and lack of discussion regarding their criticisms. The work was greatly improved through their observations. Thanks also to the SCIRP editorial staff for their assistance. A warm thanks to Silvano Gioca, who engaged in one of his usual long journeys in exotic and distant lands, as soon as he learned (through mysterious ways) of this paper of mine, he wanted to cover the editorial costs. Gavin Taylor revised my English with great skill.

## Conflicts of Interest

The author declares no conflicts of interest regarding the publication of this paper.

## References

[1] Bellone, E. (2006) Isaac Newton. In: Rossi, P., Ed., *Storia della Scienza*. Vol. 1, *La rivoluzione scientifica*: *Dal Rinascimento a Newton*, Editoriale L'Espresso, Roma, 419-447.

[2] van Lunteren, F. (1991) Framing Hypotheses: Conceptions of Gravity in the 18th and 19th Centuries. Unpublished Dissertation, The Author, Utrecht, 338 p.

[3] van Lunteren, F. (2002) Nicolas Fatio de Duillier on the Mechanical Cause of Universal Gravitation. In: Edwards, M.R., Ed., *Pushing Gravity*: *New Perspectives on LeSage's Theory of Gravitation*, Apeiron, Montreal, 41-59.

[4] Newton, I. (1675) Newton's Second Paper on Color and Light, Read at the Royal Society in 1675/6. Harvard University Press, Cambridge, 181.

[5] Cohen, I.B. (1958) Isaac Newton's Papers and Letters on Natural Philosophy and Related Documents. Newton's Second Paper on Color and Light, Read at the Royal Society in 1675/6, Harvard University Press, Cambridge, 501 p.

[6] Evans, M.G. (1958) *American Journal of Physics*, **26**, 619-624. https://doi.org/10.1119/1.1934717

[7] Bernoulli, J. (1735) Essai d'une nouvelle physique celeste. Imprimerie Royale, Paris, 144 p.

[8] Taylor, W.B. (1876) Kinetic Theories of Gravitation. Annual Report of the Board of Regents, Smithsonian Institution, Washington DC, 205-282.

[9] Laplace, P. (1802) Mechanique Celeste. Tome Troisime, Seconde Partie, Livre X, Chapitre VII, L'Imprimerie De Crapelet, Paris, 325-326.

[10] Maxwell, J.C. (1856) *Transactions of the Cambridge Philosophical Society*, **10**, 158-159.

[11] Heaviside, O. (1893) *The Electrician*, **31**, 281-282, 359.

[12] Riemann, B. (1853) Natural Philosophy (Section: New Mathematical Principles of Natural Philosophy). In: *Collected Papers*, Translated on 2004 by Baker, R., Christenson, C. and Orde, H., Kendrick Press, Heber City, 505-517.

[13] Beekman, G. (2005) *Journal of the British Astronomical Association*, **115**, 207-212.

[14] Beekman, G. (2006) *Journal for the History of Astronomy*, **37**, 71-86. https://doi.org/10.1177/002182860603700106

[15] Yarkovsky, I.O. (1888) Hypothèse cinétique de la gravitation universelle en connexion avec la formation des éléments chimiques. The Author, Moscow, 139 p. (In French)

[16] Yarkovsky, I.O. (1901) The Density of Luminiferous Aether and the Resistance It

Offers to Motion. The Author, Bryansk, 17 p. (In Russian)

[17] Majorana, Q. (1930) *Journal de Physique et Le Radium*, **1**, 314-324. (In French) https://doi.org/10.1051/jphysrad:0193000109031400

[18] Caputo, M. (1962) *Accademia Nazionale Lincei, Rendiconti della Classe di Scienze Fisiche, Matematiche e Naturali*, **32**, 509-515. (In Italian)

[19] Caputo, M. (2006) *Journal of Astrophysics and Astronomy*, **27**, 439-441. https://doi.org/10.1007/BF02709369

[20] Scalera, G. and Braun, T. (2003) Ott Christoph Hilgenberg in Twentieth-Century Geophysics. In: Scalera, G. and Jacob, H., Eds., *Why Expanding Earth?—A Book in Honour of Ott Christoph Hilgenberg*, INGV Publication, Rome, 25-41.

[21] Scalera, G. (2020) *Rendiconti Online della Società Geologica Italiana*, **52**, 103-119. https://doi.org/10.3301/ROL.2020.18

[22] Hilgenberg, O.C. (1967) Why Earth Expansion? Talk Held to the Technical University Berlin on February 7 1967. The author, Berlin, 16 p.

[23] Hilgenberg, O.C. (1974) *Geotektonische Forshungen*, **45**, 194 p. (In German)

[24] Whittaker, E.T. (1910) Theories of Aether and Electricity—From the Age of Descartes to the Close of the Nineteenth Century. Longmans, Green, and Co., London, 475 p. https://doi.org/10.5962/bhl.title.19630

[25] Selleri, F. (1993) On the Meaning of Special Relativity If a Fundamental Frame Exists. In: Arp, H.C., Keys, C.R. and Rudnicki, K., Eds., *Progress in New Cosmologies*, Plenum Press, New York, 269-284. https://doi.org/10.1007/978-1-4899-1225-1_18

[26] Kostro, L. (2000) Einstein and the Ether. Apeiron, Montreal, 242 p. (Italian Edition: (2001) Einstein e l'etere. Edizioni Dedalo, Bari, 317 p.)

[27] Wilczek, F. (2008) The Lightness of Being: Mass, Ether, and the Unification of Forces. Basic Books, Hachette, 270 p.

[28] Bhattacharyya, S., Minwalla, S., Hubeny, V.E. and Rangamani, M. (2008) Nonlinear Fluid Dynamics from Gravity. Institute of Physics Publishing for SISSA, Trieste, 39 p. https://doi.org/10.1088/1126-6708/2008/02/045

[29] Rangamani, M. (2009) *Classical and Quantum Gravity*, **26**, Article ID: 224003. https://doi.org/10.1088/0264-9381/26/22/224003

[30] Barceló, C., Liberati, S. and Visser, M. (2011) *Living Reviews in Relativity*, **14**, Article No. 3. https://doi.org/10.12942/lrr-2011-3

[31] Christianto, V. and Smarandache, F. (2008) *Progress in Physics*, **3**, 63-67.

[32] Wang, X.-S. (2008) *Progress in Physics*, **4**, 25-30.

[33] Ngucho, Y.J.M. (2019) Analogies between Gravity and Fluid Dynamics. Master Degree Thesis, African Institute for Mathematical Sciences (AIMS), Cameroon, 23 p.

[34] Blinov, V.F. (2012) Kinetic Gravity and Growing Earth. The Author, Kiev, 27 p.

[35] Petry, W. (2021) *Journal of Modern Physics*, **12**, 1749-1757. https://doi.org/10.4236/jmp.2021.1213102

[36] Cahill, R.T. (2009) Dynamical 3-Space: A Review. In: Duffy and Levy, Eds., *Ether Spacetime and Cosmology: New Insights into a Key Physical Medium*, Apeiron, Montreal, 135-200.

[37] Consoli, M., Pluchino, A., Rapisarda, A. and Tudisco, S. (2014) *Physica A*, **394**, 61-73. https://doi.org/10.1016/j.physa.2013.09.070

[38] Arminjon, M. (2004) *Foundations of Physics*, **34**, 1703-1724.

https://doi.org/10.1007/s10701-004-1312-3

[39] Bullard, E., Everett, J.E. and Smith, A.G. (1965) *Philosophical Transactions of the Royal Society of London. Series A*, **258**, 41-51. https://doi.org/10.1098/rsta.1965.0020

[40] Smith, A.G. and Hallam, A. (1970) *Nature*, **225**, 139-144. https://doi.org/10.1038/225139a0

[41] Owen, H.G. (1983) Some Principles of Physical Palaeogeography. In: Sims, R.W., Price, J.H. and Whalley, P.E.S., Eds., *Evolution, Time and Space: The Emergence of the Biosphere*, Systematic Association Special Vol. 3, Academic Press, London, 85-114.

[42] Mantovani, R. (1930) Troublante découverte: La Terre grandit. Notice preliminaire sur la découverte de la dilatation planétaire destinée aux mathématiciens, physiciens, astronomes, géologues et à tous ceux qui s'intéressent aux grandes énigmes de l'Univers (Intriguing Discovery: The Earth Grows. Preliminary Note on the Discovery of Planetary Dilation Intended for Mathematicians, Physicists, Astronomers, Geologists and All Those Interested in the Great Enigmas of the Universe). The Author, Tipografia Ferrari, Parma, 20 p. (In French)

[43] Egyed, L. (1961) *New York Academy of Sciences*, **23**, 424-432. https://doi.org/10.1111/j.2164-0947.1961.tb01369.x

[44] Creer, K.M. (1965) *Nature*, **205**, 539-544. https://doi.org/10.1038/205539a0

[45] Jordan, P. (1971) The Expanding Earth: Some Consequences of Dirac's Gravitation Hypothesis. Translated by A. Beer from the 1966 German Edition, Pergamon Press, Oxford, 202 p.

[46] Carey, S.W. (1976) The Expanding Earth. Elsevier, Amsterdam, 488 p.

[47] Owen, H.G. (1976) *Philosophical Transactions of the Royal Society of London. Series A, Mathematical and Physical Sciences*, **281**, 223-291. https://doi.org/10.1098/rsta.1976.0026

[48] Heezen, B.C. and Tharp, M. (1977) World Ocean Floor (a Map). U.S. Navy Office of Naval Research, Washington DC.

[49] Shields, O. (1983) Trans-Pacific Biotic Links That Suggest Earth Expansion. In: Carey, S.W., Ed., *Expanding Earth Symposium*. Sydney 1981, University of Tasmania, Hobart, 199-205.

[50] Shields, O. (1996) *Palaeobotanist*, **43**, 85-95. https://doi.org/10.54991/jop.1994.1191

[51] Neiman, V.B. (1984) Geological and Geophysical Proofs and Possible Causes of the Earth's Expansion. Nauka, Moscow, 166-173.

[52] Vogel, K. (1984) *Zeitschrift für Geologische Wissenschaften*, **12**, 563-573. (In German)

[53] Larin, V.N. (1993) Hydridic Earth: The New Geology of Our Primordially Hydrogen-Rich Planet. Translated and Edited by C.W. Hunt from the 2nd Russian Edition of 1980, Polar Publishing, Calgary, 242 p.

[54] Kremp, G.O.W. (1996) *Palaeobotanist*, **45**, 152-180. https://doi.org/10.54991/jop.1996.1231

[55] Chudinov, Y.V. (1998) Global Eduction Tectonics of the Expanding Earth. VSP-BV, Utrecht, 201 p.

[56] Mardfar, R.A. (2000) Relationship between Gravity and Evolution: The Theory of the Increasing of Gravity. Zeinab, Tabriz, 124 p.

[57] Maxlow, J. (2002) *Australian Geologist*, **122**, 22-26.

[58] Cwojdziński, S. (2003) The Tectonic Structure of the Continental Lithosphere Considered in the Light of the Expanding Earth Theory—A Proposal of a New Interpretation of Deep Seismic Data. Polish Geological Institute, Warszawa, Special Papers, No. 9, 80 p.

[59] McCarthy, D. (2005) *Journal of Biogeography*, **32**, 2161-2177. https://doi.org/10.1111/j.1365-2699.2005.01355.x

[60] Shehu, V. (2005) The Growing and Developing Earth. BookSurge, North Charleston, 218 p.

[61] Betelev, N.P. (2009) *Journal of Volcanology and Seismology*, **3**, 355-362. https://doi.org/10.1134/S0742046309050054

[62] Hurrell, S. (2012) Ancient Life's Gravity and Its Implications for the Expanding Earth. In: Scalera, G., Boschi, E. and Cwojdziński, S., Eds., *The Earth Expansion Evidence—A Challenge for Geology, Geophysics and Astronomy*, Aracne Editrice, Roma, 307-325.

[63] Scalera, G. (1990) General Clues Favouring Expanding Earth Theory. In: Augustithis, S.S., *et al.*, Eds., *Critical Aspects of the Plate Tectonics Theory, Volume II* (*Alternative Theories*), Theophrastus Publications, Athens, 65-93.

[64] Scalera, G. (1993) *Annali di Geofisica*, **36**, 47-53.

[65] Scalera, G. (1994) Earth Complexity vs. Plate Tectonic Simplicity. In: Barone, M. and Selleri, F., Eds., *Frontiers of Fundamental Physics*, Plenum Press, New York, 257-273. https://doi.org/10.1007/978-1-4615-2560-8_29

[66] Scalera, G. (2001) *Annali di Geofisica*, **44**, 13-32. https://doi.org/10.4401/ag-3616

[67] Scalera, G. (2009) *Annals of Geophysics*, **52**, 615-648. https://doi.org/10.4401/ag-4622

[68] Scalera, G. (2010) Earthquakes, Phase Changes, Fold Belts: From Apennines to a Global Perspective. GeoActa, Special Publications No. 3, "Geology of the Adriatic Area", 25-43.

[69] Scalera, G. (2011) Roots of Modern Geodynamical Views in Schiaparelli's Thought—The Volcano-Seismic Correlation Events on the Andes. In: Trinchieri, G. and Manara, A., Eds., *Schiaparelli and His Legacy*, *Memorie della Società Astronomica Italiana*, Vol. 82, 377-384.

[70] Scalera, G. (2012) Distensional Mediterranean and World Orogens—Their Possible Bearing to Mega-Dykes Active Rising. In: Scalera, G., Boschi, E. and Cwojdziński, S., Eds., *The Earth Expansion Evidence—A Challenge for Geology, Geophysics and Astronomy*, Aracne Editrice, Roma, 115-160.

[71] Scalera, G. (2013) Variable Radius Cartography—Birth and Perspectives of a New Experimental Discipline. 26*th International Cartographic Conference*, Dresden, 25-30 August 2013, 37 p. https://www.researchgate.net/publication/270393982

[72] Scalera, G. (2017) Can the History of the Ether Receive New Boost from Geosciences? *Atti del XXXVII Convegno annuale SISFA*, Bari, 26-29 September 2017, 307-316.

[73] Ollier, C.D. (2012) Extension Everywhere—Rifts, Continental Margins and Island Arcs. In: Scalera, G., Boschi, E. and Cwojdziński, S., Eds., *The Earth Expansion Evidence—A Challenge for Geology, Geophysics and Astronomy*, Aracne Editrice, Roma, 61-76.

[74] Liu, Y., Chen, Z., Liu, J. and Wei, J. (2013) *Advances in Geosciences*, **3**, 319-326. (In Chinese) http://www.hanspub.org/journal/ag.html https://doi.org/10.12677/AG.2013.36043

[75] Nyambuya, G.G. (2014) *International Journal of Astronomy and Astrophysics*, **4**,

244-249. https://doi.org/10.4236/ijaa.2014.41021

[76] Xu, C. and Sun, W. (2014) *Geophysical Journal International*, **199**, 1655-1661. https://doi.org/10.1093/gji/ggu364

[77] Shen, W.-B., Shen, Z.-Y., Sun, R. and Barkin, Y. (2015) *Geodesy and Geodynamics*, **10**, 1-5. https://doi.org/10.1016/j.geog.2015.05.006

[78] Xu, C., Wei, D. and Sun, W. (2016) *Journal of Geodynamics*, **99**, 10-15. https://doi.org/10.1016/j.jog.2016.05.001

[79] Khan, Z.A. and Tewari, R.C. (2017) *Journal of Tethys*, **5**, 218-239.

[80] Retejum, A.J. (2020) *Open Journal of Geology*, **10**, 1-12. https://doi.org/10.4236/ojg.2020.101001

[81] Borexino Collaboration (2017) *Annals of Geophysics*, **60**, S0114. https://doi.org/10.4401/ag-7389

[82] Shimizu, I. (2017) *Annals of Geophysics*, **60**, S0113. https://doi.org/10.4401/ag-7388

[83] Fiorentini, G., Lissia, M. and Mantovani, F. (2007) Geo-Neutrinos and Earth's Interior. https://doi.org/10.1016/j.physrep.2007.09.001

[84] Anderson, D.L. (2009) Energetics of the Earth and the Missing Heat Source Mystery. Tech. Rep. http://www.mantleplumes.org/Energetics.html

[85] Bellini, G., Inoue, K., Mantovani, F., Serafini, A., Strati, V. and Watanabe, H. (2021) *La Rivista del Nuovo Cimento*, **45**, 1-105. https://doi.org/10.1007/s40766-021-00026-7

[86] Herndon, J. (1993) *Journal of Geomagnetism and Geoelectricity*, **45**, 423-437. https://doi.org/10.5636/jgg.45.423

[87] Degueldre, C. and Fiorina, C. (2016) *Solid Earth Sciences*, **1**, 49-63. https://doi.org/10.1016/j.sesci.2016.08.002

[88] Scalera, G. (2018) Sequenza di mappe paleogeografiche del Tardo Triassico assistite dal GPMDB (Late Triassic Sequence of Paleogeographic Maps Assisted by the GPMDB). *Proceedings GNGTS* (*Gruppo Nazionale Geofisica Terra Solida—National Group Solid Earth Geophysics*) *Annual Conference*, Bologna, 217-222.

[89] Pisarevsky, S. (2005) *EOS*, **86**, 170. https://doi.org/10.1029/2005EO170004

[90] Buffoni, E. (2015) Idrodinamica (Hydrodynamics). Tipografia Editrice Pisana, Pisa, 179 p. (In Italian)

[91] Assis, A.K.T., Neves, M.C.D. and Soares, D.S.L. (2009) Hubble's Cosmology: From a Finite Expanding Universe to a Static Endless Universe. In: Potter, F., Ed., 2*nd Crisis in Cosmology Conference*, *CCC*-2 *ASP Conference Series*, Vol. 413, 255-267.

[92] Kragh, H.S. (2017) *Journal of Astronomical History and Heritage*, **20**, 2-12.

[93] Van Flandern, T. (1998) *Physics Letters A*, **250**, 1-11. https://doi.org/10.1016/S0375-9601(98)00650-1

[94] De Sangro, R., Finocchiaro, G., Patteri, P., Piccolo, M. and Pizzella, G. (2015) *The European Physical Journal C*, **75**, 10 p. https://doi.org/10.1140/epjc/s10052-015-3355-3

[95] Hu, Q. and Mao, H. (2021) *Matter and Radiation at Extremes*, **6**, Article ID: 068101. https://doi.org/10.1063/5.0069643

[96] Tagawa, S., Sakamoto, N., Hirose, K., Yokoo, S., Hernlund, J., Ohishi, Y. and Yurimoto, H. (2021) *Nature Communications*, **12**, Article No. 2588. https://www.nature.com https://doi.org/10.1038/s41467-021-22035-0

[97] Sumner, T. (2015) Mystery at the Center of the Earth. *Science News*, Sept. 19, 18-21.

https://doi.org/10.1002/scin.2015.188006016

[98] Wang, H.-Z. (1990) *Chinese Astronomy and Astrophysics*, **14**, 361-370. https://doi.org/10.1016/0275-1062(90)90015-6

[99] Jones, S.E. and Ellsworth, J.E. (2003) Geo-Fusion and Cold Nucleosynthesis. 10*th International Conference on Cold Fusion*, Cambridge, August 2003, 617-622.

[100] Fukuhara, M. (2020) *Journal of Physics Communications*, **4**, Article ID: 095007. https://doi.org/10.1088/2399-6528/abb2e6

[101] Fukuhara, M. (2020) *AIP Advances*, **10**, Article ID: 035126. https://doi.org/10.1063/1.5108922

[102] Jiang, S. and He, M. (2012) *Plasma Science and Technology*, **14**, 438-441. https://doi.org/10.1088/1009-0630/14/5/25

[103] Terez, E.I. and Terez, I.E. (2013) *International Journal of Astronomy and Astrophysics*, **3**, 362-365. https://doi.org/10.4236/ijaa.2013.33040

[104] Makarenko, O.M. (2012) *Geological Journal*, **2012**, 104-115. https://doi.org/10.30836/igs.1025-6814.2012.2.138954

[105] Beck, A.E. (1960) *Nature*, **185**, 677-678. https://doi.org/10.1038/185677b0

[106] Beck, A.E. (1961) *Journal of Geophysical Research*, **66**, 1478-1490. https://doi.org/10.1029/JZ066i005p01485

[107] Cook, M.A. and Eardley, A.J. (1961) *Journal of Geophysical Research*, **66**, 3907-3912. https://doi.org/10.1029/JZ066i011p03907

[108] Birch, F. (1968) *Physics of the Earth and Planetary Interiors*, **1**, 141-147. https://doi.org/10.1016/0031-9201(68)90001-0

[109] Burša, M. and Hovorková, O. (1994) *Studia Geophysica et Geodaetica*, **38**, 235-245. https://doi.org/10.1007/BF02295999

[110] Edwards, M.R. (2019) *Geodesy and Geodynamics*, **10**, 173-178. https://doi.org/10.1016/j.geog.2019.03.002

[111] Scalera, G. (2006) TPW and Polar Motion as due to an Asymmetrical Earth Expansion. In: Lavecchia, G. and Scalera, G., Eds., *Frontiers in Earth Sciences*: *New Ideas and New Interpretations*, *Annals of Geophysics*, Supplement to Vol. 49, No. 1, 483-500.

[112] Schiaparelli, G.V. (1891) Della rotazione della Terra sotto l'influenza delle azioni geologiche (The Earth's Rotation under the Influence of Geological Actions). *The Poulkova Observatory on the Occasion of His Half-Century Celebration*, Vol. 30, 5-33. (In Italian) https://doi.org/10.1007/BF02718469

[113] Sakharov, A.D. (1967) *JETP Letters*, **5**, 24-27.

[114] Buffoni, E. (2013) I Quanti e la Teoria Generale Dello Spazio Fluido. Tipografia Editrice Pisana, Pisa, 91 p. (In Italian)

Journal of Modern Physics, 2022, 13, 1440-1451
https://www.scirp.org/journal/jmp
ISSN Online: 2153-120X
ISSN Print: 2153-1196

# Orthogonal Collision of Particles Produces New Physical State

**Weihong Qian**[1,2]

[1]School of Physics, Peking University, Beijing, China
[2]Guangzhou Institute of Tropical and Marine Meteorology, CMA, Guangzhou, China
Email: qianwh@pku.edu.cn

**How to cite this paper:** Qian, W.H. (2022) Orthogonal Collision of Particles Produces New Physical State. *Journal of Modern Physics*, **13**, 1440-1451.
https://doi.org/10.4236/jmp.2022.1311089

**Received:** October 19, 2022
**Accepted:** November 22, 2022
**Published:** November 25, 2022



## Abstract

Collider is a machine or device that usually causes two beams of high-speed particles moving to collide in a straight line. The fundamental purpose of a collision is to obtain an abnormal mass-energy density and attempt to discover new physics and new substances namely new physical states. However, linear collisions are not easy to achieve the above purpose. Through the comparable experiment of rear-end collision, head-on collision and orthogonal collision of two low-velocity particles, this paper theoretically proposes a new idea that the orthogonal collision between two-beam high-velocity particles can really produce an abnormal mass-energy density. This machine based on the new idea of orthogonal collision can not only greatly reduce the construction cost of colliders, but also is the most effective way to achieve the purpose of collision.

## Keywords

Collider, Orthogonal Collision, Mass-Energy Density, New Physical State

## 1. Introduction

Exploring mysteries of the universe and finding new matter are the basic goal of physical research. The equipment for such an exploration is a collider. Usually, a linear collider is a constructed device in which two-type or one-type particles with high speeds collide each other in a straight line to form a concentrated energy or a new physical state, such as the appearance of Higgs particles [1] [2] [3]. The conventional linear collider is constructed in a way that it first uses several accelerators to gradually accelerate the two streams of particles that are injected, and then a head-on collision happens when they reach a certain beam strength and energy [4] [5]. It means that accelerator and collider are actually

one system. In the storm of particle collisions, only a few particles collide. People are going to measure the signs of particle collisions from electric light and flint. The collider is an instrument for measuring experiments with high-energy particles and discovering "new states" or "new matter". Therefore, colliders have a wide range of applications in high-energy particle physics, condensed matter physics, plasma physics and astrophysics [6] [7] [8] [9].

In order to get the energy of a linear collider, it is first necessary to produce high-energy (or high-speed) particles. The acquisition of high-energy particles requires a variety of particle accelerators. Since the 1960s, many types of accelerators or colliders have emerged [10] [11] [12]. For example, according to the type of accelerated particles, they can be divided into positron-electron collider, electron-proton collider, electron-ion collider, heavy ion collider, and other particle colliders [13] [14] [15]. According to the accelerated particle energy, they can be divided into low-energy, medium-energy and high-energy accelerators, even ultrahigh energy accelerators [16] [17] [18].

Centroid or center-of-mass dynamics of particles is complex in all linear colliders [19] [20] [21] [22]. The effectiveness of a collider can be simply compared with a moving-static collision and a moving-moving collision. When high-energy particles bombard a stationary target in a collider, only the center-of-mass energy (CME) is effective during particle collision, which accounts for only a part of total energy. However, if two beams of high-energy particles moved head-on with high energies $E_{1,2}$ collide, the combined centroid system has the beam energies about $2E$ [22]. Their total energy from moving-static collision and moving-moving collision can be simply calculated by using an addition.

There are two famous colliders in the world [23]. One is the Relativistic Heavy Ion Collider at the Brookhaven National Laboratory in Long Island, USA, which was the only heavy ion collider in the world from 1984 when it was proposed to build the plan until it was put into operation in 2000 [24] [25]. The other is the Large Hadron Collider, located near Geneva, across the border between Switzerland and France, which officially opened on September 10, 2008, becoming the world's largest particle accelerator facility [26] [27]. The cost is in the billions of Euros [28] [29]. The existence of the Higgs boson was confirmed in 2012 [2] [30]. Recently, new exotic particle structures, including exotic four-quark particles, have been observed at the Large Hadron Collider [5]. The discovery of new particles has led to the desire to build larger ring colliders [3] [31] [32]. Of course, such collider would cost tens of billions of Euros.

Physicists are going to keep accelerating elementary particles and then having them collide head-on, for taking apart elementary particles that are smaller than atoms to get smaller particles. In order to create new tiny elementary particles, one must concentrate a large amount of energy into a very small volume, which is to obtain a higher energy density. The Relativistic Heavy Ion Collider is a device that connects particles at all levels of acceleration one after another. Heavy ions start from the series of electrostatic accelerators, pass particles through a transmission line to a linear accelerator and inject them into an intensifier, then

send them to alternating gradient synchrotrons to accelerate, and finally inject them to a relativistic heavy ion collider through a beam transmission line. In the relativistic heavy ion collider, the same heavy ions collide with each other, accumulating and storing in two independent superconducting storage rings. Finally, two beams of heavy ion collide to obtain a higher energy density and look for a state of matter called quark-gluon plasma.

In the universe, matter and particles have three basic properties: mass, charge (electric charge and color charge), and spin (momentum). Among them, spin is the basic form of motion of matter (particles) in the universe. For the motion of stars in the Milky Way, it has both the tangential velocity around the center and the radial velocity towards the center. When two stars (particles) reach to each other, they may not move in a straight line, but in different directions, and will rotate with each other and even merge or collide in the end.

If two stars of equal mass and velocity collide head-on in a straight line, the energy of their collision is the sum of their respective energies which can be expected. New energy (or extra energy or abnormal energy) produced by a linear collision is not expected. How can a collider produce new unpredictable energies and new unpredictable matter (particles)? This paper first examines the form of linear collision with a rear-end collision and a head-on collision respectively. Then, an orthogonal collision is described and compared with the linear collision. However, in order to physically describe the performance of the three forms of collisions, we will focus on describing the interaction of the two low-velocity particles. It can be easily to generalize the collision performance of two particles to the interaction of two beams of high-velocity particles. At the end of the paper, conclusions and discussion are given. The study could answer a part of questions proposed by particle physicists who are fretting that they do not know what their next collider will be [33].

## 2. Linear Collision Form

In the real world, common collision events occur between vehicles or ships or airplanes with their relative moving speeds. Two cars can have a rear-end collision or a head-on collision in a straight-line road. Right angle collisions and other collisions at different angles can also occur between them on a crossing road point. Among them, the most definitive events can be mathematically described by three special angles of a 0-degree rear-end collision, a 180-degree head-on collision and a 90-degree right-angle collision. We focus on studying the energy formed by the collision of these three different angles.

We here design a test structure shown in **Figure 1** that compares a positron-electron collision in different forms. First, on the left-hand side of **Figure 1**, positrons and electrons are accelerated in a linear accelerator. They then separate and enter into a circular cavity on the right-hand side. The circular radius of the annular cavity is $r$.

In general, two beams of high-energy particles are widely used in the theoretical description of accelerator-colliders. The goal of accelerators is trying to

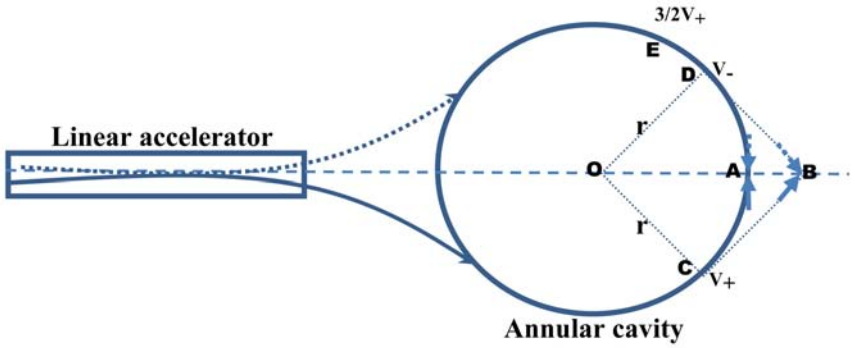


**Figure 1.** Three ways for negative-positive particles collided in a collider. Letter A denotes the linear collision point and letter B is at the orthogonal collision point. Point O indicates the center of an annular cavity with a radius of $r$, $v_+$ is the velocity of a positive particle at the tangent point C, $v_-$ is the velocity of a negative particle at the tangent point D, and $3/2\,v_+$ is the velocity of a positive particle at the point E. Four points of the square are at O, C, B, D. The rectangular box is a linear accelerator. Solid arrows indicate the moving of positive particles and dashed arrows indicate the moving of negative particles.

accelerate particles and form a state of high speed, close to the speed of light $c$, so the interaction of particles in a collider needs to be expressed in relativistic terms, and one of the important factors is the Lorentz factor

$$\gamma_i = \frac{1}{\sqrt{1-v_i^2/c^2}}. \tag{1}$$

It is a parameter (an elastic ruler) varied from the velocity $v_i$ of an object (or particle) relative to the speed of light $c$. Einstein introduced it into the relativistic momentum $p_i = \gamma_i m_i v_i$ and energy $E_i = \gamma_i(m_i c^2)$. The description of the center-of-mass energy and momentum and the interaction of two particles or two beams of particles must be carried out within the frame of this factor [22]. The usual collider uses a head-on collision of two beams of high-speed particles. Within a collider, there are different influence relationships and different collision opportunities between charged particles, so that there will be different collisions and moving angles among particles. Describing the complex interaction of these particles requires the use of wave dynamics, dynamical systems, instability analysis, external controlling fields, fluid modeling, nonlinear mathematics, and statistics [9] [34] [35] [36] [37] [38]. Colliders usually employ bunched beans of particles with approximately Gaussian distributions, where two bunch particles collided head-on with a frequency distribution can be expressed as the luminosity [22]. The development and application of these methods should be a broad field of particle physics.

Regardless of the particle number and speed of the two beams used by modern colliders, the purpose of colliders is to achieve how many pairs of particles exactly collide head-on per unit time. Only pairs of head-on collisions can achieve maximum energy density. Therefore, we focus on one of the pairs of oncoming particles to see how they interact. There are three special and valid cases of collision of two particles: head-on collision, rear-end collision, and orthogonal colli-

sion. Orthogonal collisions produce the most severe extreme events, indicating that the collisions produce the greatest energy density. In the development and design of colliders, this idea of orthogonal collision needs to be considered. Although the two beams of particles used in the future orthogonal colliders are also composed of a large number of particles, only the interaction of two particles is analyzed in this study in order to clearly describe the energy difference between orthogonal collisions and head-on collisions. Understanding the orthogonal collision of two low-velocity particles is the basis for further studying the orthogonal interaction of a large number of high-velocity particles.

A central part of this paper is an attempt to introduce the idea of orthogonal particle collisions for building future colliders. Therefore, it is not necessary to directly use the particle velocities obtained by high-speed and ultra-high-speed accelerators. Instead, we mainly compare the effects of the three-type collisions with low-velocity particles on various energies in this study.

According to the two low-velocity particles in the non-relativistic limit *i.e.*, when the velocities $v_{1,2} \ll c$ where $c$ is the speed of light, we first examine a rear-end collision. The velocity at which an electron with mass $m$ reaches the point D of the annular cavity is $v_-$. Also, we suppose that the velocity of a positron with its mass $m$ reaching the point E is $3/2\,v_+$. Thereafter, we use a positive particle indicating a positron and a negative particle indicating an electron. Finally, the positive particle marked by + and the negative particle marked by − with their velocities collide each other at the point A and form new energy

$$m\left[3/2\,v_+\right]^2/2 - mv_-^2/2 = 5/8\,mv^2. \tag{2}$$

The relative difference in the velocity between two particles is only $1/2\,v$, but the collision energy between them is $5/8\,mv^2$ (or $0.625mv^2$) as indicated in Equation (2), which is slightly larger than a particle energy $1/2\,mv^2$ (or $0.5mv^2$).

If the velocity of a positive particle is $2\,v_+$, its velocity is faster than that of negative one about a relative difference $1\,v$. In this case, the collision energy of a rear-end collision is $3/2\,mv^2$ (or $1.5mv^2$) showing in Equation (3).

$$m\left[4/2\,v_+\right]^2/2 - mv_-^2/2 = 3/2\,mv^2. \tag{3}$$

We now look at the situation where two particles collide head-on each other. In **Figure 1**, a positive particle and a negative particle leave the linear accelerator and enter the annular cavity. They continue to travel in the annular cavity at the same velocity, but in different directions. When they reach the point A, a head-on collision event occurs. Before the point A, they are moving along a circular curve. But when they reach the limit of point A, the angle between two particles in the direction of motion is 180 degrees. The energy of this head-on collision is

$$mv_+^2/2 + mv_-^2/2 = mv^2. \tag{4}$$

The energy at the time and at the point A for the head-on collision is the sum of two particle energies as indicated in Equation (4). Curiously, when the relative velocity difference of a rear-end collision is $1\,v$ while the relative velocity differ-

ence of a head-on collision is as large as $2v$, the energy of the rear-end collision is 1.5 times as large as the energy of the head-on collision. Actually, the velocity of a positive particle is $2v$ in the rear-end collision, which means that the positive particle must additionally increase a part of velocity $v$ or a part of energy $0.5mv^2$.

The linear collision is the basic form of all modern colliders. In this way, all builders of colliders are working to increase the particle velocity expected before a collision. Therefore, the goal of a front-mounted multi-step acceleration device is to increase the velocity of particles for the final collision. In the case of the Relativistic Heavy Ion Collider, for example, particles which finally collide require the cumulative velocity accelerated during the pre-accelerators. First of all, a series of accelerators is to inject charged particles from the ground end of an accelerator into an acceleration tube, which is accelerated for the first time into a high-voltage electrode and changes the polarity of particle band through a charge conversion device. Then they enter the second acceleration tube to accelerate again, even for a third and fourth times, gradually increasing the velocity of particles. The final result is increasing the energy of heavy ions.

In order to gradually increase the velocity or energy of particles, the internal structure of a collider is complex and the length of a linear accelerator is also desirable to be long. In this way, the complexity of a constructed accelerator increases, and the spatial range also increases, which ultimately makes the cost of a collider greatly increased. This costs not only money, but also costs valuable resources and negatively impacts on the earth's environment.

## 3. Right-Angle Collision Form

We now switch another way to orthogonally collide a negative particle with a positive particle. In **Figure 1**, two low-velocity particles leave the linear accelerator to enter the annular cavity. They have velocities $v_+$ and $v_-$ when they reach the point C and the point D, respectively. Then, instead of following the circular path to the point A, they start from the point C and the point D, and move at the same velocity along their tangent direction. They collide at the point B. At this time, the angle of collision between the negative particle and the positive particle is 90 degrees. It is a right-angle collision. Obviously, on the circumference of the annular cavity, the determination of point C and point D is unique. On the annular cavity, four points O, C, B, and D form a square while three points O, A, and B are in a straight line.

In the following, we look at their energies at the point B when they collide. Before point C and point D, two particles are moving along a circular track. They have centripetal forces with their unit vectors $\boldsymbol{n}_C$ and $\boldsymbol{n}_D$.

$$\boldsymbol{F}_C = \frac{m_+}{r} v_+^2 \boldsymbol{n}_C, \tag{5}$$

$$\boldsymbol{F}_D = \frac{m_-}{r} v_-^2 \boldsymbol{n}_D. \tag{6}$$

Two forces act at the point B, forming an event of collision which is named as

a shear stress. Its expression is the vector product of two forces, *i.e.*,

$$\boldsymbol{\tau}_B = \left(\frac{m_+}{r}v_+^2\right)\cdot\left(\frac{m_-}{r}v_-^2\right)\cdot\left(\boldsymbol{n}_C\times\boldsymbol{n}_D\right). \tag{7}$$

The process of interaction is to bring the mass and energy of two particles from points C and D to collide at the point B. At the point B, the collision of particles is the formation of new physics, new energy, and new matter. New physics can be expressed in a new mathematical form. The formation of new energy is like a nuclear explosion while its extreme energy density is difficult to predict. New matter is the appearance of smaller particles that people have not yet discovered. Finding the newest and the smallest particles from colliders are a dream of physical scientists [30] [39].

When points C and D approach the point A, the collision of two particles is on a straight line. At this point, the angle at which two oncoming particles collide is $\alpha = 180$ degrees, i.e. $\boldsymbol{n}_C\times\boldsymbol{n}_D = \sin\alpha = 0$. Their shear stress is

$$\boldsymbol{\tau}_A = \left(\frac{m_+}{r}v_+^2\right)\cdot\left(\frac{m_-}{r}v_-^2\right)\cdot\left(\boldsymbol{n}_A\times\boldsymbol{n}_A\right) = 0. \tag{8}$$

Differing from at the point A, their angle between two particles is $\alpha = 90$ degrees at the point B, so the vector product equals to 1, namely $\boldsymbol{n}_C\times\boldsymbol{n}_D = \sin\alpha = 1$. The shear stress is

$$\tau_B = \left(\frac{m_+}{r}v_+^2\right)\cdot\left(\frac{m_-}{r}v_-^2\right) = \left(m_+v_+^2\right)\left(m_-v_-^2\right)/r^2. \tag{9}$$

In the right-hand side of Equation (9), it expresses the mass-energy density per unit area. Equation (7) and Equation (9) show that the result of the collision between two forces is no longer a force, but a mass-energy density.

We can also select a point at which two particles collide on the extension line outside point B. Then the angle between two moving vectors of particles is $\alpha < 90$ degrees, so that

$$\boldsymbol{n}_C\times\boldsymbol{n}_D = \sin\alpha < 1,\ 0^\circ < \alpha < 90^\circ. \tag{10}$$

If we choose a point at where two particles collide on the inside extension line between point A and point B. Then the angle between two moving vectors of particles is $180 > \alpha > 90$ degrees, thus

$$\boldsymbol{n}_C\times\boldsymbol{n}_D = \sin\alpha < 1,\ 90^\circ < \alpha < 180^\circ. \tag{11}$$

Therefore, the mass-energy (or energy) density of their collision is the greatest only when two particles orthogonally collide at the point B as indicated in Equation (9).

From **Figure 1** and Equation (9), the mass-energy density of two particles leaving the annular cavity is $\left(m_+v_+^2\right)\left(m_-v_-^2\right)/r^2$. This mass-energy density can be quantitatively estimated. According to the conservation of mass and energy, when two particles orthogonally collide at the point B, the collision point is a very small three-dimensional space. Then, the mass-energy $\left(m_+v_+^2\right)\left(m_-v_-^2\right)$ that was originally distributed over the large area $r^2$ should now be concentrated in

a very small volume. It is interesting that the mass-energy density on the square area $r^2$ will be concentrated in a very small volume $r_B^3$ with $r_B \ll r$ through this process of orthogonal collision. Here, the mass-energy dimension of two particles before collision is per unit area (in fact, particles also have thickness), and then the dimension at the time of collision is per unit volume (the volume space has the particle scale). The three-dimensional mass-energy density after collision is huge and incalculable. This is the formation of new physics and new matter.

## 4. Comparison of Different Collision Energies

To facilitate a comparison of the ratio between energy magnitudes of three collision scenarios, we take each mass of negative and positive particles as $m$. According to Equations (2) and (3), the energy ratio of a head-on collision to a rear-end collision is

$$R_{h-r} = \frac{mv^2}{(5/8)mv^2} = 8/5. \tag{12}$$

The energy of a head-on collision is 1.6 times as large as the energy of a rear-end collision. Conversely, a rear-end collision energy is 0.6 times to that of a head-on collision. In reality, the damage caused by the collision of two cars in the rear-end collision is smaller than that caused by the head-on collision. This also shows that no one is trying to construct a machine of rear-end collision in physical field.

Here, a question is remained. What is the energy ratio of an orthogonal collision to a linear collision in this type of collider? We consider that the radius of an annular cavity is one unit length $r = 1$, then the mass-energy density on the unit area of the collision at the point B is

$$\tau_B = \left(mv_+^2\right)\left(mv_-^2\right) = \left(mv^2\right)mv^2. \tag{13}$$

When it compares to the case of a head-on collision, the energy ratio is

$$R_{o-h} = \left(mv^2\right)mv^2 \Big/ mv^2 = mv^2. \tag{14}$$

It can be found that the energy ratio formed from an orthogonal collision to a head-on collision is not a definite value, but a multiple of the change in mass and velocity of a particle.

When comparing the two energies of orthogonal collision and rear-end collision, their energy ratio is

$$R_{o-r} = \left(mv^2\right)mv^2 \Big/ \left(\frac{5}{8}mv\right)^2 = \frac{8}{5}mv^2. \tag{15}$$

Interestingly, the difference between Equations (14) and (15) is only 1 and 8/5 (or 1.6). This comparison shows that the energy of a head-on collision is slightly larger than that of a rear-end collision.

It can be noted that the addition of total energy is used in the collision of two particles along a straight line while the multiplication of total energy is used in

the right-angle collision of two particles. The total energy of multiplication is larger than that of addition as long as the unit of each particle energy is larger than 2. It is true that we can get different mathematical values but used only multiplication and addition in a smaller number such as $(1\times1=1)<(1+1=2)$, $(1\times2=2)<(1+2=3)$, $(2\times2=4)=(2+2=4)$, $(2\times3=6)>(2+3=5)$, and $(3\times3=9)>(3+3=6)$. These cases show that the value of one by any number is less than the sum between them while the value of two by two is equal to their sum.

The mass of a particle is very small, but the velocity when the particle is accelerated is very large. Of course, it is difficult to accelerate particles to the speed of light. For a particle with a mass unit of 1 gram, as long as the velocity of a negative particle or a positive particle reaches 1 m/s, the energy of an orthogonal collision is equivalent to the energy of two head-on collision particles. Actually, the velocity of a negative particle or a positive particle is rather large when they left accelerator to collide each other.

If we identify the head-on linear collision energy in Equation (3) and the orthogonal collision energy density in Equation (9), the energy ratio of the latter to the former increases with the square of particle velocity, as expressed in Equation (14). This analysis shows that the energy density of a collider in the form of orthogonal collision is rather large. This mechanism should be considered in the development of the next generation of colliders.

## 5. Conclusions and Discussion

Two particles or two beams of particles can collide at different angles. Specially, two particles can achieve a rear-end collision or a head-on collision along a straight line. In the rear-end collision, the particle in the back is 1.5 times faster than the particle in the front, but their energy of collision is only 0.6 times as large as that of a head-on collision. This shows that the energy of a head-on collision is larger than the energy of a rear-end collision. Whether two particles adopt linear acceleration or circular acceleration and if the final collision form of two particles is completed in a straight line, the collision energy is the sum of two-particle energies. The total energy of two beams of particles colliding head-on is roughly the sum of the energy that all pairs of particles can collide head-on. Therefore, the maximum energy produced by all current types of linear colliders can be expected. Of course, with the increase of an expected energy, the result of linear collision can also possibly form a fragmentation of original particles, but it is difficult to expect the formation of new physics, new energy and new matter or new particles. Thus, the linear collision is only a smashing machine.

In recent decades, the United States, Europe, Japan, China and other countries and agencies have built accelerators with different types, different energy levels and different motion tracks [3] [40] [41] [42]. The shape of particle motion orbit can be divided into a linear accelerator and a circular (ring) accelerator, but the final collision form of particles in a collider is the same, which is a head-on colli-

sion. To increase energy in the event of a head-on collision, one way is to increase expenses in constructing series of particle accelerators, such as the Large Hadron Collider, and other linear colliders in plans of Europe and China [3] [32] [43] [44]. This is called colliding dreams from physical scientists in Japan, China and Europe [33].

The study in this paper shows that orthogonal colliders can be currently manufactured by modifying the various annular head-on colliders that already exist around different places in the world. The basic principle of an orthogonal collider has been clearly expressed by the interaction of two low-velocity particles in this paper. This story described from two-particle orthogonal collision to two-beam-particle orthogonal collision can be well understood and generalized by public and scientific community under the non-relativistic limit. The orthogonal collision of two-beam high-velocity or high-energy particles can create more chances to form new matters in the relativistic frame. Therefore, various statistical and dynamic methods can also be applied to estimate the mass-energy density of orthogonal collisions.

The manufacture of orthogonal collider is relatively simple, just at the two determined points of a ring cavity with high-velocity or high-energy positrons and electrons moving along their tangent line and forming a crossing collision point outside the ring cavity. Another method is to construct a device that the particles emitted from two linear accelerators collide orthogonally. The ratio of the energy of an orthogonal collider to the energy of a linear collider is proportional to the square of their particle velocity. We believe that new physics and new matter can be produced by the orthogonal collision of two beam particles. Thus, the results in this paper could be useful for constructing a new generation of colliders and achieving the dream of physical scientists.

## Acknowledgements

The author wishes to thank Dr. Du, J. for improving this paper's expression and the two anonymous reviewers for their constructive suggestions which have improved the paper. The author also discussed with Drs. Guan, Y.P., Li, W. J. and Zhang B. L. for some equations. This work was supported by the innovative R&D project in Guangdong Province in China (2019ZT08G669) and the National Natural Science Foundation of China (Grant Number: 41775067).

## Conflicts of Interest

The author declares no conflicts of interest regarding the publication of this paper.

## References

[1] Tomlin, S. (2007) *Nature*, **446**, 836. https://doi.org/10.1038/446836a

[2] CMS Collaboration (2022) *Nature*, **607**, 60. https://doi.org/10.1038/s41586-022-04892-x

[3] Gibney, E. (2014) *Nature*, **511**, 394-395. https://doi.org/10.1038/511394a

[4] Ohmi, K. and Zimmermann, F. (2015) *Physical Review Accelerators and Beams*, **18**, Article ID: 121003. https://doi.org/10.1103/PhysRevSTAB.18.121003

[5] Castelvecchi, D. (2021) *Nature*, **596**, 330. https://doi.org/10.1038/d41586-021-02174-6

[6] Sau, G., Biswas, S.K., De, B., *et al.* (2008) *Canadian Journal of Physics*, **86**, 883-897. https://doi.org/10.1139/p07-207

[7] Gao, J. and Jin, S. (2015) *Chinese Science Bulletin*, **60**, 1251-1260. https://doi.org/10.1360/N972014-00820

[8] Wang, Y.F. and Lu, W. (2022) *Chinese Science Bulletin*, **67**, 805-808. https://doi.org/10.1360/TB-2022-0077

[9] Chandra, S., Sarkar, J., Das, C. and Ghosh, B. (2021) *Plasma Physics Reports*, **47**, 306-317. https://doi.org/10.1134/S1063780X21030041

[10] Bernardini, C. (2004) *Physics in Perspective*, **6**, 156-183. https://doi.org/10.1007/s00016-003-0202-y

[11] Cho, A. (2020) *Science*, **367**, 235-236. https://doi.org/10.1126/science.367.6475.235

[12] Gao, J. (2021) *International Journal of Modern Physics*, **36**, Article ID: 2142002. https://doi.org/10.1142/S0217751X21420021

[13] Abramowicz, H. and Caldwell, A.C. (1999) *Reviews of Modern Physics*, **71**, 1275-1409. https://doi.org/10.1103/RevModPhys.71.1275

[14] Crișan, E.L., Salanță, I.I., Beleiu, I.N., *et al.* (2021) *The Journal of Technology Transfer*, **46**, 62-89. https://doi.org/10.1007/s10961-019-09754-9

[15] Cho, A. (2018) *Science*, **361**, 317-318. https://doi.org/10.1126/science.361.6400.317

[16] Cimino, R., *et al.* (2004) *Physical Review Letters*, **93**, Article ID: 014801. https://doi.org/10.1142/S0217751X16300052

[17] Sterman, G. (2016) *International Journal of Modern Physics*, **31**, Article ID: 1630005.

[18] Mazzolari, A., *et al.* (2021) *Physical Review Research*, **3**, Article ID: 013108.

[19] Zhang, W.W., Zhang, K.Z. and Liu, C.J. (2003) *High Power Laser and Particle Beams*, **15**, 617-620.

[20] Moraes, J.S., Pakter, R. and Rizzato, F.B. (2005) *Physics of Plasmas*, **12**, Article ID: 023104. https://doi.org/10.1063/1.1848546

[21] Lindstrom, C.A., D'Arcy, R., Garland, M.J., Gonzalez, P., Schmidt, B., Schroeder, S., Wesch, S. and Osterhoff, J. (2020) *Physical Review Accelerators and Beams*, **23**, Article ID: 052802. https://doi.org/10.1103/PhysRevAccelBeams.23.052802

[22] Workman, *et al.* (2022) *Progress of Theoretical and Experimental Physics*, **2022**, 083C01.

[23] Baron, N. and Baur, G. (1994) *Physical Review C*, **49**, 1127-1131. https://doi.org/10.1103/PhysRevC.49.1127

[24] Jacak, B.V. (1999) *Acta Physica Hungarica New Series—Heavy Ion Physics*, **10**, 305-314.

[25] Litvinenko, A.G. (2007) *Physics of Particles and Nuclei*, **38**, 204-231. https://doi.org/10.1134/S1063779607020037

[26] Bruning, O., Burkhardt, H. and Myers, S. (2012) *Progress in Particle and Nuclear Physics*, **67**, 705-735. https://doi.org/10.1016/j.ppnp.2012.03.001

[27] Acharya, S., Acosta, F.T., Adamova, D., *et al.* (2020) *Nature*, **588**, 232-238. https://doi.org/10.1038/s41586-020-3001-6

[28] Adam, D. (2001) *Nature*, **413**, 441. https://doi.org/10.1038/35097216

[29] Florio, M., Forte, S. and Sirtori, E. (2016) *Technological Forecasting and Social Change*, **112**, 38-53. https://doi.org/10.1016/j.techfore.2016.03.007

[30] Gibney, E. (2022) *Nature*, **605**, 604-607. https://doi.org/10.1038/d41586-022-01388-6

[31] Bruning, O. and Collier, P. (2007) *Nature*, **448**, 285-289. https://doi.org/10.1038/nature06077

[32] Witze, A. (2022) *Nature*, **608**, 666. https://doi.org/10.1038/d41586-022-02287-6

[33] Normile, D. and Cho, A. (2019) *Science*, **363**, 911-912. https://doi.org/10.1126/science.363.6430.911

[34] Alekseev, B.V. (1995) *High Temperature*, **33**, 834-845.

[35] Lebedev, V., Burov, A. and Nagaitsev, S. (2017) *Physical Review Accelerators and Beams*, **20**, Article ID: 121301. https://doi.org/10.1103/PhysRevAccelBeams.20.121301

[36] Gilljohann, M.F., Ding, H., *et al.* (2019) *Physical Review X*, **9**, Article ID: 011046.

[37] Maiti, A., Chowdhury, S., Singha, P., Ray, S., Dasgupta, R. and Chandra, S. (2020) *The African Review of Physics*, **15**, 97-101.

[38] Sarkar, J., Chandra, S., Goswami, J., Das, C. and Ghosh, B. (2021) *AIP Conference Proceedings*, **2319**, Article ID: 030006.

[39] Feldman, D.F. (2020) *Science*, **368**, 131. https://doi.org/10.1126/science.abb3552

[40] Swinbanks, D. (1990) *Nature*, **345**, 467. https://doi.org/10.1038/345467a0

[41] Ohlsson, T. (2013) *Nature*, **494**, 35. https://doi.org/10.1038/494035d

[42] Gibney, E. (2018) *Nature*, **553**, 257-258. https://doi.org/10.1038/d41586-018-00162-x

[43] Brainard, J. (2018) *Science*, **362**, 1220. https://doi.org/10.1126/science.362.6413.390

[44] Guterman, L. (2019) *Science*, **363**, 210.

Journal of Modern Physics, 2022, 13, 1452-1473
https://www.scirp.org/journal/jmp
ISSN Online: 2153-120X
ISSN Print: 2153-1196

# General Relativity and the Tully-Fisher Relation for Rotating Galaxies

**Yogendra Srivastava[1,2], Giorgio Immirzi[3], John Swain[4], Orlando Panella[5], Simone Pacetti[2]**

[1]Emeritus Professor of Physics, Northeastern University, Boston, MA, USA
[2]Dipartimento di Fisica e Geologia, Università di Perugia, Perugia, Italy
[3]Retired, Dipartimento di Fisica e Geologia, Università di Perugia, Perugia, Italy
[4]Physics Department, Northeastern University, Boston, MA, USA
[5]Istituto Nazionale di Fisica Nucleare, INFN Sezione di Perugia, Perugia, Italy
Email: yogendra.srivastava@gmail.com, giorgio.immirzi@gmail.com, jswain02115@yahoo.com, orlando.panelle@pg.infn.it, simone.pacetti@unipg.it

**How to cite this paper:** Srivastava, Y., Immirzi, G., Swain, J., Panella, O. and Pacetti, S. (2022) General Relativity and the Tully-Fisher Relation for Rotating Galaxies. *Journal of Modern Physics*, **13**, 1452-1473.
https://doi.org/10.4236/jmp.2022.1311090

**Received:** October 2, 2022
**Accepted:** November 25, 2022
**Published:** November 28, 2022



## Abstract

The flat limit of rotational velocity ( $v_\varphi$ ) approximately equal to the "edge"-velocity of a galaxy is related to the baryonic mass ( $M_B$ ) via the T-F relationship $M_B \propto v_\varphi^n$ with $n \approx 4$. We explore the connection between mass and the limiting velocity in the framework of general relativity (GR) using the Weyl metric for axially-symmetric galaxies that are supported entirely by their rotational motion. While for small distances from the center, the Newtonian description is accurate as one moves beyond the (baryonic) edge of the galaxy, Lenz's law and non-linearity of the gravitational field inherent in GR not only lead to a flat velocity (obviating its Keplerian fall), but also provide its tight log-log relationship with the enclosed (baryonic) mass.

## Keywords

GR, Weyl Metric, Rotating Galaxies, Flat Rotation Curves, TF Relation

## 1. Introduction

The *rotation curves*, *i.e.*, the rotational velocity as a function of the distance from the center do not appear to follow a Keplerian drop as $1/\sqrt{r}$ ; instead they tend to reach a constant plateau velocity ( $v_\varphi$ ). This experimental fact, discovered by Vera Rubin [1] in the 1980's and confirmed by many later observations, poses one of the most challenging problems in theoretical physics. At present, the most widely accepted explanation is to suppose that the observed (luminous) mass

and radius of a galaxy is only a small part of the total; the rest is a vast (spherically symmetric) distribution of hypothetical dark matter (DM), which interacts only through gravitation; this is the basis of the widely accepted ΛCDM model [2] (cosmological constant plus cold dark matter). It is important to note that ΛCDM is itself anchored upon Einstein's general relativity (GR) with a cosmological constant.

The DM model when applied to (rotating) galaxies has its problems. First of all, in spite of extensive searches no trace of this mysterious dark matter has been found. Secondly, there is an empirical but successful relation, the Opik-Tully-Fischer law [3] [4] [5], between the plateau velocity of the gas ( $v_\varphi$ ) and the visible, hence baryonic, mass of the galaxy: ( $M_{\text{baryonic}} \propto v_\varphi^4$ ). But if the baryonic mass is supposed to be only a few percent of the total, how does this tiny fraction determine the rotational velocity of the galaxy? (Recall that in DM, an asymptotic $v_\varphi$ is generated by the *dark mass* not the baryonic mass). Thirdly, there has been no satisfactory explanation offered in DM for the magnitude of the observed (intrinsic) angular momentum ( $J_z$ ) of a galaxy. By contrast, in general relativity (GR), we can compute $J_z$ in terms of rotation velocity and the baryonic mass-current density that only extends over the visible size of any galaxy [6]. In fact, Salucci's review on DM concludes with a somber note: *It seems impossible to explain the observational evidences gathered so far in a simple dark matter framework* [7].

Building on previous work by other authors [8]-[17], and our own earlier work [18], we propose in the present paper that general relativity (GR), when appropriately applied, is perfectly capable of explaining the observed phenomena above, provided one takes into account the finite size (and a non-spherical mass distribution) of most galaxies and the basic fact that they rotate.

To be concrete, let us consider our own galaxy [19]. The Milky Way has a diameter of 25 Kilo parsec and a thickness of 2 Kilo parsec with a visible baryonic mass of about $(1 \div 2.5) \times 10^{11} M_\odot$. The considerably non-spherical geometry fixes the (stable) axis of rotation and our galaxy acquires a rotational velocity of about 200 km/sec at the edge (of the diameter). As previously noted in Ref. [18], rotations bring about a well-known but often forgotten fundamental difference between the Newtonian theory & GR.

In the Newtonian theory, *there is no dependence of the gravitational field upon the rotation of a body* [20]. In GR, on the other hand, the rotation of a system makes the metric nondiagonal (*i.e.*, the time-space component $g_{oi} \propto A_i$ becomes non-zero and a 3-vector-field $A_i$ is generated). A *preferred* direction (in space) is thus chosen and the *sense* of rotation (clock-wise or anti-clockwise) is established and fixed. This leads to the introduction of parity ( $\mathcal{P}$ ) and time-reversal ( $\mathcal{T}$ )-violating but ( $\mathcal{PT}$ ) conserving terms. Thus, a geo-magnetic field $\boldsymbol{B} = \nabla \wedge \boldsymbol{A}$ emerges (already at the linearized level in GR) that gives rise to the GEM (geo-electromagnetic) theory of Thirring & Lense [21] [22] [23]. (The ensuing Lense-Thirring effect has been beautifully confirmed experimentally in Ref.

[24]). An intrinsic angular momentum $\boldsymbol{J}$ is generated (through the non diagonal term). These issues are discussed in detail in later sections.

Another important fact distinguishing the Newtonian theory from GR is that a non-spherical mass distribution in GR necessarily radiates gravitational waves through its quadrupole moment. In ΛCDM, by contrast, as explicitly noted by Peebles [2], *it assumes... no gravitational waves.* Neglecting gravitational radiation from non-spherical rotating galaxies that have been in existence for several billion years and that have been continuously radiating, would be an extravagant assumption. It is also important to note that (massless) gravitational waves produce no *scalar* curvature $[\, T\left(\text{gravitational wave}\right) = g_{\mu\nu}T^{\mu\nu}\left(\text{gravitational wave}\right) \equiv 0\,]$, yet they contribute to the overall energy-momentum balance $[\, T_{\mu\nu}\left(\text{gravitational wave}\right) \neq 0\,]$. Also, as we shall see later, the length parameter $a$ in the Weyl metric provides a precise relationship between the asymptotic rotation velocity and the radiation field.

The paper is organized as follows. In Section (II), we briefly discuss our previous work [18] that was anchored upon the most general class of stationary, axially-symmetric metrics in GR found by Weyl [25] [26]. In particular, we here reproduce 1) the Einstein equations valid in the vacuum (*i.e.*, outside the galaxy); 2) motion of a test particle outside of the galaxy; 3) Exact Weyl constraints in the vacuum; 4) choice of the matter energy-momentum density appropriate for a galaxy that is supported entirely by rotations with zero pressure; 5) the nature of the solutions of the Einstein equations for the matter within the galaxy and 6) obtain Ludwig's extended GEM theory from the exact Weyl metric upon truncating the scalar potential $U$ to linear order in the constraint equations but keeping the exact non-linearity in the rotation field intact. In Section (3), we reemphasize a key role that Lenz's law plays in always boosting the rotation velocity up. In Section (4), we consider the rotation velocity and the TF law. In Section (5), we show that both the Weyl class of metrics and the Kerr metric possess an intrinsic angular momentum. It is worthy of note that the Schwarzschild metric has zero (intrinsic) angular momentum simply because it is spherical and thus lacks a vector field fixing a direction in space. A simple phenomenological analysis using an analytic, factorized mass density is applied to obtain the rotation velocity and the intrinsic angular momentum for our own galaxy and compared with experimental data in Section (7). The paper concludes in Section (8) with a summary of results obtained, work in progress and future prospects.

## 2. The Weyl Metric

In various subsections below, we list results relevant for the present paper from our previous work [18]:

1) Einstein equations for the Weyl metric outside the galaxy;

2) Motion of a test particle outside of the galaxy;

3) Exact Weyl constraints in the vacuum;

4) Matter energy-momentum density for galaxies supported entirely by rota-

tions with zero pressure;

5) Einstein equation constraints within the galaxy;

6) Ludwig's extended GEM theory results from the Einstein equations.

## 2.1. Weyl Metric and Einstein Equations outside the Galaxy

The axially-symmetric Weyl metric for a cylindrically symmetric space-time [27], with coordinates $(ct,\varphi,\rho,z)$, including explicitly the rotation term (see, for example [20]) may be written as:

$$\mathrm{d}s^2 = -\mathrm{e}^{2U}\left(c\mathrm{d}t - a\mathrm{d}\varphi\right)^2 + \mathrm{e}^{-2U}\rho^2\mathrm{d}\varphi^2 + \mathrm{e}^{2\nu-2U}\left(\mathrm{d}\rho^2+\mathrm{d}z^2\right), \tag{2.1}$$

$$g_{\mu\nu} = \begin{pmatrix} -\mathrm{e}^{2U} & \mathrm{e}^{2U}a & 0 & 0 \\ \mathrm{e}^{2U}a & -\mathrm{e}^{2U}a^2+\mathrm{e}^{-2U}\rho^2 & 0 & 0 \\ 0 & 0 & \mathrm{e}^{2\nu-2U} & 0 \\ 0 & 0 & 0 & \mathrm{e}^{2\nu-2U} \end{pmatrix};$$

$$g = \det g_{\mu\nu} = -\mathrm{e}^{4\nu-4U}\rho^2;$$

the inverse metric has the form:

$$g^{\mu\nu} = \begin{pmatrix} \dfrac{\mathrm{e}^{2U}a^2}{\rho^2}-\mathrm{e}^{-2U} & \dfrac{\mathrm{e}^{2U}a}{\rho^2} & 0 & 0 \\ \dfrac{\mathrm{e}^{2U}a}{\rho^2} & \dfrac{\mathrm{e}^{2U}}{\rho^2} & 0 & 0 \\ 0 & 0 & \mathrm{e}^{2U-2\nu} & 0 \\ 0 & 0 & 0 & \mathrm{e}^{2U-2\nu} \end{pmatrix};$$

and the invariant (spatial) volume element reads

$$\begin{aligned} &\mathrm{d}V = \mathrm{d}\rho\mathrm{d}\varphi\mathrm{d}z\sqrt{-g} = \mathrm{e}^{-2(U-\nu)}\left(\rho\mathrm{d}\rho\mathrm{d}z\mathrm{d}\varphi\right); \\ &\mathrm{d}V \geq \mathrm{d}V_{flat} \end{aligned} \tag{2.2}$$

Below, we list some salient aspects of the above axially-symmetric metric:

- 1: $U, a$ & $\nu$ are functions only of $\rho = \sqrt{x^2+y^2}$ and $z$. independent of $\varphi$. Hence, there are two Killing vectors; one time-like and the other space-like (outside of the horizon) of the system.
- 2: The function $U$ is related to the Newtonian potential $\Phi$ through $\mathrm{e}^{2U} = 1+2\dfrac{\Phi}{c^2}$.
- 3: The function $a$ would be related to the angular momentum of the system.
- 4: The gravito-magnetic potential-field $A_\phi = \dfrac{ca}{\rho}$, is a vector potential $\boldsymbol{A} = \left(0, \dfrac{ca}{\rho}, 0\right)$.
- 5: The three potential fields ($U, a$ & $\nu$) characterizing the metric are not all independent. The Einstein equations in the vacuum, that is outside the boundaries of a confined system such as a galaxy, impose the following *exact* non-linear differential constraints on these functions [20]:

$R_{\mu\nu}=0;$ in the vacuum of the system implies :

$$\frac{\partial^2 U}{\partial\rho^2}+\frac{\partial U}{\rho\partial\rho}+\frac{\partial^2 U}{\partial z^2}=-\frac{e^{4U}}{2\rho^2}\left[\left(\frac{\partial a}{\partial\rho}\right)^2+\left(\frac{\partial a}{\partial z}\right)^2\right];(\text{i})$$

$$\frac{\partial}{\partial z}\left(\frac{e^{4U}}{\rho}\frac{\partial a}{\partial z}\right)+\frac{\partial}{\partial\rho}\left(\frac{e^{4U}}{\rho}\frac{\partial a}{\partial\rho}\right)=0;(\text{ii}) \tag{2.3}$$

$$\text{and } \frac{\partial\nu}{\rho\partial\rho}=\left[\left(\frac{\partial U}{\partial\rho}\right)^2-\left(\frac{\partial U}{\partial z}\right)^2\right]-\frac{e^{4U}}{4\rho^2}\left[\left(\frac{\partial a}{\partial\rho}\right)^2-\left(\frac{\partial a}{\partial z}\right)^2\right];(\text{iii})$$

$$\frac{\partial\nu}{\rho\partial z}=2\frac{\partial U}{\partial\rho}\frac{\partial U}{\partial z}-\frac{e^{4U}}{2\rho^2}\frac{\partial a}{\partial\rho}\frac{\partial a}{\partial z};(\text{iv})$$

N.B.: Since $U$ and $a$ begin at order $G$, $\nu$ begins at second order (*i.e.*, is of order $G^2$). Once $U$ & $a$ satisfy the top two equations relating them Equation (2.3(i), (ii)), a solution for $\nu$ exists since the last two equations Equations (2.3(iii), (iv)) become the integrability conditions for it; $\nu\to 0$ as $\rho\to 0$ for any $z$.

- 6: The inequality in Equation (2.2) that tells us that the invariant spatial volume element is larger than its value in the flat-limit is useful for proving bounds on integrals of (positive definite) integrands, in gravitational asymptotic perturbation theory such as that developed by Landau-Lifshitz [27] & by Weinberg [6].

## 2.2. Motion of a Test Particle outside the Galaxy

A test particle in this axially symmetric metric would have two constants of motion, that we indicate as $p_0=E/c$ for time translations, $p_\phi=J/c$ for rotational motion in the x-y plane. We shall write $E=\gamma mc^2$, or $E=mc^2+\mathcal{E}_{NR}$ to study the non-relativistic limit.

We now write the geodesic equation for a test particle of mass $m$ for the above metric. The simplest formalism that extends to a Riemannian space blessed with a metric is through the action principle. Calling the action $S$, $m$ the mass and $\tau$ the proper time $\tau$, we have

$$\begin{aligned}&\mathrm{d}S=-\left(mc^2\right)\mathrm{d}\tau;\left(\mathrm{d}S\right)^2=\left(mc\right)^2\left(c\mathrm{d}\tau\right)^2;\\&\text{Let } p_\mu=\frac{\partial S}{\partial x^\mu};\text{Hamilton-Jacobi Eqn. implies : } g^{\mu\nu}\frac{\partial S}{\partial x^\mu}\frac{\partial S}{\partial x^\nu}=-\left(mc\right)^2;\\&\text{We have } p_\mu p_\nu g^{\mu\nu}=-\left(mc\right)^2\end{aligned} \tag{2.4}$$

As stated earlier, an axially symmetric system has two conserved quantities: the energy $E$ and the component of angular momentum $J_z$ say, for rotational motion in the xy-plane. Hence, the dependence on time-interval ($t$) and that on $\varphi$ can be prescribed as

$$\begin{aligned}&S\left(ct;\rho;\varphi;z\right)=-Et+J\varphi+\hat{S}\left(\rho;z\right);\\&-\frac{\partial S}{\partial ct}=E/c;\frac{\partial S}{\partial\varphi}=J;\frac{\partial S}{\partial\rho}=p_\rho;\frac{\partial S}{\partial z}=p_z\end{aligned} \tag{2.5}$$

Hence, for the Weyl metric, we have

$$
\begin{aligned}
&(mc)^2 = \left(\frac{E}{c}\right)^2\left[\mathrm{e}^{-2U} - \left(\frac{a}{\rho}\right)^2 \mathrm{e}^{2U}\right] - 2\frac{a}{\rho}\frac{J}{\rho}\frac{E}{c}\mathrm{e}^{2U} - \left(\frac{J}{\rho}\right)^2 \mathrm{e}^{2U} - \mathrm{e}^{2(U-\nu)}\left[p_\rho^2 + p_z^2\right]; \text{(i)}\\
&\left(\frac{E}{c}\right)^2 \mathrm{e}^{-2U} - \left[\frac{J}{\rho} + \frac{a}{\rho}\frac{E}{c}\right]^2 \mathrm{e}^{2U} = (mc)^2 + \mathrm{e}^{2(U-\nu)}\left[p_\rho^2 + p_z^2\right]; \text{(ii)}\\
&\text{Or}: \left[\frac{E}{c}\left\{\mathrm{e}^{-U} + \frac{a}{\rho}\mathrm{e}^{U}\right\} + \frac{J}{\rho}\mathrm{e}^{U}\right]\left[\frac{E}{c}\left\{\mathrm{e}^{-U} - \frac{a}{\rho}\mathrm{e}^{U}\right\} - \frac{J}{\rho}\mathrm{e}^{U}\right] = (mc)^2 + \mathrm{e}^{2(U-\nu)}\left(p_\rho^2 + p_z^2\right); \text{(iii)}
\end{aligned}
\tag{2.6}
$$

Let $E = mc^2\gamma$ and as both $E$ & $J$ are constants of motion, we can define a reduced (a-dimensional) angular momentum, *i.e.*, angular momentum per unit energy per unit $\rho$ (the perpendicular distance or, the impact parameter): $j \equiv Jc/E\rho$; and through it a *rotational* velocity $v_\varphi \equiv jc$. Similarly, the rotational parameter $a$ from the metric, can be employed to define a *vector potential*: $A_\varphi \equiv ca/\rho$ that has the dimensions of a velocity. With these definitions, Equation (2.6(ii)) reads:

$$
\begin{aligned}
&J = \rho\frac{E}{c}j;\ v_\varphi = cj;\ a = \rho\frac{A_\varphi}{c};\ \pi_\varphi \equiv v_\varphi + A_\phi;\\
&\gamma^2\left[\mathrm{e}^{-2U} - \left(\frac{\pi_\varphi}{c}\right)^2 \mathrm{e}^{2U}\right] = 1 + \mathrm{e}^{2(U-\nu)}\frac{p_\rho^2 + p_z^2}{(mc)^2}
\end{aligned}
\tag{2.7}
$$

For a galaxy supported totally by rotations along $\varphi$, that is the focus of this paper, we set $p_z = 0$ & $p_\rho = 0$. Then the above equation is reduced to

$$
\begin{aligned}
&\gamma = \frac{1}{\sqrt{\mathrm{e}^{-2U} - \left(\pi_\varphi/c\right)^2 \mathrm{e}^{2U}}};\\
&\text{Keeping leading terms only}: \gamma \approx \frac{1}{\sqrt{1 - 2U - \left(\pi_\varphi/c\right)^2}};\\
&\text{Test particle energy}: E = \gamma\left(mc^2\right) \approx mc^2 + \mathcal{E}_{NR};\\
&\mathcal{E}_{NR} = m\Phi + \frac{m}{2}\pi_\varphi^2;\ \pi_\varphi = v_\varphi + A_\varphi; \text{(ii)}
\end{aligned}
\tag{2.8}
$$

Equation (2.8(ii)) shows clearly what the Newtonian theory leaves out that GR supplies: viz., the vector potential $A_\varphi$. That in turn generates the GEM magnetic field. The lack of the dynamics generated by mass current density in the Newtonian theory is a serious lacuna that has important consequences. We discuss one such important improvement that GR provides.

As $U < 0$, the particle will remain bound so long as $\left|v_\varphi + A_\varphi\right| < \sqrt{-2\Phi}$ and not $v_\varphi < \sqrt{-2\Phi}$ (their values at the coordinates $\rho, z$ in question) as the Newtonian theory asserts.

This leads to the well known quandary when one computes, using Newtonian gravity, the escape velocity of our Sun were it to escape from our Galaxy. The mean rotational velocity of our Sun is about 220 km/sec and it is approximately 8.2 Kilo-parsec away from the center of our Galaxy. There is apparently very little (baryonic) mass beyond this distance. Thus, Newtonian theory for the Sun's escape velocity predicts $\sqrt{2}\times 220 \approx 310$ km/sec [28] in the vicinity of our Sun,

experimental astrophysicists estimate the Sun's escape velocity to be between (500 ÷ 550) km/sec.

In GEM, by contrast, the escape velocity reads: $v_{escape} \approx -A_{\varphi} + \sqrt{-2\Phi}$ . As we shall discuss later in more detail, Lenz's law (reminding us that all masses attract so that the GEM magnetic field obeys the *left hand rule*) forces us to have $A_{\varphi} < 0$ , thus boosting the escape velocity up [*vedi* Section (3)]. From the phenomenology of the Milky Way in Section (7), we estimate the magnetic term to add about 200 km/sec, thereby bringing the escape velocity much closer to its estimated experimental value. A quantitative analysis of this matter shall be presented in a later work.

### 2.3. Exact Weyl Constrains in the Vacuum

Having delineated a few important aspects that distinguish GR from the Newtonian theory regarding the dynamics of a rotation-supported galaxy, let us return to a discussion of the exact Weyl constraints.

At first glance, Equations (2.3(i-iv)) appear quite opaque and daunting, but they acquire a physically more appealing aspect through the following *dictionary* in terms of the GEM electric $\boldsymbol{E}$ & magnetic $\boldsymbol{B}$ fields of order *G*, along with a higher order field $\hat{\boldsymbol{B}}$ that is of order $G^2$. They are defined as follows:

$$\begin{aligned}
&\boldsymbol{E} = \left(E_{\rho}, 0, E_z\right) = \left(-\frac{\partial \Phi}{\partial \rho}, 0, -\frac{\partial \Phi}{\partial z}\right) = -\nabla\Phi; \text{(i)} \\
&\boldsymbol{B} = \left(B_{\rho}, 0, B_z\right) = \left(-\frac{\partial A_{\varphi}}{\partial z}, 0, \frac{\partial A_{\varphi}}{\partial \rho}\right) = \nabla \wedge \boldsymbol{A}; \text{(ii)} \\
&\hat{\boldsymbol{B}} = \left(\hat{B}_{\rho}, 0, \hat{B}_z\right) = \left(-\frac{1}{\rho}\frac{\partial \nu}{\partial z}, 0, \frac{1}{\rho}\frac{\partial \nu}{\partial \rho}\right); \text{(iii)} \\
&\text{Thus, we have : } \hat{\boldsymbol{B}}^2 = \frac{1}{\rho^2}\left(\nu_{\rho}^2 + \nu_z^2\right); \text{(iv)} \\
&\& \quad -\rho\left(\nabla \wedge \hat{\boldsymbol{B}}\right)_{\varphi} = \nu_{\rho\rho} + \nu_{zz} - \frac{1}{\rho}\nu_{\rho}; \text{(v)}
\end{aligned} \tag{2.9}$$

Before considering the equations they obey, let us pause to say a few words about the genesis of the nomenclature in Equation (2.9). This EM analogy was first noticed and Equations (2.9(i) and (ii)) were used by Thirring. His initial purpose was to compute the gravitational field inside a hollow rotating sphere (in linearized GR). Later with Lense, he extended the analysis of the effect of proper rotation of a central body on the motion of other celestial bodies, which led to the discovery of the Lense-Thirring effect [24]. In a set of four beautiful papers, Ludwig [13] [14] [15] [16] has extended GEM by including additional field energy (that are second order in *G*) and obtained a closed set of non-linear equations for the rotational velocity ( $v_{\varphi}$ ) in terms of the Newtonian velocity (via its acceleration) and the matter distribution within the galaxy. We shall return to discuss them in a later subsection and show that indeed they are reproduced in the appropriate limit.

In terms of the field variables defined in Equation (2.9), the Weyl equations in

the vacuum given in Equation (2.3) read:

$$\begin{aligned}
&\nabla\cdot\boldsymbol{E} = -\frac{2}{c^2}\mathrm{e}^{-2U}\boldsymbol{E}^2 + \frac{c^2}{2}\mathrm{e}^{6U}\boldsymbol{B}^2;\text{(i)}\\
&\nabla\wedge\boldsymbol{B} = -\frac{4}{c^2}\left(\boldsymbol{E}\wedge\boldsymbol{B}\right);\text{(ii)}\\
&\hat{\boldsymbol{B}}_\rho = \frac{\rho}{c^2}\left[E_z^2 - E_\rho^2\right] + \frac{\mathrm{e}^{4U}}{4}\left[B_\rho^2 - B_z^2\right];\text{(iii)}\\
&\hat{\boldsymbol{B}}_z = 2\frac{\rho}{c^2}E_\rho E_z + \frac{e^{4U}}{2}B_\rho B_z;\text{(iv)}
\end{aligned} \tag{2.10}$$

Within the galaxy, the *Gauß law* in Equation (2.10(i)) shall get the mass density term on the right-hand side ($-4\pi G\rho_m$). Similarly the *Ampere law* in Equation (2.10(ii)) shall get the mass current density ($-4\pi G\rho_m v_\varphi$) when we continue the solution within the galaxy. On the other hand, Equations (2.10(iii) and (iv)) remain valid both inside and outside of the galaxy, due to our choice of the matter energy-momentum density as discussed in a later subsection.

The various exponentials in these expressions add on higher order polynomials in the Newtonian potential due to the non-linearity of GR. In all the four equations above, the quadratic terms in $\boldsymbol{E}$ & $\boldsymbol{B}$ appear; these are easily interpretable as different components of the field energy-momentum density.

An attentive reader might wonder how (& why) one can possibly succeed in describing the dynamics of a spin-2 gravitational field in terms of just the GEM-electric and magnetic (spin-1 vector) fields? The answer to this question lies in the non-linearity of GR. Already at the second order (in G), there are constraints between the $\boldsymbol{E}$-field (whose longitudinal part is defined through the gradient of the Newtonian potential $\Phi$ and whose transverse part arises through the time derivative of the transverse part of the vector potential, $\partial\boldsymbol{A}_T/\partial t$) and there are constraints between them, *vedi* Equations (2.3(i) and (ii)). Further on, at order $G^2$, a subsidiary field $\nu$ appears in the metric as well as in the equations of motion, that is completely constrained by the behavior of the GEM fields and the boundary condition that $\nu\left(\rho=0;z\right)\equiv 0$. Thus, in the far field region, once the origin is appropriately chosen, the gravitational field is limited to its two degrees of freedom and its multipole expansion beginning with the quadrupole. Not so, in the near field within or in the vicinity of the galaxy where both longitudinal and transverse fields are present with constraints between them playing a crucial role in limiting the dynamics, as the following discussion illustrates.

The assumption that there is no motion along the (radial) $\rho$-direction or along the z-direction, brings in constraints for the dynamical system. Weinberg's Equation (9.12) [6] gives the following expression for a particle's (spatial) acceleration $\mathcal{A}^i$ ($i=2,3,4$ with coordinates labeled as $x^\mu$: ($x^1=ct$, $x^2=\varphi$; $x^3=\rho$; $x^4=z$)

$$\begin{aligned}
\mathcal{A}^i = &-\Gamma^i_{1,1} - 2\Gamma^i_{1,j}\frac{\mathrm{d}x^j}{\mathrm{d}t} - \Gamma^i_{j,k}\frac{\mathrm{d}x^j}{\mathrm{d}t}\frac{\mathrm{d}x^k}{\mathrm{d}t}\\
&+\frac{\mathrm{d}x^i}{\mathrm{d}t}\left[\Gamma^1_{1,1} + 2\Gamma^1_{1,j}\frac{\mathrm{d}x^j}{\mathrm{d}t} + \Gamma^1_{j,k}\frac{\mathrm{d}x^j}{\mathrm{d}t}\frac{\mathrm{d}x^k}{\mathrm{d}t}\right];
\end{aligned} \tag{2.11}$$

Assuming only circular motion (about the z-axis), we have non-vanishing velocity only along the $\varphi$-axis: $\mathrm{d}\varphi/\mathrm{d}t = v/\rho$ and $\mathrm{d}x^i/\mathrm{d}t = 0$ for $i = 3,4$. Under this premise, also the accelerations along the 3- & 4-axes must vanish:

$$\begin{aligned}
&\text{(i) } \mathcal{A}^{\rho} = -c^2 \mathrm{e}^{4U-2\nu} U_{,\rho} + c\mathrm{e}^{4U-2\nu} \frac{v}{\rho}\left[a_{,\rho} + 2aU_{,\rho}\right] \\
&\qquad - \mathrm{e}^{-2\nu}\left(\frac{v}{\rho}\right)^2 \left[-\rho + \mathrm{e}^{4U} a a_{,\rho} + \rho^2 U_{,\rho} + \mathrm{e}^{4U} a^2 U_{,\rho}\right] = 0; \\
&\text{(ii) } \mathcal{A}^{z} = -c^2 \mathrm{e}^{4U-2\nu} U_{,z} + c\mathrm{e}^{4U-2\nu} \frac{v}{\rho}\left[a_{,z} + 2aU_{,z}\right] \\
&\qquad - \mathrm{e}^{-2\nu}\left(\frac{v}{\rho}\right)^2 \left[\rho^2 U_{,z} + \mathrm{e}^{4U} a^2 U_{,z} + \mathrm{e}^{4U} a a_{,z}\right] = 0;
\end{aligned} \tag{2.12}$$

Equations (2.12) along with Equations (2.3(i, ii)) allow us to obtain an exact non-linear, first order differential equation for the velocity field $\beta(\rho, z=0) = v(\rho, z=0)/c$ on the equatorial plane in terms of the (normalized dimensionless) Newtonian (velocity squared) defined as usual $g(\rho) = (\rho/c^2)(\partial\Phi(\rho,0)/\partial\rho)$, where $\Phi(\rho,0)$ is the Newtonian potential in the equatorial plane. This rather complicated expression can be found in Appendix A of [18]. Here we shall illustrate the strategy employed to derive the result valid to the lowest non-vanishing order. To the desired order of accuracy, Equations (2.12), yield the following expressions for $a,\rho$ & $a_{,z}$:

$$\frac{a,\rho}{\rho} = -\frac{\beta}{\rho} + \left(\frac{1}{\beta} + \beta\right)\frac{\Phi_{,\rho}}{c^2}; \quad \frac{a,z}{\rho} = +\left(\frac{1}{\beta} + \beta\right)\frac{\Phi_{,z}}{c^2}; \tag{2.13}$$

We can thus eliminate $a_{,\rho}; a_{,z}$ in Equation (2.3(ii)), to obtain an expression for the second derivatives of *U*. To the desired order of accuracy:

$$\left[\mathrm{e}^{4U}\left(\frac{1}{\beta} + \beta\right)U_{,z}\right]_{,z} + \left[\mathrm{e}^{4U}\left\{-\frac{\beta}{\rho} + \left(\frac{1}{\beta} + \beta\right)U_{,\rho}\right\}\right]_{,\rho} = 0; \tag{2.14}$$

Keeping only terms linear in the *U*-field:

$$\left(\frac{1}{\beta} + \beta\right)\left[U_{,\rho,\rho} + U_{,z,z}\right] = \frac{1-\beta^2}{\beta^2}\beta_{,z}U_{,z} + \frac{1-\beta^2}{\beta^2}\beta_{,\rho}U_{,\rho} - \frac{\beta}{\rho^2} + \frac{\beta_{,\rho}}{\rho}; \tag{2.15}$$

Thus:

$$\begin{aligned}
&U_{,\rho,\rho} + U_{,z,z} + \frac{U_{,\rho}}{\rho} \\
&= \frac{1-\beta^2}{\beta\left(1+\beta^2\right)}\beta_{,z}U_{,z} - \frac{\beta^2}{\rho^2\left(1+\beta^2\right)} + \frac{\rho\beta_{,\rho}}{\rho^2}\frac{\beta^2 + \left(1-\beta^2\right)g(\rho,z)}{\beta\left(1+\beta^2\right)} + \frac{g(\rho,z)}{\rho^2}; \text{(i)}
\end{aligned} \tag{2.16}$$

According to Equation (2.3(i)), lhs is of order $G^2$, outside the galaxy. Thus, to linear order in G, we have at $z=0$ upon using the up-down symmetry, for the rate of increase of $\beta(\rho)$ (outside the galaxy)

$$\rho\frac{\partial\beta}{\partial\rho} = \beta\frac{\beta^2 - g(\rho)\left(1-\beta^2\right)}{\beta^2 + g\left(\rho\left(1+\beta^2\right)\right)}; \tag{2.17}$$

Equation (2.17) is of course only valid outside the galaxy. It agrees exactly with Ludwig's Equation (4.13) [13] when his solution is continued to outside the galaxy where the matter density term $f = 0$.

It is easy to obtain the rate equation inside the galaxy (to linear order) upon including the matter density term on the rhs of Equation (2.3(i)). To lowest order, the (2-dimensional) Laplacian of U receives the matter field contribution ($4\pi G\rho_m$). Explicitly, inside the galaxy, we have

$$\nabla^2 U(\rho,z) = \frac{4\pi G\rho_m(\rho,z)}{c^2} + \text{terms of order } G^2;$$

$$\text{Define for } z=0;\ f(\rho) = \frac{4\pi G\rho_m(\rho,z=0)\rho^2}{c^2};$$

$$\text{Equation (2.14(i))} \rightarrow (f-g) + \frac{\beta^2}{1+\beta^2} = \frac{1}{\beta(1+\beta^2)}\rho\frac{\partial\beta}{\partial\rho}\left[\beta^2 + g\left(1-\beta^2\right)\right];$$

$$\rho\frac{\partial\beta}{\partial\rho} = \beta\frac{\beta^2 + (1-\beta^2)(f-g)}{\beta^2 + g(1+\beta)^2} \tag{2.18}$$

This essentially reproduces Ludwig's result inside the galaxy and reduces to Equation (2.17) outside the galaxy for which $f = 0$.

## 2.4. Matter Energy-Momentum Density

Within the boundaries of the galaxy, the dynamics of course changes:

$$E_{\mu\nu}(\rho,z) = R_{\mu\nu} - \frac{1}{2}Rg_{\mu\nu} = \frac{8\pi G}{c^4}T_{\mu\nu} \tag{2.19}$$

and thus we need a model for the energy-momentum density of the rotating galaxy and a choice for the metric inside. Hoping that no confusion ensues, we shall continue to use the same form of the metric as given in Equation (2.1). The simplest and most commonly used model for matter is that of *free dust* with in general an equation of state relating the mass density to the pressure. We shall assume further that our galaxy has zero-pressure, which implies that it is *totally* supported by rotations around its stable axis, with no further extraneous motion. Choosing the axis of rotation along the z-axis (with an angular velocity $\dot{\phi}$), our extreme simplifying assumptions, allow us to restrict the matter energy-momentum density to the following form [with coordinates $(o,\varphi,\rho,z)$]:

$$\begin{aligned}
&T^{\mu\nu} = \rho_m u^\mu u^\nu;\\
&u^\mu(\rho,z) = \gamma c\left(1,\frac{\beta}{\rho},0,0\right);\\
&u_o = -\gamma c\mathrm{e}^{2U}\left[1-\beta\frac{a}{\rho}\right];u_\varphi = \gamma c\left[\mathrm{e}^{2U}a\left(1-\beta\frac{a}{\rho}\right)+\beta\rho\mathrm{e}^{-2U}\right];u_\rho = 0;u_z = 0;\\
&\text{The trace}: T^\mu_\mu = -\rho_m c^2 \Rightarrow \frac{1}{\gamma^2} = \left(1-\beta\frac{a}{\rho}\right)^2\mathrm{e}^{2U} - \beta^2\mathrm{e}^{-2U}
\end{aligned} \tag{2.20}$$

While lack of motion along the $\rho$ (radial) & $z$ (vertical) directions simplify

the structure of the matter energy-momentum density tensor from a (4 × 4) matrix to a (2 × 2) matrix form, this simplification also brings some unexpected peculiarities such as:

- 1: Even though the reduced matrix $T_{\mu\nu}$ is real-Hermitean, it is non-diagonal and because it is factorizable its determinant is zero. We recall that in the general case, this matrix has 4 eigenvalues: a positive definite (time-like) mass density with 3 (space-like) pressures ( $p_1, p_2, p_3$ along its principal axes). By setting all pressures $p_i$ to zero, we have made the matrix *singular* with the lone non-vanishing eigenvalue the scalar (generally invariant) mass density $\rho_m c^2$.
- 2: For any finite $\beta$, the Lorentz factor $\gamma$ in Equation (2.20) does not reduce to its expected value $\left(1-\beta^2\right)^{-1/2}$, unless the rotation parameter $a \to 0$. But, if we let $a = 0$, the metric becomes *diagonal*, since then $g_{o\varphi} = 0$ thereby rendering the (matter + field) angular-momentum zero. Clearly, this is unphysical and thus unacceptable. We must have $a \neq 0$ (it can be positive or negative, of course).
- 3. In the expression for $\gamma$, the linear term in $\beta$ induced by a non-vanishing length parameter $a \neq 0$, would exceed the expected $\beta^2$ correction unless *for any value of* $\rho \leq \rho_{edge}$ *within the galaxy*, $2\left|a(\rho)/\rho\right| < \beta(\rho)$. In short, $\beta$ cannot be too small if the rotational velocity alone has to support a galaxy with zero internal pressure.
- 4: The metric and its first derivatives must be matched at the boundary for their inside versus outside values.

Thus, $\beta$ just outside cannot be too small either. A clear indication from GR that Newtonian values for $\beta$ that are becoming too small at the edge must get supplemented by (the mass current density) contributions to stabilize the system.

## 2.5. Einstein Constraints within the Galaxy

To emphasize the affinity and the difference between Einstein gravity and electromagnetism, and partly to follow the works by Ludwig [13] [14] [15] [16], it is convenient to write the Einstein equations for this metric in terms of the three vectors $\boldsymbol{E}, \boldsymbol{B}, \hat{\boldsymbol{B}}$ defined earlier. Overall we have a dictionary with which we can write the Einstein equations

$$E_{\mu\nu} \equiv R_{\mu\nu} - \frac{1}{2} g_{\mu\nu} R = \frac{8\pi G}{c^4} T_{\mu\nu} \tag{2.21}$$

We have:

$$\begin{aligned} R = g^{\mu\nu} R_{\mu\nu} &= \frac{8\pi G}{c^4} g^{\mu\nu} T_{\mu\nu} \\ &= \mathrm{e}^{2U-2\nu}\left(2\nabla^2 U + \frac{\mathrm{e}^{4U}}{\rho^2}\left(a_{,\rho}^2 + a_{,z}^2\right) - 2\left(\nu_{,\rho,\rho} + a_{,zz} + U_{rho}^2 + U_{,z}^2\right)\right) \\ &= \mathrm{e}^{2U-2\nu}\left(-2\frac{\mathrm{e}^{-2U}}{c^2}\nabla\cdot\boldsymbol{E} - 4\frac{\mathrm{e}^{-4U}}{c^4}\boldsymbol{E}^2 + 16\frac{\mathrm{e}^{4U}}{c^2}\boldsymbol{B}^2 + 2\rho\left(\nabla\wedge\hat{\boldsymbol{B}}\right)_{\varphi} + \hat{B}_{\rho}\right) \end{aligned}$$

and therefore a "Gauß law"

$$\nabla\cdot\boldsymbol{E}=-4\pi G\rho_m \mathrm{e}^{2\nu}\left(1+\mathrm{e}^{-2U}\left(\beta\gamma\right)^2\right)-2\frac{\mathrm{e}^{-2U}}{c^2}\boldsymbol{E}^2+8\mathrm{e}^{6U}\boldsymbol{B}^2 + \rho c^2\mathrm{e}^{2U}\left(\nabla\wedge\hat{\boldsymbol{B}}\right)_\varphi-\frac{1}{2}c^2e^{2U}\hat{B}_z \tag{2.22}$$

To single out the non-diagonal part of $E_{\mu\nu}$ in terms of the matter current density $J_m=\rho_m v_\varphi$, we consider the combination

$$\begin{aligned} aE_{ctct}+E_{ct\varphi} &= \frac{8\pi G}{c^2}\left(aT_{ctct}+T_{ct\varphi}\right)=\frac{8\pi G}{c^2}\left(-\left(J_m\right)_\varphi\gamma^2\rho\left(1-\frac{a}{\rho}\beta\right)\right) \\ &= -\frac{1}{2}\mathrm{e}^{4U-2\nu}\left(a_{,\rho,\rho}+a_{,z,z}-\frac{1}{\rho}a_{,\rho}+4\left(a_{,\rho}U_{,\rho}+a_{,z}U_{,z}\right)\right) \\ &= \frac{2\rho}{c}\mathrm{e}^{4U-2\nu}\left(\left(\nabla\wedge\boldsymbol{B}\right)\right)-4\left(E\wedge\boldsymbol{B}\right)_\varphi\Big) \end{aligned} \tag{2.23}$$

and therefore an "Ampère law" emerges:

$$\nabla\wedge\boldsymbol{B}=\frac{4\pi G}{c}\mathrm{e}^{-4U+2\nu}\left(-\boldsymbol{J}_m\gamma^2\left(1-\frac{a}{\rho}\beta\right)\right)+\frac{c}{2\rho}\mathrm{e}^{-4U+2\nu}\boldsymbol{E}\wedge\boldsymbol{B} \tag{2.24}$$

In Appendix B of Ref. [18], we have reproduced some details of the traditional iterative scheme in GR (developed over a century ago). Anyone interested can readily compare the higher order contributions as they arise from the perturbative scheme with the exact Einstein-Weyl equations.

### 2.6. Ludwig's Extended GEM Theory Results from Einstein Equations

Neglecting higher order term in $G$ and (special) relativistic corrections, we can summarize Gauß and Ampère law as:

$$\nabla\cdot\boldsymbol{E}=-4\pi G\rho_m,\quad \nabla\wedge\boldsymbol{B}=-\frac{4\pi G}{c}\boldsymbol{J}_m \tag{2.25}$$

It is important to note (and very useful to remember to implement) the negative sign of the matter fields on the rhs of Equations (2.25), especially in the Ampére law that leads to a *left hand rule* for the GEM magnetic field. Precisely because gravitation has only attraction (unlike E & M that has both), the Lenz's law for gravity implies that there is a net boost to the acceleration due to other masses. We illustrate in Section (3) that the model obeying Lenz's law produces a rotation velocity curve consistent with mass-to-luminosity data whereas another model while successful in producing the rotation curve was inconsistent with the light intensity data.

## 3. Lenz's Law Always Boosts Rotational Velocities for Stable Galaxies

An attentive reader might rightly wonder why there is always a counter rotating GEM magnetic field produced by the velocity-field of material masses. Such is not always the case in Maxwellian electrodynamics due to the fact that both at-

tractive and repulsive forces are generated as both positive and negative charges exist in the electro-magnetic theory of Maxwell. In GEM however, the force is always attractive [29] [30]. For the problem at hand, it is most easily seen in the equation for the GEM magnetic field

$$\nabla \times \boldsymbol{B} = -\frac{4\pi G}{c^2}\rho \boldsymbol{v} + \frac{\partial \boldsymbol{E}}{c^2 \partial t} \tag{3.26}$$

The minus sign in the first term on the right hand side of Equation (6.6) tells us that the magnetic field induced on the left side (due to the velocity field) follows the *left-hand rule* always. In standard electrodynamics with different signs of charge, Lenz's law implies that a negatively charged electron in a beam of co-moving electrons loses momentum due to other negatively charged electrons in the beam. On the other hand, the same Lenz's law implies that an electron gains momentum if there are say positively charged parallel moving protons. In GEM, there is only attraction between masses and thus the situation is similar to that between an electron and a proton. Ergo, Lenz's law implies that there is always an increase in the rotational velocity of galaxies due to GEM. In the following, we shall confirm these results explicitly that the resultant rotational velocity is indeed boosted through a GEM magnetic term $B_z < 0$. We may consider it as a strict *boundary condition* to be imposed for the stability of a galaxy that is supported entirely by rotations.

We have shown in Ref. [18] that the model obeying Lenz's law produces a rotation velocity curve consistent with mass-to-luminosity data whereas another model while successful in producing the rotation curve was inconsistent with the light intensity data.

The example of galaxy NGC 1560 has been discussed at length by Ludwig in Ref. [13] using two different parametrizations, we shall call them model 1 & model II with two different Newtonian g-functions $g_I$ & $g_{II}$. These are shown in Figure 1 of Ref. [18]. They both produce roughly the same $\beta(\rho)$. The GEM magnetic field is defined as

$$\frac{B_z}{c} = \frac{g(\rho) - \beta^2}{\beta\rho}. \tag{3.27}$$

For model I, $B_z > 0$ and for model II, $B_z < 0$. In Figure 2 of Ref. [18], are shown the magnetic fields, $B_{z_I}$ for model I and $-B_{z,II}$ for model II. Lenz's law is not obeyed in model I but it is in model II. In Figure 3 of Ref. [18], are shown the corresponding Newtonian velocities

Ludwig's model II obeys Lenz's law and at the same time is also consistent with the mass-to-luminosity data, whereas model I does not agree with the mass-to-luminosity data. This shows the efficacy of Lenz's law in limiting the class of acceptable solutions.

## 4. Rotation Velocity and the Tully-Fisher Law

As discussed in Section (3), the induced GEM magnetic field $\boldsymbol{B}$ is always

counter-rotating (follows the left hand rule) with respect to velocity-field of material masses that produce it. Also, as shown earlier, the Einstein-Weyl equations acquire the form of Gauß-like and Ampère-like laws, even at the linearized level.

Upon assuming that $\boldsymbol{A}_g = A_\varphi \hat{\varphi}; \boldsymbol{v} = v\hat{\varphi}$ and that we are in stationary conditions, the equations (in cylindrical coordinates) read [13]:

$$\begin{aligned} &\phi_g = \frac{\Phi}{c^2}; \\ &\frac{1}{\rho}\frac{\partial}{\partial\rho}\left(r\frac{\partial\phi_g}{\partial\rho}\right) + \frac{\partial^2\phi_g}{\partial z^2} = \nabla^2\phi_g = 4\pi G\rho_m; \\ &\frac{\partial}{\partial\rho}\left(\frac{1}{\rho}\frac{\partial\left(\rho A_\varphi\right)}{\partial\rho}\right) + \frac{\partial^2 A_\varphi}{\partial z^2} = \frac{4\pi G}{c^2}\rho_m v \end{aligned} \tag{4.1}$$

The assumption is that $v(\rho, z)$ describes continuously the motion of the rotating matter inside the galaxy and the motion of the ionized gas that circles round it. While the geodesic equations for the (spatial) acceleration of a particle $\mathcal{A}^i$ have been shown to be non-linear and complicated, however, we here limit our discussion and consider only equatorial circular motion around the z-axis with $\frac{\mathrm{d}\varphi}{\mathrm{d}t} = \frac{v}{\rho}$ and $\mathcal{A}^\rho = \mathcal{A}^z = 0$. Under these provisions, to lowest order we have the Lorentz force equations:

$$\begin{aligned} &\frac{\partial\Phi}{\partial\rho} - \frac{v^2}{\rho} = \frac{v}{\rho}\frac{\partial(ca)}{\partial\rho},\ \frac{\partial\Phi}{\partial z} = \frac{v}{\rho}\frac{\partial(ca)}{\partial z} \leftrightarrow E_z - vB_\rho = 0;\ E_\rho + vB_z = -\frac{v^2}{\rho}; \\ &\text{Define, a magnetic velocity term}: \beta_{mag} \equiv \frac{\rho(-B_z)}{c} \geq 0; \\ &\text{Thus, with } g \text{ the Newtonian velocity squared}: \beta^2 = g + \beta\beta_{mag} \geq g; (\mathrm{i}) \\ &\beta = \frac{1}{2}\left[\beta_{mag} + \sqrt{4g + \beta_{mag}^2}\right]; (\mathrm{ii}) \end{aligned} \tag{4.2}$$

Thus, as we proposed to show in Section (1), GR with its inherent Lenz's law does indeed produce the remarkable result that the rotational velocity always exceeds its Newtonian value: [ $\beta^2 \geq g$ Equation (4.2(i))].

The above inequality is a powerful constraint that has been amply confirmed through 2700 data points from 153 SPARC galaxies. For details, we refer the reader to Ref. [5], especially Figure 3 in it.

We have also shown that up to the order of required accuracy, Ludwig's rate equations for the rotation velocity emerge from the Weyl metric, thereby giving strong support to Ludwig's computational program. We shall return to it in Section (6).

We reproduce here from Ref. [18], a simple qualitative argument for constant asymptotic velocity deduced from these equations, with a Newtonian term augmented by the magnetic term. At small distances from the center, the Newtonian term dominates but as one proceeds further towards the edge of the galaxy, the picture changes dramatically due to the onset of the magnetic term.

If we consider our own galaxy, the Newtonian velocity has roughly speaking

two bumps and then it goes down in the Keplerian fashion as $1/\sqrt{\rho}$. If we simply add a magnetic term that begins from zero and grows up near the edge to produce a constant (negative) vector potential $A_\varphi$ in obedience to the Lenz's law, we have the desired result of a constant rotational velocity. Also, the same asymptotically constant vector potential allows us to obtain a reasonable estimate both for the rotation velocity & the angular momentum of our galaxy.

For our galaxy, the maximum of the Newtonian term coincides approximately with the onset of asymptotic velocity, $\beta^2(\infty)=\frac{R_s}{2R_{edge}}$, where the Schwarzschild radius $R_s=2GM/c^2$ with $M$ denoting the baryonic mass (plus that of the gravitational field). For a pillbox like galaxy, $V=\pi R_{edge}^2 h$, $M=\rho_m V$, so that $\beta^2(\infty)\sim\frac{M}{M^{1/2}}\sim M^{1/2}$, reproducing the Tully-Fisher law: $M\propto\beta^4$. As we change the geometry, we expect that $M\propto\beta^n$ with $n=4\pm0.5$. Thus, while the scatter in the index $n$ is to be expected, the log-log relationship would be maintained.

We note that the mass parameter here refers to the baryonic mass (+that of the GR radiation). A linear light-to mass ratio $\Upsilon^*\approx 0.5 M_\odot/L_\odot$ is employed for all disk galaxies in Ref. [5] to convert the light data from 3.6 μm band of Spitzer into mass. Thus, to use the terminology in Ref. [7], we are discussing the baryonic TF relation.

## 5. Weyl Class of Metrics & the Particular Kerr Metric

We briefly note here the similarities and differences between the large distance behaviour of the Weyl class of metrics to the particular one of the Kerr solution of the Einstein equations [20]. This solution apparently describes a rotating black hole in terms of a mass $M$ and a (constant) length parameter $a$ that is known to be linearly related to its angular momentum.

Taking $\hat{z}$ as axis of rotation, $g_{\mu\nu}\equiv\eta_{\mu\nu}+h_{\mu\nu}$, at large distance, the Kerr metric asymptotic behaviour is given by ([6] pg. 240):

$$\begin{aligned} &h_{ij}\to-\frac{R_s}{r^3}x_i x_j,\ \ h_{0i}\to\frac{R_s}{r^2}\left(x_i+\frac{1}{r}(\boldsymbol{a}\wedge\boldsymbol{x})_i\right),\\ &R_s\equiv\frac{2GM}{c^2},\ \boldsymbol{a}=(0,0,a),\ i,j=1,2,3 \end{aligned} \tag{5.3}$$

As amply discussed in an Appendix in Ref. [18], this is quite generally all that one needs to calculate the total mass and angular momentum. For the Kerr metric (5.3), it yields $E_{tot}=Mc^2$, $\boldsymbol{J}=Mc\boldsymbol{a}$, as expected. If $a=0$ the Kerr metric coincides with the Schwarzschild metric and $J=0$. We can see that for the system to have a finite intrinsic angular momentum, it is crucial that the space-time part of $h_{\mu\nu}$ does not vanish asymptotically beyond $1/r^2$.

Let us now consider the general class of Weyl's axially-symmetric metrics as in Section (2) focusing on their space-time part in the equatorial plane (*i.e.*, at $z=0$ so that $\rho=r$) and we have:

$$
\begin{aligned}
&g_{o\varphi}(r)=\frac{a(r)}{c}\mathrm{e}^{2U(r)}, \text{can be written in pseudo-Euclidean}\\
&\text{coordinatesas the special case of } g_{oi}=\varepsilon_{ijk}a_j x_k\frac{\mathrm{e}^{2U}}{r^2};\\
&\text{with Weyl's being the special case } \boldsymbol{a}=(0,0,a);\\
&\text{Expanding in perturbation theory :}\\
&g_{oi}=g_{oi}^{(1)}+g_{oi}^{(2)}=\varepsilon_{ijk}\frac{a_j x_k}{r^2}\left[1+2U(r)+\cdots\right],\\
&\text{with } g_{oi}^{(1)}=\varepsilon_{ijk}\frac{a_j x_k}{r^2};\ \&\ g_{oi}^{(2)}=\varepsilon_{ijk}\frac{a_j x_k}{r^2}2U(r)
\end{aligned}
\tag{5.4}
$$

We are interested in the second part ( $g_{oi}^{(2)}$ ) that relates to the angular momentum ( $\boldsymbol{J}$ ) of the system. Asymptotically, we have (*vedi* Ref. [6]) for the second term,

$$
g_{oi}^{(2)}=\frac{2G}{r^3}(\boldsymbol{r}\times\boldsymbol{J})_i;\ \text{ we find } J_z=Mca \tag{5.5}
$$

exactly the same as that for the Kerr metric provided we associate the (constant) Kerr length parameter *a* with the (asymptotic) Weyl length parameter *a*.

The implication is that a finite value of the total (material + that of the gravitational field) angular momentum of the galaxy requires that the rotational velocity asymptote to a constant value and *vice versa*.

A mental picture of what is happening may be formed through the following rough guide about the Weyl parameter *a*. For small *r*, *a* increases from zero linearly until the edge, beyond which, while continuous at the edge, it eventually becomes a constant. At very large *r*, as expected the GEM magnetic field ( $-B_z\to 1/r$ ), as all radiation fields do.

## 6. Ludwig's Non-Linear Differential Equation for the Velocity Field

While in Section (4) Equation (4.2) we have tried to keep our equations *linear* by keeping both the Newtonian and the magnetic contributions at the same level, the strategy followed by Ludwig [13] (see also Ref. [16] [17]) has been to eliminate the magnetic term entirely, at the expense of course of ending up with a non-linear equation for the velocity field. Below we follow his formalism to pinpoint a few aspects.

As stated in the last paragraph, we can use Equation (4.1) to eliminate $A_\varphi$ from the expression of the Ampère law, that becomes

$$
\frac{\partial}{\partial\rho}\left(\frac{1}{v}\frac{\partial\phi}{\partial\rho}-\frac{v}{\rho}\right)+\frac{\partial}{\partial z}\left(\frac{1}{v}\frac{\partial\phi}{\partial z}\right)=\frac{4\pi G}{c^2}\rho_m v. \tag{6.6}
$$

This equation multiplied by *v* and subtracted from the expression of Gauß' law given earlier, eliminates the double derivatives and yields:

$$
4\pi G\rho_m\left(1-\frac{v^2}{c^2}\right)=\left(\frac{1}{\rho}+\frac{1}{v}\frac{\partial v}{\partial\rho}\right)\frac{\partial\phi_g}{\partial\rho}+\frac{1}{v}\frac{\partial v}{\partial z}\frac{\partial\phi_g}{\partial z}+v\frac{\partial}{\partial\rho}\frac{v}{\rho} \tag{6.7}
$$

a non linear first order differential equation for $v(\rho,z)$ for given $\rho(\rho,z)_m$, $\Phi_g(\rho,z)$. In the equatorial plane $z=0$ by the up-down symmetry we can drop the $\frac{\partial\phi_g}{\partial z}$; then:

$$\left(\beta^2+\rho\frac{\partial\varphi}{\partial\rho}\right)r\frac{\partial\beta}{\partial\rho}=\frac{\beta}{\rho}\left(\left(\beta^2-r\frac{\partial\varphi}{\partial\rho}\right)+\frac{4\pi G\rho_m}{c^2}\rho^2\left(1-\beta^2\right)\right);$$

$$\beta=\frac{v(\rho,0)}{c},\varphi=\frac{\phi_g}{c^2}$$

Outside the galaxy, where $\rho(\rho,0)_m=0$, the equation becomes

$$\frac{\rho}{\beta}\frac{\partial\beta}{\partial\rho}=\frac{\beta^2-\rho\frac{\partial\varphi}{\partial\rho}}{\beta^2+\rho\frac{\partial\varphi}{\partial\rho}}=\frac{\beta^2-g(\rho)}{\beta^2+g(\rho)} \tag{6.8}$$

This equation shows the key role played by the GEM magnetic field, that is now:

$$\frac{B_z}{c}=\frac{\rho\frac{\partial\varphi}{\partial\rho}-\beta^2}{\beta\rho}=\frac{g(\rho)-\beta^2}{\beta\rho}. \tag{6.9}$$

Equation (6.8) is an elegant rate equation for the velocity outside the galaxy. However, in any phenomenology, care must be taken to ensure that the GEM magnetic field employed (*vedi* Equation (6.9)) $B_z<0$ is indeed negative. A realistic example confirming this fact has already been provided in Section (3).

## 7. Rotation Velocity and Angular Momentum for the Milky Way

Our own galaxy the Milky Way is presumably the one we ought to know the best and yet it is most arduous to discuss it realistically given its rings and spiral arms that belie our assumption of axial symmetry as its structure in no way can be considered independent of the angle $\varphi$[1]. In the Weyl formalism under consideration in this paper, rings and spiral arms can occur due to instabilities generated by the motion of the interstellar medium (ISM). See, for example, Ref. [31]. Following a hollowed theoretical custom, presently we shall ignore these as of no consequence and proceed with confidence that the Einstein theory with an extended Weyl metric and a pressure-less source is applicable to it and we shall be satisfied if our description is even approximately successful for the angular momentum and rotational velocity of this massive bar like object in terms of its known diameter (about 25 kpc); thickness (about 2 kpc) and its baryonic mass; that is, use only the *visible* part of the galaxy in trying to understand it. After all, we do feel less guilty in our maneuvers in that we are not assuming that our galaxy consists of a vast (over an order of magnitude more massive) amount of *unseen* dark matter (of *unknown* origin) spread out (over a radius of 380 kpc)

[1]To say nothing of a massive black hole of mass ($4\times10^6 M_\odot$) and a Schwarzschild radius ($1.2\times10^7$ km) that exists at the center of the galaxy.

rotating with perfect *spherical symmetry* obeying *Newtonian* mechanics [32].

To begin our phenomenology, we need an input mass density $\rho_m(\rho,z)$ that describes the bulge, the disk and a co-rotating gas surrounding it, a Newtonian potential and the corresponding Newtonian (squared, normalized) velocity $g(\rho,z=0)$ generated from it and an estimate of its baryonic mass ($M$). Unfortunately, there is less than unanimity as to what this mass is: Allen's astronomical data lists $M_{galaxy}=1.4\times10^{11}M_{\odot}$ [19]; Trimble quotes $M_{galaxy}=1\times10^{11}M_{\odot}$ [33]; Nagai-Miyamoto estimate it to be about $2.567\times10^{11}M_{\odot}$ [34]; Lipovka estimate is $2.3\times10^{11}M_{\odot}$ [35]; Sofue obtains for the bulge and the disk mass $M_{b+d}=7.9\times10^{10}M_{\odot}$, however this analysis also has a DM halo mass of $2.23\times10^{11}M_{\odot}$ (within a DM halo radius $h\sim22$ kpc) [32]. It is important to note that the Sofue estimates include the DM component to the regular baryonic bulge and disk components in fitting the galaxy rotation curve at *small* distances. The total fraction of baryons from WMAP cosmic value is 17% [36], it is estimated to be 12% as the mean for a group of galaxies, whereas for our own galaxy it is only 5.9% of DM considered spread out up to 380 kpc (chosen arbitrarily as the half-distance between our and M31 galaxy nearby [32].

In view of the above uncertainties, we limited our task to the following: Assume a baryonic mass density $\rho_m(\rho,z)$ spread out only over the visible domain of our galaxy (roughly 25 kpc in diameter and 2 kpc in thickness) whose Newtonian potential provides a reasonable description of the rotation velocity including the two visible bumps in the velocity along with the expected Keplerian fall-off at larger distances. We computed using the GR formalism described in the text: the total mass $M$ (baryonic + radiation); the total angular momentum $J$ and the rotation velocity. As we have stressed, the continuity constraints in GR imply that the *magnetic* contribution that keeps the velocity up at larger distances cannot be ignored since it is related to the Newtonian term. Thus followed the simple illustrative example described in detail in Ref. [18]. We here briefly summarize the results obtained therein.

We chose a convenient analytic (& factorizable) mass distribution due to Lipovka [35] so as to facilitate our computations of the total mass, angular momentum and the Newtonian velocity vs. distance. The geo-magnetic velocity has been chosen to asymptote to a constant as discussed in the text. In units of kpc, it reads

$$V_{mag}(\rho)=\frac{160}{3.09\times10^{16}}\frac{\rho}{\rho+70}, \tag{7.10}$$

where $\rho$ is in units of kpc.

The modified velocity is

$$V_{mod}(\rho)=\frac{V_{mag}(\rho)+\sqrt{4V_{\perp}^{2}(\rho)+V_{mag}^{2}(\rho)}}{2}. \tag{7.11}$$

**Figure 1** shows the modified velocity. For the angular momentum, we obtain

$$J\simeq1.155\times10^{67}\left(\text{Joules}\cdot\text{sec}\right);\ J_{mod}\simeq1.193\times10^{67}\left(\text{Joules}\cdot\text{sec}\right). \tag{7.12}$$

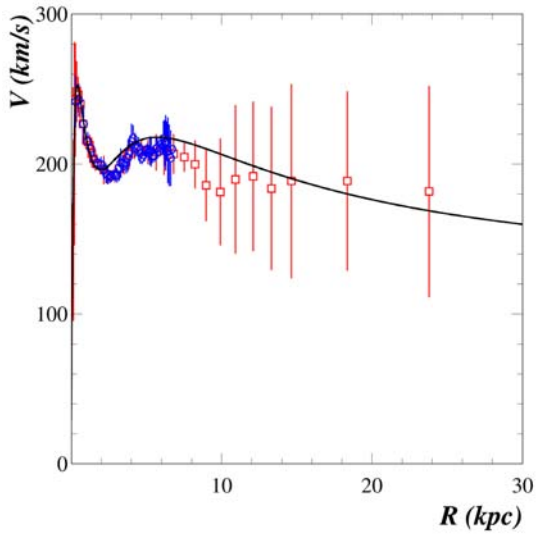


**Figure 1.** We show rotation velocity for our Milky Way using Equation (7.10).

This estimate can be compared to Trimble's estimate [33] of the angular momentum $6 \times 10^{66}$ (Joules-sec), obtained using *only the disk* part of the Milky Way.

## 8. Conclusions & Future Prospects

We first summarize results obtained previously, then describe research in progress and close with prospects for the future.

- Our work began with the Weyl class of axisymmetric metrics in GR for whom solutions to the Einstein-Weyl equations in the vacuum are known in terms of a few differential equations. Even more fortunately, for what we call the extended Weyl class that includes rotations explicitly, exact differential equations are also known.
- Unlike the Kerr metric, Weyl metric can be easily (and has been) continued within the galaxy and physically meaningful results obtained.
- Armed with exact solutions, it became possible to show how Gauß and Ampère laws emerged and under what conditions Ludwig's extended GEM theory and his non-linear rate equations for the rotation velocity field could be deduced.
- Using the century old iterative procedure in GR and further elaborated by Weinberg, we could discuss the value of the mass M (baryonic mass + that of the gravitational field) & that of the intrinsic angular momentum $J$ of a rotationally-supported galaxy. The extended Weyl metric analysis allowed us to conclude rigorously that Weyl's (vectorial) length parameter $a$ must have a finite limit to obtain a finite $J$. As the same parameter also controls the asymptotic limit of the rotation velocity, we can conclude that GR is indeed capable of obtaining a flat plateau in the rotation velocity.
- We have attempted an alternative strategy to that of Ludwig as far as the phenomenology of the rotation curves is concerned. Ludwig eliminated the

magnetic contribution to obtain his non-linear rate equation for the velocity field in terms of the input from the Newtonian potential and the mass distribution within the galaxy. Instead, we kept the Newtonian input & the magnetic input together; thus our velocity equations remained linear. This allowed us to provide a clearer physical picture: at small distances, the velocity is basically described by the Newtonian term and as it begins to fall off it is supported near the edge by essentially a constant vector potential. It also brought to focus the crucial role of Lenz's law and the left hand rule for the GEM magnetic field.

- As byproducts of our analysis, we were able to deduce a few other practical results: 1) imposition of Lenz's law implies the rigorous inequality: $\beta^2 \geq g$, the Newtonian value. A result supported by 2700 data points from 153 rotating galaxies; 2) a better estimate (≥500 km/sec.) for our Sun's escape velocity from our galaxy; 3) an easy to remember pneumonic for the asymptotic velocity $\beta^2 \approx R_s/(2R_{edge})$; 4) how Tully-Fisher law emerges from a rotating *pill-box* galaxy; 5) simple dimensional analysis implies $J \propto M^{7/4}$ if Tully-Fischer holds.

Our present focus is four-fold: A: A satisfactory GR description of the deflection of light from large galaxies & from galaxy clusters; B: To obtain a better understanding of the TF-law ($M \propto \beta^4$) and the Virginia Trimble law ($J \propto M^{1.9}$), the latter covering data that run over 50 orders of magnitude [33]; C: A comprehensive phenomenology of the rotation curves with realistic densities and more refined Newtonian inputs; D: Testing our conjecture that spiral arms in rotating galaxies such as ours are generated dynamically through non-linear effects inherent in GR.

Further let us hope for yet more brilliant advances in astrophysical observations (for example, via renewed investigations involving Hanbury-Brown-Twiss techniques) to reduce the error bars in rotation curves. Only then, it would be feasible to truly distinguish between different theoretical models.

## Acknowledgements

YS would like to thank Professor Gerson Ludwig for numerous correspondence and discussions about his pioneering work on rotationally supported galaxies. He would also like to thank members of the dipartimento di fisica e geologia di Universitá di Perugia for their hospitality & to Dr. Patrizia Cenci, Direttore di INFN, Sezione di Perugia for her continued encouragement and warm support.

## Conflicts of Interest

The authors declare no conflicts of interest regarding the publication of this paper.

## References

[1] Rubin, V.C., Thonnard, N. and Fotd Jr., W.K. (1978) *The Astrophysical Journal*,

**225**, L107. https://doi.org/10.1086/182804

[2] Peebles, P.J.E. (2017) How the Non-Baryonic Dark Matter Theory Grew.

[3] Opik, E. (1922) *The Astrophysical Journal*, **55**, 406-410. https://doi.org/10.1086/142680

[4] Tully, R.B. and Fisher, J.R. (1977) *Astronomy & Astrophysics*, **54**, 661-673.

[5] McGaugh, S., Lelli, F. and Schombert, J. (2016) *Physical Review Letters*, **117**, Article ID: 201101. https://doi.org/10.1103/PhysRevLett.117.201101

[6] Weinberg, S. (1972) Gravitation & Cosmology. John Wiley & Sons, New York.

[7] Salucci, P. (2019) *The Astronomy and Astrophysics Review*, **27**, Article No. 2. https://doi.org/10.1007/s00159-018-0113-1

[8] Balasin, H. and Grümiller, G. (2008) *International Journal of Modern Physics D*, **17**, 475-488. https://doi.org/10.1142/S0218271808012140

[9] Crosta, M.T., Gianmaria, M., Lattanzi, M. and Poggio, E. (2018) Testing Dark Matter Geometry Sustained Circular Velocities in the Milky Way with Gaia DR2.

[10] Cooperstrock, F. and Tieu, S. (2007) *International Journal of Modern Physics*, **22**, 2293.

[11] Cross, D.J. (2006) Comments on the Cooperstock-Tieu Galaxy Model.

[12] Cornejo, A.G. (2021) *International Journal of Astronomy*, **9**, 27-30.

[13] Ludwig, G. (2021) *The European Physical Journal C*, **81**, Article No. 186.

[14] Ludwig, G. (2021) *The European Physical Journal Plus*, **136**, Article No. 373.

[15] Ludwig, G. (2021) *The European Physical Journal Plus*, **136**, Article No. 465.

[16] Ludwig, G. (2022) *European Journal of Physics C*, **82**, Article No. 281.

[17] Ludwig, G. (2022) Galactic Rotation Curve without Dark Matter. Private Communication. (Unpublished)

[18] Srivastava, Y., Immirzi, G., Swain, J., Panella, O. and Pacetti, S. (2022) General Relativity versus Dark Matter for Rotating Galaxies. (Submitted for Publication)

[19] Allen, C.W. (1976) Astronomical Quantities. 3rd Edition, The Athlone Press, London.

[20] Stephani, H. (1990) General Relativity. Second Edition, Cambridge University Press, Cambridge.

[21] Thirring, H. (1918) *Physikalische Zeitschrift*, **19**, 204.

[22] Pfister, H. (2012) *General Relativity and Gravitation*, **44**, 3217-3224. https://doi.org/10.1007/s10714-012-1450-4

[23] Lense, J. and Thirring, H. (1918) *Zeitschrift für Physik*, **19**, 156-163.

[24] Ciufolini, I. and Pavlis, E.C. (2004) *Nature*, **431**, 958-960. https://doi.org/10.1038/nature03007

[25] Weyl, H. (1917) *Annals of Physics*, **54**, 117-145. https://doi.org/10.1002/andp.19173591804

[26] Weyl, H. (1918) Gravitation und Elettrizät. Sitz. Preuss. Acad. Wiss., Berlin, 465.

[27] Landau, L. and Lifshitz, E. (1965) The Classical Theory of Fields. 4th Revised English Edition, Course of Theoretical Physics, Vol. 2, Oxford University Press, Oxford.

[28] Smith, M., *et al.* (2007) *Monthly Notices of the Royal Astronomical Society*, **379**, 755-772. https://doi.org/10.1111/j.1365-2966.2007.12021.x

[29] Ruggiero, M.L. and Tartaglia, A. (2002) *Il Nuovo Cimento B*, **117**, 743.

[30] Mashoon, B. (2008) Gravitoelectromagnetism: A Brief Review.

arXiv:gr-qc/0311030v2 (2008)

[31] Frenkler, J. (2022) How the Spirals in the Milky Way's ISM Form. arXiv: 2203.08672 [astro-ph. GA]

[32] Sofue, Y. (2017) Rotation and Mass in the Milky Way and Spiral Galaxies. Oxford University Press, Oxford. https://doi.org/10.1093/pasj/psw103

[33] Trimble, V. (1984) *Comments Astrophysics*, **10**, 127-135.

[34] Miyamoto, M. and Nagai, R. (1975) *Publications of the Astronomical Society of Japan*, **27**, 533-543.

[35] Lipovka, A. (2018) *Publications of the Astronomical Society of Japan*, **70**, Article No. 86. https://doi.org/10.1093/pasj/psy082

[36] Dehnen, W. and Binney, J. (1998) *Monthly Notices of the Royal Astronomical Society*, **294**, 429-438.

Journal of Modern Physics, 2022, 13, 1474-1498
https://www.scirp.org/journal/jmp
ISSN Online: 2153-120X
ISSN Print: 2153-1196

# The Progenitor of the Big Bang and Its Connection to the Flatness and Acceleration of the Universe

**Ahmad A. Hujeirat**

IWR, Universität Heidelberg, Heidelberg, Germany
Email: AHujeirat@uni-hd.de

**How to cite this paper:** Hujeirat, A.A. (2022) The Progenitor of the Big Bang and Its Connection to the Flatness and Acceleration of the Universe. *Journal of Modern Physics*, **13**, 1474-1498.
https://doi.org/10.4236/jmp.2022.1311091

**Received:** October 17, 2022
**Accepted:** November 26, 2022
**Published:** November 29, 2022



## Abstract

It was argued that old and massive neutron stars end up as black objects that are made of purely incompressible superconducting gluon-quark superfluid matter (henceforth SuSu-objects). Based on theoretical investigations and numerical solving of the field equations with time-dependent spacetime topologies, I argue that a dense cluster of SuSu-objects at the background of flat spacetime that merged smoothly is a reliable candidate for the progenitor of the big bang. Here, we present and use a new time-dependent spacetime metric, which unifies the metrics of Minkowski, Schwarzschild, and Friedmann as well as a modified TOV-equation for modeling dynamical contractions of relativistic objects. Had the progenitor undergone an abrupt decay, a hadronizing front forms at its surface and starts propagating from outside-to-inside, thereby hadronizing its entire content and changing the topology of the embedding spacetime from a flat into a dynamically expanding curved one. For an observer located at the center of the progenitor, $\mathcal{H}_0$, the universe would be seen as isotropic and homogeneous, implying therefore that the last big bang event must have occurred in our neighborhood. For $t \gg \tau_{dyn}$ the curved spacetime re-converges into a flat one, whereas the outward-propagation topological front, which separates the enclosed curved spacetime from the exterior flat one, would appear spatially and temporally accelerating outwards. The here-presented scenario suggests possible solutions to the flatness problem, the origin of acceleration of the universe and the pronounced activities of high redshift QSOs. We anticipate that future observations by the James-Webb-Telescope to support our scenario when active QSOs with $z > 12$ would be detected.

## Keywords

General Relativity: Big Bang, Black Holes, QSOs, Neutron Stars, QCD,

Condensed Matter, Superfluidity

## 1. Introduction

Data from supernovae statistics predict that at least 1% of star populations in star-forming clouds should be neutron stars (NSs). Yet this rate is expected to be even higher in the early universe when the first generation of stars was formed, roughly 500 Myr after the big bang (henceforth BB). These should have been massive, extraordinary luminous and therefore short-living, which subsequently collapsed to form BHs or massive NSs [1] [2]. However, their relatively large sizes, masses and energy contents would give rise to fragmentation, preferably forming massive NSs rather than BHs. This may reasonably explain why the mass-function of BHs exhibits the mass-gap: $[2.5M_\odot \le \mathcal{M} \le 5.5M_\odot]$, where stellar BHs have not been detected.

Indeed, for the currently measured average density and dimensions, we expect the universe to inhibit $10^{20}$ NSs [3] [4]. The actual number of NSs may turn out to be much larger, as the universe prior to the BB might have been populated with old objects and inactive galaxies. This is in line with recent observations that reveal the existence of certain stellar components and QSOs formed earlier than the redshift $z \ge 10$ (see [2] and the references therein), *i.e.* within only several hundred million years after the BB. Also, formation of the high redshift galaxy GN-z11 within 600 Myr after the BB and the possibility that it may host a SMBH cannot be explained by the current evolutionary scenarios [5] [6]. Therefore, NSs may significantly affect the dynamics of the universe on time scales longer than or even comparable to the age of the universe (henceforth $\tau_{14}$.)

On $\tau \ge \tau_{14}$, NSs have ample time to conglomerate into clusters and subsequently merge to form progenitors to numerous BB-events that take off sequentially and in parallel.

**But what is the nature of NS-cores?** Most theoretical and numerical studies of NS-interiors predict the central density to be larger than the nuclear density, $\rho_0$. Due to the vanishing thermal energy production inside the core, the average gradient of the temperature throughout the NS should be positive, and therefore the core is practically a "freezer" of zero-temperature. Under these conditions, supranuclear dense matter has little choice, but to be superfluid. These arguments are in line with well-observed glitch phenomena in pulsars (see [7] [8] [9] [10] for further details).

Superconductivity ensures that magnetic fields are expelled from the zero-temperature core into the boundary layer between the core and the overlaying compressible and dissipative normal matter. Based on our previous studies (e.g. [10]), the spacetime embedding the SuSu-core should be flat, whereas the overlaying normal matter is embedded in a curved spacetime (**Figure 1**).

In fact, the over- and under-shooting that have been observed to associate the glitching events of the Vela pulsar in 2016 provide further evidence for the

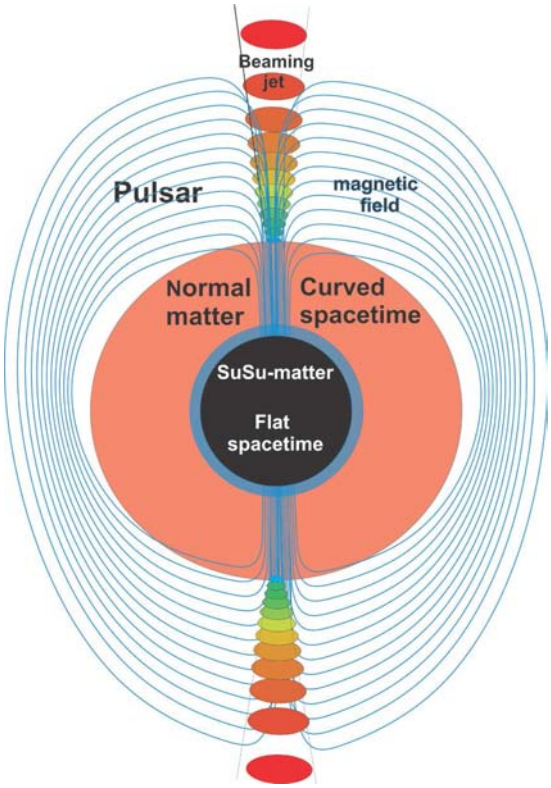


**Figure 1.** A pulsars with an embryonic quantum core and different spacetime topologies.

conductivity and superfluidity of the cores in massive NSs [11] [12]. The overall configuration is strikingly similar to the tachocline between the convection zone of the sun and the underlying rigid body rotating core, where dynamo action is considered to be operating.

Demanding the core's matter to be purely incompressible is a very strong requirement with far-reaching consequences in astrophysics and cosmology. To clarify the point, a fluid is said to be incompressible, if the density-gradient vanishes everywhere in the domain, *i.e.* $\nabla\mathcal{E}=0$. In terrestrial incompressible fluids, the pressure ceases to describe the thermodynamical state of matter locally, but it turns into a mathematical term only, called the Lagrangian multiplier, which affects the dynamical behavior of the fluid globally, irrespective of causality.

In stars, incompressibility is a requirement that is fulfilled through the imposed regularity condition at the center of astrophysical objects. In the case of NSs, the pressure gradient $\nabla P$ is generally balanced by the spatial variation of the curvature $\nabla_\mu g^{\mu\nu}$, which is dominated by $\nabla_\mu g^{\mu\nu}\approx \Delta g_{tt}/\Delta r$. On length scales comparable to the average separation between two arbitrary nucleons $\Delta r_{bb}$, the relative spatial variation of $\left|g_{\mu\nu}\right|$ is of order $10^{-19}$ [13], and therefore too weak compared to the governing nuclear forces.

On the other hand, the cores of old and massive NSs are made of zero-temperature supranuclear dense matter. Under these conditions, it was conjectured that the matter must be made of an incompressible superconducting gluon-

quark superfluid [14]. While superconductivity and superfluidity are direct consequences of zero-temperature dense matter even under terrestrial conditions, the incompressibility of gluon-quark matter would remain a hypothesis that may not be verified under normal conditions. However, there is a reasonable argument in favor of the incompressibility of gluon-quark matter at zero-temperature: Given that gluon-quark-plasmas inside hadrons are hidden from the outside world, this may indicate that the energy states of QGP inside hadrons are incompatible with the surrounding particle-free vacuum structure [15] [16]. At zero-temperature however, a QGP is expected to undergo a phase transition into QG-condensate, where QG settles down into the lowest possible quantum energy state predicted to be compatible with that of the surrounding particle-free vacuum. In this case, putting a certain number of QG-condensates together, the vacuum would share the same energy states. Here, the QG-condensates become transparent to each other, and so they merge to form a parent QG-condensate, whose size is the linear addition of the individuals.

As the spacetime embedding vacuum is flat, then the spacetime embedding the parent zero-temperature QG-condensate should be flat too, which is equivalent to requiring the QG-cloud to be macroscopically incompressible. In fact, recent results from the Relativistic Heavy Ion Collider (RHIC) confirm that the quark-gluon-plasmas emerging from smashed nuclei behave nearly as perfect liquids [17] [18], though the physical conditions governing the QGP here are totally different from those inside the cores of massive NSs.

Based thereon, the scenario here may be extended to suggest an alternative model for BB without invoking inflation to solve the horizon and flatness problems, as well as prohibit the progenitor from collapsing into a hypermassive BH (see [19] [20] [21] [22] for a review). Using recent WIMP observations, the total mass content of normal matter in the universe can be calculated and, when divided by the universal maximum energy-density $\rho_{cr}^{uni}$ ($\approx 3\,\rho_0$ see [14] for further details), then a radius of several AUs may be obtained. Prior to the BB-explosion, the progenitor, which was entirely made of incompressible SuSu-matter, was levitating freely in a flat spacetime.

Any model of the BB should still fulfill the classical conditions of isotropy and homogeneity [23]. However, according to our scenario, the progenitor must have a finite measurable size and a certain location in spacetime. These conditions may safely be met for observers located at the center of the progenitor, which implies that the BB of our universe must have occurred in our close neighborhood. Of course, this would violate the cosmological principle grossly, but the model should be taken seriously as long as its implications agree with observations.

## 2. Theory of the Time-Dependent Spacetime Topology of the Fireball

Our model is based on the hypothesis that the spacetime embedding incompressible SuSu-matter is flat, and that the progenitor of the BB is a hypermassive

DEO that formed from the merger of trillions of stellar mass DEOs on time scales comparable to or longer than the age of the universe.

Hence, $t \le 0$ relative to $\mathcal{H}_0$ the spacetime both inside and outside the progenitor was Minkowski flat, *i.e.* $\mathrm{d}s^2_{Mink} = \eta_{\mu\nu}\mathrm{d}x^\mu \mathrm{d}x^\nu$. However, at $t = 0^+$, the confining force at the surface of the progenitor suffered an irreversible destructive decay, which triggered a hadronization front that propagated from outside-to-inside, thereby converting the rings of SuSu-matter into a dissipative and compressible matter successively, which is dubbed normal matter. This matter interacts with the embedding spacetime and dictates its curvature. In the stationary case, Birkhoff theorem states that the spacetime surrounding the newly formed rings of normal matter should be of the Schwarzschild-type metric, $\mathrm{d}s^2_{Sch} = g_{\mu\nu}\mathrm{d}x^\mu \mathrm{d}x^\nu$.

If the metric is time-dependent, then the transitions from $\mathrm{d}s^2_{Mink}$ into $\mathrm{d}s^2_{Sch}$ or even into the Friedmann-Robertson-Wakker metric (FRW), $\mathrm{d}s^2_{FRW}$, and vice versa, should be possible, depending on the amount and type of the embedded matter .

Let $\mathrm{d}s^2$ be a metric, which has the following form:

$$\mathrm{d}s^2 = g_{\mu\nu}\mathrm{d}x^\mu \mathrm{d}x^\nu = g_{00}\mathrm{d}t^2 + g_{11}\mathrm{d}\bar{r}^2 + g_{22}\mathrm{d}\theta^2 + g_{33}\mathrm{d}\varphi^2 \tag{1}$$

where

$$\begin{aligned} &g_{00} = c^2\mathrm{e}^{2\mathcal{V}(r,t)},\ \ g_{11} = -\mathrm{e}^{2\lambda(r,t)} \\ &g_{22} = -\mathrm{e}^{2\mathcal{C}(t)}r^2,\ \ g_{33} = -\mathrm{e}^{2\mathcal{C}(t)}r^2\sin^2\theta \end{aligned} \tag{2}$$

Here $\mathcal{V}$ and $\lambda$ are functions of the comoving radius $\bar{r}(r,t) = r\mathrm{e}^{\mathcal{C}}$, and $\mathcal{C}(t)$ is a function of time only. All physical and geometrical events are measured with respect to $\mathcal{H}_0$ located at $r = 0$.

When contracting the Riemann tensor and calculating the Ricci tensor (see [23] for further details):

$$R_{\mu\nu} = \Gamma^\alpha_{\mu\alpha,\nu} - \Gamma^\alpha_{\mu\nu,\alpha} + \Gamma^\alpha_{\mu\beta}\Gamma^\beta_{\alpha\nu} - \Gamma^\alpha_{\mu\nu}\Gamma^\beta_{\alpha\beta}, \tag{3}$$

using the Christoffel symbol:

$$\Gamma^\lambda_{\mu\nu} = \frac{1}{2}g^{\lambda\kappa}\left\{g_{\kappa\nu,\mu} + g_{\kappa\mu,\nu} - g_{\mu\nu,\kappa}\right\}, \tag{4}$$

we obtain the following Ricci components:

$$\begin{aligned} R_{00} &= \ddot{\lambda} + \dot{\lambda}^2 - \dot{\mathcal{V}}\dot{\lambda} + 2\ddot{\mathcal{C}} + 2\dot{\mathcal{C}}^2 - 2\mathcal{V}'/r + \left(-\mathcal{V}'' + \mathcal{V}'\lambda' - (\mathcal{V}')^2 - 2\mathcal{V}'/r\right)\mathrm{e}^{2(\mathcal{V}-\lambda)} \\ R_{11} &= \left(-\ddot{\lambda} - \dot{\lambda}^2 + \dot{\mathcal{V}}\dot{\lambda} - 2\dot{\lambda}\dot{\mathcal{C}}\right)\mathrm{e}^{2(\lambda-\mathcal{V})} + \mathcal{V}'' + (\mathcal{V}')^2 - \mathcal{V}'\lambda' - 2\lambda'/r \\ R_{22} &= -\left\{\ddot{\mathcal{C}} + \dot{\mathcal{C}}\dot{\lambda} + 2\dot{\mathcal{C}}^2 - \dot{\mathcal{V}}\dot{\mathcal{C}}\right\}r^2\mathrm{e}^{2(\mathcal{C}-\mathcal{V})} + \left(1 + r\mathcal{V}' - r\lambda'\right)\mathrm{e}^{2(\mathcal{C}-\lambda)} - 1 \\ R_{33} &= -r^2\sin^2\theta\left[\ddot{\mathcal{C}} + 2\dot{\mathcal{C}}^2 - \dot{\mathcal{V}}\dot{\mathcal{C}} + \dot{\mathcal{C}}\dot{\lambda}\right]\mathrm{e}^{2(\mathcal{C}-\mathcal{V})} + \sin^2\theta\left[1\left(\ + r\mathcal{V}' - r\lambda'\right)\mathrm{e}^{2(\mathcal{C}-\lambda)} - 1\right] \end{aligned} \tag{5}$$

$\dot{\square}, \square'$ denote the time and spatial-derivatives of the variables, respectively.

The field equations may be re-arranged into the convenient form:

$$\begin{aligned} &R^{(t)}_{00} + R^{(s)}_{00}\mathrm{e}^{2(\mathcal{V}-\lambda)} = RHS_{00} \\ &R^{(t)}_{11}\mathrm{e}^{2(\lambda-\mathcal{V})} + R^{(s)}_{11} = RHS_{11} \\ &R^{(t)}_{22}r^2\mathrm{e}^{2(C-\mathcal{V})} + R^{(s)}_{22}\mathrm{e}^{2(C-\lambda)} - 1 = RHS_{22} \end{aligned} \tag{6}$$

where

$$\begin{aligned}
R_{00}^{(t)} &= \ddot{\lambda} + \dot{\lambda}^2 - \dot{\mathcal{V}}\dot{\lambda} + 2\ddot{\mathcal{C}} + 2\dot{\mathcal{C}}^2 - 2\dot{\mathcal{V}}/r \\
R_{11}^{(t)} &= -\ddot{\lambda} - \dot{\lambda}^2 + \dot{\mathcal{V}}\dot{\lambda} - 2\dot{\mathcal{C}}\dot{\lambda} \\
R_{22}^{(t)} &= -\left(\ddot{\mathcal{C}} + 2\dot{\mathcal{C}}^2 - \dot{\mathcal{C}}\dot{\mathcal{V}} + \dot{\mathcal{C}}\dot{\lambda}\right) \\
R_{00}^{(s)} &= -\mathcal{V}'' + \mathcal{V}'\lambda' - \left(\mathcal{V}'\right)^2 - 2\mathcal{V}'/r \\
R_{11}^{(s)} &= \mathcal{V}'' + \left(\mathcal{V}'\right)^2 - \mathcal{V}'\lambda' - 2\lambda'/r \\
R_{22}^{(s)} &= 1 + r\mathcal{V}' - r\lambda'
\end{aligned} \tag{7}$$

To make the problem tractable, the field equations:

$$\mathcal{R}_{\mu\nu} - \frac{1}{2} g_{\mu\nu}\mathcal{R} + \Lambda g_{\mu\nu} = -\kappa \mathcal{T}_{\mu\nu}, \tag{8}$$

may be re-written in the following equivalent form:

$$\mathcal{R}_{\mu\nu} = -\kappa\left(\mathcal{T}_{\mu\nu} - \frac{T}{2} g_{\mu\nu}\right) + \Lambda g_{\mu\nu} = RHS_{\mu\nu}, \tag{9}$$

where $\mathcal{T} = \mathcal{T}_{\mu}^{\mu}$, $\mathcal{T}_{\mu\nu}$ and $\Lambda$ correspond to the stress-energy tensor and the cosmological constant, respectively (see [13] [23] for further details).

Expanding the tensor $RHS_{\mu\nu}$ we obtain:

$$\begin{aligned}
RHS_{\mu\nu} &= -\kappa\left(T_{\mu\nu} - \frac{T}{2} g_{\mu\nu}\right) + \Lambda g_{\mu\nu} \\
&= -\kappa g_{\mu\nu}\left[\left(\rho + p\right)u_{\mu}u^{\nu} - \frac{1}{2}\left(\rho - p\right)\right] + \Lambda g_{\mu\nu} \\
&= \left\{-\kappa\left[\left(\rho + p\right)u_{\mu}u^{\nu} - \frac{1}{2}\left(\rho - p\right)\right] + \Lambda\right\} g_{\mu\nu}
\end{aligned} \tag{10}$$

The diagonal components have the following forms:

$$\begin{aligned}
RHS_{00} &= \left\{-\kappa\left[\left(\rho + p\right)\Gamma^2 g_{00} - \frac{1}{2}\left(\rho - p\right)\right] + \Lambda\right\} g_{00} = \overline{RHS}_{00} g_{00} \\
RHS_{11} &= \left\{-\kappa\left[\left(\rho + p\right)\Gamma^2 V^2 g_{11} - \frac{1}{2}\left(\rho - p\right)\right] + \Lambda\right\} g_{11} = \overline{RHS}_{11} g_{11} \\
RHS_{22} &= \left\{\frac{\kappa}{2}\left(\rho - p\right) + \Lambda\right\} g_{22} = \overline{RHS}_{22} g_{22}
\end{aligned} \tag{11}$$

Here $\Gamma = 1/\sqrt{g_{00} + g_{11}V^2}$ and $V$ are the Lorenz factor and the transport velocity as measured by $\mathcal{O}_0$, respectively.

The above set of equations may be re-written in a more convenient form:

$$\begin{aligned}
R_{00}^{(t)}\mathrm{e}^{-2\mathcal{V}} + R_{00}^{(s)}\mathrm{e}^{-2\lambda} &= \overline{RHS}_{00} \\
R_{11}^{(t)}\mathrm{e}^{-2\mathcal{V}} + R_{11}^{(s)}\mathrm{e}^{-2\lambda} &= -\overline{RHS}_{11} \\
R_{22}^{(t)}\mathrm{e}^{-2\mathcal{V}} + R_{22}^{(s)} r^2 \mathrm{e}^{-2\lambda} - \mathrm{e}^{-2\mathcal{C}} r^2 &= -\overline{RHS}_{22}
\end{aligned} \tag{12}$$

Subtracting the second equation from the first in (12), and dividing by 2, yields:

$$\frac{1}{2}\left(R_{00}^{(t)} + R_{11}^{(t)}\right)\mathrm{e}^{-2\mathcal{V}} - \frac{\mathcal{V}' + \lambda'}{r}\mathrm{e}^{-2\lambda} = -\frac{1}{2}\kappa\left[\left(\mathcal{E} + p\right)\Gamma^2\left(g_{00} - g_{11}V^2\right)\right]. \tag{13}$$

Now, adding the last equation to the third, we obtain:

$$\begin{aligned}&\left[\frac{1}{2}\left(R_{00}^{(t)}+R_{11}^{(t)}\right)+R_{22}^{(t)}\right]\mathrm{e}^{-2\mathcal{V}}-\frac{1}{r^2}\frac{\mathrm{d}}{\mathrm{d}r}\left(r\left(\mathrm{e}^{-2\mathcal{C}}-\mathrm{e}^{-2\lambda}\right)\right)\\&=-\frac{1}{2}\kappa\left[\left(\mathcal{E}+p\right)\Gamma^2\left(g_{00}-g_{11}V^2\right)+\left(\rho-p\right)\right]-\Lambda,\end{aligned}\tag{14}$$

where,

$$\begin{aligned}&\frac{1}{2}\left(R_{00}^{(t)}+R_{11}^{(t)}\right)=\ddot{\mathcal{C}}+\dot{\mathcal{C}}^2-\dot{\lambda}\dot{\mathcal{C}}-\frac{\dot{\mathcal{V}}}{r}\\&\frac{1}{2}\left(R_{00}^{(s)}+R_{11}^{(s)}\right)=-\frac{\mathcal{V}'+\lambda'}{r}\\&\frac{1}{2}\left(R_{00}^{(t)}+R_{11}^{(t)}\right)+R_{22}^{(t)}=-\dot{\mathcal{C}}^2+\left(\dot{\mathcal{V}}-2\dot{\lambda}\right)\dot{\mathcal{C}}-\frac{\dot{\mathcal{V}}}{r}\\&\frac{1}{2}\left(R_{00}^{(s)}+R_{11}^{(s)}\right)+R_{22}^{(s)}=-\frac{1}{r^2}\frac{\mathrm{d}}{\mathrm{d}r}\left(r\left(\mathrm{e}^{-2\mathcal{C}}-\mathrm{e}^{-2\lambda}\right)\right)\end{aligned}\tag{15}$$

As the last equation in (14) must be applicable both to stationary and time-dependent cases, then $\mathrm{e}^{-2\lambda}=\mathrm{e}^{-2\mathcal{C}}\times f\left(r,t\right)$. However, in the stationary case, Birkhoff theorem states that outside the object, $f\left(r,t\right)\sim 1/\left(1-\mathcal{X}\left(r\right)\right)$. Therefore, without loss of generality, we may set the metric components to be of the forms:

$$g_{11}=-\mathrm{e}^{2\lambda}=\frac{\mathrm{e}^{2C}}{1-\mathcal{X}_b}\quad\text{and}\quad\mathrm{e}^{2C}=R^2,\tag{16}$$

where $R=R\left(t\right)$ and $\mathcal{X}_b=\mathcal{X}_b\left(r,t\right)$. The subscript "$b$" corresponds to the function in the comoving frame.

Further inspection of the equations (see Equation (20)), shows that, for a slowly varying $\mathcal{V}$ and $V\ll c$, we obtain:

$$\frac{1}{r^2R^2}\frac{\mathrm{d}}{\mathrm{d}r}\left(r\mathcal{X}_b\right)\sim\kappa\mathcal{E},$$

whose integration yields $\mathcal{X}\sim m/r$, where $m=4\pi\int\mathcal{E}r^2\mathrm{d}r$ is the enclosed mass. It turns out that setting $\mathcal{X}_b\left(r,t\right)=m_b\left(r,t\right)/r$ provides consistent solutions for almost all reasonable metrics. In this case, the derivatives of $\mathcal{V}$ read as follows:

$$\dot{\lambda}=\begin{cases}\dot{\mathcal{C}}; & \text{if } \dot{\mathcal{X}}_b=0,\\ \dot{\mathcal{C}}+\dfrac{1}{2}\dfrac{\dot{\mathcal{X}}_b}{1-\mathcal{X}_b} & \\ =\left(1+\mathcal{Z}_b\right)\dot{\mathcal{C}}+\dot{F}; & \text{otherwise}\end{cases}\tag{17}$$

where $\dot{\mathcal{C}}=\dot{R}/R$, $\mathcal{Z}_b=\mathcal{X}_b/\left(1-\mathcal{X}_b\right)$ and $\dot{F}$ is a material flux function of the form:

$$\dot{F}=\frac{1}{2}\frac{\alpha_{bb}}{r}\frac{\dot{m}_b^{nor}}{1-\mathcal{X}_b}.\tag{18}$$

Hence the set of field equations that describes the time-evolution of the space-time topology reads:

$$\left[\frac{\ddot{R}}{R}-\left(1+\mathcal{Z}_b\right)\left(\frac{\dot{R}}{R}\right)^2-\dot{F}\left(\frac{\dot{R}}{R}\right)\right]\mathrm{e}^{-2\mathcal{V}}+\frac{1}{2r}\left[\frac{\partial}{\partial t}\left(\mathrm{e}^{-2\mathcal{V}}\right)+\frac{\mathrm{e}^{-2\lambda}}{\mathrm{e}^{-2\mathcal{V}}}\frac{\partial}{\partial r}\left(\mathrm{e}^{-2\mathcal{V}}\right)+\frac{\partial}{\partial r}\mathrm{e}^{-2\lambda}\right] \tag{19}$$
$$=-\frac{1}{2}\kappa\left(\mathcal{E}+p\right)\left[\Gamma^2\left(g_{00}-g_{11}V^2\right)\right]$$

$$\frac{1}{2}\left(\frac{1}{r}-Y\right)\frac{\partial}{\partial t}\left(\mathrm{e}^{-2\mathcal{V}}\right)-\left[\left(3+2\mathcal{Z}_b\right)\left(\frac{\dot{R}}{R}\right)^2+2\dot{F}\left(\frac{\dot{R}}{R}\right)\right]\mathrm{e}^{-2\mathcal{V}} \tag{20}$$
$$=-\kappa\left(\mathcal{E}+p\right)V^2\mathrm{e}^{-2(\mathcal{V}-\lambda)}+\frac{1}{r^2R^2}\frac{\mathrm{d}}{\mathrm{d}r}\left(r\mathcal{X}_b\right)-\kappa\mathcal{E}.$$

In addition, the conservation of energy and momentum of matter is taken into account by requiring that the stress-energy tensor must be divergence-free, *i.e.* $\nabla_\mu T^{\mu\nu}=0$. This yields the following set of GR hydrodynamical equations:

$$\frac{1}{\sqrt{-g}}\frac{\partial}{\partial t}\left(\sqrt{-g}\mathcal{D}\right)+\frac{1}{R}\frac{1}{\sqrt{-g}}\frac{\partial}{\partial r}\sqrt{-g}\left(\mathcal{D}V\right)=0 \tag{21}$$

$$\frac{1}{\sqrt{-g}}\frac{\partial}{\partial t}\left(\sqrt{-g}\mathcal{M}^r\right)+\frac{1}{R}\frac{1}{\sqrt{-g}}\frac{\partial}{\partial r}\left(\sqrt{-g}\mathcal{M}^rV\right) \tag{22}$$
$$=-\frac{1}{R}\frac{\partial P}{\partial r}+\frac{\mathcal{M}^t}{2R}\left(g_{tt,r}+V^2g_{rr,r}\right),$$

where $\sqrt{-g}=r^2R^3\sin(\theta)/\sqrt{GW}$, $\mathcal{D}$, and $V$ are the determinant of the metric, the relativistic energy-density, and the transport velocity, respectively. The four-momenta is defined as $\mathcal{M}^\sigma=\mathcal{D}hu^\sigma$, where $h$ stands for enthalpy and $u^\sigma$ for the four-velocity; $\sigma=\{t,r,\theta,\varphi\}$. Here, the Lorentz factor reads:

$$u^t=\frac{1}{g_{tt}+V^2g_{rr}}. \tag{23}$$

The continuity equation may be re-written in the following compact form:

$$\frac{\partial}{\partial t}\left(\bar{\mathcal{D}}_b\right)+\frac{1}{R}\frac{1}{r^2}\frac{\partial}{\partial r}\left(r^2\bar{\mathcal{D}}_bV\right)=0, \tag{24}$$

where $\bar{\mathcal{D}}_b=\mathcal{D}_b/\sqrt{GW}$ and $\mathcal{D}_b=\mathcal{D}R^3$.

To close the system, an equation of state (EOS) should be included, e.g.

$$P=P\left(\mathcal{E}\right)=P\left(\mathcal{D}/u^t\right).$$

## 2.1. Special Cases

In the above-mentioned derivations both the metric coefficients $g_{tt}$ and $g_{rr}$ are spatially and temporally varying functions. The simplest special case is Minkowski spacetime, where $g_{tt}\to 1$ and $g_{tt}\to -1$. The Schwarzschild metric may be recovered by relaxing the time-dependency, setting $R=1$, $V=0$ and $\mathcal{X}=\frac{2G}{c^2}\frac{m(r)}{r}$, where $m(r)$ denotes the enclosed mass of normal matter. The FRW metric is recovered by setting both the energy density and the metric coefficient $g_{tt}$ to constants.

However, it is tempting to see how the above set of equations yields the TOV equation in the case of an object in hydrostatic equilibrium, embedded in a

Schwarzschild spacetime as well as the Friedmann equations in the case of an expanding universe.

### 2.1.1. The Modified TOV Equation for Modeling Slowly Contracting Relativistic Objects

Assume we are given a non-rotating and demagnetized relativistic object of normal matter with a constant energy-density. Following Birkhoff theorem, the surrounding spacetime topology may be described by the Schwarzschild metric. Depending on the EOS, the object may undergo a dynamical collapse or contract slowly, where in both cases the matter is transported from outside-to-inside with the transport velocity $V \ll c$. Similar to other stationary observers, our preferred central observer, $O_0$ may measure the contraction of the object with $R(t)=1$. In this case, Equation (19) reduces to:

$$\begin{aligned}&\frac{1}{2r}\frac{\partial}{\partial t}\left(\mathrm{e}^{-2\nu}\right)+\frac{\mathrm{e}^{-2\lambda}}{\mathrm{e}^{-2\nu}}\frac{\partial}{\partial r}\left(\mathrm{e}^{-2\nu}\right)+\frac{\partial}{\partial r}\mathrm{e}^{-2\lambda}\\&=-\frac{1}{2}\kappa(\mathcal{E}+p)\left[\Gamma^2\left(g_{00}-V^2 g_{11}\right)\right]=-\frac{1}{2\kappa}(\mathcal{E}+p)\bar{\bar{\Gamma}},\end{aligned}\tag{25}$$

where $\bar{\bar{\Gamma}}$ is the modified Lorentz factor. Inserting:

$$\frac{\partial \mathrm{e}^{-2\lambda}}{\partial r}=\frac{\mathcal{X}'}{R^2}=\frac{\alpha_{bb}}{R}\left(\frac{m_b}{r}\right)'=\frac{\alpha_{bb}}{R}\left(\frac{m_b'}{r}-\frac{m_b}{r^2}\right),$$

where $\alpha_{bb}=\dfrac{2G}{c^2}$ and re-arranging terms, we end up with the following equation:

$$\mathrm{e}^{-2\lambda}\frac{\partial \mathrm{e}^{-2\nu}}{\partial t}+\frac{\partial \mathcal{V}}{\partial r}=-3\frac{\alpha_{bb}}{R}\left(\bar{\bar{\Gamma}}^2+\right)\frac{\mathcal{E}_b r}{1-\mathcal{X}_b}-\frac{\alpha_{bb}}{R}\frac{m_b+3r^3P_b\bar{\bar{\Gamma}}^2}{r^2\left(1-\mathcal{X}_b\right)}.\tag{26}$$

Since a small mass perturbation would hardly affect the global topology of spacetime on time scales much shorter than the dynamical time scale, the time-derivative of $\mathcal{V}$ may be replaced by a numerical smoother, which enables the $\mathcal{V}$-integration throughout the whole domain, where the conditions at the outer boundary are used.

Note that when the transport velocity vanishes, the modified Lorentz factor reduces to one, *i.e.*, $\bar{\bar{\Gamma}}^2=1$, and the classical TOV equation:

$$\frac{\partial \mathcal{V}}{\partial r}=-\frac{\alpha_{bb}}{R}\frac{m_b+3r^3P_b}{r^2\left(1-\mathcal{X}_b\right)},\tag{27}$$

is then recovered. The effect of the first term on the RHS of Equation (26) is to steepen the gradient of the energy density in the vicinity of the surface, which yields smaller radii of NSs than usually obtained using the classical TOV equation.

### 2.1.2. Friedmann Universe

The Friedmann universe may be recovered by setting $V=P=0$, and $\mathcal{V}=\mathcal{E}=\text{constants}$. In this case, the components of the material tensor on the RHS of Equation (11) reduce to:

$$\begin{aligned}
\overline{RHS}_{00} &= -\frac{\kappa}{2}(\rho+3p)+\Lambda \overset{dust}{\rightarrow} -\frac{\kappa}{2}\rho+\Lambda \\
\overline{RHS}_{11} &= \frac{\kappa}{2}(\rho-p)+\Lambda \rightarrow \frac{\kappa}{2}\rho+\Lambda \\
\overline{RHS}_{22} &= \frac{\kappa}{2}(\rho-p)+\Lambda \rightarrow \frac{\kappa}{2}\rho+\Lambda
\end{aligned} \tag{28}$$

Setting $\dot{\mathcal{X}}=\mathcal{X}'=0$ and inserting $\mathcal{X}(r)=kr^2$ on the LHS of the Equation (13), it can be easily verified that the different terms reduce to the following expressions:

$$\begin{aligned}
&\frac{1}{2}\left(R_{00}^{(t)}+R_{11}^{(t)}\right)\mathrm{e}^{-2\mathcal{V}} \rightarrow \frac{\ddot{R}}{R}-\left(\frac{\dot{R}}{R}\right)^2 \\
&-\left(\frac{\mathcal{V}'+\lambda'}{r}\right)\mathrm{e}^{-2\lambda} \rightarrow -\frac{k}{R^2} \\
&-\frac{1}{2}\kappa(\mathcal{E}+p)\left[1+2V^2\frac{W}{G}\right] \rightarrow -\frac{1}{2}\kappa\mathcal{E}
\end{aligned} \tag{29}$$

Adding these terms together yields the first Friedmann equation:

$$\frac{\ddot{R}}{R}-\left(\frac{\dot{R}}{R}\right)^2-\frac{k}{R^2}=-\frac{1}{2}\kappa\mathcal{E}. \tag{30}$$

Similarly, Equation (14) reduces to:

$$\begin{aligned}
&\left[\frac{1}{2}\left(R_{00}^{(t)}+R_{11}^{(t)}\right)+R_{22}^{(t)}\right]\mathrm{e}^{-2\mathcal{V}} \rightarrow -3\left(\frac{\dot{R}}{R}\right)^2 \\
&-\frac{1}{r^2}\frac{\mathrm{d}}{\mathrm{d}r}\left(r\left(\mathrm{e}^{-2\mathcal{C}}-\mathrm{e}^{-2\lambda}\right)\right) \rightarrow -3\frac{k}{R^2} \\
&-\frac{1}{2}\kappa\left[(\mathcal{E}+p)\Gamma^2\left(g_{00}-g_{11}V^2\right)+(\rho-p)\right]+2\Lambda \rightarrow -(\kappa\mathcal{E}+\Lambda)
\end{aligned} \tag{31}$$

Hence, adding these terms together, we obtain:

$$\left(\frac{\dot{R}}{R}\right)^2=\frac{\kappa}{3}\mathcal{E}+\frac{\Lambda}{3}-\frac{k}{R^2}. \tag{32}$$

Substituting $\left(\frac{\dot{R}}{R}\right)^2$ into Equation (30), we recover the classical form of Friedmann's first equation:

$$\frac{\ddot{R}}{R}=-\frac{1}{2}\frac{\kappa}{3}\mathcal{E}+\frac{\Lambda}{3}. \tag{33}$$

In terms of the classical cosmological parameters $\Omega_i$, the dimensionless scale parameter $a=R/R_0$, and the dimensionless time-variable $\tau=H_0(t-t_0)$, Equation (30) may be transformed into the following form:

$$\left(\frac{\mathrm{d}a}{\mathrm{d}\tau}\right)^2=\frac{\Omega_{m,0}}{a}+\frac{\Omega_{r,0}}{a^2}+\Omega_{k,0}+\Omega_{\Lambda,0}a^2. \tag{34}$$

The subscript "0" denotes the value of the corresponding parameter in the present time (see [23] for further details). Depending on the specific values of $\Omega_{i,0}$, the dimensionless scale parameter *a* may converge or diverge as the sys-

tem evolves with time.

## 3. The Numerical Approach

For solving the set of field equations a new numerical solver has been developed. The solver is unconditionally stable, as it is based on implicit time-integration using preconditioning techniques of Krylov sub-space iterative methods. In the finite space, the equations are discretized using finite volume formulation to ensure mass and energy conservation. In Figure 2, a schematic description of the solution method is depicted (for further details on the projection method and preconditioning techniques see [24] [25]):

## 4. Time Evolution of the Fireball: Numerical Investigation

The form of $g_{rr}$ in both stationary and time-dependent cases, has the following form:

$$g_{rr}=\frac{1}{1-\mathcal{X}_b} \text{ where } \mathcal{X}(r,t)_b=\frac{2G}{c^2}R^2\left(\frac{m(r,t)}{r}\right)=\alpha_{bb}\left(\frac{m_b(r,t)}{rR}\right) \tag{35}$$

$\mathcal{X}(r,t)$ is practically the communicator that tells spacetime how to curve. Let us address the following possibilities for $\mathcal{X}$:

$$\mathcal{X}(r,t)\sim\begin{cases} r^2: \text{Schwarzschild} \\ \quad \text{TOM}: \text{incompressible normal fluids} \\ r^{\alpha}: \text{Schwarzschild} \\ \quad \text{Normal compressible}, \alpha<2 \\ r^2: \text{Friedmann} \\ \quad \text{dust} \\ 0: \text{Flat} \\ \quad \text{Vacuum}(\text{particle-free spacetime}) \\ 0: \text{Flat} \\ \quad \text{Incompressible SuSu-matter} \end{cases} \tag{36}$$

where TOM stands for the "Type Of Matter".

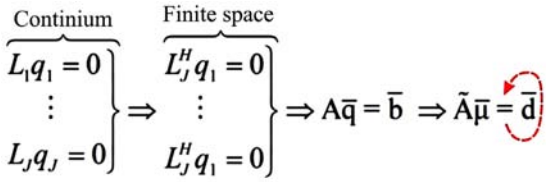


Figure 2. The numerical procedure: the set of analytical equations is transformed into the finite space, $\mathcal{H}$, using the finite volume discretization strategy. The set of equations in $\mathcal{H}$ in operator form read: $L^Hq=b^H$, which may be re-written in matrix form as $Aq=b$, where A is the corresponding matrix of coefficients. The matrix equation is then simplified and replaced by $\tilde{A}\mu=d$, where $\tilde{A}$ is a preconditioner that shares the eigenvalues of $A$, $\bar{\mu}$ is a correction vector that entails deviations from the original solution and $d$ is the defect. The iteration procedure should continue until the maximum norm of $\bar{\mu}$ has dropped below the tolerance value.

It should be noted here that in the case of incompressible normal matter with $\mathcal{E}=\mathcal{O}(\mathcal{E}_0)$, the field equations lose their predictability power and would enforce the pressure to become ultrabaric and acausal.

The dependence on time endows $\mathcal{X}_b(r,t)$ with another degree of freedom: The topology of spacetime depends not only on the total mass, but on the nature of matter also, and in particular, the spacetime should be prepared to immediately change its topology, depending on whether it embeds normal compressible matter, SuSu-matter, or particle-free vacuum.

In the present case, the progenitor of the BB is made of incompressible SuSu-matter. Hence prior to the BB, *i.e.*, for $t\le 0$ relative to $\mathcal{O}_0$, the embedding spacetime was flat.

However, at $t=0$ the fine-tuned surface tension confining the enclosed ocean of the SuSu-matter inside the progenitor, undergoes an abrupt decay, through which a hadronizing front is formed, which propagates from outside-to-inside. Behind the front, the deconfined SuSu-matter converts into hadrons. The released energy, which is expected to be of the order of 1 GeV per hadron, creates an extraordinary huge pressure, whose $\nabla P$ enforces the newly created normal matter to propagate outwards with ultrarelativistic velocity. This velocity may be predicated from the momentum Equation (22) as follows:

$$\frac{\partial \bar{u}^u}{\partial t}\approx -\frac{\nabla P}{D}+f_{grav}\Rightarrow\left(\bar{u}^u\right)^2\approx\frac{P_u}{D}=V_S^2\approx c^2, \tag{37}$$

where $\bar{u}^u$ is the radial component of the contravariant four-velocity. We used $\Delta r=\Delta_{bb}$ as the length scale over which $\nabla P$ changes significantly.

As it will be explained later, since $\left|f_{grav}\right|\xrightarrow[r\to\infty]{}0$, and therefore its decelerating effect decreases with the distance to $\mathcal{O}_0$, and therefore the outward-moving particles would naturally be seen as accelerating outwards. In particular, the particles in the outermost shells, where the topology hardly differs from that of a flat spacetime.

To manifest these arguments, we carry out our calculations, using the following reference quantities

$$\left[\tilde{\rho}\right]=3\rho_0,\ \left[\tilde{M}\right]=10^{22}M_\odot,\ \left[\tilde{V}\right]=c.$$

These are used to non-dimensionalize the field equations. Based thereon the reference radius reads: $\left[\tilde{r}\right]=\left[\left(3/4\pi\right)\left(\left[\tilde{M}\right]/\tilde{\rho}\right)^{1/3}\right]\approx 1.21$ AU. which yields $\left[\tilde{t}\right]\approx 10$ min.

Although the inward propagational speed, $V_f$, of the hadronization front, $\mathcal{F}^{HD}$, should be taken as an input parameter, we simply set $V_f$ to be equal to the speed of light. The reason is that inside incompressible SuSu-matter with $\nabla P=0$, communications are conducted with the speed of light only.

Hence, the hadronization front would reach the center roughly after 10 minutes, whilst the expansion front, $\mathcal{F}^{EX}$, should have reached $r=2\times\left[\tilde{r}\right]$.

The production rate of normal matter $\dot{M}^{nor}$ and the corresponding total mass $M^{nor}$ at time = $t$ read:

$$\dot{M}^{nor} = F_0\left[ +\left(\frac{tV_f}{r_0}\right)^2 + \left(\frac{tV_f}{r_0}\right)\right] 2$$
$$M^{nor} = M_0\left[ \left(\frac{tV_f}{r_0}\right)3 - \left(\frac{tV_f}{r_0}\right)^2 3 + \left(\frac{tV_f}{r_0}\right)^3\right] \quad (38)$$

where $M_0 = (4\pi/3)\rho_{cr} r_0^3$ and $F_0 = (4\pi r_0^2)\times(\rho_{cr} V_f)$ are the reference total initial mass of the progenitor and the initial outward-oriented flux of energy, respectively.

In Figure 3, we show the time-evolution of the spacetime topology during the propagation of the hadronization front without hydrodynamics. Here, the mass of SuSu-fluid decreases whilst the mass of the newly created normal matter increases, thereby enforcing the spacetime to change its topology from flat into curved. On the other hand, the expansion front, $\mathcal{F}^{EX}$, which separates the enclosed curved spacetime from the unperturbed surrounding flat spacetime, starts propagating outwards at the speed of light.

When including hydrodynamics, the flow configuration mimics the classical relativistic shock tube problem (RSTP, see [24] for further details). In Figure 4, the time-dependent motion of normal matter triggered by the pressure gradient under flat spacetime conditions is shown. Here, the matter is jettisoned into the

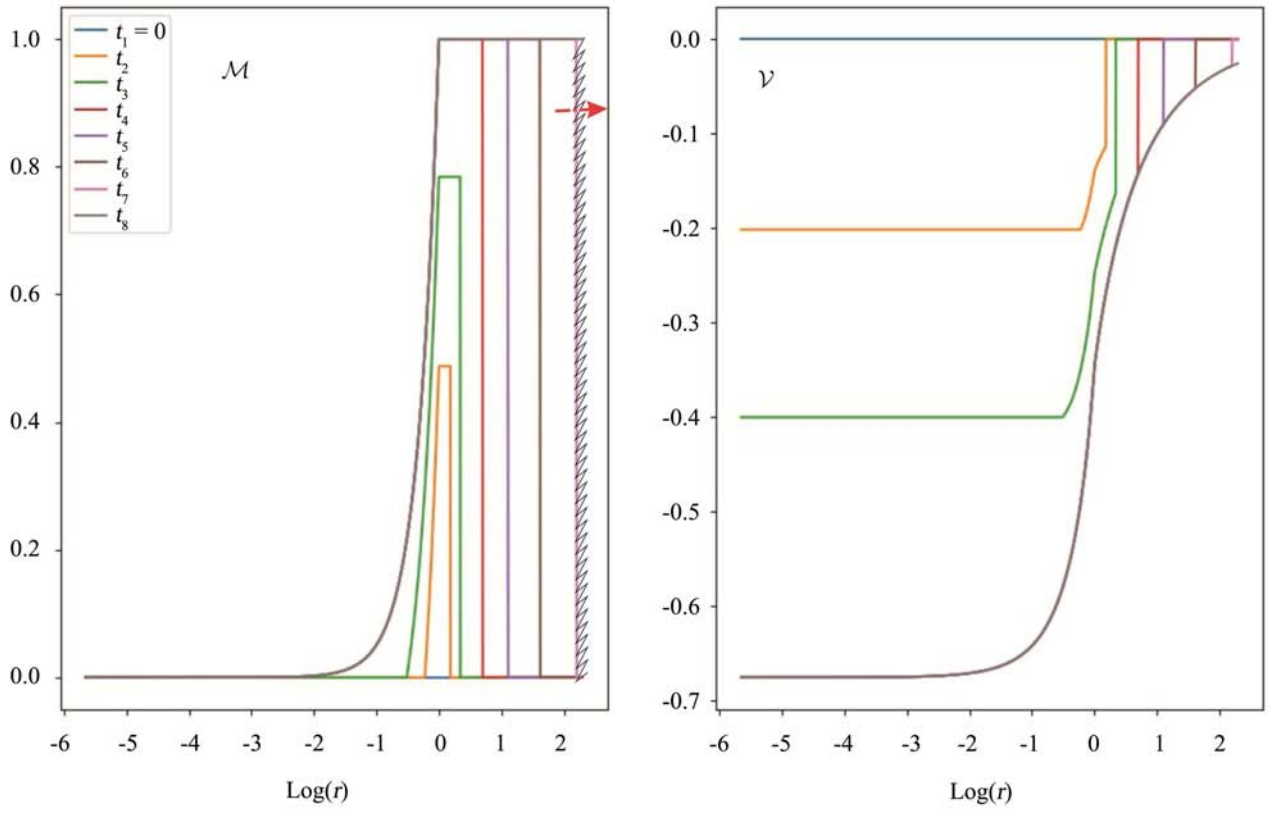


Figure 3. Different snapshots of the profile of total mass of normal matter, $\mathcal{M}$, and the gravitational potential $\mathcal{V}$, during the propagations of both the inward-oriented hadronization, $\mathcal{F}^{HA}$, and the outward-oriented expansion front, $\mathcal{F}^{EX}$. In these calculations, hydrodynamics are not included.

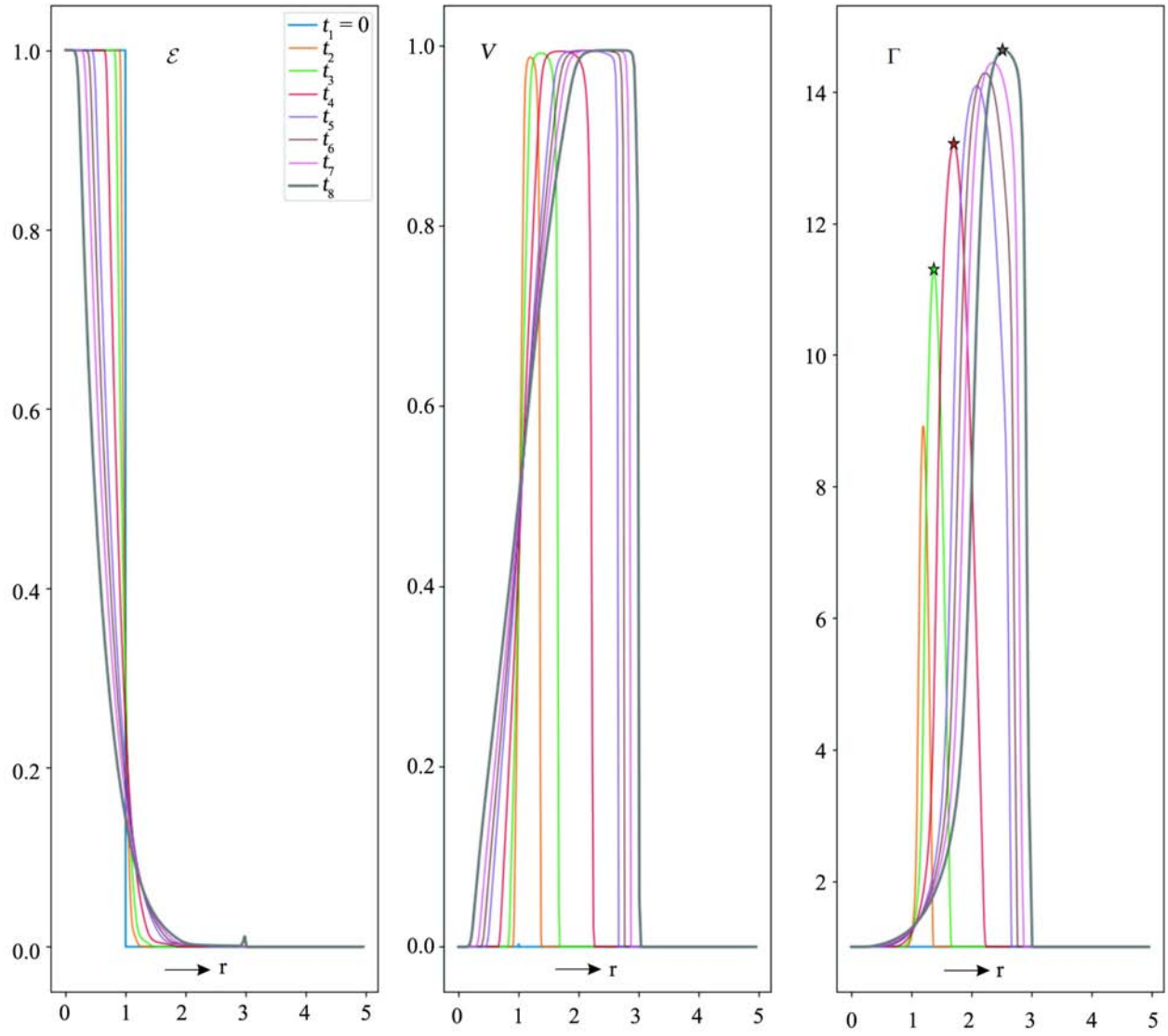


**Figure 4.** Radial distributions of the energy-density $\mathcal{E}$, transport velocity, $V$, and Lorentz factor, $\Gamma$, at different times are shown. When the quantum surface tension confining the SuSu-matter inside the progenitor is destructively perturbed, a hadronization front forms at the surface which, in turn, generates pressure, whose $\nabla P$ sets the newly created normal matter into outward-oriented motion at ultra-high relativistic speeds. The spacetime shortly after the formation of the hadronization front is flat and therefore the flow configuration is identical to the classical relativistic Riemann problem.

surrounding flat spacetime with ultrarelativistic velocity, reaching very high Lorentz factors. In these calculations, the thermal energy is accounted for by modifying the total pressure as follows: $P_{tot} = P(\mathcal{E}) + P_{ram} = \mathcal{E} + \mathcal{E}V^2$, where $P_{ram}$ stands for the ram pressure. Similar to the non-relativistic shock-tube problem, a rarefaction wave forms, which propagates in the opposite direction, expands the matter and lowers its pressure (first panel, **Figure 4**).

In the following step, we allow spacetime to evolve according to Equation (19). The initial configuration is a progenitor with incompressible SuSu-matter embedded in a flat spacetime. However, at $r = r_0$ boundary conditions were imposed, that prohibit escape of matter from the initial domain of the progenitor.

Depending on the compactness parameter, $\kappa = r_0/r_S = \alpha_{bb}$ and the EOS, the surrounding curved spacetime compresses the matter in the central region toward forming a hydrostatic core. Indeed, in the limit of $t \to \infty$ the equation for $\mathcal{V}$, which we term as the gravitational potential, converges to the TOV, which is usually used to model the interior of NSs in hydrostatic equilibrium (see Figure 5 and Figure 6). Whilst the matter accumulates in the very central region, the gravitational potential well becomes increasingly deeper.

When removing the BCs on the velocity and pressure at $r = r_0$, the resulting large pressure gradient jettisons the newly created hadrons into the surrounding spacetime with ultrarelativistic velocities, leaving little time for the matter to accumulate in the central region to form a core in hydrostatic equilibrium.

As anticipated, when the SuSu-matter in the outermost shell of the progenitor decays into hadrons, the surrounding spacetime starts curving. This, in turn, compresses the newly created normal matter via a compression front that follows, but is still slower than the inward-propagating hadronization front (see the first panel in Figure 6). Had the compression front hit the center, then the infalling matter bounces back and turns into outflow (second panel in Figure 7). Note that the transport velocity increases with both time and distance from the

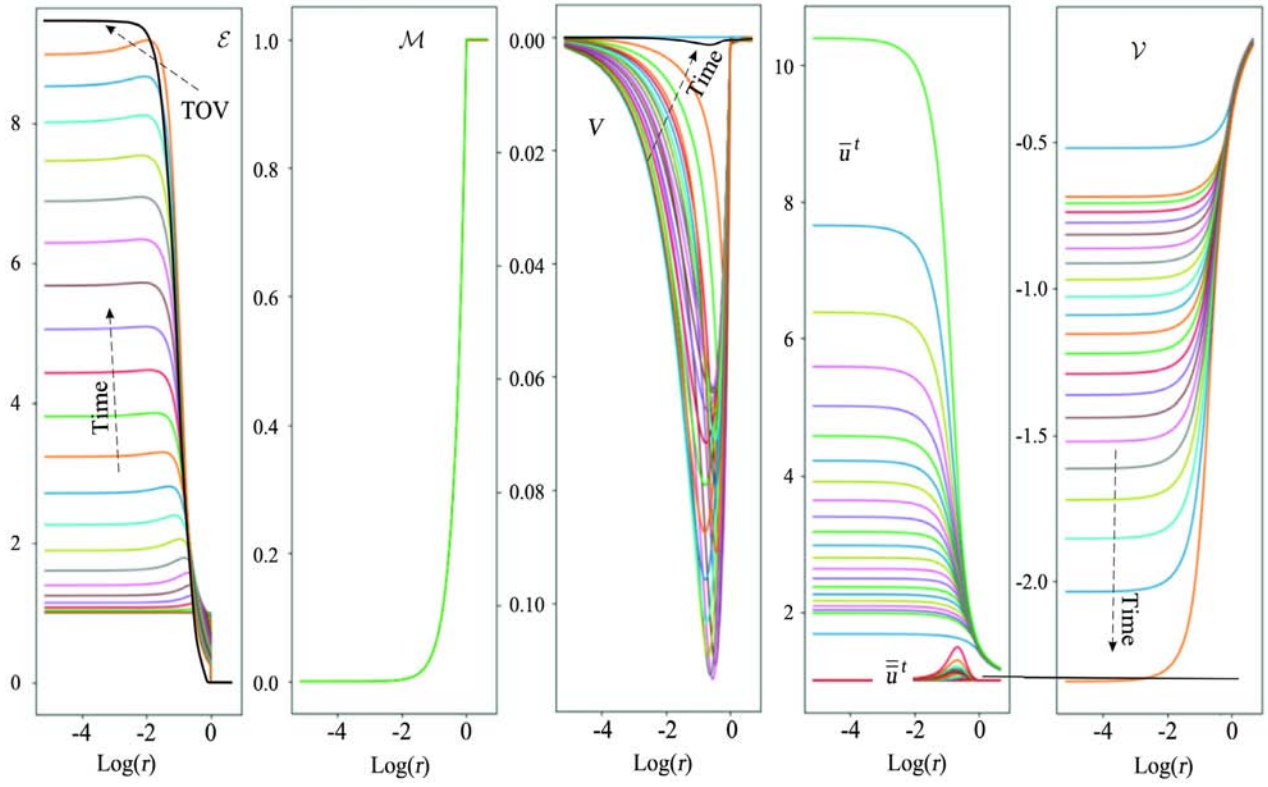


Figure 5. Snapshots of the radial distribution of the energy density $\mathcal{E}$, the total mass of normal matter, $\mathcal{M}$, the transport velocity, V, the modified Lorentz factor, $\bar{\Gamma}$, and the gravitational potential, $\mathcal{V}$, during contraction of a DEO. The boundary conditions here do not allow transport of normal matter into the surrounding space. In these calculations, an enhanced shock-capturing method is developed to avoid bouncing. The final configuration here is shown to converge smoothly into forming a core in hydrostatic equilibrium, whose interior may be well-described by the classical TOV equation.

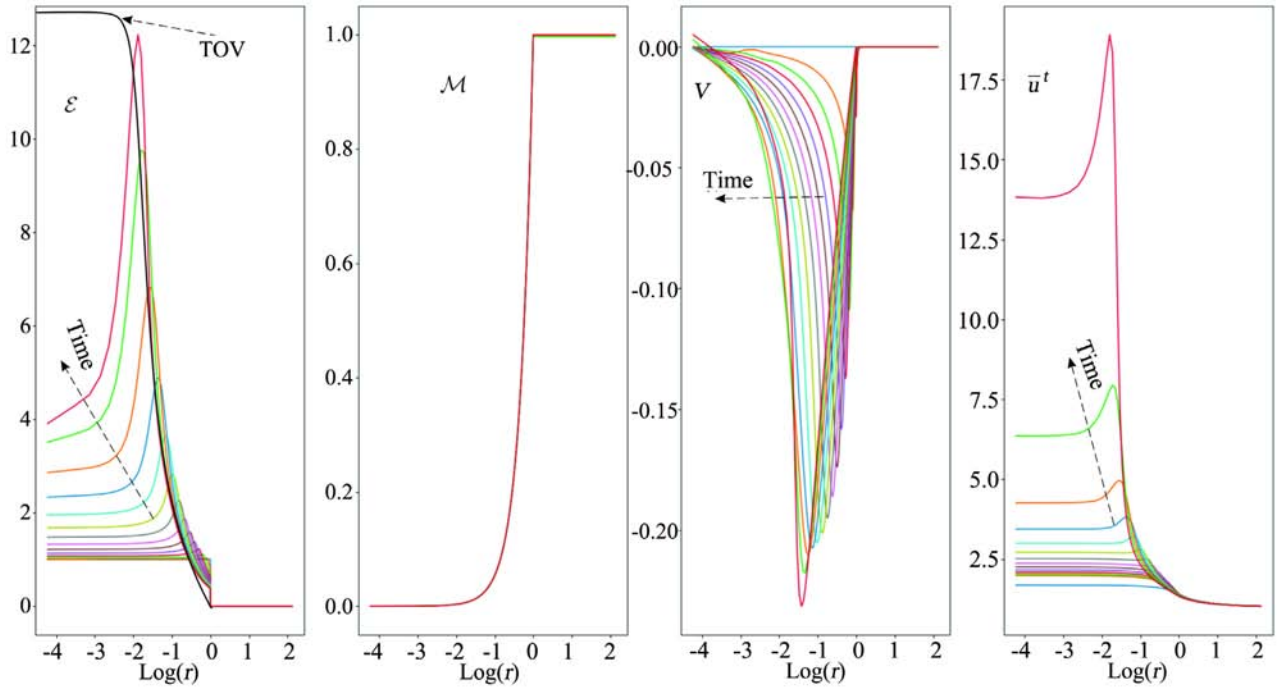


**Figure 6.** Snapshots of the radial distributions of the energy density $\mathcal{E}$, the total mass of normal matter, $\mathcal{M}$, the transport velocity V and the modified Lorentz factor $\bar{\Gamma}$ during the early stages of the contraction of the progenitor. In these calculations, the boundary conditions do not allow transport of normal matter into the surrounding. Obviously, the compressional front initially forms at the surface, starts propagating inwards. Depending on the EOS, the final configuration is a core in hydrostatic equilibrium whose interior is described by the modified TOV equation.

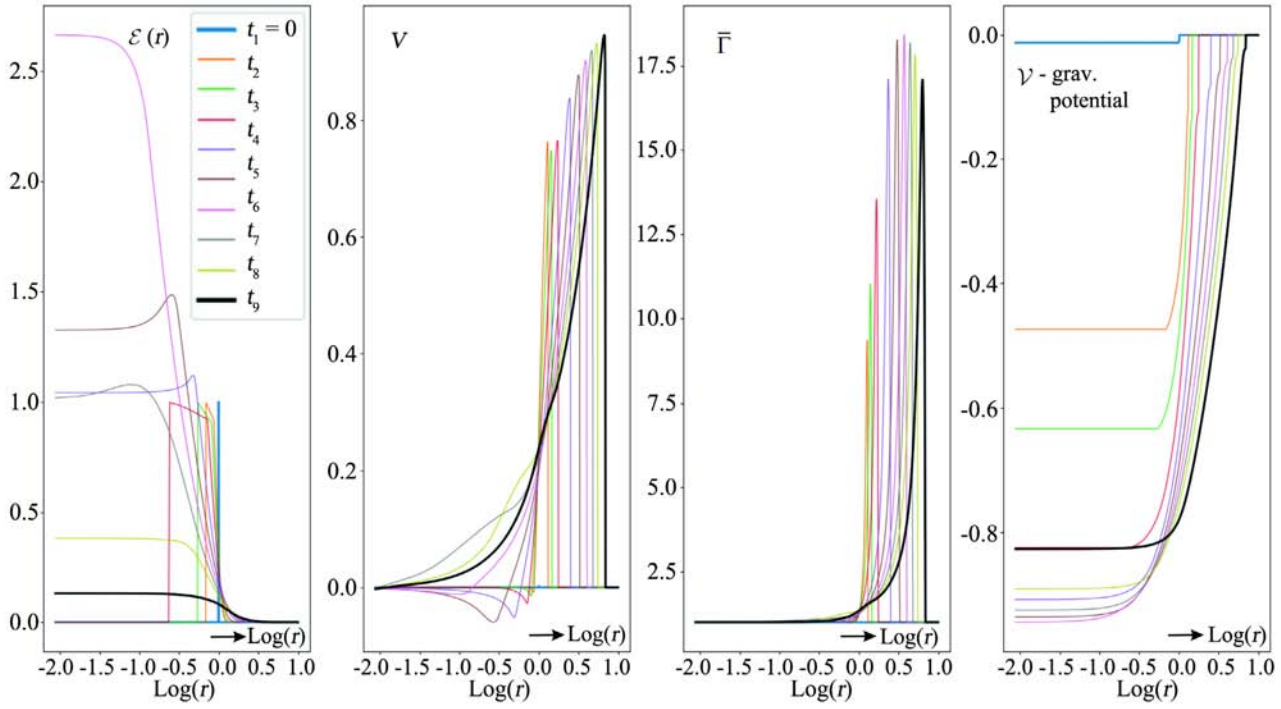


**Figure 7.** Snapshots of the radial distributions of the energy density $\mathcal{E}$, the transport velocity $V$, the modified Lorentz factor $\bar{\Gamma}$ and the gravitational potential $\mathcal{V}$ for different times during the hadronization process of the progenitor and beyond, starting from $t_1 = 0$ (blue) and ending up at $t_9 = 6$ (black).

center, and therefore is practically accelerating outwards relative to $\mathcal{O}_0$. In the third panel the modified Lorentz factor, $\bar{\Gamma}$ is displayed versus distance. We recall that:

$$\bar{\Gamma}^2 = \begin{cases} \dfrac{g_{tt}+V^2 r_{rr}}{g_{tt}-V^2 r_{rr}} : \text{General form} \\ 1 : \text{Hydrostatic core embedded in curved spacetime} \\ \dfrac{1+\beta^2}{1-\beta^2} : \text{Flat spacetime} \end{cases} \tag{39}$$

Obviously, for matter configurations that are slowly contacting or in hydrostatic equilibrium, $\bar{\Gamma}^2$ is more indicative than the classical Lorentz factor.

In the fourth panel the time-evolution of $\mathcal{V}$, which is dubbed gravitational potential, is displayed. Here, during the accumulation of matter in the central region, the gravitational potential becomes increasingly deeper, which agrees with the numerical experiment in **Figure 3**. However, had the core entered the bouncing phase, which is expected to occur on the dynamical time scale, the spacetime at the background would start flattening, in accord with the minimum energy theorem (see Equation (40) below).

To clarify this point we note that in the stationary case, the minimum energy theorem states that the gravitational energy/mass, $\mathcal{E}_g$, of an object can be extracted from the curvature of the embedding spacetime as follows:

$$\begin{aligned} \mathcal{E}_g &= \frac{1}{16\pi}\lim_{r\to\infty}\int_{S^2} n^i g^{k\ell}\left(\frac{\partial}{\partial x^k}g_{\ell i}-\frac{\partial}{\partial x^i}g_{\ell k}\right)\mathrm{d}S \\ &= \begin{cases} 0 & \text{flat spacetime} \\ M_0 & \text{Schwarzschild spacetime} \end{cases} \end{aligned} \tag{40}$$

For further details see [14] [26].

In obtaining the last equality, we relied on the Birkhoff theorem, which states that the surrounding spacetime topology may be described by the Schwarzschild metric.

In the present time-dependent case, Birkhoff theorem is valid only in the domain between the shock front, $\mathcal{F}^{SH}$, and the expansion front $\mathcal{F}^{EX}$, only. Here the time-dependent gravitational potential reads:

$$\mathcal{V}(r,t) = \begin{cases} \mathcal{V}(r,t) : r \le r_{SH} \\ \log\sqrt{1-M_0/r} : r_{SH}(t) \le r \le r_{EX}(t) \\ 0 : r \ge r_{EX}(t) \end{cases} \tag{41}$$

where $r_{SH} \doteq V_{SH} t$ and $r_{EX} \doteq ct$ are the radial distances of both the shock and expansion fronts, respectively.

The integral may be transformed into an infinite series, where each summand represents the enclosed mass of a newly created ring of normal matter at a time $t_n$. Since the series converges to $\mathcal{M}_0$, the integral should be transformable into the sum of infinite discrete summands as follows:

$$\frac{1}{16\pi}\lim_{r\to\infty}\int_{S^2}(*)\mathrm{d}S \xrightarrow[t=\frac{r}{c}\to\infty]{} \frac{1}{16\pi}\sum_{t_0=0}^{\infty} f(t_n) = \mathcal{M}_0, \tag{42}$$

where $f(t_n)$ corresponds to the time-dependent form of the integrand at time $t_n$. For $t \le r_0/c$, the total mass of normal matter increases with time and the corresponding potential well becomes increasingly deeper.

For $t \ge r_0/c$ the total mass of normal matter enclosed within the outward-moving radius $r \ge r_{sh}(t)$ is $\mathcal{M}_0$, whereas the gravitational potential $\mathcal{V}(r,t) \sim \log\sqrt{1-\mathcal{M}_0/r_{EX}}$, and therefore decreases with time and distance. As a consequence, due to the significant increase of the volume enclosing the normal matter, the gravitational potential starts flattening in the inner part (see $\mathcal{V}$ in Figure 7). In the limit of $\tau \gg \Delta\tau_0$, the curved spacetime would converge to a flat one and our observer $\mathcal{H}_0$ would hardly see anything, but a flat spacetime.

A comoving observer sitting at the shock front would experience deceleration if the expansion front is much faster than the shock front, whereas a stationary observer at the center would see the shock front accelerating outwards.

It should be noted here that the large outward-oriented relativistic velocities of normal matter must be extremely redshifted, so that $\mathcal{H}_0$ would fail to observe their motions unless they collide with existing objects and galaxies. In this case, a considerable amount of mass of the inflowing normal matter sticks to the galaxy's constituents, thereby transferring a huge amount of momentum and enforcing the galaxy to start moving outwards; hence accelerating outwards with respect to $\mathcal{H}_0$. This process has a significant effect, as, in addition to setting the galaxy in outward-oriented global motion, it turns old and inactive galaxies into active mode, in which accretion is activated and jets are initiated, so that they can be easily seen by remote observers.

## 5. Summary and Discussion

Based on our previous studies of glitching pulsars, an alternative model for the BB has been presented. Accordingly, pulsars are born with embryonic cores that are made of incompressible SuSu-matter. As pulsars evolve over cosmic times, these embryonic cores grow in mass and dimension to finally metamorphose into invisible dark energy objects. This phase corresponds to the lowest quantum energy state. According to our conjecture, the spacetime embedding SuSu-matter must be flat.

For $\tau \ge \tau_{14}$, these DEOs should have ample time to conglomerate into a cluster, and then subsequently merge to form the $10^{20} M_\odot$ massive progenitor of the BB with a flat spacetime at the background.

At $t = 0^+$ with respect to $\mathcal{O}_0$, the progenitor underwent an abrupt decay, thereby initiating four fronts that started propagating in different directions and speeds (see Figure 8):

- A hadronization front, $\mathcal{F}^{HA}$, that formed at the surface and propagated inward at the speed of light, behind which SuSu-matter was converted into virially hot and dissipative normal matter, which, in turn, interacted with spacetime and converted it into a curved one.

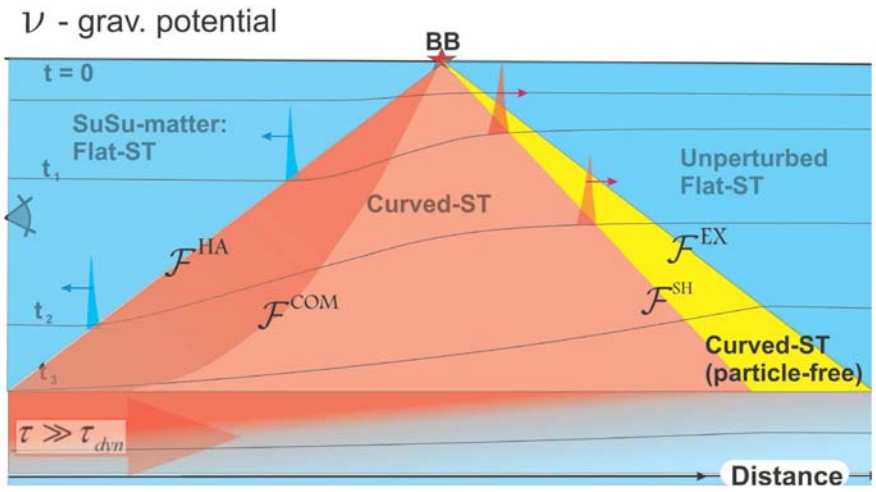


**Figure 8.** A schematic description of the evolution of spacetime (ST) topologies during the big bang event. Starting at the surface of the progenitor (BB), the hadronization front, $\mathcal{F}^{HA}$, starts propagating inwards with the speed of light, thereby converting the SuSu-matter into normal matter, and changing the topology of the embedding spacetime from flat into a curved one. The newly created normal matter is jettisoned in the direction of $-\nabla P$, thereby forming a shock-front $\mathcal{F}^{SH}$, which is then immediately overtaken by the outward-propagating expansion front $\mathcal{F}^{EX}$. The latter changes the spacetime topology from flat into a curved one. Relative to $\mathcal{O}_0$, both curved spacetimes between $\mathcal{F}^{HA}$ and $\mathcal{F}^{SH}$ (red colored) as well as between $\mathcal{F}^{SH}$ and $\mathcal{F}^{EX}$ (yellow colored) increase with time. However, as the total mass of normal matter is finite, the curved spacetime starts to flatten and converge to a flat on time scales much longer than the dynamical one, *i.e.* $\tau \gg \tau_{dyn}$.

- An expansion front, $\mathcal{F}^{EX}$, of spacetime, which formed at the surface and propagated outwards at the speed of light, thereby changing the topology of spacetime from flat into a curved one.
- $\mathcal{F}^{HA}$ would be followed by the compression front $\mathcal{F}^{COM}$, which the surrounding curved spacetime exerts on the enclosed normal matter, but not on the incompressible SuSu-matter. Due to the opposing force of the pressure, $\mathcal{F}^{COM}$ would propagate much more slowly than $\mathcal{F}^{HA}$.
- Triggered by the gradient of the pressure of normal matter at the surface of the progenitor, a shock front, $\mathcal{F}^{SH}$, started propagating outwards, whose speed is determined by both the EOS and the ratio of the pressure across the surface. Given the perfect spherical symmetry of the progenitor and that $\mathcal{E} = P = 0$ in the surrounding flat spacetime, $\mathcal{F}^{SH}$ of the normal matter in the outermost shell would hardly differ from, though more slowly than $\mathcal{F}^{EX}$. This implies that the matter-free domain which is bounded between $\mathcal{F}^{SH}$ and $\mathcal{F}^{EX}$, increases with time. However, the outward propagational speed of the matter in the following shells must be smaller, as the corresponding matter still has to climb up the gravitational well in which it is located. For the stationary observer $\mathcal{H}_0$, this matter appears accelerating outwards, rendering its re-collapse into a BH.

In this paper, we have presented also the theoretical foundation of the scenario, by deriving the time-dependent GR field equations in combination with the general relativistic hydrodynamical equations.

A new metric, which unifies the Minkowski, Schwarzschild and Friedmann metrics has been presented and implemented in the present model of the BB. Moreover, a modified TOV-equation for modeling contracting relativistic objects has been presented.

A highly robust time-implicit numerical solver, which relies on preconditioning techniques within the framework of Krylov subspace iterative methods, has been employed to solve the above-mention set of equations numerically.

The numerical results obtained are in line with the here-presented scenario. In **Figure 9** and **Figure 10**, we schematically outline the different aspects of the scenario, but the main consequences may be read as follows, though theoretical investigations and observational data are still needed to ensure their validities further:

- We conjectured that the spacetime inside zero-temperature QG-condensates that are motionless relative to remote stationary observers ought to be flat. This corresponds to the lowest quantum energy state, which should be compatible with the surrounding vacuum states [15] [16]. Putting a certain number of such QG-condensates, each component would be transparent to the other, and so they ought to overlap towards forming a parent condensate, whose mass and dimension are the linear addition of those of the individuals. The matter in the cores of massive NSs is expected most to share these properties, and therefore the spacetime embedding these cores should be flat. We note that the flatness requirement of spacetime inside zero-temperature QG-condensates is equivalent to demanding them to be in an incompressible state.
- Another implication of the above-mentioned conjecture is that the laws of nature would permit the existence of a universal maximum energy-density, $\rho_{max}^{uni}$, beyond which matter becomes purely incompressible. In this case, the matter is well-prepared to resist all types of external destructive perturbations, as communications are maintained at the speed of light. Consequently, the collapse of astrophysical objects with incompressible SuSu-cores need not end up forming BHs, but the SuSu-cores would enforce the infalling matter to bounce off, through which they increase in masses and size.

Indeed, based on the numerical solution of the Gross-Pitaevskii equation for modeling Boss-Einstein condensates (see Section 2.4 in [14]), it was shown that the merger of two DEOs proceeds rather stably and smoothly, without developing destructive perturbations. This in turn may indicate that the NS-merger GW170817 may have formed a NS with a much more massive core, rather than collapsing into a stellar BH (see [27] [28] [29] for further details).

In an infinite universe, these BB-cycles may occur in the sub-domains sequentially and/or in parallel as depicted in the lower panel.

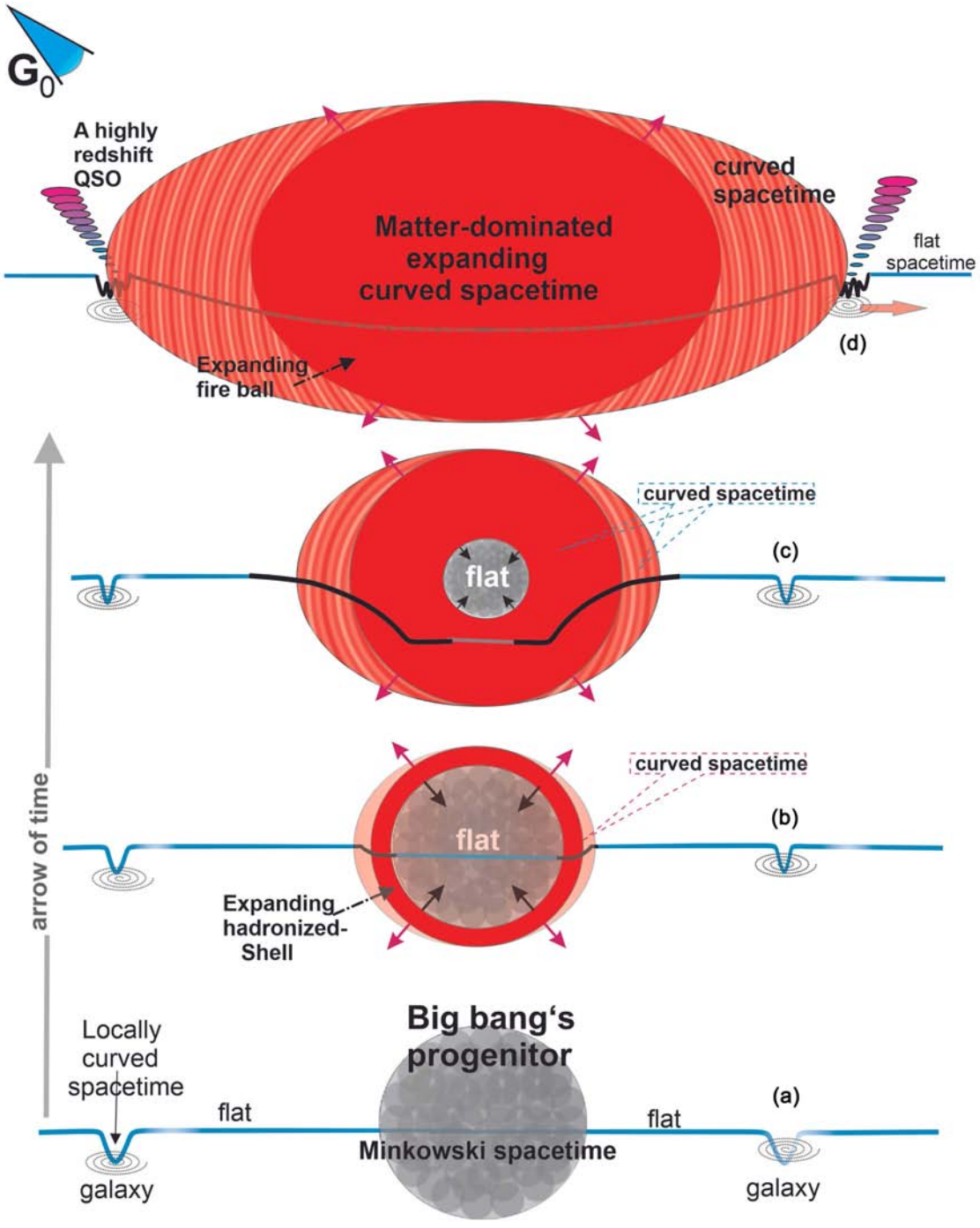


**Figure 9.** A schematic description of the BB-scenario as seen by the supra-observer $G_0$: on time scales comparable to or even larger than the age of the universe, a certain number of DEOs find their ways to conglomerate and form a tight cluster, where they subsequently merge smoothly and form the hypermassive progenitor of the BB. At a certain time, it undergoes an abrupt decay, triggering a hadronization front, $\mathcal{F}^{HA}$, which starts propagating from outside-to-inside, thereby converting the SuSu-matter into normal dissipative matter and changing the spacetime topology from flat into a curved one. At the same time, the decay triggers an expansion front $\mathcal{F}^{EX}$, which starts propagating outwards, thereby changing the topology of the surrounding matter-free spacetime from flat into a curved one. Once $\mathcal{F}^{EX}$ has hit and marched throughout old and quiet galaxies, it sets them in active mode, which we identify as high redshift QSOs. For $\tau \gg \tau_{dyn}$ the curvature of spacetime embedding the BB-explosion starts flattening in accordance with the minimum energy theorem.

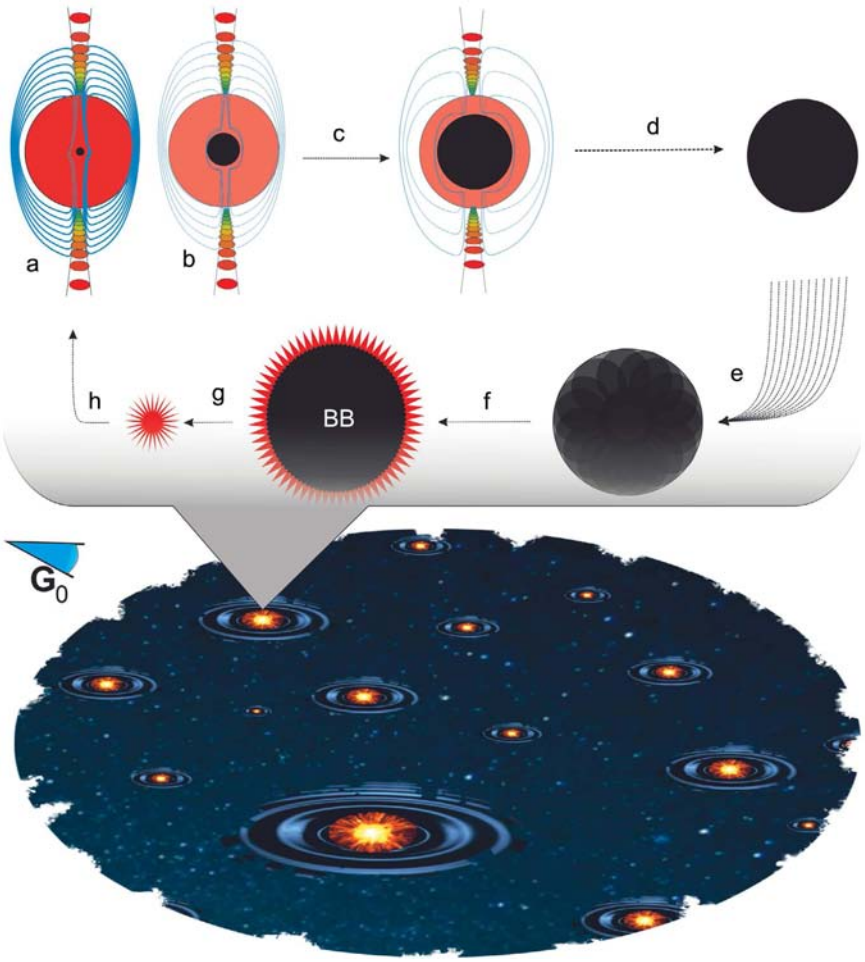


**Figure 10.** A schematic description of BB-cycles in the multiverse scenario as seen by the supra-observer $G_0$. Pulsars are born with embryonic cores of incompressible SuSu-matter (a), these cores grow in mass and dimension in a discrete manner (b, c) and finally metamorphose the entire dead NSs into invisible DEOs (d). On time scales comparable to or longer than the age of the universe, part of these objects conglomerate to form a cluster of DEOs (e), that subsequently merge to form a hypermassive DEO (f), which serves as the progenitor of the next BB. At a certain time, it undergoes an abrupt decay (f), thereby hadronizing the entire progenitor and giving rise to a BB-explosion (f), later on the jettisoned matter cools down and forms stars, part of which collapse to form the next generation of pulsars.

It should be noted here that the event horizon of a $10^{22} M_{\odot}$ massive object made of normal matter is of order $10^{27}$ cm. Hence, without invoking inflation and violating causality, our universe must theoretically have collapsed into a hypermassive BH. In the here-presented scenario, however, our universe is shown to expand forever, without invoking inflation and dark energy, whilst still respecting causality.

- The ADM mass is generally calculated from the integral (40), provided that the concerned object is standing there forever. However, in the time-dependent case, the causality condition requires the curved spacetime from which gravitational mass-energy is extracted, to have a finite dimension. Recalling that

the convergence of SuSu-matter into normal matter was completed after 10 minutes, generating a fireball with a fixed mass of $10^{22} M_{\odot}$, which must remain constant. As both the fireball and the embedding spacetime are expanding, the curvature must start flattening from inside-to-outside (see Figure 7). In this case, the following two logical consequences emerge:

1) Once the outward-propagating expansion front, $\mathcal{F}^{EX}$, has hit and marched through faint and quiet galaxies, the local spacetime is perturbed and their contents must re-arrange their trajectories, thereby transforming the galaxies into active modes, that we observe today as active galaxies and powerful QSOs.

2) After the first 10 min, the total mass of normal matter was $10^{22} M_{\odot}$, and was enclosed inside a sphere of radius 2.4 AU. Since then the curvature of spacetime has been continuously flattening, which yields a relative curvature: $Q(t=\text{today})/Q(t=10\,\text{min}) \sim \left[r(t=10\,\text{min})/r(t=\text{today})\right]^2 \approx 10^{-30}$. This implies that the universe today must be extraordinarily flat.

- Based on the here-presented scenario, we conclude that BB-explosions are local recurrence phenomena in an infinite universe, that may take off from time to time in different sub-domains sequentially and in parallel. These sub-domains are dynamical; they may overlap with others, disappear, or even be created anew. Each sub-domain may be populated by all types of objects and its dimension and age are determined by the time it takes to restore the spacetime topology into a flat one. The life-cycle of each sub-spacetime follows the same evolutionary scenario of the BB in our universe: here pulsars evolve into NSs, these become DEOs. Large number of DEOs may conglomerate in a certain location in the sub-domain, they merge and form a giant progenitor made of SuSu-matter.

Note that in an infinitely large universe, the mathematical probability of assembling a sufficient number of DEOs in a certain location is vanishingly small, but certainly not zero. Also, expansion of spacetimes of certain sub-domains of the infinite universe cannot rule out the possibility that they may be contracting in other sub-domains. These expansions/contractions may not affect the topologies of local spacetimes inside galaxies, which in turn may facilitate assembling of objects. Once assembled and smoothly merged to form the progenitor, the latter may undergo an abrupt decay that leads to its entire hadronization, thereby creating a giant fireball. Its content cools down and stars are formed, part of which collapse to form pulsars and so on.

- The total mass of normal matter-made objects that evolved from the BB of our universe may most likely be much lower than expected, as spacetime surrounding the progenitor of the BB may have been populated by numerous dead objects and galaxies.
- SuSu-matter can be found in pulsars, NSs, magnetars and even in stellar and supermassive BH-candidates. This implies that these objects may be much more massive than predicted from observing normal and luminous matter.

This is a direct consequence of the flat spacetime topology that embeds Su-Su-matter.

## Acknowledgements

The author acknowledges the financial support of the IWR and KAUST, Profs. Mario Livio and Adi Nasser for their valuable comments and Dr. Umar for proofreading the manuscript.

## Conflicts of Interest

The author declares no conflicts of interest regarding the publication of this paper.

## References

[1] Bromm, V. (2013) Formation of the First Stars.

[2] Laporte, N., Meyer, R.A., Ellis, R.S., *et al.* (2021) *Monthly Notices of the Royal Astronomical Society*, **505**, 3336-3346. https://doi.org/10.1093/mnras/stab1239

[3] Diehl, R., Halloin, H., Kretschmer, K., *et al.* (2006) *Nature*, **439**, 45-47. https://doi.org/10.1038/nature04364

[4] Sartore, N., Ripamonti, E., Treves, A. and Turolla, R. (2010) *Astronomy & Astrophysics*, **510**, A23. https://doi.org/10.1051/0004-6361/200912222

[5] Fan, X., Wang, F., Yang, J., *et al.* (2019) *The Astrophysical Journal Letters*, **870**, L11. https://doi.org/10.3847/2041-8213/aaeffe

[6] Oesch, P.A., *et al.* (2016) *The Astrophysical Journal*, **819**, 129.

[7] Espinoza, C.M., Lyne, A.G., Stappers, B.W. and Kramer, C. (2011) *Monthly Notices of the Royal Astronomical Society*, **414**, 1679-1704. https://doi.org/10.1111/j.1365-2966.2011.18503.x

[8] Roy, J., Gupta, Y. and Lewandowski, W. (2012) *Monthly Notices of the Royal Astronomical Society*, **424**, 2213-2221. https://doi.org/10.1111/j.1365-2966.2012.21380.x

[9] Hujeirat, A.A. (2018) *Journal of Modern Physics*, **9**, 554-572. https://doi.org/10.4236/jmp.2018.94038

[10] Hujeirat, A.A. and Samtaney, R. (2019) *Journal of Modern Physics*, **10**, 1696-1712. https://doi.org/10.4236/jmp.2019.1014111

[11] Ashton, G., Lasky, P.D., Graber, V. and Pal-freyman, J. (2019) Rotational Evolution of the Vela Pulsar during the 2016 Glitch.

[12] Hujeirat, A.A. (2020) *Journal of Modern Physics*, **11**, 1779-1784. https://doi.org/10.4236/jmp.2020.1111110

[13] Glendenning, N.K. (2007) Special and General Relativity. Springer, Berlin. https://doi.org/10.1007/978-0-387-47109-9

[14] Hujeirat, A.A. (2021) *Journal of Modern Physics*, **12**, 937-958. https://doi.org/10.4236/jmp.2021.127057

[15] Lee, T.D. (1979) Lecture at Columbia University.

[16] Donoghue, J.F. (1980) *Physical Review D*, **22**, 1780. https://doi.org/10.1103/PhysRevD.22.1780

[17] Shuryak, E.V. (2004) *Nuclear Physics A*, **750**, 64-83.

[18] Pasechnik, R. and Šumbera, M. (2017) *Universe*, **3**, Article No. 7. https://doi.org/10.3390/universe3010007

[19] Guth, A.H. (1981) *Physical Review D*, **23**, Article No. 347. https://doi.org/10.1103/PhysRevD.23.347

[20] Linde, A.D. (1982) *Physics Letters B*, **108**, 389-393. https://doi.org/10.1016/0370-2693(82)91219-9

[21] Bardeen, M., Steinhardt, P.J. and Turner, M.S. (1983) *Physical Review D*, **28**, 679.

[22] Bozza, V. (2022) *Universe*, **8**, 379. https://doi.org/10.3390/universe8070379

[23] Hobson, M.P., Efstathiou, G. and Lasenby, A.N. (2015) General Relativity: An Introduction for Physicists. Cambridge University Press, New York.

[24] Fischer, M.S. and Hujeirat, A.A. (2020) Time-Implicit Schemes in Fluid Dynamics?

[25] Hujeirat, A.A. and Thielemann, F.-K. (2009) *Informatik-Spektrum*, **32**, 496-504. https://doi.org/10.1007/s00287-009-0391-0

[26] Witten, E. (1981) *Communications in Mathematical Physics*, **80**, 381-402. https://doi.org/10.1007/BF01208277

[27] Abbott, *et al.* (2017) *The Astrophysical Journal Letters*, **848**, L12.

[28] Piro, L., Troja, E. and Zhang, B. (2019) *Monthly Notices of the Royal Astronomical Society*, **483**, 1912-1921. https://doi.org/10.1093/mnras/sty3047

[29] Hujeirat, A.A. and Samtaney, R. (2020) *Journal of Modern Physics*, **11**, 1779-1784. https://doi.org/10.4236/jmp.2020.1111110

Journal of Modern Physics, 2022, 13, 1499-1517
https://www.scirp.org/journal/jmp
ISSN Online: 2153-120X
ISSN Print: 2153-1196

# The Experimental Exploration and Discovery of DNA Communication between the Plants

**Xinzhou Yuan, Jiafeng Yuan, Zhongxian Deng, Shikui Wang, Zhen Yang, Qiao Bi***

Shenzhen Xinzhou Biological Information Technology Co., Ltd., Shenzhen, China
Email: *biqiao@gmail.com

**How to cite this paper:** Yuan, X.Z., Yuan, J.F., Deng, Z.X., Wang, S.K., Yang, Z. and Bi, Q. (2022) The Experimental Exploration and Discovery of DNA Communication between the Plants. *Journal of Modern Physics*, **13**, 1499-1517.
https://doi.org/10.4236/jmp.2022.1311092

**Received:** October 5, 2022
**Accepted:** November 26, 2022
**Published:** November 29, 2022





## Abstract

For the first time, through the invention of Compensating Bio-information Energy (CBE) technology and bioinformatics breeding machine, we have completed a number of experiments by using plant signals to transfer plant genetic traits in the same family or across families, and discovered the transfer phenomenon of life genetic information. The test results show that plants can change from random variation to controllable and directional variation, thus opening up plant asexual, no molecular transfer, fast and low-cost breeding. The new approach provides new evidence for the connection of information energy waves between plant DNA, which deserves the attention and in-depth study of the scientific community.

## Keywords

Biological Signal, Biological Microwave Radiation, DNA Communication, Bio-Information Breeding Machine

## 1. Introduction

Last century twenties the former Soviet Union biologist Gulevitch first discovered biological signals and non-contact biological physics effects through the famous onion experiment [1]. For more than 100 years, many experts and scholars have persisted in their explorations and have achieved many research results of historical significance and uncovered the mystery of biological field [2] [3] [4] [5] [6]. Under certain conditions, the communication of information energy between organisms can also be realized, that is, biological microwave communication. Jiang Canzheng, a Chinese scientist in the former Soviet Union, applied the technology of physical shielding to complete many experiments to be verified

the phenomenon of biological microwave communication, and many incredible experimental results have been achieved in the transfer of genetic traits in animals and plants and human rehabilitation [7] [8] [9] [10].

On this basis, we conducted in-depth exploration and found that the interaction between plant molecules is indeed not limited to chemical interaction. The phenomenon of non-contact random variation between plants is the transfer of biological information through the energy wave radiated by plants under certain specific conditions, that is, biological microwave communication [11]. Through a number of repeatable biological experiments, we also found that the transduction of biological signals can transfer the genetic traits of plants [12]. Therefore, we believe that the core of biological signals is the existence of DNA signals containing life information. In recent years, scientists have discovered the biological material basis of this life phenomenon. More and more evidence shows that miRNA can serve as a link between animals, plants and microorganisms across species, and is closely related to the substances that form genes [13] [14] [15]. For millions of years, the co-evolution of life has not only formed the close connection of all organisms in terms of genetic material, but also formed the connection of energy (wave) between genes. This energy wave, namely life signal, is a physical way of life information transmission. We call it information energy, which is the basis for the realization of DNA communication [16]. This ultra-weak information energy wave can affect the protein activity of biological receptors [17]-[24], and correspondingly many reproducible biological experiments provide evidence for the transmission of life signals, that is, the transfer of DNA information.

The practice of crop improvement shows that there are two effective ways to improve crop yield potential through plant breeding, namely morphological improvement and utilization of heterosis. However, if only the way of morphological improvement is adopted, the improvement potential is very limited, and heterosis breeding will not produce satisfactory results if it is not combined with morphological improvement [25]. In the past 20 years, we have found a new way to use high and new technology to make the random variation without contact between plants in nature. One of important progress for us is CBE technology and bioinformatics breeding machine are invented [26], as shown in **Figure 1**.

The invention relates to a new technical field of compensating biological information energy to plants and polar molecular liquids, involving quantum physics, bioinformatics, molecular biology and other sciences. These methods may be widely used in scientific research, breeding, drinks, health care and other field. Since 2008, with the strong support of relevant scientific research and institutional experts, we have completed a number of new and exploratory experiments by using proportional sampling method, repeatedly verified the phenomenon of DNA communication, and found the existence of DNA signals. **Figure 2** is part of the experimental photos, hereinafter referred to as information processing.


**Figure 1.** The bioinformatics breeding machine, which realizes the directional transfer of donor genetic traits to the receptor through energy wave transmission, and opens up a new way of asexual and molecular free bioinformatics breeding.


**Figure 2.** The changes of genetic characters of the first generation of wheat (HS) in the bioinformatics breeding test field and the detection information receptor.

## 2. Experiment and Detection of Plant Radiation Signal

### 2.1. Donor Information Promotes Reproduction of Cordyceps Mycelium

We directionally transmitted the information of the donor wheat sprouts to the recipient Cordyceps mycelium through the breeding machine, as shown in Figure 3. After receiving the wheat information in the three treatment groups, the

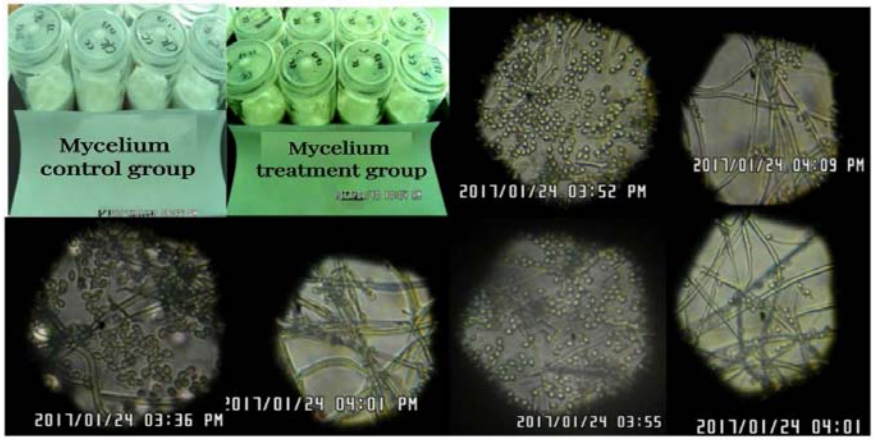


**Figure 3.** The three groups of comparative photos of transferring wheat information to Cordyceps mycelium. It can be seen that the mycelium reproduction of the three treatment groups is significantly better than that of the control group, indicating that wheat information promotes mycelium reproduction.

mycelial reproduction was significantly better than that of the control group, indicating that wheat information promoted mycelial reproduction.

### 2.2. Donor Plant Information Changes Color and Taste of Recipient Plant

We used the bioinformation breeding machine to transfer respectively the radiation information of the donor green vegetable bud and the pepper bud to the budding cabbage of the recipient; the budding cabbages were then seeded in the experimental fields. After harvest, the offspring (HS) 1 generation were compared for appearance, color and taste, as shown in **Figure 4**. And the relevant taste was compared by double-blind method, as shown in **Table 1**. The color of cabbage in treatment group 1 and 2 was significantly different from that in control group (middle), the color of information processing group 1 was lighter than that of control group, and the color of information processing group 2 was darker than that of the control group, and the change of chlorophyll was obvious. And the taste of treatment group 1 and 2 was also significantly different from that of the control group. This experiment provides evidence that different plants radiate different information, and have different influences and effects on the recipient. At the same time, it indicates that the information transmitted by the bioinformation breeding machine is the real information of the donor.

### 2.3. Donor Information Promotes the Germination Potential of Recipient Buds

**Figure 5-1** and **Figure 5-2** show the significant changes in the growth trend of radish seeds after receiving the information of donor wheat sprouts during germination and then planting in the experimental field. The signal processing group is on the left, and the control group is on the right. The germination of the treatment group is faster and stronger than that of the control group. **Figure 5-3**


**Figure 4.** The left is cabbage information processing group 1, which is lighter in color than the control group (middle); on the right is pepper information processing group 2, whose color is darker than that of the control group, indicating that the chlorophyll of the treatment group has changed.

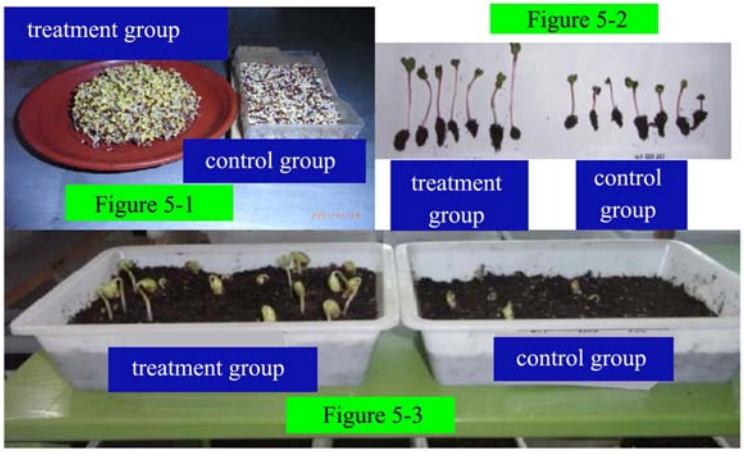


**Figure 5.** Showing donor information promotes the experimental results of germination potential. **Figure 5-1** and **Figure 5-2** show that wheat information transfer to water radish promotes the germination and growth of water radish seeds, with the treatment group on the left and the control group on the right. **Figure 5-3** shows the transfer of wheat information to soybeans. The growth of the treatment group was significantly better than that of the control group.

**Table 1.** Statistical table of taste experiment of Chinese cabbage by double-blind method (2017.3.1).

| NO | List of participants | Control group 1 (stem) | Control group 2 (leaves) | Treatment 1 group (stem) | Treatment 1 group (leanes) | Treatment 2 group (stem) | Treatment 2 groups (stem) |
|---|---|---|---|---|---|---|---|
| 1 | Yuan | bland | tasteless | peculiar smell | delicious | not tasty | bitter taste |
| 2 | Liu | bland | tasteless | peculiar smell | delicious | not tasty | bitter taste |
| 3 | Han | bland | tasteless | peculiar smell | delicious | not tasty | bitter taste |
| 4 | Zhu | bland | tasteless | peculiar smell | delicious | not tasty | bitter taste |
| 5 | Li | bland | tasteless | peculiar smell | delicious | not tasty | bitter taste |
| 6 | Dong | bland | tasteless | peculiar smell | delicious | not tasty | bitter taste |
| 7 | Qu | bland | tasteless | peculiar smell | delicious | not tasty | bitter taste |

shows that after receiving the information of donor wheat during soybean germination, the treatment group (left) grew stronger than the control group (right). We have done repeated experiments and have seen the same results. These show that the radiation information of donor wheat plants can affect the growth trend of recipient plants.

### 2.4. Detection of Plant Radiation Signals

In the absence of detection data, many people doubt that living plants radiate biological signals (microwaves) during their life activities. In 2020, we developed a biological radiation signal power detector, as shown in Figure 6. After verification, it can detect the noise power of signals below 8G radiated by human body, plants and fungi at room temperature, that is, it can detect some biological radiation signals, and use data to prove the true existence of radiation signals of plants and other living bodies. For example, the average data of the three groups of vegetables detected for six consecutive days after germination are shown in Table 2. The test was divided into three experimental groups: A, B and C. The sprouts of green vegetables were tested at 9 am, 12 noon and 5 pm every day, 10 time consecutive tests were performed in each time period and calculate the average value. After each measured data is stable for 3 minutes, observe for one minute, read the value every 5 seconds during this minute, take the average value of three groups as the measured value, and then subtract the natural noise power value of the same plant in the shielding box. The difference obtained is the measured radiant power value of the green vegetable seedling, which is listed in

Figure 6. The staff are using the biological radiation signal power detector to detect the radiation signal power of plants, and use the data to judge the growth state of plants.

**Table 2.** Summary of average values of radiation signal power detection of green vegetable seedlings. Detection location: Shielding box; temperature 22˚C - 23˚C; Relative humidity 90%; Unit: DBM.

| Observe date The subjects | time (day) | 1 | 2 | 3 | 4 | 5 | 6 | Average shielding box |
|---|---|---|---|---|---|---|---|---|
| The experimental group A. | Morning | 43.06 | 45.1 | 44.87 | 46.06 | 44.29 | 44.8 | 40.06 |
| | Noon | 47.85 | 45.07 | 44.79 | 43.81 | 43.76 | 43.47 | |
| | Evening | 45.04 | 45.22 | 44.97 | 42.6 | 42.15 | 42.3 | |
| The experimental group B | Morning | 44.06 | 46.12 | 44.43 | 45.79 | 43.68 | 45.15 | |
| | Noon | 45.63 | 44.37 | 44 | 44.04 | 43.98 | 43.59 | |
| | Evening | 44.5 | 44.65 | 43.84 | 42.51 | 40.62 | 42.89 | |
| The experimental group C | Morning | 44.57 | 45.97 | 44.29 | 45.38 | 44.6 | 44.93 | |
| | Noon | 45.29 | 43.26 | 43.47 | 44.46 | 45.85 | 44.17 | |
| | Evening | 44.86 | 45.42 | 45.28 | 43.16 | 42.81 | 43.63 | |
| The experimental mean | Morning | 43.89 | 45.73 | 44.53 | 45.74 | 47.6 | 44.96 | |
| | Noon | 46.25 | 44.23 | 44.08 | 44.1 | 44.53 | 43.74 | |
| | Evening | 44.8 | 45.09 | 44.69 | 42.75 | 41.86 | 42.94 | |
| Average difference of experimental groups A, B and C | Morning | 3.83 | 5.67 | 4.47 | 5.68 | 7.54 | 4.9 | |
| | Noon | 6.19 | 4.17 | 4.02 | 4.04 | 4.47 | 3.68 | |
| | Evening | 4.74 | 5.03 | 4.63 | 2.69 | 1.8 | 2.88 | |

the column of the average value in the table, and the unit is the noise power dbm. The measured data were obtained by testing under the same conditions, and finally the average value of the three experimental groups A, B, and C was taken as the testing result. From the above three groups of average data, they basically reflect the real detection results, that is, the power of plant radiation signals in different periods of time is significantly different, fluctuates with time, and has the basic characteristics of nonlinearity. This shows that the energy of the radiation changes with varies from time to time, which provides quantitative data for further exploration of complex metabolic functions of plants. **Figure 7** is the drawing of measured data from the average detection data of groups A, B and C in **Table 1**, after subtracting the shielding box ontological natural noise power value, we can directly observe the life activity rhythm of green vegetable seedlings within 10 days. As can be seen from the broken line in the morning, there are two radiation power peaks at the detection data points on the second and five day; at noon, the broken line can be seen that the radiation power of green vegetable seedlings in the development process presents a general trend of decline; the broken line in the evening also showed an overall downward trend of radiation power of green vegetable seedlings. The results also showed that living plants can radiate energy outward as they grow; moreover, the intensity of the radiation power is nonlinear fluctuations with time, showing the characteristics of biological clock. The results of detection data provide quantitative basis for us to identify plant growth status and select plants with good growth status.

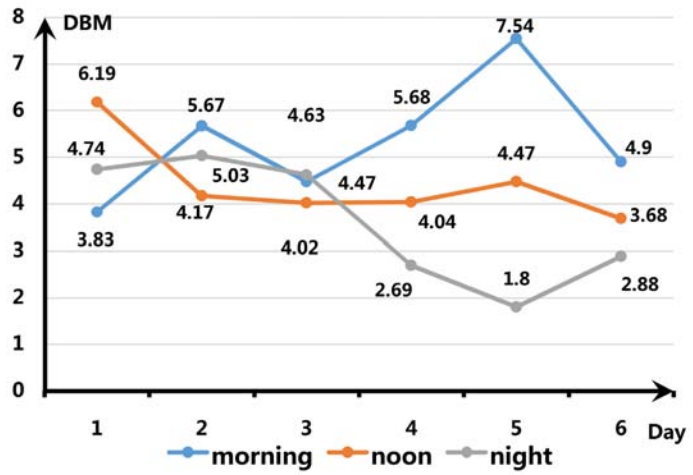


**Figure 7.** The chart drawn by subtracting the noise value in the environment from the average value of the radiation signals detected by the biological signal detector at different times in the morning, middle and evening of three groups of green vegetable seedlings within 6 days. From the data chart, we can see that the power of the radiation signal fluctuates at different times during the growth process of green vegetable seedlings, which provides a quantitative basis for us to judge the growth state of plants and select plants.

## 3. Experiments on Directional Transfer of Genetic Traits

### 3.1. Experimental Materials

The experimental results show that biological information is expressed through the energy of biological signal transmission. The famous onion experiment found that biological signals come from the process of cell division. The experimental results show that in the process of plant growth, that is, the process of DNA replication, the signal power density is large and the amount of information is large, which can accelerate the recovery of human cell function [27]. The biological experiment results of many repeatable and no molecular transfer genetic traits show that DNA signal is the most basic and important signal in biological signals. Also according to the theory of atomic emission spectrum and absorption spectrum [28], we think that changes in the energy of DNA atoms also are the physical processes that govern life, when DNA atoms drop from high energy state to a low energy state, RNA releases energy quanta; conversely, when it rises from a low to a high energy state, it absorbs quantum of energy. This could be one of the ways for DNA to radiate or absorb signals, express or obtain life information.

Based on the above theories or hypotheses, we chose the information donor and receptor during germination because the signal is the strongest in the rapid division process of plant cells, the germination is also the easiest to absorb foreign signals.

In practice, we have invented a biological radiation signal power detection device, for detect the radiation signals of selected plant donors and receptor, as shown in **Figure 6**. After detection, we conducted statistical data analysis and found that the strongest signal was indeed released during the rapid division of

plant cells. Therefore, we selected the information donor and recipient of the experiment as the buds in the vigorous growth stage.

According to the purpose of the experiment, we first determine the genetic traits to be transferred, and then select the more prominent plant genetic traits as the biological signal donor, and the recipient should select the buds and seedlings that need to obtain the genetic traits.

## 3.2. Experimental Equipment

The experimental equipment is a biological information breeding machine, as shown in **Figure 1**. It is developed and manufactured by ourselves, and its interior is equipped with biological signal processing, acceleration and transfer systems.

## 3.3. Basic Principles and Components of CBE Technology

### 3.3.1. Basic Principles

When the function or structure of cells, tissues, organs and systems changes, the biological signals radiated by them will first change, such as the detection of cardio brain electrical signals and the application of judging diseases; conversely, when the signals radiated by cells, tissues, organs and systems are modulated by foreign matched biological signals, their functions or structures will also be affected [16].

### 3.3.2. Three Parts of CBE Technology

1) Design and select the technical scheme of information donor and recipient plants; 2) Cultivate information donors and receptors according to the technical bid; 3) Genetic information transfer is completed by biological information breeding machine.

Through experiments, we have found that different plants will radiate different biological signals and have different effects on different cells of human body, and have different improvement effects on human functions [29], therefore, we believe that DNA signals in different can express different life information and can receive the corresponding life information, so different life signal effects will be produced.

According to the famous physicist David Bohm's theory of quantum potential and the second law of thermodynamics (information is negative entropy), we believe that the high part of biological information energy in the entanglement process determines the direction and biological effect of information transfer. The life information of the trait contained in plant DNA with prominent genetic traits should be in a relatively high information potential, so it is easier to transmit information to the genes of the receptor, therefore, plants with outstanding genetic traits should be selected as donors.

In addition, in the process of information energy wave entanglement, the outstanding genetic trait information of the donor will be transferred to the receptor in the form of biological radiation signal. After the receptor DNA obtains

this life information energy that can express outstanding genetic traits, it will be expressed in the process of controlling protein synthesis and affect the activity of the protein, that is, to realize the transfer of genetic information. Therefore, we have formulated strict technical requirements for seed selection, cultivation and management of information donors and recipients.

According to the basic principles of quantum physics and low energy particle accelerator, we have invented the biological signal transfer system in CBE technology by adopting a variety of new technologies [30]. CBE signal transfer system can be installed inside the machine. On this basis, a bioinformation breeding machine has been invented, which realized the directional gather, processing, acceleration, maximum signal-to-noise ratio and directional transfer of the donor plant signals to the recipient in a shielded environment. The new technology developed a new structure and biological signal wave handling process, greatly reduced the manufacturing cost, through the directional acceleration of plant signal, realized the maximum power density of plant signal, increased the information received by recipient cells per unit time, and completed the directional transfer of donor genetic information in a short time.

Experiments show that the signals radiated by plants in the process of vigorous growth contain a large amount of information, and are more vulnerable to the influence of various external signals. Therefore, we should pay attention to preventing the interference of various signals such as electricity, magnetism, light and sound, so we have strict technical control over the cultivation, management, use, information transfer process of plants, and the custody of samples, etc.

### 3.4. Process of Transferring Genetic Traits of CBE Technology

The CBE technology we used in the experiment transfers genetic traits as follows:

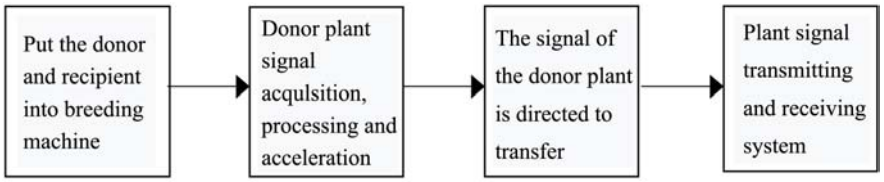


### 3.5. Experimental Methods

#### 3.5.1. Quantum Resonance Detector

TJQQ-ZDJTEQAM quantum resonance detector was used to detect the efficacy characteristics of plant emission information, and donor and recipient were selected according to the detection results of efficacy characteristics.

#### 3.5.2. Biological Signal Radiation Power Detector

The biological signal radiation power detector developed by us was used to detect the radiation power of the experimental donor and recipient plants, and the donor and recipient were determined according to the monitoring data.

#### 3.5.3. Seedling Requirements

According to the requirements of seed germination, the donor and acceptor should be cultivated separately and they can only be used when they sprout. In terms of the experimental plan, generally, the number of donors is N times more than the number of receptors, to ensure timely replacement of vigorous growth of the donor.

#### 3.5.4. Bioinformation Breeding Machine

In the experiment, the selected donors and receptors are placed in different positions of the bioinformatics breeding machine, and then the cabin door is closed, the ventilation system is opened, and the automatic working system of the bioinformatics breeding machine is started.

#### 3.5.5. Set Test Time

According to the working time and experimental steps of the breeding machine set in the plan, as well as the detection of temperature, humidity and ventilation, we check the growth status of the donor and recipient buds and seedlings, replenish water appropriately, and replace the donor buds and seedlings according to the set test time.

#### 3.5.6. Sample Package

After 50 - 100 h of work, the genetic information transfer will be completed. The receptors will be installed in shielded boxes to avoid electric, magnetic, light and sound waves pollution, and the receptors will be sown to the experimental fields in time according to the design requirements.

### 3.6. Effect and Analysis

#### 3.6.1. Transfer of Genetic Traits of Black Peanut and Protein to Radish

**Figure 8** shows the experimental results of multiple transfer genetic traits completed by us through a bioinformation breeding machine. **Figure 8-1** shows that after soybean sprout signal was transferred to corn bud, the seedlings were planted in the test field. After several days, it was found that the seedling type and root system of the treatment group were significantly changed. **Figure 8-2**, **Figure 8-3** and **Figure 8-4** show that after transferring the information of black peanut to water radish, its fruit appearance (after harvest), leaf shape and root system have changed significantly. In September 2010, the first generation of the radish son (HS) was tested by the Test Center of Institute of Ecology, Chinese Academy of Sciences [31], and various amino acids and proteins showed significant changes. The receptor is compared with the control group, there were 18 items with change rate ≥ 15%; there were 16 items with change rate ≥ 40%; there were 3 items with change rate ≥ 100%, among which ammonia increased by 177.78%, potassium increased by 26.56%, and total protein and amino acid in treatment group increased by 84.3% by compared with control group. **Figure 8-5** shows that after the soybean information was transferred to the wheat receptor, the appearance of the first generation of its offspring (HS) changed


**Figure 8.** Some experimental results of directional transfer of genetic traits using CBE technology. From **Figure 8-1**, it can be seen that after the soybean information is transferred to the corn bud and planted in the experimental field, a few days later, random sampling shows that the plant type and root of the first generation of Maize (HS) are transferred to the genetic traits of soybean. **Figure 8-2**, **Figure 8-3** and **Figure 8-4** show that the fruit shape, leaf shape and root of generation 1 of black peanut information processing group (HS) have changed significantly. **Figure 8-5** shows that after transferring the soybean information to wheat, the soybean information processing group was significantly shorter than the control group after the first generation (HS) mature harvest, and the seeds of the treatment group were fuller than the control group, with an estimated yield increase of more than 20%. **Figure 8-6**, **Figure 8-7** and **Figure 8-8** are the experimental results of transferring the information of soybeans, garlic and flax to corn respectively. The plant type of corn in the information processing group has changed significantly, and the taste has also changed. **Figure 8** shows that after the receptor receive the information wave from the donor, the genetic characters of the receptor change towards the genetic characters of the donor, rather than random distribution, indicating that the genetic information transferred through the biological breeding machine is not distorted, and the real genetic information of the donor has been transferred.

significantly. On the left is the information processing group, and on the right is the control group. The trees in the information processing group were shorter than those in the control group, and the grain weight was increased by about 20%.

In 2012, the experimental seeds were provided by Liaoning Academy of Agricultural Sciences, which repeated the above experiment of black peanut information transfer water supply radish. After the test center of Shenyang Institute of ecology, Chinese Academy of Sciences [32], it was found that the change of the subgeneration (HS) generation 1 treatment group was still very significant. The Center tested 21 items in total. Among them there were 8 items with a change rate ≥ 15%, 4 items with change rate ≥ 40%, and 2 items with change rate ≥ 100%. Where the protein increased by 468.42%, the selenium increased by 42.8%, and the cystine increased by 133%.

The significance of the above experiment is to realize the transfer of genetic traits through plant information transmission: it is the first time to realize the directional transfer of various genetic traits of the donor plant to the recipient by

the information wave in the biological information breeding machine through CBE technology, and to realize the selective, cross space, directional transfer to the recipient without molecular transfer, so it is essentially different from transgenic.

### 3.6.2. Experiments on Directional Transfer of Soluble Sugar and Soluble Protein

With the support of experts from Liaoning Academy of Agricultural Sciences and Shenyang Agricultural University, a number of biological information transfer experiments have also been carried out, and all of them have achieved success. In 2015, we used the same method above to complete the experiment of transferring cantaloupe information to dry cucumber. The treatment group and the control group were planted in the experimental field respectively. After they matured, the first generation of their son (HS) was sent to Shenyang Agricultural University for testing see **Figure 9** and the data in the table. We found that the soluble sugar content of the treatment group increased by 44.9% compared with the control group, and the soluble protein content increased by 45%.

We adopted the same method to directionally transfer the genetic traits of soluble sugar and soluble protein of melon or watermelon to cucumbers, as shown in **Figure 10**. The first generation of the son (HS) was sent to Shenyang Agricultural University for soluble sugar and soluble protein testing [33], and the test results are shown in the chart. After watermelon information processing, the soluble sugar content of water cucumber in treatment group increased by 416% and the soluble protein content increased by 421% compared with control group. The soluble sugar of water cucumber is increased by 350% after cantaloupe information treatment and the soluble protein content is increased by 356%.

The results indicated that the genetic characters of soluble sugar and soluble protein of watermelon and melon have been transferred to the genetic characters of soluble sugar and soluble protein of cucumber.

9-1 The treatment group is on the left and the control group is on the right

9-2 Detection Report of Shenyang Agricultural University

| test item | unit | experimental result | |
|---|---|---|---|
| | | contents of soluble sugar | soluble protein content |
| control group | mg/g | 2.85 | 1.42 |
| treatment group | mg/g | 4.13 | 2.06 |

**Figure 9.** The experimental results of directional transfer of genetic traits of muskmelon polysaccharide and protein to dry cucumber; from the test data of Postharvest progeny (HS) 1 generation, it can be seen that soluble sugar and protein in the treatment group increased significantly compared with the control group.

10-1 Cucumber information processing group on the left and control group on the right

10-2 Melon information processing group on the left and control group ontheright

Detection report of soluble sugar and protein

| test item | unit | experimental result | |
|---|---|---|---|
| | | contents of soluble sugar | soluble protein content |
| The control group | mg/g | 0.75 | 0.37 |
| Treatment group 1 | mg/g | 3.87 | 1.93 |
| Treatment group 2 | mg/g | 3.38 | 1.69 |

**Figure 10.** The experimental results of directional transfer of genetic traits of watermelon/cantaloupe polysaccharide and protein to water cucumber. It can be seen from the test data of the first generation of offspring (HS) after harvest that the indexes of soluble sugar and protein in the treatment group have doubled compared with the control group.

In 2016, we also cooperated with experts from Shenyang Agricultural University to transfer the genetic traits of polysaccharide in northeast Round jujube (wild kiwi fruit) to the original potato species through a bioinformatics breeding machine, as shown in **Figure 11**. **Figure 11-1** is the information donor, namely the north square round jujube seedling; **Figure 11-2** is the information receptor, that is, the original seed of potato; **Figure 11-3** is potato control group; **Figure 11-4** is potato treatment group; **Figure 11-5** is the test result of soluble sugar [34]. The soluble sugar content of the treatment group increased significantly compared with the control group, at least by more than 2 times, and at most by more than 6 times. After that, we tested the molecular weight of nucleic acid and found that the molecular weight of nucleic acid in the treatment group increased significantly compared with that in the control group, as shown in **Table 3**.

### 3.7. Directional Transfer Experiment of Soybean Isoflavones

In 2017, we cooperated with experts from the College of Life Sciences of Beijing University of Chinese Medicine. We provided experimental equipment for biological information transfer, and students independently completed the experiment of transferring information from soybean sprouts to corn sprouts, through genetic testing, it was found that soybean isoflavone genes were obviously expressed in multiple treatment groups, as shown in **Figure 12**.

### 3.8. Discussion on Experiments of Transfer Genetic Traits

Kulian. P. pointed out that the DNA double helix breaking process is also

**Table 3.** Nucleic acid test report of genetic information transferred from Northeast Jujube to potato.

| Signal processing time | Exp. Num. | Exp.1 | Exp.2 | Average value | Group D | Control group | Multiple 1 | Multiple 2 |
|---|---|---|---|---|---|---|---|---|
| 70 h | 1-1 | 0.587444 | 0.626555 | 0.607 | 0.485888 | 0.450333 | 1.249256 | 1.347890 |
| 90 h | 1-2 | 0.566555 | 0.657444 | 0.612 | 0.427666 | | 1.431021 | 1.358993 |
| 110 h | 1-3 | 0.506555 | 0.493111 | 0.499 | 0.5200555 | | 0.961115 | 1.109918 |


| Tes content | | | |
|---|---|---|---|
| test item | unit | experimental result: contents of soluble sugar | experimental result: soluble protein content |
| Potato (control group) | mg/g | 0.08 | 4.13 |
| Treatment group 1 | mg/g | 0.33 | 4.07 |
| Treatment group 2 | mg/g | 0.28 | 3.71 |
| Treatment group 3 | mg/g | 0.59 | 3.86 |
| Treatment group 4 | mg/g | 0.45 | 5.07 |

**Figure 11.** The results of four groups of parallel experiments that transferred the genetic traits of northern jujube polysaccharide to potatoes. From the test data of the first generation of offspring (HS), it can be seen that the soluble sugar in the treatment group increased significantly compared with the control group, at least by more than 3 times, and at most by more than 6 times.

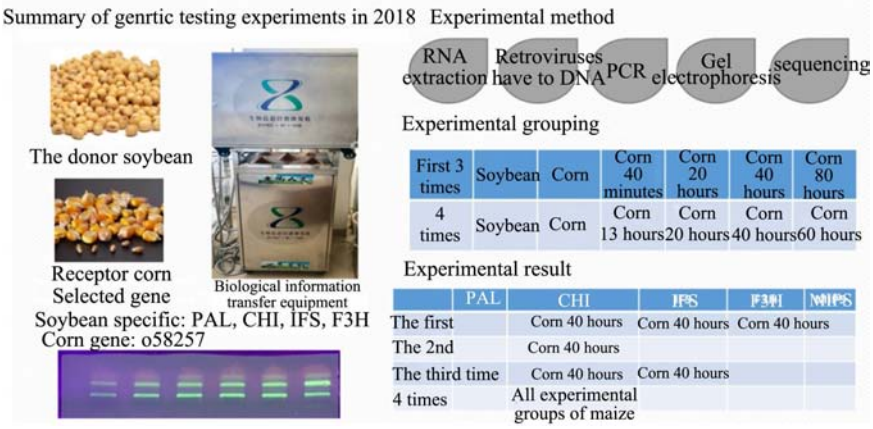


**Figure 12.** The experimental results of transferring soybean isoflavones to maize completed by students of the Academy of life sciences of Beijing University of traditional Chinese medicine using the experimental machine of bioinformatics breeder. They conducted gene detection and found that in the 40 hour information transfer experimental results, there were multiple groups of soybean isoflavones genes in the treatment group were expressed in maize genes.

accompanied by the internal quantum entanglement effect of DNA, indicating that there is a quantum entanglement phenomenon in DNA [35] [36], that may be a biological information transfer mechanism. Biological signal transduction is

essentially a physical process of life quantum information transfer. The results of the above repeatable experiments showed that different recipient plants would have different biological effects by receiving the signals of radiation from different donor plant seedlings in the bioinformation breeding machine processing. Whether the same family or cross family of plants, after receiving the signal from the budding donor for 50 - 100 h by bioinformation breeding machine, the germination potential, leaf shape, vein, plant type, root and fruit shape of the parent or son (HS) 1 generation can be significantly changed. Not only that, it was also found that the genetic traits of the receptor (HS) generation 1 were transferred to the prominent genetic traits from the donor. After receiving the radiation signal from the donor plant in the bioinformatics breeding machine the genetic traits are directed to transfer, the changes of genetic traits were not random orientation and distribution. This indicates that the transferred information expresses the selected and prominent genetic traits of the donor plant, which is a directional transfer. And the genetic information transferred by the biological breeding machine is not distorted, which is indeed a transfer of the real genetic information of the donor.

The German scholar Konstantin Meyl believes that the metabolism controlled by genes can only occur when energy and information are introduced [37]. The above-mentioned various biological experiments show that there is such a unified signal of energy and information in the biological signal, that is, the signal of DNA radiation, and the information is expressed by the change of the donor's radiation energy. The above test results provide new evidence: in the biological signals radiated by the donor plant, there are signals that can affect the DNA replication and protein activity of the recipient plant. It is the most important and basic biological signal, which is of great significance for exploring the biological field and exploring life. By using the bioinformatics breeding machine, the life information of the donor plant can be transferred directly to the receptor in a short time, and the appearance or genetic traits of the receptor can be changed directionally; the genetic information transfer of the same family and cross family plants can also been realized, which will open up a new way of molecular free transfer for the cultivation of new varieties.

## 4. Conclusion and Discussion

1) A number of test results once again show that different structures of different plants will radiate different biological signals and express different information in the metabolic process, which can affect the life activities of different levels of allogeneic species. DNA signal is the most basic and important signal, and its information and energy cannot be separated. In many cases, information is expressed through the nonlinear and complex changes of energy, which can directly affect the replication and expression of cell DNA. It is a signal with important vital characteristics that is unique to life.

2) Asexual and molecular free DNA communication can be realized between

plants. It is not interfered by the complex electromagnetic environment in plants, indicating that DNA signals are different from other electromagnetic signals. Therefore, it can transmit life information while transmitting energy, especially the information that can truly transmit and express genes, and affect the activities of allogeneic proteins. Therefore, it is of great significance and deserves attention and in-depth research.

3) The experimental results of this paper provide new evidence for not only the connection of genetic material, but also the close connection of genetic information energy between plants, that is, DNA communication.

4) The invention of CBE technology and bioinformatics breeding machine has realized the transmission of biophysical signals and the directional transfer of plant specific information. Moreover, this kind of plant information will not directly produce the chemical reaction in the recipient body, will not destroy the molecular structure, and has no ethical problems. It has opened up a new way of non-sexual, non-molecular transfer, selective, directional, low-cost, new variety cultivation, so it has broadly application prospects.

## Acknowledgements

The authors would like to express their heartfelt thanks to the Microbial Engineering Center of the Liaoning Academy of Agricultural Sciences, the School of Horticulture of Shenyang Agricultural University, the Science and Technology Committee of the Liaoning Veteran Professors Association, Professor Song Kongzhi, and former researcher Li Xianghui of the Institute of Genetics of the Chinese Academy of Sciences for their strong support!

## Availability of Data and Materials

The datasets obtained and analyzed for this study will be made available from the corresponding author in a reasonable request.

## Contributions

Xinzhou Yuan, Jiafeng Yuan, Zhongxian Deng, Shikui Wang, Zhen Yang, and Qiao Bi wrote the main manuscript text, and Xinzhou Yuan and Jafeng Yuan prepared the experimental data, forms and related figures. All authors have reviewed the manuscript.

## Consent for Publication

All authors contributed to the article and approved the submitted version for publication.

## Conflicts of Interest

The authors are employed by Shenzhen Xinzhou Biological Information Technology Co., Ltd. All authors declare no other competing interests.

## Funding Statement

This study received funding from Shenzhen Xinzhou Biological Information Technology Co., Ltd. The funder was not involved in the study design, collection, analysis, and interpretation of data, the writing of this article or the decision to submit it for publication. All authors declare no other competing interests.

## References

[1] Pang, X.F. (2008) Bioelectromagnetics. National Defense Industry Press, Beijing, 279.

[2] Gu, Q. (2014) Biophotonics (Chinese Edition). Science Press, Beijing.

[3] Jia, L.H. (1984) General Theory of Biological Structure and Biological Field. Taiyuan Shanxi Agricultural University, Taiyuan.

[4] Chen, J.G., Shi, F., Jin, Z., *et al.* (1995) *Chinese Journal of Biophysics*, No. 1, 119-124.

[5] Yuan, X.Z. (2006) *American Natural Science Research*, **6**, 140-141.

[6] Yuan, X.Z. (2006) *Chinese Journal of Practical Medicine*, **6**, 44-46.

[7] Qian, Z., *et al.* (1994) *Chinese Medicine University*, *College Journal*, **23**, 519.

[8] Jiang, C.Z. (1996) *Nexus Magazine*, *USA-Canadian Edition*, **3**, 39.

[9] Jiang, C.Z. and Yuan, X.Z. (2010) Biological Electromagnetic Wave Disclosure: Field Guiding Discovery. Dakang Press, Taibei, 83-108, 305-308.

[10] Jiang, C.Z. and Yuan, X.Z. (2011) Biological Electromagnetic Wave Disclosure. Medical Science and Technology Press, Beijing, 48-73.

[11] Yuan, X.Z. (2016) Exploration and Discovery of Life Signal. Somatic Science Research Progress Papers Collection, 156-187.

[12] Yuan, X.Z. (2017) *Frontier Science*, **11**, 80-85.

[13] Chen, X., Ba, Y., Ma, L.J., *et al.* (2008) *Cell Research*, **18**, 997-1006. https://doi.org/10.1038/cr.2008.282

[14] Zhu, K.G., Liu, M.H., Fu, Z., *et al.* (2017) *PLOS Genetics*, **13**, e1006946. https://doi.org/10.1371/journal.pgen.1006946

[15] Yin, Y., Cai, X., Chen, X., *et al.* (2014) *Cell Research*, **24**, 1164-1180. https://doi.org/10.1038/cr.2014.121

[16] Yuan, X.Z., Yuan, J.F., Bi, Q. and Song, K.Z. (2022) *Open Journal of Biophysics*, **12**, 265-283. https://doi.org/10.4236/ojbiphy.2022.124013

[17] Zheng, Q., *et al.* (1994) *Journal of China Medical University*, **23**, 519.

[18] Jiang, C.Z., Zheng, Q. and Tang, B.H. (2000) *Chinese Journal of Applied Physiology*, No. 4, 326-329.

[19] Fan, S.D., Zheng, Q., Tian, W., *et al.* (1995) *Journal of China University of Physical Education*, **4**, 13.

[20] Fan, S.D., Zheng, Q., Tian, W., *et al.* (1996) *Journal of Shenyang Institute of Physical Education*, No. 3, 13-14.

[21] Xia, Z.D., Chen, S.Z., Wu, G.J., *et al.* (1999) *Chinese Journal of Modern Medicine*, No. 7, 18-19.

[22] Jiang, C.Z., Qian, Z. and Tang, B.H. (2007) *Natural Science Research*, **10**, 68-77.

[23] Jiang, K.Z., Zheng, Q. and Yuan, X.Z. (2008) *China Practical Medicine*, No. 9, 31-31.

[24] Jiang, K.Z., Zheng, Q. and Yuan, X.Z. (2008) The improvement effect of bio electromagnetic field on human myocardial ischemia, China Practical Medicine, No. 4, 72-73.

[25] Yuan, L.P. (2018) *Journal of Agronomy*, **8**, 71-73.

[26] Yuan, X.-Z. and Yuan, J.-F. (2013) Biological Information Breeding Machine. China Patent Number: 201320587392.7.

[27] Xia, Z.D., *et al.* (2000) *Journal of Hunan Medical University*, **25**, 151-153.

[28] Wang, H.Y., Zhang, W.J. and Li, G.X. (2000) Basic Physics of University. China Higher Education Press, Beijing, 394-397.

[29] Yuan, X.Z., *et al.* (2009) *China Health Monthly*, **29**, 203-205.

[30] A System for Directional Transfer of Biological Information Energy. China Patent CN201710842076.22017.

[31] Shenyang Institute of Ecology, Chinese Academy of Sciences (2010) Detection Report; Chinese Academy of Sciences Measurement Words 2010-01-047, Radish (Control Group); 2010-01-049 Radish (Experimental Group, Black Peanut Biofield Induced Radish Variation).

[32] Shenyang Institute of Ecology, Chinese Academy of Sciences (2012) Detection Report; 2012-1-86 Water Radish (Control Group); 2012-01-087 Radish (Experimental Group, Biological Field of Black Peanut Induced Radish Variation).

[33] College of Horticulture, Shenyang Agricultural University (2015) Sample Detection Experimental Report, Potato and Other Control Group and Treatment Group (Soft Jujube Biological Field Treatment Potato; Cantaloupe/Watermelon Biological Field Treatment of Dry Cucumber/Water Cucumber, etc.).

[34] College of Horticulture, Shenyang Agricultural University (2016) Experimental Test Results Report, Potato Control Group, Treatment Group Detection.

[35] Kurian, P., Dunston, G. and Lindesay, J. (2016) *Journal of Theoretical Biology*, **391**, 102-112. https://doi.org/10.1016/j.jtbi.2015.11.018

[36] Bordonaro, M. (2019) *Biosystems*, **178**, 16-24. https://doi.org/10.1016/j.biosystems.2019.01.010

[37] Meyl, K. (2012) *DNA and Cell Biology*, **31**, 422-426. https://doi.org/10.1089/dna.2011.1415

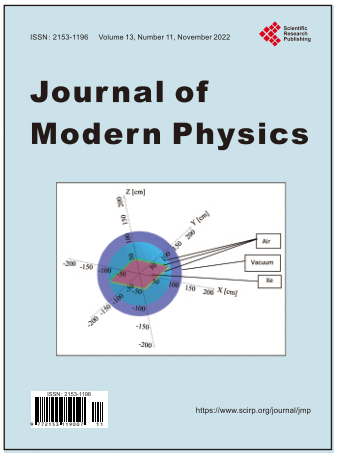


# Call for Papers

# Journal of Modern Physics

ISSN: 2153-1196 (Print) ISSN: 2153-120X (Online)
https://www.scirp.org/journal/jmp

***Journal of Modern Physics*** **(JMP)** is an international journal dedicated to the latest advancement of modern physics. The goal of this journal is to provide a platform for scientists and academicians all over the world to promote, share, and discuss various new issues and developments in different areas of modern physics.

## Subject Coverage

Journal of Modern Physics publishes original papers including but not limited to the following fields:

Biophysics and Medical Physics
Complex Systems Physics
Computational Physics
Condensed Matter Physics
Cosmology and Early Universe
Earth and Planetary Sciences
General Relativity
High Energy Astrophysics
High Energy/Accelerator Physics
Instrumentation and Measurement
Interdisciplinary Physics
Materials Sciences and Technology
Mathematical Physics
Mechanical Response of Solids and Structures
New Materials: Micro and Nano-Mechanics and Homogeneization
Non-Equilibrium Thermodynamics and Statistical Mechanics
Nuclear Science and Engineering
Optics
Physics of Nanostructures
Plasma Physics
Quantum Mechanical Developments
Quantum Theory
Relativistic Astrophysics
String Theory
Superconducting Physics
Theoretical High Energy Physics
Thermology

We are also interested in: 1) Short Reports—2-5 page papers where an author can either present an idea with theoretical background but has not yet completed the research needed for a complete paper or preliminary data; 2) Book Reviews—Comments and critiques.

## Notes for Intending Authors

Submitted papers should not have been previously published nor be currently under consideration for publication elsewhere. Paper submission will be handled electronically through the website. All papers are refereed through a peer review process. For more details about the submissions, please access the website.

## Website and E-Mail

**https://www.scirp.org/journal/jmp** **E-mail: jmp@scirp.org**

## What is SCIRP?

Scientific Research Publishing (SCIRP) is one of the largest Open Access journal publishers. It is currently publishing more than 200 open access, online, peer-reviewed journals covering a wide range of academic disciplines. SCIRP serves the worldwide academic communities and contributes to the progress and application of science with its publication.

## What is Open Access?

All original research papers published by SCIRP are made freely and permanently accessible online immediately upon publication. To be able to provide open access journals, SCIRP defrays operation costs from authors and subscription charges only for its printed version. Open access publishing allows an immediate, worldwide, barrier-free, open access to the full text of research papers, which is in the best interests of the scientific community.

- High visibility for maximum global exposure with open access publishing model
- Rigorous peer review of research papers
- Prompt faster publication with less cost
- Guaranteed targeted, multidisciplinary audience


Scientific Research Publishing

**Website: https://www.scirp.org**
**Subscription: sub@scirp.org**
**Advertisement: service@scirp.org**